

UNIVERSIDADE TÉCNICA DE LISBOA
INSTITUTO SUPERIOR TÉCNICO

Quasinormal Modes
and
Gravitational Radiation
in
Black Hole Spacetimes

Vitor Cardoso

(Licenciado)

Dissertação para obtenção do Grau de Doutor em Física

Orientador: Doutor José Pizarro de Sande e Lemos

Presidente: Reitor da Universidade Técnica

Vogais: Doutor José Tito da Luz Mendonça

Doutor Jorge Venceslau Comprido Dias de Deus

Doutor Alfredo Barbosa Henriques

Doutor Kostas Kokkotas

Doutor José Pizarro de Sande e Lemos

Doutor Luís Filipe Lopes Bento

Dezembro de 2003

**Quasinormal Modes
and
Gravitational Radiation
in Black Hole Spacetimes**

VITOR CARDOSO

February 4, 2008

Resumo

Buracos negros desempenham um papel fundamental na física actual. Os buracos negros possuem modos de vibração próprios, semelhantes aos de um sino ou de uma guitarra, a que chamamos modos quasinormais. Investigações passadas mostram que os modos quasinormais são importantes no entendimento da vibração de buracos negros astrofísicos. Investigações recentes mostram que são importantes na conexão entre gravitação e mecânica quântica. O estudo de modos quasinormais é assim de extrema importância.

Estes modos controlam todo e qualquer processo envolvendo buracos negros, em particular a emissão de ondas gravitacionais geradas, por exemplo, na colisão de dois buracos negros. Existe a possibilidade de se criarem buracos negros em aceleradores, segundo conjecturas que invocam a existência de dimensões extra no universo. Torna-se portanto imperativo fazer um estudo detalhado da radiação gravitacional emitida na colisão de buracos negros em várias dimensões, bem assim como o estudo de ondas gravitacionais em dimensões mais altas.

Na presente dissertação apresenta-se um estudo aprofundado dos modos quasinormais de buracos negros, em vários espaços-tempo de fundo. Investiga-se também a radiação gravitacional gerada na colisão de buracos negros com partículas e na colisão entre dois buracos negros. Finalmente, apresenta-se o estudo de ondas gravitacionais em dimensões gerais onde, por exemplo, se generaliza a fórmula do quadrupolo de Einstein.

PALAVRAS-CHAVE:

Buracos negros; Modos quasinormais; Radiação gravitacional; Colisões entre buracos negros; Propagação de ondas; Dimensões extra;

Abstract

Black holes play a fundamental role in modern physics. They have characteristic oscillation modes, called quasinormal modes. Past studies have shown that these modes are important to our understanding of the dynamics of astrophysical black holes. Recent studies indicate that they are important as a link between gravitation and quantum mechanics. Thus, the investigation of these modes is a timeliness topic.

Quasinormal modes dominate almost every process involving black holes, in particular gravitational wave emission during, for example, the collision between two black holes. It may be possible to create black holes at future accelerators, according to recent theories advocating the existence of extra dimensions in our universe. It is therefore important to study in depth the gravitational radiation emitted in high energy collision between two black holes in several dimensions, and also to make a theoretical study of gravitational waves in higher dimensions.

In this thesis we shall make a thorough study of the quasinormal modes of black holes in several kinds of background spacetimes. We shall investigate the gravitational radiation given away when highly energetic particles collide with black holes, and also when two black holes collide with each other. Finally, we shall study the properties of gravitational waves in higher dimensions, for instance, we generalize Einstein's quadrupole formula.

KEY-WORDS:

Black holes; Quasinormal modes; Gravitational radiation; High energy black hole collision; Wave propagation; Extra dimensions.

Este trabalho foi financiado pela Fundação Para a Ciência e a Tecnologia,
sob o contrato Praxis XXI/BD/21284/99 (01/01/2000-31/12/2003).

This work was supported by Fundação Para a Ciência e a Tecnologia,
under the grant Praxis XXI/BD/21284/99 (01/01/2000-31/12/2003).

Acknowledgements

I am extremely grateful to my supervisor José Lemos, for all the things he taught me and for all the physics we have done together. It was a pleasure and an honor to work with him, and i'm certain I could not have asked for a better adviser. Thanks José!

I am also very grateful to Óscar Dias, my best and long-dated friend, for such wonderful moments we had together thinking about physics and life. His sharp mind and gentle personality has made a better physicist and human being of me.

I am very thankful to Mário Pimenta, for showing me how a teacher is supposed to teach, and of course also for the great meals we had at his place.

It is my pleasure to thank all the elements of CENTRA, specially Jorge Dias de Deus, Barbosa Henriques and Ana Mourão, for all the support and encouragement during the completion of this thesis, and also Dulce Conceição and Paula Espada, for their infinite patience, and for having the gift to make apparently complex things turn simple.

I am indebted to Emanuele Berti, Kostas Kokkotas, Roman Konoplya, José Lages, Lubos Motl, José Natário, Andrew Neitzke, Hisashi Onozawa, Tito Mendonça, Ricardo Schiappa and Shijun Yoshida for very interesting discussions and collaborations, in which part of this work was done. I have learned a lot from you.

To my family, where I always find unconditional support, I cannot thank enough in words. I love you all! Mother, I am trying.

Carlota, thank you! This thesis is half yours.

Of course, peace of mind is important when doing research. Only special people are able to put up with my continuous non-sense, and still smile for me. Thanks Pedro (Ching-Cheng) and Ana (Bacaninha). I love you.

Estér, I'll see you some day.

Contents

Preface	xv
Brief general introduction	1
I Quasinormal modes in four and higher dimensions	3
1 Quasinormal modes: an introduction	5
1.1 Quasinormal modes: an introduction	5
1.1.1 Motivation	5
1.1.2 Definition of quasinormal modes	7
1.2 What is the importance of QNMs in fundamental physics	10
1.2.1 QNMs and black hole parameter estimation	11
1.2.2 QNMs and thermalization in the AdS/CFT	11
1.2.3 QNMs and black hole area quantization	12
1.3 Outline of Part I	14
2 Quasinormal modes of the three dimensional BTZ (AdS) black hole	17
2.1 Introduction	17
2.2 Perturbing a non-rotating BTZ black hole with scalar and electromagnetic fields	19
2.2.1 The wave equation	19
2.2.2 QNMs for scalar and electromagnetic perturbations	20
2.3 Perturbing a black hole with Dirac and Weyl spinor fields	22
2.3.1 The wave equation	22
2.3.2 QNMs for Weyl perturbations	24
2.4 Discussion	24
3 Quasinormal modes of the four dimensional Schwarzschild-AdS black hole	27
3.1 Introduction	27
3.2 Scalar, Electromagnetic and Gravitational perturbations in a Schwarzschild AdS background	28
3.2.1 Maxwell perturbations	28
3.2.2 Gravitational perturbations	29
3.3 QNMs and some of its properties	31
3.3.1 Analytical properties	31
3.4 Equations and numerical Method	33
3.5 Numerical results	35
3.5.1 Scalar QN frequencies	35

3.5.2	Electromagnetic QN frequencies	38
3.5.3	Gravitational QN frequencies	41
3.6	Discussion of the results	45
3.6.1	On the isospectrality breaking between odd and even perturbations	45
3.6.2	Why are the scalar and gravitational perturbations isospectral in the large black hole regime?	46
3.6.3	Future directions	47
3.7	The limit $m \rightarrow 0$	49
3.8	Conclusion	50
3.9	APPENDIX: Pure AdS normal modes for electromagnetic and gravitational perturbations	50
4	Quasinormal modes of the four dimensional toroidal (AdS) black hole	53
4.1	Introduction	53
4.2	Scalar, electromagnetic and gravitational perturbations in a toroidal, cylindrical or planar black hole in an AdS background	54
4.2.1	Scalar field perturbations	55
4.2.2	Maxwell field perturbations	56
4.2.3	Gravitational perturbations	56
4.3	Quasi-normal modes and some of its properties	59
4.3.1	Numerical calculation of the QN frequencies	59
4.4	Conclusions	62
5	Quasinormal modes of the near extremal four dimensional Schwarzschild-dS black hole	63
5.1	Introduction	63
5.2	Equations	64
5.3	Conclusions	67
6	Quasinormal modes of Schwarzschild black holes in four and higher dimensions	69
6.1	Introduction	69
6.2	QN frequencies of the four-dimensional Schwarzschild black hole	72
6.3	QN frequencies of D -dimensional Schwarzschild black holes	77
6.3.1	Equations and conventions	77
6.3.2	Perturbative calculation of QNMs of D -dimensional Schwarzschild BHs	79
6.3.3	Numerical procedure and results	81
6.4	Discussion of results and future directions	87
7	A complete survey on the quasinormal modes of the four dimensional Kerr black hole	89
7.1	Introduction	89
7.2	Numerical method	91
7.3	Gravitational perturbations	92
7.3.1	Modes having $l = m = 2$: a more extensive discussion	92
7.3.2	Modes having $l = 2, l \neq m$	95

7.3.3	Modes having $l = 3$	96
7.4	Scalar and electromagnetic perturbations	97
7.4.1	Scalar modes	97
7.4.2	Electromagnetic modes	98
7.5	The asymptotic behaviour of the modes' imaginary part	98
7.6	Algebraically special modes	99
7.6.1	An introduction to the problem	99
7.6.2	Numerical search and QNM multiplets	101
7.7	Conclusions	102

II Encounters of black holes with particles in four and higher dimensions: quasinormal modes, gravitational and scalar radiation **111**

8	Gravitational radiation: an introduction	113
8.1	Introduction	113
8.2	Astronomical sources of gravitational waves	114
8.3	Microscopic sources of gravitational waves	116
8.4	Outline of Part II	119
9	Gravitational radiation in a curved asymptotically flat four dimensional background : encounters of non-rotating black holes with particles	121
9.1	Introduction	121
9.2	Basic Formalism	122
9.3	Numerical Results	124
10	Gravitational radiation in a curved asymptotically flat four dimensional background: encounters of Kerr black holes with particles	129
10.1	Introduction	129
10.2	The Teukolsky and Sasaki-Nakamura formalism	131
10.3	The Sasaki-Nakamura equations for a point particle falling along a geodesic of the Kerr black hole spacetime	133
10.3.1	The Sasaki-Nakamura equations for an highly relativistic point particle falling along the symmetry axis of the Kerr black hole	133
10.3.2	The Sasaki-Nakamura equations for an highly relativistic point particle falling along the equatorial plane of the Kerr black hole	134
10.4	Implementing a numerical solution	134
10.5	Numerical Results and Conclusions	135
11	Scalar radiation in asymptotically anti-de Sitter in three, four and higher dimensional spacetimes	141
11.1	Introduction	141
11.2	Scalar radiation from infall of a particle into a BTZ black hole	143
11.2.1	Formulation of the problem and basic equations	143
11.2.2	The initial data and boundary conditions	144
11.2.3	Green's function solution	145

11.2.4	Numerical results for the waveforms and spectra	147
11.3	Scalar radiation from infall of a particle into a D -dimensional Schwarzschild-anti-de Sitter black hole	149
11.3.1	The Problem, the Equations and the Laplace transform, and the initial and boundary conditions for D -dimensions	149
11.3.2	Results	153
11.4	Conclusions	159
III Gravitational waves in higher dimensions		161
12	Gravitational waves in higher dimensions	163
12.1	Introduction	163
12.2	Outline of Part III	165
13	Gravitational waves in a flat higher dimensional background	167
13.1	Introduction	167
13.2	Linearized D -dimensional Einstein's equations	168
13.2.1	The inhomogeneous wave equation	168
13.2.2	The plane wave solutions	169
13.2.3	The D -dimensional retarded Green's function	170
13.2.4	The even D -dimensional retarded solution in the wave zone	172
13.3	The even D -dimensional quadrupole formula	173
13.3.1	Derivation of the even D -dimensional quadrupole formula	173
13.3.2	Applications of the quadrupole formula: test particles in a background geometry	174
13.4	Instantaneous collisions in even D -dimensions	177
13.4.1	Derivation of the radiation formula in terms of a cutoff for a head-on collision	177
13.4.2	Applications: the cutoff frequency when one of the particles is a black hole and radiation from black hole pair creation	178
13.4.3	Spherical coordinates in $(D - 1)$ -dimensions	183
13.5	Summary and discussion	183
14	Late-time tails in higher dimensional spacetimes	185
14.1	Introduction	185
14.2	A brief summary of previous analytical results for a specific class of potentials	187
14.3	The evolution equations and late-time tails in the D -dimensional Schwarzschild geometry	188
14.3.1	The evolution equations and the reduction of the potential to the standard form	188
14.3.2	Late-time tails	190
14.4	Conclusions	192
Bibliography		195

Preface

The research included in this thesis has been carried out at Centro Multidisciplinar de Astrofísica (CENTRA) in the Physics Department of Instituto Superior Técnico. I declare that this thesis is not substantially the same as any that I have submitted for a degree or diploma or other qualification at any other University and that no part of it has already been or is being concurrently submitted for any such degree or diploma or any other qualification.

Chapters 2, 4, 5, 9, 10 and 11 are the outcome of collaborations with Professor José Lemos. Chapter 3 was done in collaboration with Professor José Lemos and Roman Konoplya. Chapter 7 was done in collaboration with Professor Kostas Kokkotas, Dr. Emanuele Berti and Dr. Hisashi Onozawa. Chapter 6 is the outcome of a collaboration with Professor José Lemos and Dr. Shijun Yoshida. Chapter 13 is the outcome of a collaboration with Professor José Lemos and Óscar Dias. Chapter 14 is the outcome of a collaboration with Professor José Lemos, Dr. Shijun Yoshida and Óscar Dias. Most of these chapters have been published, and some are being submitted for publication.

Chapter 9 referring to encounters of black holes with particles in an anti-de Sitter background, was submitted with some modifications, under the title “Numerical Analysis of Partial Differential Equations in General Relativity and String Theory: Applications to Gravitational Radiation and to the AdS/CFT Conjecture”, and won the Gulbenkian Prize of Scientific Investigation 2001 (Prémio Gulbenkian de Estímulo à Investigação Científica, 2001).

A list of the works published included in this thesis is included below.

- . V. Cardoso, J. P. S. Lemos, “Scalar, electromagnetic and Weyl perturbations of BTZ black holes: quasi normal modes”, *Phys. Rev. D* **63**, 124015 (2001); gr-qc/0101052. (Chapter 2)
- . V. Cardoso, J. P. S. Lemos, “Quasi-normal modes of Schwarzschild black holes in anti-de Sitter spacetimes: electromagnetic and gravitational perturbations”, *Phys. Rev. D* **64**, 084017 (2001); gr-qc/0105183. (Chapter 3)
- . V. Cardoso, R. Konoplya, J. P. S. Lemos, “Quasinormal frequencies of Schwarzschild black holes in anti-de Sitter spacetimes: A complete study on the asymptotic behavior”, *Phys. Rev. D* **68**, 044024 (2003); gr-qc/0305037. (Chapter 3)
- . V. Cardoso, J. P. S. Lemos, “Quasi-normal modes of toroidal, cylindrical and planar black holes in anti-de Sitter spacetimes”, *Class. Quantum Grav.*, **18**, 5257 (2001); gr-qc/0107098. (Chapter 4)
- . V. Cardoso, J. P. S. Lemos, “Quasinormal modes of the near extremal Schwarzschild-de Sitter black hole”, *Phys. Rev. D* **67**, 084020 (2003); gr-qc/0301078. (Chapter 5)
- . V. Cardoso, J. P. S. Lemos, S. Yoshida, “Quasinormal modes of Schwarzschild black holes in four and higher dimensions”, *Phys. Rev. D*, in press (2003), gr-qc/0309112; (Chapter 6)
- . E. Berti, V. Cardoso, K. Kokkotas and H. Onozawa, “Highly damped quasinormal modes of Kerr black holes”, *Phys. Rev. D*, in press (2003); hep-th/0307013. (Chapter 7)
- . V. Cardoso, J. P. S. Lemos, “Gravitational radiation from collisions at the speed of light: a massless particle falling into a Schwarzschild black hole”, *Phys. Lett. B* **538**, 1 (2002); gr-qc/0202019. (Chapter 9)
- . V. Cardoso, J. P. S. Lemos, “The radial infall of a highly relativistic point particle into a Kerr black hole along the symmetry axis”, *Gen. Rel. Gravitation* **35**, L327-333 (2003); gr-qc/0207009. (Chapter 10)

- . V. Cardoso, J. P. S. Lemos, “Gravitational radiation from the radial infall of highly relativistic point particles into Kerr black holes”, *Phys. Rev. D* **67**, 084005 (2003); gr-qc/0211094. (Chapter 10)
- . V. Cardoso, J. P. S. Lemos, S. Yoshida, “Electromagnetic radiation from collisions at almost the speed of light: an extremely relativistic charged particle falling into a Schwarzschild black hole”, *Phys. Rev. D*, in press (2003); gr-qc/0307104. (mentioned in Chapter 10)
- . V. Cardoso, J. P. S. Lemos, “Black hole collision with a scalar particle in three dimensional anti-de Sitter spacetime”, *Phys. Rev. D* **65**, 104032 (2002); hep-th/0112254. (Chapter 11)
- . V. Cardoso, J. P. S. Lemos, “Black hole collision with a scalar particle in four, five and seven dimensional anti-de Sitter spacetimes: ringing and radiation”, *Phys. Rev. D* **66**, 064006 (2002); hep-th/0206084. (Chapter 11)
- . V. Cardoso, J. P. S. Lemos, “Scalar synchrotron radiation in the Schwarzschild-anti-de Sitter Geometry”, *Phys. Rev. D* **65**, 104033 (2002); hep-th/0201162. (Chapter 11)
- . V. Cardoso, Ó. J. C. Dias, J. P. S. Lemos, “Gravitational radiation in D-dimensional spacetimes”, *Phys. Rev. D* **67**, 064026 (2003); hep-th/0212168. (Chapter 13)
- . J. T. Mendonça, V. Cardoso, “Gravitational optics: Self-phase modulation and harmonic cascades”, *Phys. Rev. D* **66**, 104009 (2002); gr-qc/0209076. (mentioned in Chapter 13)
- . J. T. Mendonça, V. Cardoso, M. Servin, M. Marklund and G. Brodin, “Self-phase modulation of spherical gravitational waves”, *Phys. Rev. D*, in press (2003); gr-qc/0307031. (mentioned in Chapter 13)
- . M. Servin, M. Marklund, G. Brodin, J. T. Mendonça and V. Cardoso, “Nonlinear self-interaction of plane gravitational waves”, *Phys. Rev. D* **67**, 087501 (2003); astro-ph/0303412. (mentioned in Chapter 13)
- . V. Cardoso, S. Yoshida, O. J. C. Dias, J. P. S. Lemos, “Late-Time Tails of Wave Propagation in Higher Dimensional Spacetimes”, *Phys. Rev. D* **68**, 061503(R)[Rapid Communications](2003); hep-th/0307122. (Chapter 14)

Brief general introduction

This thesis is devoted to the study of (i) the characteristic vibration modes of black holes, called quasinormal modes (QNMs), (ii) radiative processes in non-asymptotically flat spacetimes and gravitational waves from processes involving black holes, specially high energy collisions, and (iii) gravitational waves in higher dimensions. This thesis has accordingly been divided into three parts: Part I deals with QNMs of black holes, Part II deals with gravitational radiation from encounters of black holes with particles, and Part III deals with gravitational wave physics in higher dimensions.

A few years ago, the very concept of QNMs of black holes was closely linked to the gravitational radiation emitted by the object, and one studied quasinormal modes, specially the lowest lying modes, in order to get a better understanding of the properties of the gravitational wave signal. For example, the decay time of the gravitational signal is directly connected to the imaginary part of the associated quasinormal frequency, and the characteristic frequency of the signal is related to the real part of the lowest quasinormal frequency. There are now a couple of significant breakthroughs in fundamental physics that separated the direct dependence of QNMs on gravitational radiation, and changed the way we faced gravitational radiation, as something important only in an astrophysical set. First supergravity brought a whole new interest to anti-de Sitter spacetimes and the AdS/CFT conjecture gave a new special meaning to the notion of quasinormal modes of black holes living in anti-de Sitter spacetimes. According to it, the imaginary part of the lowest quasinormal frequency should describe the typical timescale of approach to thermal equilibrium in a dual conformal field theory. Very recently quasinormal modes have made their way to a completely unsuspected territory: quantum gravity. Some evidence has been accumulating that highly damped quasinormal modes may be important in semi-classical attempts to quantize the black hole area. This has been confirmed, rather surprisingly, in Loop Quantum Gravity, an alternative theory to quantum gravity. Second, the recent attempts to solve the hierarchy problem have put forward the interesting possibility that there may be large extra dimensions in our Universe, besides the usual four. This is the so called TeV-scale gravity scenario. When the consequences of such a scenario are carefully studied, one comes to the conclusion that gravitational waves may be indirectly detected at accelerators such as LHC at CERN!

In Part I the quasinormal modes of black holes, both in asymptotically flat and in non-asymptotically flat spacetimes, will be thoroughly studied. In Part II we will study gravitational wave generation from the collision of black holes with particles. We begin by study high energy collisions between point particles and black holes, and black hole-black hole collisions at near the speed of light. This is a subject of the utmost importance, since one may well produce black holes at the LHC. We will go on by considering scalar radiation in asymptotically anti-de Sitter spacetime. In Part III we shall conclude this thesis by extending what we know about linearized gravitational waves in four dimensions to a general D -dimensional spacetime.

Part I

Quasinormal modes in four and higher dimensions

Chapter 1

Quasinormal modes: an introduction

Contents

1.1	Quasinormal modes: an introduction	5
1.2	What is the importance of QNMs in fundamental physics	10
1.3	Outline of Part I	14

1.1 Quasinormal modes: an introduction

1.1.1 Motivation

We are all familiar with the fact that the ringing of a bell or the strum of a guitar invariably produces a “characteristic sound”. Such systems respond to any excitation by selecting a set of natural real frequencies, the normal frequencies, and their response is given as a superposition of stationary modes, the normal modes. Black holes have a characteristic sound as well. As a simple demonstration we may let a gaussian gravitational wavepacket evolve on the Schwarzschild geometry. The results, at the linearized level, are shown in Figs. 1.1-1.2.

A striking feature, first uncovered by Vishveshwara [1] and clearly apparent in Figs.1.1-1.2, is that the signal is dominated, during a certain time, by damped single frequency oscillations. The frequency and damping of these oscillations depend only on the parameters characterizing the black hole, which in the Schwarzschild case is its mass. They are completely independent of the particular initial configuration that caused the excitation of such vibrations. That such characteristic oscillations always appear and dominate the signal at intermediate times, in any event involving black holes, has been tested time and time again. It has been verified at the linearized level [1, 2, 3], in which the fields are treated as a perturbation in the single black hole spacetime, but also for example, on fully numerical simulations of black hole-black hole collision processes [4, 5], or stellar collapse [6, 7]. They are therefore a characteristic of black holes. These characteristic oscillations have been termed “quasinormal modes” and the associated frequencies “quasinormal frequencies” [8]. The “normal” part derives from the obvious similarity between these and normal mode systems. There are however important differences between these two systems, which justifies the “quasi”: first, quasinormal modes are not stationary modes, since they are exponentially damped. This is merely reflecting the

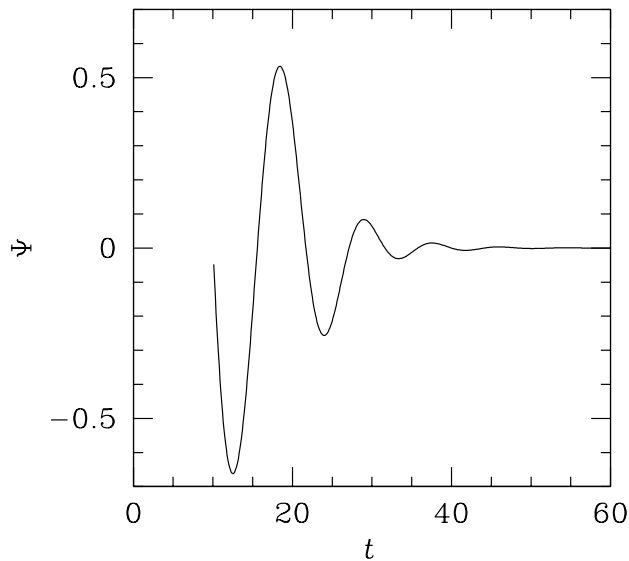


Figure 1.1: Evolution of a gravitational gaussian wavepacket in the neighborhood of a Schwarzschild black hole. One can see that the waveform is dominated by a characteristic ringing. We have chosen a gaussian wavepacket $\Psi \sim e^{-(\frac{v-v_0}{\sigma})^2}$, with $\sigma = 3$ and $v_c = 10$, but the ringing down frequency and damping time is independent of these parameters. Also, the coordinate $v = t + r_*$ is an advanced time coordinate.

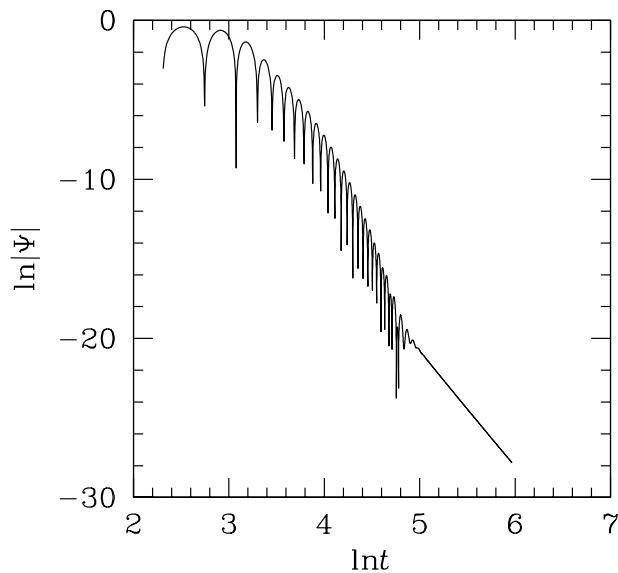


Figure 1.2: Evolution of a gravitational gaussian wavepacket in the neighborhood of a Schwarzschild black hole, here shown in a log-log plot. The dominance of quasinormal ringing is clear, and at very late times, a power-law falloff appears.

fact that the black hole spacetime is radiating energy away to infinity, through the form of gravitational (or any massless field) waves. When describing a resonant system, such as a bell, a guitar or a star, one often makes the convenient and sometimes accurate assumption, that there is no damping. This then leads to a normal mode, complete expansion of the field. The stationary mode expansion is just reflecting the no energy loss assumption. As soon as one turns to the more realistic situation, by allowing a dissipation mechanism, one expects no such naive stationary normal mode expansion to exist. Black hole oscillations occupy a very special place here. It is impossible, even in principle, even in the most idealized scenario, to turn off the dissipation mechanism. In fact, black holes are made from the fabric of spacetime, and any spacetime oscillation implies the generation of gravitational waves, carrying energy away to infinity. Indeed the very equations describing black hole oscillations are nothing more than a description of gravitational waves. Quasinormal modes were first discussed in the black hole context, but from the above discussion one anticipates they will also appear in other dissipative physical systems, such as a vibrating string coupled to a surrounding medium (and therefore transmitting energy to infinity through it), laser cavities or a star when one does not neglect gravitational radiation. Another important difference between normal and quasinormal modes is the completeness issue, which is a rather subtle one, mathematically. The response of a normal mode system can be given for all times as a superposition of normal modes. However, quasinormal modes seem to appear only over a limited time interval; this is also shown in Fig. 1.2, where it is seen that at very late times quasinormal ringing gives way to a power-law falloff. A thorough account of quasinormal modes in asymptotically flat spacetimes, their properties, a thorough comparison between normal and quasinormal mode systems, and a discussion about the incompleteness of quasinormal modes can be found in the classical reviews by Kokkotas and Schmidt [9] and Nollert [10], and references therein. From now on we shall refer to quasinormal modes as “QNM” and we shall refer to quasinormal frequencies as “QN frequencies”.

1.1.2 Definition of quasinormal modes

Most of the problems concerning wave propagation in black hole spacetimes can be reduced to a second order partial differential equation of the form

$$\frac{\partial^2}{\partial x^2}\Psi - \frac{\partial^2}{\partial t^2}\Psi - V\Psi = 0. \quad (1.1)$$

Here x is a spatial variable, usually but not always ranging (in a special coordinate system) from $-\infty$ to $+\infty$. When dealing with black hole spacetimes the horizon is usually at $-\infty$, and for the rest of this discussion we shall assume so. Also, V is an x -dependent potential. To define in a phenomenological way what a QNM is, we shall proceed in the usual way by assuming a time dependence

$$\Psi(t, x) = e^{-i\omega t}\phi(x). \quad (1.2)$$

Inserting this in (1.1) we get an ordinary differential equation in the spatial variable x ,

$$\frac{d^2}{dx^2}\phi + (\omega^2 - V)\phi = 0. \quad (1.3)$$

The form (1.2) is not restrictive, since once we have a solution for (1.3), a general time dependent solution can be given as a continuous Fourier transform of such solutions. The

form (1.3) is ideal to study QNMs in a way that parallels a normal mode analysis. We shall now restrict ourselves to asymptotically flat spacetimes, and defer a discussion of asymptotically de Sitter (i.e., a spacetime with a positive cosmological constant) or anti-de Sitter (i.e., negative cosmological constant) for the next chapters. In asymptotically flat spacetimes, the potential V is positive and satisfies

$$V \rightarrow 0, x \rightarrow -\infty \tag{1.4}$$

$$V \rightarrow 0, x \rightarrow +\infty. \tag{1.5}$$

Therefore, such potentials do not allow bound states, and this makes it impossible to do a normal mode expansion. The idea that the evolution of Ψ will generally involve a superposition of these QNMs can be shown to be correct by the use of Laplace transforms. We refer the reader to [9, 10]. Nevertheless, we saw that the signal is somehow dominated by characteristic oscillations (Figs.1-2), so we shall blindly continue with our analysis. Having in mind the form (1.4)-(1.5) of the potential we have that near the boundaries $-\infty$ and $+\infty$ the solution behaves as plane waves,

$$\phi \sim e^{\pm i\omega x}, x \rightarrow -\infty \tag{1.6}$$

$$\phi \sim e^{\pm i\omega x}, x \rightarrow +\infty. \tag{1.7}$$

The boundary conditions defining QNMs are that toward the boundaries the solutions should be purely outgoing at infinity ($x = +\infty$) and ingoing at the horizon ($x = -\infty$),

$$\phi \sim e^{-i\omega x}, x \rightarrow -\infty \tag{1.8}$$

$$\phi \sim e^{+i\omega x}, x \rightarrow +\infty. \tag{1.9}$$

Here ingoing at the horizon means entering into the black hole, therefore leaving the domain we are studying. These are physically motivated boundary conditions. Only a discrete set of complex frequencies ω_{QN} satisfy these boundary conditions. These are the QN frequencies, and the associated wavefunctions ϕ , solutions of (1.3) are the QNMs. It has been proved by Vishveshwara [11] that for the Schwarzschild geometry ω_{QN} must have a negative imaginary part; this has also been found for geometries other than Schwarzschild, for example Schwarzschild-anti-de Sitter, Schwarzschild-de Sitter, Kerr (we shall go through these geometries on the next chapters). This means on the one hand that QNMs decay exponentially in time, and the physical significance of this is that the black hole spacetime is losing energy in the form of gravitational waves. On the other hand, this also means that the spacetime is stable. In addition, the imaginary part being negative makes the numerical calculation of QN frequencies a non-trivial task: according to the boundary conditions (1.8)-(1.9), and to the fact that the QN frequencies have a negative imaginary part, one has that QNMs grow exponentially at the boundaries. Now, in order to tell if a certain frequency is or not a QN frequency one must check that, for example, there is only an out-going $e^{i\omega x}$ piece at infinity, or in other words, one must check that near infinity the $e^{-i\omega x}$ is absent. However, this last term is exponentially suppressed in relation to the other, so one must be able to distinguish numerically an exponentially small term from an exponentially large one. This has always been, and still is, a major obstacle when it comes down to an actual computation of QN

Table 1.1: The first four quasinormal frequencies for a Schwarzschild black hole, measured in units of the black hole mass M . To convert this to Hz one must multiply the numbers in the Table by $32310\frac{M_{\odot}}{M}$. Thus, a one solar mass black hole has a typical ringing frequency of 10 kHz in the quadrupole mode, and a damping timescale, due to gravitational wave emission, of $\tau = 3.74 \times 10^{-4}s$.

$\omega_{\text{QN}}M$			
n	$l = 2:$	$l = 3:$	$l = 4:$
0	0.37367-0.08896 <i>i</i>	0.59944-0.09270 <i>i</i>	0.80918-0.09416 <i>i</i>
1	0.34671-0.27391 <i>i</i>	0.58264-0.28130 <i>i</i>	0.79669-0.28449 <i>i</i>
2	0.30105-0.47828 <i>i</i>	0.55168-0.47909 <i>i</i>	0.77271-0.47991 <i>i</i>
3	0.25150-0.70514 <i>i</i>	0.51196-0.69034 <i>i</i>	0.73984-0.68392 <i>i</i>

frequencies. Still, brute numerical force sometimes works. Chandrasekhar and Detweiler [12] have succeeded in finding some of the Schwarzschild QN frequencies this way, in 1975. Since then, numerous techniques have been developed. Some of them are analytical tools like the WKJB technique of Schutz and Will [13], later refined to 3rd order [14], and recently extended to 6th order [15], or the “potential fit” [16] one, in which one tries to fit the Schwarzschild potential to one which enables us to find exact results. However, the most successful attempt has been developed by Leaver [17], using a continued fraction form of the equations, which is rather easy to implement numerically. We refer the reader to [9, 10] for a complete account of all these techniques, and many others. Exact results for QNMs of certain black hole space-times only became available very recently, and shall be later described in this thesis. They are however an exception, the rule being that an exact solution to (1.3) satisfying the boundary conditions (1.8)-(1.9) is not available. So one has to resort to any numerical or approximate method one can. In Table 1.1 we present the first four QN frequencies for gravitational perturbations of a Schwarzschild black hole, obtained using Leaver’s [17] technique.

In Table 1.1 the angular quantum number l gives the angular dependence of the gravitational wave. For example a wave with $l = 2$, the lowest gravitational radiatable multipole, has a quadrupole distribution. Some comments are in order. First, QN frequencies come in pairs. That is, if $\omega = a + ib$ is a QN frequency, then so is $\omega = -a + ib$. We only show in Table 1.1 frequencies with a positive real part. There are a countable infinity of QN frequencies. They are usually arranged by their imaginary part. Thus, the frequency with lowest imaginary part is called the fundamental frequency and is labeled with the integer $n = 0$; the one with second lowest imaginary part is the first overtone ($n = 1$) and so on. The real part can be shown to be, using a WKJB type of reasoning [13], of the order of the height of the potential barrier, i. e., $Re[\omega] \sim V_{\text{max}}$, where V_{max} is the maximum value attained by the potential V . The real part is, in the Schwarzschild geometry, bounded from above, whereas the imaginary part seems to grow without bound for overtone number $n \rightarrow \infty$. This is shown in Fig.1.3, where we show the first two thousand QNMs, using Leaver’s technique, plus an improvement devised by Nollert [18].

Notice that as the imaginary part of ω goes to infinity the real part seems to go to a constant (in this case 0.0437123) , and this has given rise to a lot of discussion recently, in connection with the quantization of black hole area. This issue will be addressed later on.

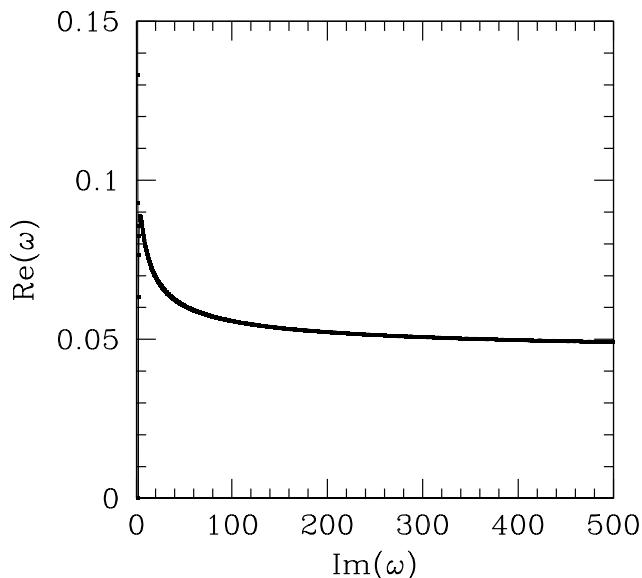


Figure 1.3: Some of the higher overtone QN frequencies for $l = 2$ gravitational perturbations. Notice that the real part seems to go to a constant, whereas the imaginary part grows without bound. In fact, one can show numerically that $M\omega_n = 0.0437123 - \frac{i}{4}(n + 1/2) + \mathcal{O}(\frac{1}{\sqrt{n}})$

1.2 What is the importance of QNMs in fundamental physics

Once one realizes the importance of black holes in fundamental physics, one can grasp the meaning and significance of their characteristic vibrations. Black holes are *the* general relativistic object by excellence. They are pure objects, in the sense that only a few parameters, like mass, charge and angular momentum are enough to describe them. In this respect they come very close to our notion of elementary particles. They have been called the hydrogen atom of general relativity and this is indeed a very good comparison. Like in the hydrogen atom \leftrightarrow quantum mechanics dichotomy, a black hole being a solution to Einstein's equations has all of the general relativistic properties embodied in it, but still is simple enough to be a model for starting a complete understanding of all the physics that go with Einstein's equations. Moreover, probing black hole physics is probing the strong field regime of general relativity, something that has still not been done (here, gravitational waves may also play an important role. We defer this discussion for Part II of this thesis.)

There are mainly three major motivations leading us to study in detail the QNMs of black holes, namely estimating black hole parameters by using the fact that QN frequencies depend only on intrinsic parameters, estimating thermalization timescales in connection with the AdS/CFT conjecture and semi-classical attempts to quantize the black hole area, that are now making heavy use of highly damped QNMs. These are described below.

1.2.1 QNMs and black hole parameter estimation

Historically, one of the main reasons for studying QNMs is that they may provide valuable help for identifying black hole parameters. Gravitational waves have not yet been detected, but their indirect influence has been seen and measured with remarkable accuracy by Hulse and Taylor for the binary pulsar PSR 1913+16. One expects to finally detect gravitational waves directly in the forthcoming years, with gravitational wave detectors already taking data [20, 21, 22]. However, gravitational waves are so weak that in order to ever hope for their detection one needs to have a very strong source of gravitational waves, for instance stellar collapse or black hole collisions. Numerical simulations have shown that in the final stage of such processes (ringdown) QNMs dominate the black hole response. Of course, since the QNMs are exponentially damped in time, only the mode corresponding to the fundamental frequency (lowest imaginary part) should show up in the signal. This is indeed the case. Now, as we said earlier, the QN frequencies depend only on the black hole fundamental parameters. For example, if we are dealing with a Kerr black hole, the QN frequencies will depend only on the black hole mass M and angular momentum per unit mass a . As such it should be possible to infer the black hole parameters solely from the knowledge of the ringing frequency and the damping time. Consider a single interferometric gravitational wave detector and a perturbed black hole. Focus attention on a single oscillation mode of the black hole, for example the $l = m = 2$ mode. Then the strain measured by the detector has the time dependence of an exponentially damped sinusoid characterized by four parameters Q , f , V and T [23]

$$h(t) = V^{-1/3} e^{-\pi f \frac{t-T}{Q}} \sin 2\pi f(t - T). \quad (1.10)$$

Here Q is the quality factor measured in units of the oscillation frequency f ,

$$Q = \pi f \tau, \quad (1.11)$$

where τ is the damping time. $V^{-1/3}$ is the amplitude of the waveform, which depends on the distance to the source, the size of the perturbation, and the relative orientation of the detector and the source. Finally, T is the starting time of the perturbation. Note the Q and f are related to the imaginary and real part of the fundamental QN frequency. In particular one finds that a good fit to the numerical results for the fundamental QN frequencies of a rotating hole is [23]

$$f \sim \frac{1}{2\pi M} \left[1 - \frac{63}{100} (1 - a)^{3/10} \right], \quad (1.12)$$

$$Q = \pi f \tau = 2(1 - a)^{-9/20}. \quad (1.13)$$

Now, by measuring the ringing frequency and decay time one could in principle derive the parameters of the black hole, by inverting (1.12) and (1.13). For a very recent work on how to effectively search for the gravitational ringing of black holes see [24].

1.2.2 QNMs and thermalization in the AdS/CFT

Quantum field theories are currently the very best we have for a microscopic description of nature, and these are verified experimentally to a high degree of accuracy. They treat particles as point-like, capable of interacting locally with other particles. Successful as quantum theories

are, we have not yet been able to incorporate gravity in such a formalism. Nevertheless, if one gives up the notion that particles are point-like, and assumes that the fundamental objects are strings, it is possible to quantize gravity in a consistent scheme [25]. All string theories include a particle with zero mass and spin two, and since gravity is the only consistent interaction for massless spin two particles, this means any string theory will contain gravity. Now, another theory that describes matter, namely quarks and gluons, is QCD. QCD is a gauge theory based on the group $SU(3)$. This is sometimes stated by saying that quarks have three colors. QCD is asymptotically free, meaning that the effective coupling constant decreases as the energy increases. At low energies QCD becomes strongly coupled and it is not easy to perform calculations. It was suggested by 't Hooft that the theory might simplify when the number of colors N is very large [26]. The plan was to try and solve exactly for $N = \infty$ and then do an expansion in $1/N = 1/3$. Furthermore there are strong indications that the large N theory is a free string theory with string coupling constant $1/N$. The correspondence between QCD when $N \rightarrow \infty$ and string theory is the AdS/CFT correspondence conjecture [27]. It states that the bulk physics in AdS_n is dual to the physics of a certain CFT_{n-1} , which may be thought of as living in the conformal boundary of AdS_n . For example, it conjectures that $U(N)$ Yang-Mills theory, with number of spinor supercharges $\mathcal{N} = 4$, which is a conformal theory, is the same as a ten-dimensional superstring theory on $AdS_5 \times S^5$. The only particular feature of these strings is that they are moving on an anti-de Sitter space. The radius of curvature of this anti-de Sitter space depends on N and large N corresponds to a large radius of curvature. Thus, by taking N to be large we can make the curvature as small as we want. The theory in AdS includes gravity since any string theory includes gravity. So it is claimed that there is an equivalence between a gravitational theory and a field theory! However the mapping between the gravitational and the field theory is quite non-trivial since the field theory lives in a lower dimension. For more details on this see the review [28]. The QN frequencies of AdS black holes have a direct interpretation in terms of the dual conformal field theory. According to the AdS/CFT correspondence, a large static black hole in AdS corresponds to an approximately thermal state in the CFT, and perturbing the black hole corresponds to perturbing this thermal state. The decay of the perturbation describes therefore the return to equilibrium. Now, we know that the fundamental QN frequency should control the decay of any perturbation, and therefore by computing QN frequencies in AdS spacetime (containing a black hole), one obtains a prediction for the thermalization timescale in the strongly coupled CFT. It seems extremely difficult to compute this timescale directly in the CFT.

1.2.3 QNMs and black hole area quantization

There are other attempts to quantize gravity, besides string theory. As we remarked earlier, one has the strong conviction that black holes may play a major role in our attempts to shed some light on a quantum theory of gravity. The quest for a consistent quantization of black holes was initiated many years ago by Bekenstein [29, 30] who, based solely on semi-classical arguments, conjectured that the horizon area of a (non extremal) black hole should have a discrete eigenvalue spectrum. By using a semi-classical version of Christodoulou's processes along with Heisenberg's quantum uncertainty principle, Bekenstein deduced the quantization

condition of the black hole area,

$$A_n = \gamma l_p^2 n, n = 1, 2, \dots, \quad (1.14)$$

where γ is a dimensionless constant and $l_p = \sqrt{\frac{G}{c^3}} \sqrt{\frac{h}{2\pi}}$ is the Planck length. This formula has been arrived at only by using Sommerfeld's quantization procedure. The quantization of horizon area in equal steps brings to mind an horizon formed by patches of equal area γl_p^2 which get added one at a time. There is no need to think of a specific shape or localization of these patches. It is their standard size which is important, and which makes them all equivalent. This patchwork horizon can be regarded as having many degrees of freedom, one for each patch. In quantum theory degrees of freedom independently manifest distinct states. Since the patches are all equivalent, each will have the same number of quantum states, say k . Therefore the total number of quantum states of the horizon is

$$N = k^{\frac{A}{\gamma l_p^2}}, \quad (1.15)$$

where k is a positive integer. The N states may not all be equally probable. But if the k states of each patch are all likely, then all N states are equally probable. In that case the statistical (Boltzmann) entropy associated with the horizon is $\log N$ or

$$S_{BH} = \frac{\log k A}{\gamma l_p^2}. \quad (1.16)$$

Comparing with Hawking's formula for the entropy, $S_{BH} = \frac{A}{4}$ one gets

$$\gamma = 4 \log k. \quad (1.17)$$

Thus, statistical physics arguments force the dimensionless constant γ to be of the form (1.17). Still, a specific value of k requires further input, which was not available up until recently. However, a sudden turning of events happened a few years ago, when Hod [31] made a proposal to determine γ . His proposal made the spacing of area levels consistent both with the area-entropy thermodynamic relation for black holes, with the Boltzmann-Einstein formula in statistical physics, and with Bohr's correspondence principle. Hod builds his conjecture on Bohr's correspondence principle, "transition frequencies at large quantum numbers should equal classical oscillation frequencies", and then goes on to associate these classical oscillation frequencies with the highly damped QN frequencies, since "quantum transition do not take time" [32]. As previously noted, the highly damped QN frequencies of a Schwarzschild black hole were numerically found to be given by

$$M\omega_n = 0.0437123 - \frac{i}{4}(n + 1/2) + \mathcal{O}\left(\frac{1}{\sqrt{n}}\right), \quad (1.18)$$

and they are independent of l , the angular quantum number characterizing the angular distribution. Hod observed that the numerical limit for the real part, 0.0437123 agreed (to the available data) with $\frac{\log 3}{8\pi}$. He therefore conjectured that asymptotically

$$M\omega_n = \frac{\log 3}{8\pi} - \frac{i}{4}(n + 1/2). \quad (1.19)$$

Using $A = 16\pi M^2$ and $dM = E = \frac{\hbar}{2\pi}\omega$ he then concluded that

$$\gamma = 4 \log 3, \quad (1.20)$$

and therefore that

$$A_n = 4l_p^2 \log(3) \times n. \quad (1.21)$$

Following Hod's suggestion, Dreyer [33] recently used a similar argument to fix a free parameter (the so-called Barbero-Immirzi parameter) appearing in Loop Quantum Gravity, an alternative approach to a quantum gravity theory. Supposing that transitions of a quantum black hole are characterized by the appearance or disappearance of a puncture with lowest possible spin j_{\min} . Dreyer found that Loop Quantum Gravity gives a correct prediction for the Bekenstein-Hawking entropy if $j_{\min} = 1$, thereby fixing the Barbero-Immirzi parameter. When Hod made his original proposal, formula (1.19) and therefore also (1.20) and (1.21) was just based on a curious numerical coincidence. It has however been recently established by Motl [34] and Motl and Neitzke [35] with analytical techniques. In this quantum gravity context, in which the correspondence principle is valid, relevant modes are those which damp infinitely fast, do not significantly contribute to the gravitational wave signal, and are therefore typically ignored in studies of gravitational radiation. It is probably too early to assess the significance of these proposals. An obvious route to follow is to generalize these results for the Kerr black hole. However, as we shall describe, the Kerr black hole has bravely resisted all attempts to do so. First, the most complete numerical studies so far (see Chapter 7) do not seem to be able to completely probe the asymptotic behaviour of the QN frequencies. The available results point to some strange behaviour.

1.3 Outline of Part I

In the first part of this thesis we shall make an extensive study of QNMs and associated QN frequencies of black holes, both in asymptotically flat and in asymptotically de Sitter or anti-de Sitter backgrounds.

In Chapter 2 we shall begin by studying the QNMs and QN frequencies of the so called BTZ black hole [36]. This is a black hole solution to Einstein's equations with a cosmological constant in (2+1) spacetime dimensions, and lives in an asymptotically anti-de Sitter background. We shall find that it is possible to solve *analytically* the wave equation in this background, and also that it is possible to find simple analytical, exact expressions for the QN frequencies. This is the first instance of an analytical solution for the QN frequencies of a black hole, and was found by Cardoso and Lemos [37]. Note that we shall study only scalar, electromagnetic and Weyl perturbations, and not gravitational perturbations, since Einstein's equations in (2+1) dimensions have no dynamical degrees of freedom, and so there are no gravitational waves in this spacetime. The fact that there is a simple exact expression for the quasinormal frequencies makes it possible to make a number of studies which would otherwise have to rely on numerical calculations. We shall see examples of this in Part II. Besides, it was possible, very recently, to use these results to test for the validity of the QNM/black hole area quantization relation, so the BTZ black hole is in fact a very useful guide.

In Chapter 3 we go on to study the QNMs and QN frequencies of the four dimensional Schwarzschild-anti-de Sitter black hole. In order to analyze gravitational quasinormal modes

we shall decompose Einstein's equations in tensorial spherical harmonics and repeat the procedure of Regge and Wheeler [38] and Zerilli [39] to arrive at the gravitational wave equation. Notice that both in Chapters 2 and 3 the regime of very high overtones, i.e., highly damped modes, is studied, and therefore it is possible to make close contact with the AdS/CFT because these black holes live in an asymptotically anti-de Sitter background, but also with the recent conjectures relating highly damped QNMs with black hole area quantization and Loop Quantum Gravity.

There are, however, families of black holes in general relativity with a negative cosmological constant with horizons having topology different from spherical. In Chapter 4 we want to focus on the family of black holes whose horizon has toroidal, cylindrical or planar topology [41], and make a complete analysis of their QNMs. The analysis of gravitational wave is a non-trivial task, which we shall carry by using Chandrasekhar's [40] formalism.

In Chapter 5 we will turn to spacetimes which are asymptotically de Sitter. We will consider a near extremal Schwarzschild-de Sitter black hole. In this case it is also possible to find an exact solution to the wave equation leading again to exact analytical results, as was shown by Cardoso and Lemos [42]. However, this procedure only yields the correct QN frequencies up to some overtone number, i.e., it fails to give the correct asymptotic behaviour. In Chapter 6 we shall make an exhaustive numerical and analytical investigation of the QNMs of Schwarzschild black holes in four and higher dimensions. We shall first start by reviewing results that are known for quite some time, and then we shall take a look at new data. Finally, in Chapter 7, the last Chapter of Part I, we will revisit the quasinormal frequencies of the Kerr black hole, with the purpose to investigate the asymptotic behaviour of QN frequencies with a large imaginary part. This will hopefully help us on deciding whether or not there is some deep connection between QNMs and Loop Quantum Gravity, or then if QNMs are really at the heart of black hole area quantization. Here we will follow Berti et al [43].

Chapter 2

Quasinormal modes of the three dimensional BTZ (AdS) black hole

Contents

2.1	Introduction	17
2.2	Perturbing a non-rotating BTZ black hole with scalar and electromagnetic fields	19
2.3	Perturbing a black hole with Dirac and Weyl spinor fields	22
2.4	Discussion	24

2.1 Introduction

Up until very recently, all these works in QNMs dealt with asymptotically flat spacetimes. In the past few years there has been a growing interest in asymptotically AdS (anti-de Sitter) spacetimes. Indeed, the Bañados-Teitelboim-Zanelli (BTZ) black hole in 2+1-dimensions [36], as well as black holes in 3+1 dimensional AdS spacetimes with nontrivial topology (see, e.g. [41]), share with asymptotically flat spacetimes the common property of both having well defined charges at infinity, such as mass, angular momentum and electromagnetic charges, which makes them a good testing ground when one wants to go beyond asymptotic flatness. Another very interesting aspect of these black hole solutions is related to the AdS/CFT (Conformal Field Theory) conjecture [27]. For instance, due to this AdS/CFT duality, quasi-normal frequencies in the BTZ black hole spacetime yield a prediction for the thermalization timescale in the dual two-dimensional CFT, which otherwise would be very difficult to compute directly. If one has, e.g., a 10-dimensional type IIB supergravity, compactified into a $BTZ \times S^3 \times T^4$ spacetime, the scalar field used to perturb the BTZ black hole, can be seen as a type IIB dilaton which couples to a CFT field operator \mathcal{O} . Now, the BTZ in the bulk corresponds to to a thermal state in the boundary CFT, and thus the bulk scalar perturbation corresponds to a thermal perturbation with nonzero $\langle \mathcal{O} \rangle$ in the CFT.

The study of QNMs in AdS spacetime was initiated, with this motivation in mind, by Horowitz and Hubeny [48], but it focused on black holes living in AdS spacetime with dimension greater or equal to four. The QNMs of the BTZ black hole were first computed by

Cardoso and Lemos [37] who investigate the non-rotating black hole solution, and turned out to reveal a pleasant surprise: one can find an exact, analytical solution for them. In fact, it was the first example of a black hole spacetime for which one could solve exactly the wave equation, and this makes it an extremely important spacetime, where one can start to prove or disprove conjectures relating QNMs and critical phenomena or black hole area quantization. This work was later extended to rotating black holes by Birmingham [49], who could also establish a relation between QN frequencies and the Choptuik parameter [50], a conjecture put forward in [48]. Recently, and still in 2+1 dimensions, the QNMs of the more general dilatonic black holes were studied in [51], and QNMs in three dimensional time dependent anti-de Sitter spacetime were studied in [52]. That the QN frequencies of the BTZ black hole lead indeed to relaxation times in the CFT was proved by Birmingham, Sachs and Solodukhin [53], who found agreement between quasi-normal frequencies and the location of the poles of the retarded correlation function of the corresponding perturbations in the dual conformal field theory. This then provides a new quantitative test of the AdS/CFT correspondence. For previous work on BTZ black holes such as entropy of scalar fields, see [54] and references therein.

We shall now describe how to compute exactly the QNMs of the 3D non-rotating BTZ black hole [36]. This will follow closely the work in [37]. The non-rotating BTZ black hole metric for a spacetime with negative cosmological constant, $\Lambda = -\frac{1}{l^2}$, is given by

$$ds^2 = \left(-M + \frac{r^2}{l^2}\right)dt^2 - \left(-M + \frac{r^2}{l^2}\right)^{-1}dr^2 - r^2d\phi^2, \quad (2.1)$$

where M is the black hole mass. The horizon radius is given by $r_+ = M^{1/2}l$. The original article [36] considers the static and rotating uncharged BTZ black hole and the static electrically charged BTZ black hole. The extension to consider the rotating electrically charged BTZ black hole (mass, angular momentum and electric charge different from zero) has been done by Clément [56] and by Martínez, Teitelboim and Zanelli [57]. The static magnetic counterpart of the BTZ solution has been considered by Clément [56], Hirschmann and Welch [58] and Cataldo and Salgado [59]. The rotating magnetic solution has been found by Dias and Lemos [60] and a physical interpretation for the magnetic field source has been given.

We shall in what follows suppose that the scalar, electromagnetic and Weyl (neutrino) fields are a perturbation, i.e., they propagate in a spacetime with a BTZ metric. We will find that all these fields obey a wave equation and the associated QNM are exactly soluble yielding certain hypergeometric functions. As for the frequencies one has exact and explicit results for scalar and electromagnetic perturbations and numerical results for Weyl perturbations. To our knowledge, this is the first exact solution of QNMs for a specific model (see [45]).

In section 2 we give the wave equation for scalar and electromagnetic perturbations, and find the QNMs themselves and their frequencies. In section 3 we find the wave equation for Dirac and Weyl (neutrino) perturbations and analyze their QNMs. We should note that Einstein's equations in 2 + 1 dimensions have no dynamical degrees of freedom, and therefore there is no such thing as gravitational waves in 2 + 1 dimensions. All the gravitational degrees of freedom can be gauged away.

2.2 Perturbing a non-rotating BTZ black hole with scalar and electromagnetic fields

2.2.1 The wave equation

In this subsection we shall analyze the scalar and electromagnetic perturbations, which as we shall see yield the same effective potential, and thus the same wave equation.

First, for scalar perturbations, we are interested in solutions to the minimally coupled scalar wave equation

$$\Phi^\mu{}_{;\mu} = 0, \quad (2.2)$$

where, a comma stands for ordinary derivative and a semi-colon stands for covariant derivative. We make the following ansatz for the field Φ

$$\Phi = \frac{1}{r^{1/2}} \Psi(r) e^{-i\omega t} e^{im\phi}, \quad (2.3)$$

where m is the angular quantum number. It is useful to use the tortoise coordinate r_* defined by the equation $dr_* = \frac{dr}{-M + \frac{r^2}{l^2}}$, and given implicitly by

$$r = -M^{1/2} \coth(M^{1/2} r_*), \quad (2.4)$$

with $r_* \in]-\infty, 0]$, ($r_* = -\infty$ corresponds to $r = r_+$, and $r_* = 0$ corresponds to $r = \infty$).

With the ansatz (2.3) and the tortoise coordinate r_* , equation (2.2) is given by,

$$\frac{d^2 \Psi(r)}{dr_*^2} + (\omega - V(r)) \Psi(r) = 0, \quad (2.5)$$

where,

$$V(r) = \frac{3r^2}{4l^4} - \frac{M}{2l^2} - \frac{M^2}{4r^2} + \frac{m^2}{l^2} - \frac{Mm^2}{r^2}, \quad (2.6)$$

and it is implicit that $r = r(r_*)$. The rescaling to the radial coordinate $\hat{r} = \frac{r}{l}$ and to the frequency $\hat{\omega} = \omega l$ is equivalent to take $l = 1$ in (2.5) and (2.6), i.e., through this rescaling one measures the frequency and other quantities in terms of the AdS lengthscale l .

Now, the electromagnetic perturbations are governed by Maxwell's equations

$$F^{\mu\nu}{}_{;\nu} = 0, \text{ with } F_{\mu\nu} = A_{\nu,\mu} - A_{\mu,\nu}, \quad (2.7)$$

where $F_{\mu\nu}$ is the Maxwell tensor and A_μ is the electromagnetic potential. As the background is circularly symmetric, it would be advisable to expand A_μ in 3-dimensional vector spherical harmonics (see [61] and [62]):

$$A_\mu(t, r, \phi) = \begin{bmatrix} g^m(t, r) \\ h^m(t, r) \\ k^m(t, r) \end{bmatrix} e^{im\phi}, \quad (2.8)$$

where m is again our angular quantum number, and this decomposition is similar to the one in eigenfunctions of the total angular momentum in flat space [61].

However, going through the same steps one finds that the equation for electromagnetic perturbations is the same as the one for scalars, equation (2.5). The reason is that in three dimensions the 2-form Maxwell field $F = F_{\mu\nu} dx^\mu \wedge dx^\nu$ is dual to a 1-form $d\Phi$.

2.2.2 QNMs for scalar and electromagnetic perturbations

Although a precise mathematical definition for a QNM can be given, as a pole in the Green's function [9], we shall follow a more phenomenological point of view. A QNM describes the decay of the field in question. For the equation (2.5) it is defined as a corresponding solution which (i) near the horizon is purely ingoing, $\sim e^{i\omega r_*}$, corresponding to the existence of a black hole, and (ii) near infinity is purely outgoing, $\sim e^{-i\omega r_*}$, (no initial incoming wave from infinity is allowed). One can see that the potential $V(r)$ diverges at infinity, so we require that the perturbation vanishes there (note that $r = \infty$ corresponds to a finite value of r_* , namely $r_* = 0$).

2.2.2.a Exact calculation

Putting $l = 1$ and using the coordinate r_* , the wave equation (2.5) takes the form

$$\frac{\partial^2 \Psi(r)}{\partial r_*^2} + \left[\omega^2 - \frac{3M}{4 \sinh(M^{1/2} r_*)^2} + \frac{M}{4 \cosh(M^{1/2} r_*)^2} + \frac{m^2}{\cosh(M^{1/2} r_*)^2} \right] \Psi(r) = 0. \quad (2.9)$$

On going to a new variable $x = \frac{1}{\cosh(M^{1/2} r_*)^2}$, $x \in [0, 1]$ equation (2.9) can also be written as

$$4x(1-x)\partial_x^2 \Psi(r) + (4-6x)\partial_x \Psi(r) + \bar{V}(x)\Psi(r) = 0, \quad (2.10)$$

where

$$\bar{V}(x) = \frac{1}{4x(1-x)} \left[\frac{4\omega^2(1-x)}{M} - 3x - x(1-x) - \frac{4m^2x(1-x)}{M} \right]. \quad (2.11)$$

By changing to a new wavefunction y (see [63] for details), through

$$\Psi \rightarrow \frac{(x-1)^{3/4}}{x^{i\omega/2M^{1/2}}} y, \quad (2.12)$$

equation (2.10) can be put in the canonical form [63, 208]

$$x(1-x)y'' + [c - (a+b+1)x]y' - aby = 0, \quad (2.13)$$

with $a = 1 + \frac{im}{2M^{1/2}} - \frac{i\omega}{2M^{1/2}}$, $b = 1 - \frac{im}{2M^{1/2}} - \frac{i\omega}{2M^{1/2}}$, and $c = 1 - \frac{i\omega}{M^{1/2}}$, which is a standard hypergeometric equation. The hypergeometric equation has three regular singular points at $x = 0, x = 1, x = \infty$, and has two independent solutions in the neighbourhood of each singular point. We are interested in solutions of (2.13) in the range $[0, 1]$, satisfying the boundary conditions of ingoing waves near $x = 0$, and zero at $x = 1$. One solution may be taken to be

$$y = (1-x)^{c-a-b} F(c-a, c-b, c; x), \quad (2.14)$$

where F is a standard hypergeometric function of the second kind. Imposing $y = 0$ at $x = 1$, and recalling that $F(a, b, c, 1) = \frac{\Gamma(c)\Gamma(c-a-b)}{\Gamma(c-a)\Gamma(c-b)}$, we get

$$a = -n, \text{ or } b = -n, \quad (2.15)$$

with $n = 0, 1, 2, \dots$, so that the quasi normal frequencies are given by

$$\omega = \pm m - 2iM^{1/2}(n+1). \quad (2.16)$$

The lowest frequencies, namely those with $n = 0$ and $m = 0$ had already been obtained by [64] and agree with our results.

Table 2.1: Lowest ($n = 0$) QNM frequencies for symmetric ($m = 0$) scalar and electromagnetic perturbations of a non-rotating BTZ black hole.

$m = 0$				
	Numerical		Exact	
$M^{1/2}$	ω_r	$-\omega_i$	ω_r	$-\omega_i$
$\frac{1}{2}$	0.000	1.000	0	1
1	0.000	2.000	0	2
5	0.000	10.000	0	10
10	0.000	20.000	0	20
50	0.000	100.000	0	100
100	0.000	200.000	0	200
1000	0.000	2000.000	0	2000

2.2.2.b Numerical calculation of the frequencies

In order to check our results, we have also computed numerically the frequencies. By going to a new variable $z = \frac{1}{r}$, $h = \frac{1}{r_+}$ one can put the wave equation (2.5) in the form (see [48] for further details)

$$s(z)\frac{d^2}{dz^2}\Theta + t(z)\frac{d}{dz}\Theta + u(z)\Theta = 0, \quad (2.17)$$

where $\Theta = e^{i\omega r^*}\Psi(r)$, $s(z) = z^2 - Mz^4$, $t(z) = 2Mz^3 - 2i\omega z^2$ and $u(z) = \frac{V}{-M + \frac{1}{z^2}}$, with V given by (2.6). Now, $z \in [0, h]$ and one sees that in this range, the differential equation has only regular singularities at $z = 0$ and $z = h$, so it has by Fuchs theorem a polynomial solution. We can now use Fröbenius method (see for example [65]) and look for a solution of the form $\Theta(z) = \sum_{n=0}^{\infty} \theta_{n(\omega)}(z - h)^n(z - h)^\alpha$, where α is to be taken from the boundary conditions. Using the boundary condition of only ingoing waves at the horizon, one sees [48] that $\alpha = 0$. So the final outcome is that Θ can be expanded as

$$\Theta(z) = \sum_{n=0}^{\infty} \theta_{n(\omega)}(z - h)^n. \quad (2.18)$$

Imposing now the second boundary condition, $\Theta = 0$ at infinity ($z = 0$) one gets

$$\sum_{n=0}^{\infty} \theta_{n(\omega)}(-h)^n = 0. \quad (2.19)$$

The problem is reduced to that of finding a numerical solution of the polynomial equation (2.19). The numerical roots for ω of equation (2.19) can be evaluated resorting to numerical computation. Obviously, one cannot determine the full sum in expression (2.19), so we have to determine a partial sum from 0 to N , say, and find the roots ω of the resulting polynomial expression. We then move onto the next term $N+1$ and determine the roots. If the method is reliable, the roots should converge. We have stopped our search when a 3 decimal digit precision was achieved. We have computed the lowest frequencies for some parameters of the angular quantum number m and horizon radius r_+ . The frequency is written as $\omega = \omega_r + i\omega_i$, where ω_r is the real part of the frequency and ω_i is its imaginary part.

Table 2.2: Lowest ($n = 0$) QNM frequencies for $m = 1$ scalar and electromagnetic perturbations of a non-rotating BTZ black hole.

$m = 1$				
Numerical		Exact		
$M^{1/2}$	ω_r	$-\omega_i$	ω_r	$-\omega_i$
$\frac{1}{2}$	1.000	1.000	1	1
1	1.000	2.000	1	2
5	1.000	10.000	1	10
10	1.000	20.000	1	20
50	1.000	100.000	1	100
100	1.000	200.000	1	200
1000	1.000	2000.000	1	2000

In tables 2.1 and 2.2 we list the numerical values of the lowest QNM frequencies, for $m = 0$ and $m = 1$, respectively, and for selected values of the black hole mass. The numerical results agree perfectly with (2.16), and one sees that the imaginary part of the frequency scales with the horizon whereas the real part depends only on the angular index m .

2.3 Perturbing a black hole with Dirac and Weyl spinor fields

2.3.1 The wave equation

We shall develop Dirac's equation for a massive spinor, and then specialize to the massless case. The two component massive spinor field Ψ , with mass μ_s obeys the covariant Dirac equation

$$i\gamma^\mu \nabla_\mu \Psi - \mu_s \Psi = 0, \tag{2.20}$$

where ∇_μ is the spinor covariant derivative defined by $\nabla_\mu = \partial_\mu + \frac{1}{4}\omega_\mu^{ab}\gamma_{[a}\gamma_{b]}$, and ω_μ^{ab} is the spin connection, which may be given in terms of the tryad e_a^μ .

As is well known there are two inequivalent two dimensional irreducible representations of the γ matrices in three spacetime dimensions. The first may be taken to be $\gamma^0 = i\sigma^2$, $\gamma^1 = \sigma^1$, and $\gamma^2 = \sigma^3$, where the matrices σ^k are the Pauli matrices. The second representation is given in terms of the first by a minus sign in front of the Pauli matrices. From equation (2.20), one sees that a Dirac particle with mass μ_s in the first representation is equivalent to a Dirac particle with mass $-\mu_s$ in the second representation. To be definitive, we will use the first representation, but the results can be interchanged to the second one, by substituting $\mu_s \rightarrow -\mu_s$. For Weyl particles, $\mu_s = 0$, both representations yield the same results.

Again, one can separate variables by setting

$$\Psi(t, r, \phi) = \begin{bmatrix} \Psi_1(t, r) \\ \Psi_2(t, r) \end{bmatrix} e^{-i\omega t} e^{im\phi}. \tag{2.21}$$

On substituting this decomposition into Dirac's equation (2.20) we obtain

$$-\frac{i(M-2r^2)}{2\Delta^{1/2}}r\Psi_2 + i\Delta^{1/2}\partial_r\Psi_2 + \frac{r^2\omega}{\Delta^{1/2}}\Psi_2 = (m + \mu_s)\Psi_1, \quad (2.22)$$

$$-\frac{i(M-2r^2)}{2\Delta^{1/2}}r\Psi_1 + i\Delta^{1/2}\partial_r\Psi_1 + \frac{r^2\omega}{\Delta^{1/2}}\Psi_1 = (m + \mu_s)\Psi_2, \quad (2.23)$$

where we have put $\Delta = -Mr^2 + \frac{r^4}{l^2}$, we have restored the AdS lengthscale l , and in general we follow Chandrasekhar's notation [40]. Defining R_1 , R_2 , and \hat{m} through the relations

$$\Psi_1 = i\Delta^{-1/4}R_1, \quad (2.24)$$

$$\Psi_2 = \Delta^{-1/4}R_2, \quad (2.25)$$

$$m = i\hat{m}, \quad (2.26)$$

we obtain,

$$(\partial_{r_*} - i\omega)R_2 = \frac{i\Delta^{1/2}}{r^2}(\hat{m} - i\mu_s r)R_1, \quad (2.27)$$

$$(\partial_{r_*} + i\omega)R_1 = \frac{i\Delta^{1/2}}{r^2}(\hat{m} + i\mu_s r)R_2. \quad (2.28)$$

Defining now ν , Υ_1 , Υ_2 , and \hat{r}_* through the relations

$$\nu = \arctan\left(\frac{\mu_s r}{\hat{m}}\right), \quad (2.29)$$

$$R_1 = e^{\frac{i\nu}{2}}\Upsilon_1, \quad (2.30)$$

$$R_2 = e^{-\frac{i\nu}{2}}\Upsilon_2, \quad (2.31)$$

$$\hat{r}_* = r_* + \frac{1}{2\omega} \arctan\left(\frac{\mu_s r}{\hat{m}}\right), \quad (2.32)$$

we get

$$(\partial_{\hat{r}_*} - i\omega)\Upsilon_2 = W\Upsilon_1, \quad (2.33)$$

$$(\partial_{\hat{r}_*} + i\omega)\Upsilon_1 = W\Upsilon_2, \quad (2.34)$$

where,

$$W = \frac{i\Delta^{1/2}(\hat{m}^2 + \mu_s^2 r^2)^{3/2}}{r^2(\hat{m}^2 + \mu_s^2 r^2) + \frac{\hat{m}\mu_s\Delta}{2\omega}}. \quad (2.35)$$

Finally, putting $Z_{\pm} = \Upsilon_1 \pm \Upsilon_2$ we have

$$(\partial_{\hat{r}_*}^2 + \omega^2)Z_{\pm} = V_{\pm}Z_{\pm}, \quad (2.36)$$

with

$$V_{\pm} = W^2 \pm \frac{dW}{d\hat{r}_*}. \quad (2.37)$$

We shall be concerned with massless spinors ($\mu_s = 0$) for which $\hat{r}_* = r_*$, and $W = \frac{i\Delta^{1/2}\hat{m}}{r^2}$. Thus,

$$V_{\pm} = \frac{m^2}{r^2}\left(\frac{r^2}{l^2} - M\right) \pm \frac{Mm}{r^2}\left(\frac{r^2}{l^2} - M\right)^{1/2}. \quad (2.38)$$

In the form (2.37) one immediately recognizes that the two potentials V_+ and V_- should yield the same spectrum. In fact they are, in SUSY language, superpartner potentials derived from a superpotential W (see [66]). Once again, we can rescale r and take $l = 1$, by measuring everything in terms of l .

2.3.2 QNMs for Weyl perturbations

Similarly, the wave equation (2.36) for Weyl (until recently also called neutrino) perturbations may be put in the form

$$\partial_{r_*}^2 Z_{\pm} + \left[\omega^2 - m \left(\frac{m}{\cosh(M^{1/2}r_*)^2} \pm M^{1/2} \frac{\sinh(M^{1/2}r_*)^2}{\cosh(M^{1/2}r_*)^2} \right) \right] Z_{\pm} = 0. \quad (2.39)$$

Going to a new independent variable, $x = -\sinh(M^{1/2}r_*)$, $x \in [\infty, 0]$, we can write

$$(1+x^2)Z'' + xZ' + \left[\frac{\omega^2(1+x^2)}{M} - \frac{m^2}{M} \pm \frac{mx}{M^{1/2}} \right] Z = 0. \quad (2.40)$$

By changing the wavefunction Z to χ

$$\chi = e^{\left(\frac{M^{1/2}x-2m}{2M^{1/2}} - \frac{x}{2} \right) \arctan(x)}, \quad (2.41)$$

we have

$$(1+x^2)\chi'' + \left(\frac{2m}{M^{1/2}} + x \right) \chi' + \left(\frac{\omega^2}{M} \right) \chi = 0. \quad (2.42)$$

On putting $s = \frac{1+iz}{2}$, $s \in [\frac{1}{2}, i\infty]$, we have again the hypergeometric equation (2.13), with $a = \frac{i\omega}{M^{1/2}}$, $b = -\frac{i\omega}{M^{1/2}}$, and $c = \frac{1}{2} \pm \frac{im}{M^{1/2}}$, so that the solution to the wave equation is again specified around each singular point, and is given by the analytic continuation of the standard hypergeometric function to the complex plane [63, 208].

Since infinity is located at $s = \frac{1}{2}$, there is no easy way to determine the QNM frequencies, so we have to resort to numerical calculations. If we put (2.35) in the form (2.17) one again sees that it has no essential singularities, so the numerical method just outlined in the previous section may be applied. Moreover, since V_+ and V_- have the same spectrum [66] and the same QNM frequencies [40] we need only to work out the frequencies for one of them. In table 2.3 we present the numerical results for the QNM frequencies for neutrino perturbations and for selected values of the black hole mass.

For large black holes one can see that the imaginary part of the frequencies scale with the horizon ($r_+ = M^{1/2}$), just as in the scalar and electromagnetic case. We have also computed some higher modes, and the real part of the frequency ω_r , does not seem to depend on which mode we are dealing with, just as in the scalar and electromagnetic case.

2.4 Discussion

We have computed the scalar, electromagnetic and neutrino QNM of BTZ black holes. These modes dictate the late time behaviour of the fields. In all cases, these modes scale with the horizon radius, at least for large black holes and, since the decay of the perturbation

Table 2.3: Lowest QNM frequencies for $m = 1$ Weyl perturbations of a non-rotating BTZ black hole.

$m = 1$		
Numerical		
$M^{1/2}$	ω_r	$-\omega_i$
2	0.378	2.174
5	0.316	5.027
10	0.224	10.006
50	0.099	50.001
100	0.071	100.000
500	0.0316	500.000

has a timescale $\tau = \frac{1}{\omega_i}$, this means that the greater the mass, the less time it takes to approach equilibrium. We have also found that for large black holes, the QNM frequencies are proportional to the black hole radius. Since the temperature of a BTZ black is proportional to the black hole radius, the QNM frequencies scale with the temperature, as a simple argument indicates [48]. As we said earlier, it was proved in [53] that the location of the poles of the retarded correlation function of the corresponding perturbations in the dual conformal field theory match the QN frequencies. This leads to a new quantitative realization of the AdS/CFT correspondence.

Can one use this exact expression for the QN frequencies to test the correspondence made by Hod [31] and alluded to earlier, that there should be a relation between the highly damped QN frequencies and the quantum of area of a black hole? Birmingham *et al.* [67] have recently given intriguing hints that one can indeed, and that the answer is positive. They considered the 2+1 dimensional BTZ black hole; They showed that the identification of the fundamental quanta of black hole mass and angular momentum with the real part of the QNM frequencies leads to the correct quantum behaviour of the asymptotic symmetry algebra, and thus of the dual conformal field theory.

Chapter 3

Quasinormal modes of the four dimensional Schwarzschild-AdS black hole

Contents

3.1	Introduction	27
3.2	Scalar, Electromagnetic and Gravitational perturbations in a Schwarzschild AdS background	28
3.3	QNMs and some of its properties	31
3.4	Equations and numerical Method	33
3.5	Numerical results	35
3.6	Discussion of the results	45
3.7	The limit $m \rightarrow 0$	49
3.8	Conclusion	50
3.9	APPENDIX: Pure AdS normal modes for electromagnetic and gravitational perturbations	50

3.1 Introduction

A great deal of effort has been spent to calculate the QNMs and their associated frequencies. New powerful methods, both analytical and numerical have been developed. The main interest in these studies is in the application to the analysis of the data from the gravitational waves to be detected by the forthcoming gravitational wave detectors. We refer the reader to [9] for reviews. In a different context, York [68] tried to explain the thermal quantum radiance of a Schwarzschild black hole in terms of quantum zero-point fluctuations of zero mean in the QNMs. QNMs in asymptotically flat spacetimes have recently acquired a further importance since, as mentioned before, it has been proposed that the Barbero-Immirzi parameter, a factor introduced by hand in order that Loop Quantum Gravity reproduces correctly the black hole entropy, is equal to the real part of the QN frequencies with a large imaginary part [31, 33]

(see [69] for a short review). For further developments in calculating QN frequencies in Kerr spacetimes and in asymptotically flat black holes spacetimes see [34, 35, 70, 71, 43, 72, 73].

All these previous works deal with asymptotically flat spacetimes, but the recent AdS/CFT correspondence conjecture [27] makes the investigation of QNMs in anti-de Sitter spacetimes more appealing. Horowitz and Hubeny [48] began the study of QNMs in AdS, by thoroughly investigating scalar perturbations in 4, 5 and 7 spacetime dimensions. Their work was completed by Konoplya [74], who computed the QN frequencies of small black holes in AdS space, something Horowitz and Hubeny did not consider. By now, the body of work in this field is immense [37, 51, 75, 76, 77, 78, 79, 42].

WE shall now consider the 4-dimensional Schwarzschild-AdS spacetime. The lowest lying modes (i.e., the less damped ones parametrized by the overtone number $n = 0$) for this spacetime were found by Horowitz and Hubeny [48], and completed by Konoplya [74] for the scalar case, and by Cardoso and Lemos [77] and Cardoso, Lemos and Konoplya [78] for the electromagnetic and gravitational case. Recently, Berti and Kokkotas [79] have confirmed all these results and extended them to Reissner-Nordström-AdS black holes. Here, we shall take a step further in carrying on this program by computing numerically, through an extensive search, the high overtone QN frequencies for scalar, electromagnetic and gravitational perturbations in the Schwarzschild-AdS black hole. We shall do an extensive search for the high overtone QN frequencies, ($n \geq 1$). We find that the modes are evenly spaced for frequencies with a large imaginary part. Moreover the scalar, electromagnetic and gravitational perturbations all possess, asymptotically for high overtones n , QN frequencies with the same spacing, and this spacing is l -independent. While we can numerically prove this with great accuracy for large black holes, it remains just a conjecture for small and intermediate black holes. We shall also see that the QN frequencies of the toroidal black hole with non-trivial topology [41] are identical to the QN frequencies of a large Schwarzschild-AdS black hole [42].

Electromagnetic perturbations are of interest due to the AdS/CFT conjecture since they can be seen as perturbations for some generic supergravity gauge field. In addition, the Maxwell field is an important field with different features from scalar or gravitational fields, which makes it worth studying. On the other hand, gravitational perturbations have the additional interest of arising from any other type of perturbation, be it scalar, electromagnetic, Weyl, etc., which in turn disturb the background geometry. Therefore, questions like the stability of spacetime for scalar or other perturbations, have a direct dependence on the stability to gravitational perturbations.

3.2 Scalar, Electromagnetic and Gravitational perturbations in a Schwarzschild AdS background

3.2.1 Maxwell perturbations

The scalar wave equation has already been derived by Horowitz and Hubeny [48] so we shall now focus on the electromagnetic and gravitational case. We consider the evolution of a Maxwell field in a Schwarzschild-anti-de Sitter spacetime with metric given by

$$ds^2 = f(r)dt^2 - \frac{dr^2}{f(r)} - r^2(d\theta^2 + \sin^2\theta d\phi^2), \quad (3.1)$$

where, $f(r) = (\frac{r^2}{R^2} + 1 - \frac{2M}{r})$, R is the AdS radius and M the black hole mass. The evolution is governed by Maxwell's equations:

$$F^{\mu\nu}{}_{;\nu} = 0 \quad , F_{\mu\nu} = A_{\nu,\mu} - A_{\mu,\nu} \quad , \quad (3.2)$$

where a comma stands for ordinary derivative and a semi-colon for covariant derivative. As the background is spherically symmetric, we can expand A_μ in 4-dimensional vector spherical harmonics (see [62]):

$$A_\mu(t, r, \theta, \phi) = \sum_{l,m} \left(\begin{bmatrix} 0 \\ 0 \\ \frac{a^{lm}(t,r)}{\sin\theta} \partial_\phi Y_{lm} \\ -a^{lm}(t,r) \sin\theta \partial_\theta Y_{lm} \end{bmatrix} + \begin{bmatrix} f^{lm}(t,r) Y_{lm} \\ h^{lm}(t,r) Y_{lm} \\ k^{lm}(t,r) \partial_\theta Y_{lm} \\ k^{lm}(t,r) \partial_\phi Y_{lm} \end{bmatrix} \right) \quad , \quad (3.3)$$

where the first term in the right-hand side has parity $(-1)^{l+1}$ and the second term has parity $(-1)^l$, m is the azimuthal number and l the angular quantum number. If we put this expansion into Maxwell's equations (3.2) we get a second order differential equation for the perturbation:

$$\frac{\partial^2 \Psi(r)}{\partial r_*^2} + [\omega^2 - V(r)] \Psi(r) = 0 \quad , \quad (3.4)$$

where the wavefunction $\Psi(r)$ is a linear combination of the functions f^{lm} , h^{lm} , k^{lm} and a^{lm} as appearing in (3.3). Ψ has a different functional dependence according to the parity: for odd parity, i.e. $(-1)^{l+1}$, Ψ is explicitly given by $\Psi = a^{lm}$ whereas for even parity $(-1)^l$ it is given by $\Psi = \frac{r^2}{l(l+1)} \left(-i\omega h^{lm} - \frac{df^{lm}}{dr} \right)$, see [62] for further details. It is assumed that the time dependence is $\Psi(t, r) = e^{-i\omega t} \Psi(r)$. The potential V appearing in equation (3.4) is given by

$$V(r) = f(r) \left[\frac{l(l+1)}{r^2} \right] \quad , \quad (3.5)$$

and the tortoise coordinate r_* is defined as

$$\frac{\partial r}{\partial r_*} = f(r) \quad . \quad (3.6)$$

We can of course rescale r , $r \rightarrow \frac{r}{R}$ and if we do this, the wave equation again takes the form (3.4) with rescaled constants i.e., $r_+ \rightarrow \frac{r_+}{R}$, $\omega \rightarrow \omega R$, where r_+ is the horizon radius. So, we can take $R = 1$ and measure everything in terms of R .

3.2.2 Gravitational perturbations

When dealing with first order gravitational perturbations one supposes that, at least in some restricted region of spacetime, the metric functions can be written as

$$g_{ab}(x^\nu) = g_{ab}^{(0)}(x^\nu) + h_{ab}(x^\nu) \quad , \quad (3.7)$$

where the metric $g_{ab}^{(0)}(x^\nu)$ is the background metric, given by some known solution of Einstein's equations, and $h_{ab}(x^\nu)$ is a small perturbation. Our background metric is a Schwarzschild-anti-de Sitter metric (3.1) and the metric $g_{ab}(x^\nu)$ will follow Einstein's equations in vacuum with a cosmological constant:

$$G_{ab} - \Lambda g_{ab} = 0 \quad . \quad (3.8)$$

Upon substituting (3.7) in (3.8) we will obtain some differential equations for the perturbations. We use the same perturbations as originally given by Regge and Wheeler [38], retaining their notation. After a decomposition in tensorial spherical harmonics (see Zerilli [80] and Mathews [81]), these fall into two distinct classes - odd and even - with parities $(-1)^{l+1}$ and $(-1)^l$ respectively, where l is the angular momentum of the particular mode. While working in general relativity one has some gauge freedom in choosing the elements $h_{ab}(x^\nu)$ and one should take advantage of that freedom in order to simplify the rather lengthy calculations involved in computing (3.8). We shall therefore work with the classical Regge-Wheeler gauge in which the canonical form for the perturbations is (see also [82]):

odd parity:

$$h_{\mu\nu} = \begin{bmatrix} 0 & 0 & 0 & h_0(r) \\ 0 & 0 & 0 & h_1(r) \\ 0 & 0 & 0 & 0 \\ h_0(r) & h_1(r) & 0 & h_0(r) \end{bmatrix} e^{-i\omega t} \left(\sin \theta \frac{\partial}{\partial \theta} \right) P_l(\cos \theta); \quad (3.9)$$

even parity:

$$h_{\mu\nu} = \begin{bmatrix} H_0(r)f(r) & H_1(r) & 0 & 0 \\ H_1(r) & H_2(r)/f(r) & 0 & 0 \\ 0 & 0 & r^2K(r) & 0 \\ 0 & 0 & 0 & r^2K(r) \sin^2 \theta \end{bmatrix} e^{-i\omega t} P_l(\cos \theta). \quad (3.10)$$

Here $P_l(\cos \theta)$ is the Legendre polynomial with angular momentum l . If we put this decomposition into Einstein's equations we get ten coupled second order differential equations that fully describe the perturbations: three equations for odd perturbations and seven for even perturbations. It is however possible to circumvent the task of solving these coupled equations. Regge and Wheeler [38] and Zerilli [39] showed how to combine these ten equations into two second order differential equations, one for each parity. So following Regge and Wheeler [38] we define, for odd parity the wave function $Q(r)$ given by perturbations,

$$Q(r) = \frac{f(r)}{r} h_1(r). \quad (3.11)$$

After some work, Einstein's equations yield

$$\frac{\partial^2 Q}{\partial r_*^2} + [\omega^2 - V_{\text{odd}}(r)] Q = 0, \quad (3.12)$$

where

$$V_{\text{odd}} = f(r) \left[\frac{l(l+1)}{r^2} - \frac{6m}{r^3} \right]. \quad (3.13)$$

Likewise, following Zerilli [39] one can define for even modes the wavefunction $T(r)$ implicitly in terms of H_0 , H_1 and K , through the equations

$$K = \frac{6m^2 + c(1+c)r^2 + m \left(3cr - 3\frac{r^3}{R^2} \right)}{r^2(3m+cr)} T + \frac{dT}{dr_*}, \quad (3.14)$$

$$H_1 = -\frac{i\omega \left(-3m^2 - 3cmr + cr^2 - 3m\frac{r^3}{R^2} \right)}{r(3m+cr)f(r)} T - i\omega \frac{r}{f(r)} \frac{dT}{dr_*}, \quad (3.15)$$

where $c = \frac{1}{2} [l(l+1) - 2]$. Then Einstein's equations for even parity perturbations can be written as

$$\frac{\partial^2 T}{\partial r_*^2} + [\omega^2 - V_{\text{even}}(r)] T = 0, \quad (3.16)$$

with

$$V_{\text{even}} = \frac{2f(r)}{r^3} \frac{9m^3 + 3c^2mr^2 + c^2(1+c)r^3 + 3m^2 \left(3cr + 3\frac{r^3}{R^2}\right)}{(3m+cr)^2}. \quad (3.17)$$

Now, by defining

$$W = \frac{2m}{r^2} + \frac{-3-2c}{3r} + \frac{3c^2 + 2c^2 + 27\frac{m^2}{R^2}}{3c(3m+cr)} + j, \quad (3.18)$$

where $j = -\frac{1}{3} \left(\frac{c}{m} + \frac{c^2}{m} + \frac{9m}{cR^2} \right)$, we obtain

$$V_{\text{odd}} = W^2 + \frac{dW}{dr_*} + \beta, \quad V_{\text{even}} = W^2 - \frac{dW}{dr_*} + \beta, \quad (3.19)$$

where $\beta = -\frac{c^2+2c^3+c^4}{9m^2}$. It is interesting to note that the two potentials, odd and even, can be written in such a simple form, a fact which seems to have been discovered by Chandrasekhar [12]. Potentials related in this manner are sometimes called super-partner potentials [66]). We note that similar equations were obtained by Mellor and Moss [83] for Schwarzschild-de Sitter spacetime, using a different approach.

3.3 QNMs and some of its properties

3.3.1 Analytical properties

To solve equation (3.4) for Maxwell fields and equations (3.12-3.16) for gravitational fields, one must specify boundary conditions. Consider first the case of a Schwarzschild black hole in an asymptotically flat spacetime (see, e.g., [9]). Since in this case the potential vanishes at both infinity and horizon, the two solutions near these points are plane waves of the type $\Psi \sim e^{\pm i\omega r_*}$, where the r_* coordinate in this case ranges from $-\infty$ to ∞ . QNMs are defined by the condition that at the horizon there are only ingoing waves, i.e., $\Psi_{\text{hor}} \sim e^{-i\omega r_*}$. Furthermore, one does not want to have fields coming in from infinity (where the potential in this case vanishes). So, there is only a purely outgoing wave at infinity, i.e., $\Psi_{\infty} \sim e^{i\omega r_*}$. Only a discrete set of complex frequencies ω meet these requirements.

Consider now a Schwarzschild black hole in an asymptotically AdS spacetime. The boundary condition at the horizon is the same, we want that near the horizon $\Psi_{\text{hor}} \sim e^{-i\omega r_*}$. However, r_* has a finite range, so the second boundary condition needs to be modified. There have been several papers discussing which boundary conditions one should impose at infinity in AdS spacetimes ([84, 85, 86]). We shall require energy conservation and thus adopt the reflective boundary conditions at infinity [84]. This means that the wavefunction is zero at infinity. For a different boundary condition see [87].

We now show that the imaginary part of the frequency ω is negative, for waves satisfying these boundary conditions, provided the potential V is positive. The proof proceeds as for

the scalar field perturbation case [48], although there are some steps we think are useful to display explicitly here. Writing ϕ for a generic wavefunction as

$$\phi = e^{i\omega r_*} Z, \quad (3.20)$$

where, Z can be Ψ , Q or T , we find

$$f(r) \frac{\partial^2 \phi}{\partial r^2} + [f' - 2i\omega] \frac{\partial \phi}{\partial r} - \frac{V}{f} \phi = 0, \quad (3.21)$$

where $f = (r^2 + 1 - \frac{2M}{r})$. In the proof, we are going to need the asymptotic behavior of the solutions of equation (3.21). For $r \rightarrow r_+$ we have $f \sim (3r_+ + \frac{1}{r_+})(r - r_+)$ and $\frac{V}{f} \sim C$, where C is a constant which takes different values depending on the case, electromagnetic, odd or even gravitational perturbations. So equation (3.21) becomes, in this limit,

$$Ay \frac{\partial^2 \phi}{\partial y^2} + [A - 2i\omega] \frac{\partial \phi}{\partial y} - C\phi = 0, \quad (3.22)$$

where $y = r - r_+$, and $A = 3r_+ + \frac{1}{r_+}$. This equation has an exact solution in terms of the modified Bessel functions $I_\nu(z)$ [208],

$$\phi = C_1 y^{i\frac{\omega}{A}} I_{-\frac{i\omega}{A}} \left(2 \left(\frac{C}{A} y \right)^{\frac{1}{2}} \right) + C_2 y^{i\frac{\omega}{A}} I_{\frac{i\omega}{A}} \left(2 \left(\frac{C}{A} y \right)^{\frac{1}{2}} \right). \quad (3.23)$$

We want the asymptotic behavior of these functions when $y \rightarrow 0$ which is given by $I_\nu(z) \rightarrow \frac{(\frac{z}{2})^\nu}{\Gamma(\nu+1)}$, $z \rightarrow 0$. So, near the horizon the wavefunction ϕ behaves as

$$\phi_{r_+} = C_1 \frac{\left(\frac{C}{A}\right)^{-\frac{i\omega}{A}}}{\Gamma\left(1 - \frac{2i\omega}{A}\right)} + C_2 \frac{y^{\frac{2i\omega}{A}} \left(\frac{C}{A}\right)^{\frac{i\omega}{A}}}{\Gamma\left(1 + \frac{2i\omega}{A}\right)}. \quad (3.24)$$

We can see that if one wants to rule out outgoing modes at the horizon, we must have $C_2 = 0$, so that ϕ in equation (3.20) does not depend on y . Let's now investigate the asymptotic behavior at infinity. For $r \rightarrow \infty$ we have $\frac{V}{f} \rightarrow \frac{l(l+1)}{r^2}$. Therefore near infinity equation (3.21) becomes

$$r^2 \frac{\partial^2 \phi}{\partial r^2} + [2r - 2i\omega] \frac{\partial \phi}{\partial r} - \frac{l(l+1)}{r^2} \phi = 0. \quad (3.25)$$

Putting $x = \frac{1}{r}$ we have

$$\frac{\partial^2 \phi}{\partial x^2} + 2i\omega \frac{\partial \phi}{\partial x} - l(l+1)\phi = 0, \quad (3.26)$$

with solution $\phi = \phi_\infty$ given by

$$\phi_\infty(x) = A e^{\left[-i\omega + i(\omega^2 - l(l+1))^{1/2}\right]x} + B e^{\left[-i\omega - i(\omega^2 - l(l+1))^{1/2}\right]x} \quad (3.27)$$

Now, $\phi_\infty(x=0) = 0$, therefore $A = -B$, and thus,

$$\phi_\infty(x) = A e^{-i\omega x} \sin \left[(\omega^2 - l(l+1))^{\frac{1}{2}} x \right] \quad (3.28)$$

We can now proceed in the proof. Multiplying equation (3.21) by $\bar{\phi}$ (the complex conjugate of ϕ), and integrating from r_+ to ∞ we obtain

$$\int_{r_+}^{\infty} dr \left[\bar{\phi} \frac{d}{dr} \left(f \frac{d\phi}{dr} \right) - 2i\omega \bar{\phi} \frac{d\phi}{dr} - \frac{V}{f} \bar{\phi} \phi \right] = 0. \quad (3.29)$$

Integrating by parts yields

$$\int_{r_+}^{\infty} dr \left[\frac{d[\bar{\phi} f \frac{d\phi}{dr}]}{dr} - f \left| \frac{d\phi}{dr} \right|^2 - 2i\omega \bar{\phi} \frac{d\phi}{dr} - \frac{V}{f} |\phi|^2 \right] = 0. \quad (3.30)$$

Now, one can show that $[\bar{\phi} f \frac{d\phi}{dr}]_{r_+} = 0$, in order to satisfy the boundary conditions. Indeed, at r_+ , $\phi(r_+) = \text{constant}$ and $f(r_+) = 0$. Now, at infinity, even though $\bar{\phi}(\infty) = 0$, we have also $f(\infty) = \infty$, so we have to show that $[\bar{\phi} f \frac{d\phi}{dr}]_{\infty} = 0$. From equation (3.28) we can check that this is indeed true. Thus, equation (3.30) gives

$$\int_{r_+}^{\infty} dr \left[f \left| \frac{d\phi}{dr} \right|^2 + 2i\omega \bar{\phi} \frac{d\phi}{dr} + \frac{V}{f} |\phi|^2 \right] = 0. \quad (3.31)$$

Taking the imaginary part of (3.31) we have

$$\int_{r_+}^{\infty} dr \left[\omega \bar{\phi} \frac{d\phi}{dr} + \bar{\omega} \phi \frac{d\bar{\phi}}{dr} \right] = 0, \quad (3.32)$$

wich, after an integration by parts reduces to

$$(\omega - \bar{\omega}) \int_{r_+}^{\infty} dr \left[\bar{\phi} \frac{d\phi}{dr} \right] = \bar{\omega} |\phi(r_+)|^2. \quad (3.33)$$

Finally, inserting this back into (3.31) yields

$$\int_{r_+}^{\infty} dr \left[f \left| \frac{d\phi}{dr} \right|^2 + \frac{V}{f} |\phi|^2 \right] = - \frac{|\omega|^2 |\phi(r_+)|^2}{\text{Im } \omega}. \quad (3.34)$$

From this relation, one can infer that, if V is positive definite then $\text{Im } \omega < 0$ necessarily. So, since electromagnetic and even gravitational perturbations have $V > 0$ one always has $\text{Im } \omega < 0$. As for odd gravitational perturbations there are instances where $V < 0$, making this theorem unreliable for these cases. However, for $r_+ < \left[\frac{l(l+1)}{3} - 1 \right]^{\frac{1}{2}}$, i.e., small enough masses, $V > 0$ (see equation (3.13)), and the theorem applies.

Another important point concerns the late time behavior of these fields, and the existence or not of power-law tails. As shown by Ching et al [88], for potentials that vanish exponentially near the horizon, there are no power-law tails, so there will be no such tails in our case.

3.4 Equations and numerical Method

To summarize, the evolution of massless (scalar, electromagnetic and gravitational) fields can be reduced to the following form

$$\frac{\partial^2 \Psi(r)}{\partial r_*^2} + [\omega^2 - V(r)] \Psi(r) = 0, \quad (3.35)$$

where the tortoise coordinate r_* is defined as

$$\frac{\partial r}{\partial r_*} = f(r), \quad (3.36)$$

and the potential V appearing in (3.35) depends on the specific field under consideration. Explicitly, for scalar perturbations [48],

$$V_s = f(r) \left[\frac{l(l+1)}{r^2} + \frac{2M}{r^3} + \frac{2}{R^2} \right], \quad (3.37)$$

while for electromagnetic perturbations the potential is given by (3.5). The gravitational perturbations decompose into two sets the odd and the even parity one. For odd perturbations the potential $V(r)$ in (3.35) is given by (3.13) while for even perturbations it is given by expression (3.17).

In all cases, we denote by l the angular quantum number, that gives the multipolarity of the field. We can of course rescale r , $r \rightarrow \frac{r}{R}$. If we do this, the wave equation takes again the form (3.21) with rescaled constants i.e., $r_+ \rightarrow \frac{r_+}{R}$, $\omega \rightarrow \omega R$, where r_+ is the horizon radius. So, we can take $R = 1$ and measure everything in terms of R , the AdS radius.

Eq. (3.21) should be solved under appropriate boundary conditions, i.e., incoming waves near the horizon,

$$\Psi \sim e^{-i\omega r_*}, \quad r \rightarrow r_+, \quad (3.38)$$

and no waves at infinity,

$$\Psi = 0, \quad r \rightarrow \infty. \quad (3.39)$$

We note that there are other reasonable boundary conditions at infinity, in particular for the gravitational perturbations. For instance, one can define Robin boundary conditions in such a way as to preserve certain dualities between the odd and the even gravitational perturbations. However, it was verified numerically by Moss and Norman [76] that Dirichlet or Robin boundary conditions yield approximately the same result, so we shall keep $\Psi = 0$, $r \rightarrow \infty$. Moreover, Cardoso and Lemos [77] proved (we shall revisit this proof in this chapter) that for high overtone QN frequencies the duality is preserved, so in this regime the distinction is irrelevant. Thus, to compute the QN frequencies ω such that the boundary conditions (3.38) and (3.39) are preserved, we follow the Horowitz-Hubeny approach [48]. Within this approach we need to expand the solution to the wave equation around $x_+ = \frac{1}{r_+}$ ($x = 1/r$),

$$\Psi(x) = \sum_{k=0}^{\infty} a_k(\omega)(x - x_+)^k, \quad (3.40)$$

and to find the roots of the equation $\Psi(x = 0) = 0$. First, one should substitute (3.40) into the wave equation (3.21) in order to obtain a recursion relation for a_k [48]. Then, one has to truncate the sum (3.40) at some large $k = N$ and check that for greater k the roots converge to some true root which is the sought QN frequency. The higher the overtone number, and the smaller the black hole size, the larger the number N at which the roots of the equation $\Psi(x = 0) = 0$ converge. Yet, since in the series (3.40) each next term depends on all the preceding terms through the recursion relations, when N is too large, the tiny numerical errors in the first terms, start growing as $N \sim 10^2 - 10^3$ or greater. As a result the roots

suffer a sharp change for a small change on any of the input parameters, displaying a “noisy” dependence. To avoid this we have to increase the precision of all the input data and the recursion relation we are dealing with from the standard 20-digit precision up to a precision such that further increasing of it will not influence the result for the QN frequency. For small black holes the roots start converging at very large N only, for instance, when $r_+ = 1/20$ we can truncate the series at $N \sim 3 \cdot 10^4$, but not before. Since for finding roots of (3.39) we have to resort to trial and error method, the above procedure consumes much time, but nevertheless allows to compute QNMs of small AdS black holes [74], and to find the higher overtones we are seeking.

3.5 Numerical results

In this section we will present the numerical results obtained using the numerical procedure just outlined in the previous section. The results will be organized into three subsections: scalar, electromagnetic and gravitational perturbations. For each field, we shall also divide the results into three different regimes: large, intermediate and small black holes, since the results depend crucially on the regime one is dealing with. Here a large black hole stands for a black hole with $r_+ \gg 1$, an intermediate black hole is one with $r_+ \sim 1$, and a small black hole has a horizon radius $r_+ \ll 1$. We shall then try to unify these results. For each horizon radius r_+ and angular quantum number l there is an infinity of QN frequencies (or overtones). We shall order them according to the standard procedure, by increasing imaginary part. Accordingly, the fundamental QN frequency is defined as the one having the lowest imaginary part (in absolute value) and will be labeled with the integer $n = 0$. The first overtone has the second lowest imaginary part and is labeled with $n = 1$, and so on. The QN frequencies also have a real part, which in general display an increase along with the imaginary part. To the lowest value of the imaginary part corresponds the lowest value of the real part, to the second lowest value of the imaginary part corresponds the second lowest value of the real part, and so on. Thus n , the overtone number, is also a number that in general increases with the real part of the frequency (or energy) of the mode. This seems to be a characteristic of AdS space only, due to the special boundary conditions associated with this spacetime. This, in a sense, is to be expected since the wave equation to be studied is a Schrödinger type equation, where for quantum non-dissipative bound systems, such as the hydrogen atom or a particle in an infinite well potential, the principal quantum number n (which here has been called the overtone number) appears due to the boundary conditions of the radial equation, a typical eigenvalue problem, and is related directly with the frequency of vibration of the orbital. The similarity is not full, though, since the boundary condition at the black hole is of a different kind. However, for pure AdS spacetimes, when there is no black hole and the boundary conditions are of infinite well type, the overtone number n is indeed a principal quantum number (see Appendix A).

3.5.1 Scalar QN frequencies

The fundamental scalar QN frequencies were first computed by Horowitz and Hubeny [48] for intermediate and large black holes. Konoplya [74] extended these calculations to the case of small black holes. Recently Berti and Kokkotas [79] rederived all these results. Here we do

for the first time an extensive search for higher overtones of scalar perturbations. Some of the lowest lying modes we find are shown in Tables 3.1, 3.2 and 3.3 for large, intermediate and small black holes, respectively.

(i) Large black holes - As proven by Horowitz and Hubeny [48] in the large black hole regime the frequencies must scale as the horizon radius (this can also be proven easily and directly from the differential equation (3.21)). We show in Table 3.1 the results for a spherically symmetric mode ($l = 0$) for a black hole with $r_+ = 100$ which is therefore sufficient to infer the behaviour of all large black holes. The fundamental frequency agrees with previous results [48]. Perhaps the most interesting result in this large black hole regime is that asymptotically for high overtone number n the frequencies become evenly spaced and behave like, for $l = 0$,

$$\frac{\omega_s}{r_+} = (1.299 - 2.25i)n + 1.856 - 2.673i, \quad (n, r_+) \rightarrow \infty. \quad (3.41)$$

Thus the spacing between frequencies is

$$\frac{\omega_{s_{n+1}} - \omega_{s_n}}{r_+} = (1.299 - 2.25i), \quad (n, r_+) \rightarrow \infty. \quad (3.42)$$

Moreover, although the offset $1.856 - 2.673i$ in (3.41) is l -dependent (this number is different for $l = 1$ scalar perturbations for example), this asymptotic behaviour for the spacing (3.42) holds for any value of l . In fact our search of the QN frequencies for higher values of l reveal that the results are very very similar to those in Table 3.1. We have gone up to $l = 4$ for scalar perturbations and the results were quite insensitive to l . The asymptotic behaviour sets in very quickly as one increases the mode number n . Typically for $n = 10$ equation (3.41) already gives a very good approximation. Indeed, for $n = 10$ we find numerically (see Table 1) $\omega_s = 1486.23753 - 2516.90740i$ for a $r_+ = 100$ black hole, while the asymptotic expression gives $\omega_s = 1484.6 - 2517.3i$.

(ii) Intermediate black holes - In Table 3.2 we show some of the lowest lying scalar QN frequencies for an intermediate black hole with $r_+ = 1$. For a black with this size, one finds again that the spacing does not depend on the angular number l for very high overtone number n . With an error of about 2% the limiting value for the frequency is, for $l = 0$,

$$\omega_s \sim (1.97 - 2.35i)n + 2.76 - 2.7i, \quad n \rightarrow \infty. \quad (3.43)$$

For QN frequencies belonging to different l 's the offset in (3.43) is different, but as far as we can tell numerically, not the asymptotic spacing implied by (3.43). Expression (3.43) for the asymptotic behaviour works well again for $n > 10$.

(iii) Small black holes - Our search for the QN frequencies of small black holes, i.e, black holes with $r_+ \ll 1$ revealed what was expected on physical grounds, and was uncovered numerically for the first time in [74] for the fundamental mode: for small black holes, the QN frequencies approach the frequencies of pure AdS spacetime [86] (see also Appendix A). In fact we find

$$\omega_s = 2n + l + 3, \quad r_+ \rightarrow 0. \quad (3.44)$$

In Table 3.3 we show some results for a small black hole with $r_+ = 0.2$. We stress that the values presented in Table 3.3 for the asymptotic spacing between modes may have an error

Table 3.1: QN frequencies corresponding to $l = 0$ scalar perturbations of a large Schwarzschild-AdS BH ($r_+ = 100$). It can be seen that for large n the modes become evenly spaced. Although not shown here, our numerical data indicates that this happens for all values of l and also that the spacing is the same, regardless of the value of l . For $l = 0$ and for high n the QN frequencies go like $\frac{\omega_s}{r_+} = (1.299 - 2.25i)n + 1.856 - 2.673i$. The corresponding spacing between consecutive modes seems to be l -independent.

n	Re $[\omega_{QN}]$:	Im $[\omega_{QN}]$:	n	Re $[\omega_{QN}]$:	Im $[\omega_{QN}]$:
0	184.95344	-266.38560	7	1096.44876	-1841.88813
1	316.14466	-491.64354	8	1226.38317	-2066.89596
2	446.46153	-716.75722	9	1356.31222	-2291.90222
3	576.55983	-941.81253	10	1486.23753	-2516.90740
4	706.57518	-1166.8440	50	6682.78814	-11516.9823
5	836.55136	-1391.8641	299	39030.810	-67542.308
6	966.50635	-1616.8779	300	39160.7272	-67767.3091

Table 3.2: QN frequencies corresponding to $l = 0$ scalar perturbations of an intermediate Schwarzschild-AdS BH ($r_+ = 1$). Asymptotically for large n one finds approximately $\omega_s \sim (1.97 - 2.35i)n + 2.76 - 2.7i$.

n	Re $[\omega_{QN}]$:	Im $[\omega_{QN}]$:	n	Re $[\omega_{QN}]$:	Im $[\omega_{QN}]$:
0	2.7982	-2.6712	10	22.44671	-26.20913
1	4.75849	-5.03757	11	24.41443	-28.55989
2	6.71927	-7.39449	12	26.38230	-30.91059
3	8.46153	-9.74852	13	28.35029	-33.26123
4	10.6467	-12.1012	14	30.31839	-35.61183
5	12.6121	-14.4533	15	32.28658	-37.96238
6	14.5782	-16.8049	16	34.25485	-40.31290
7	16.5449	-19.1562	17	36.22318	-42.66340
8	18.5119	-21.5073	18	38.19157	-45.01387
9	20.4792	-23.8583	19	40.16002	-47.36431

Table 3.3: QN frequencies corresponding to $l = 0$ scalar perturbations of a small Schwarzschild-AdS BH ($r_+ = 0.2$). Asymptotically for large n one finds approximately $\omega_s \sim (1.69 - 0.57i)n + 2.29 - 0.46i$.

n	Re $[\omega_{QN}]$:	Im $[\omega_{QN}]$:	n	Re $[\omega_{QN}]$:	Im $[\omega_{QN}]$:
0	2.47511	-0.38990	6	12.45222	-3.89179
1	4.07086	-0.98966	7	14.14065	-4.46714
2	5.72783	-1.57600	8	15.83026	-5.04186
3	7.40091	-2.15869	9	17.52070	-5.61610
4	9.08118	-2.73809	10	19.21191	-6.18997
5	10.7655	-3.31557	11	20.90359	-6.76355

of about 2%. In fact it is extremely difficult to find very high overtones of small black holes, and so it is hard to give a precise estimate of the value they asymptote to.

In summary, we can say that the QN frequencies tend to be evenly spaced asymptotically as n gets very large, no matter if the black hole is large, intermediate or small. Moreover the spacing between consecutive modes is, as far as we can tell, independent of the angular quantum number l .

3.5.2 Electromagnetic QN frequencies

The fundamental electromagnetic QN frequencies were computed for the first time by Cardoso and Lemos [77]. Recently Berti and Kokkotas [79] have redone the calculation showing excellent agreement. Here we extend the results to higher overtones. Some of the lowest lying electromagnetic frequencies are shown in Tables 3.4-3.8.

(i) Large black holes - As found in [77, 78] large black holes show a somewhat peculiar behaviour: some of the lowest lying modes have pure imaginary frequencies, and these are well described by an analytical formula [77], due to Liu [89]. A surprising aspect unveiled for the first time by the present search is that the number of such modes decreases as the horizon radius becomes smaller, as can be seen from Tables 3.4 and 3.5. In other words, for very large black holes the number of imaginary modes grows. For example, for $r_+ = 1000$ (Table 3.4) there are eight pure imaginary modes, for $r_+ = 100$ there are four such modes (see Table 3.5), and for $r_+ = 10$ there are only two. If one wants to go for r_+ larger than 1000, the computation is very time consuming since we use a trial and error method for finding new modes.

Again, we find that for large black holes and $l = 1$, the frequencies are evenly spaced with

$$\frac{\omega_{\text{em}}}{r_+} = (1.299 - 2.25i)n - 11.501 + 12i, \quad (n, r_+) \rightarrow \infty. \quad (3.45)$$

And a spacing given by

$$\frac{\omega_{\text{em}_{n+1}} - \omega_{\text{em}_n}}{r_+} = (1.299 - 2.25i), \quad (n, r_+) \rightarrow \infty. \quad (3.46)$$

For different values of the angular quantum number l , we find the same spacing (3.46) between consecutive modes, although the offset in (3.45) depends on l . So, asymptotically for large n and large horizon radius the spacing is the same as for the scalar case! This is surprising, specially since the behaviour of the scalar and electromagnetic potentials are radically different. It is even more surprising the fact that this asymptotic behaviour does not depend on l , as the electromagnetic potential is strongly l -dependent. Furthermore from the first electromagnetic overtones one could surely not anticipate this behaviour.

(ii) Intermediate black holes - In Table 3.6 we show some of the lowest lying electromagnetic QN frequencies for an intermediate black hole with $r_+ = 1$. For a black with this size, one finds again that the spacing does not depend on the angular number l for very high overtone number n . With an error of about 2% the limiting value for the frequency is, for $l = 1$,

$$\omega_{\text{em}} \sim (1.96 - 2.36i)n + 1.45 - 2.1i, \quad n \rightarrow \infty. \quad (3.47)$$

Table 3.4: QNMs corresponding to $l = 1$ electromagnetic perturbations of a large Schwarzschild-AdS BH ($r_+ = 1000$). Notice that now there are eight pure imaginary modes, still well described by Liu's formula.

n	Re $[\omega_{QN}]$:	Im $[\omega_{QN}]$:	n	Re $[\omega_{QN}]$:	Im $[\omega_{QN}]$:
0	0	-1500.004789	5	0	-8985.232
1	0	-2999.982599	6	0	-10596.03
2	0	-4500.093600	7	0	-11644.76
3	0	-5999.513176	8	1219.7	-13566.42
4	0	-7502.69385	9	2494.6	-15847.06

Table 3.5: QNMs corresponding to $l = 1$ electromagnetic perturbations of a large Schwarzschild-AdS BH ($r_+ = 100$). The first four modes are pure imaginary and are well described by Liu's approximation [77, 78]. For high n the QN frequencies obey, for $l = 1$, $\frac{\omega_{em}}{r_+} = (1.299 - 2.25i)n - 11.501 + 12i$. The corresponding spacing between consecutive modes seems to be l -independent.

n	Re $[\omega_{QN}]$:	Im $[\omega_{QN}]$:	n	Re $[\omega_{QN}]$:	Im $[\omega_{QN}]$:
0	0	-150.0479	10	799.6171	-2171.826
1	0	-299.8263	11	927.812	-2398.208
2	0	-450.9458	12	1056.153	-2624.438
3	0	-595.3691	13	1184.620	-2850.543
4	22.504	-799.194	14	1313.192	-3076.546
5	162.256	-1035.098	15	1441.856	-3302.464
6	289.028	-1263.537	16	1570.601	-3528.310
7	416.247	-1491.223	17	1699.416	-3754.094
8	543.792	-1718.409	18	1828.295	-3979.824
9	671.598	-1945.246	19	1957.229	-4205.508

Table 3.6: QNMs corresponding to $l = 1$ electromagnetic perturbations of an intermediate Schwarzschild-AdS BH ($r_+ = 1$). Asymptotically for large n the modes become evenly spaced in mode number and behave as $\omega_{em} \sim (1.96 - 2.36i)n + 1.45 - 2.1i$.

n	Re $[\omega_{QN}]$:	Im $[\omega_{QN}]$:	n	Re $[\omega_{QN}]$:	Im $[\omega_{QN}]$:
0	2.163023	-1.699093	10	21.067466	-25.61714
1	3.843819	-4.151936	11	23.015470	-27.98278
2	5.673473	-6.576456	12	24.965381	-30.34713
3	7.553724	-8.980538	13	26.916889	-32.71037
4	9.458385	-11.37238	14	28.869756	-35.07265
5	11.37722	-13.75633	15	30.823790	-37.43413
6	13.30526	-16.13482	16	32.778838	-39.79488
7	15.23974	-18.50933	17	34.734776	-42.15499
8	17.17894	-20.88081	18	36.691500	-44.51455
9	19.12177	-23.24993	19	38.648922	-46.87360

Table 3.7: QNMs corresponding to $l = 1$ electromagnetic perturbations of a small Schwarzschild-AdS BH ($r_+ = 0.2$). Asymptotically for large n one finds approximately $\omega_{\text{em}} \sim (1.68 - 0.59i)n + 1.87 - 0.04i$.

n	Re $[\omega_{QN}]$:	Im $[\omega_{QN}]$:	n	Re $[\omega_{QN}]$:	Im $[\omega_{QN}]$:
0	2.63842	-0.05795	6	12.00066	-3.53148
1	3.99070	-0.47770	7	13.66436	-4.12974
2	5.49193	-1.08951	8	15.33370	-4.72479
3	7.07835	-1.70859	9	17.00715	-5.31725
4	8.70165	-2.32191	10	18.68370	-5.90758
5	10.3450	-2.92920	11	20.36268	-6.49615

Table 3.8: The fundamental ($n = 0$) QNMs corresponding to $l = 1$ electromagnetic perturbations of a small Schwarzschild-AdS BH for several values of r_+ .

r_+	Re $[\omega_{QN}]$:	Im $[\omega_{QN}]$:	r_+	Re $[\omega_{QN}]$:	Im $[\omega_{QN}]$:
1/2	2.25913	-0.65731	1/10	2.85188	-0.00064
1/3	2.40171	-0.29814	1/12	2.88058	-0.00030
1/4	2.53362	-0.13364	1/16	2.91363	-0.00016
1/5	2.63842	-0.05795	1/18	2.92406	-0.00009
1/8	2.80442	-0.00565	1/20	2.93200	-0.00002

We note that here too the offset in (3.47) does depend on l , but not the asymptotic spacing.

(iii) Small black holes - For small black holes, see Tables 3.7 and 3.8, the spacing seems also to be equal as for the scalar case, but since it is very difficult to go very high in mode number n in this regime, the error associated in estimating the asymptotic behaviour is higher, and one cannot be completely sure. Again, the electromagnetic QN frequencies of very small black holes asymptote to the pure AdS electromagnetic modes (see Appendix A, where we sketch their computation). Indeed we find that

$$\omega_{\text{emAdS}} = 2n + l + 2, r_+ \rightarrow 0. \quad (3.48)$$

This can be clearly seen from Table 3.8, where we show the fundamental mode for small black holes of decreasing radius. As the horizon radius gets smaller and smaller, the fundamental frequency approaches the value of $3 + 0i$, which is indeed the correct pure AdS mode for $l = 1$, $n = 0$, electromagnetic perturbations. It was conjectured by Horowitz and Hubeny [48] that for very small black holes in AdS space, the imaginary part of the QN frequency for spherically symmetric perturbations should scale with the horizon area, i.e., with r_+^2 . Their argument was based on a previous result [92] for the absorption cross section for the $l = 0$ component. This conjecture was later verified numerically to be correct by Konoplya [74] for the $l = 0$ case. From Table 3.8 it is however apparent that this scaling is no longer valid for $l = 1$ perturbation, and indeed we find it is not valid for $l \neq 0$ perturbations, be it scalar, electromagnetic or gravitational perturbations. The reason why the imaginary part no longer scales with the horizon area for $l \neq 0$ perturbations is due to the fact that the partial absorption cross section only scales with the horizon area for $l = 0$ perturbations. For other l 's the behaviour is more complex, and it could be that there is no simple scaling, or even

that the behaviour is oscillatory with the mass M of the black hole. We refer the reader to [93] for details on the absorption cross section of black holes.

3.5.3 Gravitational QN frequencies

The fundamental gravitational QN frequencies were computed for the first time by Cardoso and Lemos [77]. We remind that there are two sets of gravitational wave equations, the odd and even ones. Although it was found [77, 78] that there is a family of the odd modes which is very slowly damped and pure imaginary, it was possible to prove that for high frequencies both odd and even perturbations must yield the same QN frequencies. We present the results for higher overtones of odd perturbations in Tables 3.9-3.12, and even perturbations in Tables 3.13-3.16.

3.5.3.a Odd perturbations

(i) Large black holes - As discussed for the first time in [77] these exhibit a pure imaginary fundamental mode (see Table 3.9.). For large black holes, this mode is slowly damped and scales as the inverse of the horizon radius. Our analysis for higher l 's indicates that in the large black hole regime an excellent fit to this fundamental pure imaginary mode is

$$\omega_{\text{odd } n=0} = -\frac{(l-1)(l+2)}{3r_+}i, \quad r_+ \rightarrow \infty. \quad (3.49)$$

This generalizes a previous result by Berti and Kokkotas [79] for the $l = 2$ case. The simplicity of this formula (which is just a fit to our numerical data), leads us to believe it is possible to find an analytical explanation for it, but such explanation is still lacking. In the large black hole regime, asymptotically for high overtones one finds, for $l = 2$ for example,

$$\frac{\omega_{\text{odd}}}{r_+} = (1.299 - 2.25i)n + 0.58 - 0.42i, \quad (n, r_+) \rightarrow \infty. \quad (3.50)$$

This leads to the spacing

$$\frac{\omega_{\text{odd } n+1} - \omega_{\text{odd } n}}{r_+} = (1.299 - 2.25i), \quad (n, r_+) \rightarrow \infty, \quad (3.51)$$

which, as our results indicate is again l -independent. Again, the offset in (3.50) depends on l .

(ii) Intermediate black holes - Results for the odd QN frequencies of an intermediate ($r_+ = 1$) black hole are shown in Table 3.10. With an error of about 5% the limiting value for the frequency is, for $l = 2$,

$$\omega_{\text{odd}} \sim (1.97 - 2.35i)n + 0.93 - 0.32i, \quad n \rightarrow \infty. \quad (3.52)$$

We note that here too the offset in (3.52) does depend on l , but not the asymptotic spacing, with a numerical error of about 5%.

(iii) Small black holes - The behavior for small black holes is shown in Tables 3.11 and 3.12. As the black hole gets smaller, the pure imaginary mode gets more damped: the imaginary

Table 3.9: QNMs corresponding to $l = 2$ odd gravitational perturbations of a large Schwarzschild-AdS BH ($r_+ = 100$). The fundamental QN frequency is pure imaginary and seems to be well described by the formula $\omega_{n=0} = \frac{-(l-1)(l+2)}{3r_+}i$ valid only in the large black hole regime. In the large n limit one finds $\frac{\omega_{\text{odd}}}{r_+} = (1.299 - 2.25i)n + 0.58 - 0.42i$. The corresponding spacing between consecutive modes seems to be l -independent.

n	Re $[\omega_{QN}]$:	Im $[\omega_{QN}]$:	n	Re $[\omega_{QN}]$:	Im $[\omega_{QN}]$:
0	0	- 0.013255	6	836.55392	-1391.86345
1	184.95898	- 266.38403	7	966.50872	-1616.87735
2	316.14887	- 491.64242	8	1096.45098	-1841.88755
3	446.46505	- 716.75629	9	1226.38527	-2066.89540
4	576.56293	- 941.81172	10	1356.31422	-2291.90170
5	706.57797	- 1166.8433	50	6552.87704	-11291.9807

Table 3.10: QNMs corresponding to $l = 2$ odd gravitational perturbations of an intermediate Schwarzschild-AdS BH ($r_+ = 1$). Asymptotically for large n one finds approximately $\omega_{\text{odd}} \sim (1.97 - 2.35i)n + 0.93 - 0.32i$.

n	Re $[\omega_{QN}]$:	Im $[\omega_{QN}]$:	n	Re $[\omega_{QN}]$:	Im $[\omega_{QN}]$:
0	0	-2	10	20.604949	-23.803860
1	3.033114	-2.404234	11	22.567854	-26.157246
2	4.960729	-4.898194	12	24.531429	-28.510214
3	6.905358	-7.289727	13	26.495564	-30.862849
4	8.854700	-9.660424	14	28.460169	-33.215214
5	10.80784	-12.02344	15	30.425175	-35.567355
6	12.76384	-14.38266	16	32.390524	-37.919308
7	14.72199	-16.73969	17	34.356173	-40.271103
8	16.68179	-19.09530	18	36.322082	-42.622761
9	18.64286	-21.44994	19	38.288221	-44.974301

part increases, as can be seen from Table 3.12, where we show the two lowest QN frequencies for small black holes with decreasing radius. As mentioned by Berti and Kokkotas [79] the ordering of the modes here should be different. However, since one can clearly distinguish this pure imaginary mode as belonging to a special family, we shall continue to label it with $n = 0$. We have not been able to follow this mode for black holes with $r_+ < 0.5$, and so Table 3.12 does not show any pure imaginary modes for horizon radius smaller than 0.5. We note that, as for the scalar and electromagnetic cases, here too the modes are evenly spaced, with a spacing which seems to be independent of l no matter if the black hole is large or small. For very small black holes, the frequencies reduce to their pure AdS values, computed in Appendix A, to wit

$$\omega_{\text{odd}} = 2n + l + 2, \quad r_+ \rightarrow 0. \quad (3.53)$$

One can see this more clearly from Table 3.12, where in fact for very small black holes the frequency rapidly approaches (3.53). Again, for small black holes, the imaginary part does not scale with the horizon area, by the reasons explained before.

In conclusion, the higher overtones of odd perturbations follow a pattern very similar to

Table 3.11: QNMs corresponding to $l = 2$ odd gravitational perturbations of a small Schwarzschild-AdS BH ($r_+ = 0.2$). Asymptotically for large n one finds approximately $\omega_{\text{odd}} \sim (1.69 - 0.59i)n + 2.49 + 0.06i$.

n	Re $[\omega_{QN}]$:	Im $[\omega_{QN}]$:	n	Re $[\omega_{QN}]$:	Im $[\omega_{QN}]$:
0	2.404	-3.033	6	12.67161	-3.43609
1	4.91594	-0.30408	7	14.33020	-4.05366
2	6.30329	-0.89773	8	15.99881	-4.66448
3	7.82330	-1.53726	9	17.67433	-5.26955
4	9.40720	-2.17744	10	19.35465	-5.86978
5	11.0279	-2.81083	11	21.03839	-6.46596

Table 3.12: The fundamental ($n = 0$) QNMs corresponding to $l = 2$ odd gravitational perturbations of a small Schwarzschild-AdS BH for several values of r_+ .

r_+	Re $[\omega_{QN}]$:	Im $[\omega_{QN}]$:	r_+	Re $[\omega_{QN}]$:	Im $[\omega_{QN}]$:
0.8 ($n = 0$)	0	-3.045373	0.5 ($n = 1$)	3.03759	-0.71818
0.8 ($n = 1$)	2.89739	-1.69556	0.4	3.16209	-0.43092
0.7 ($n = 0$)	0	-3.83538	0.3	3.35487	-0.17320
0.7 ($n = 1$)	2.90665	-1.34656	0.2	3.62697	-0.01792
0.6 ($n = 0$)	0	-4.901973	0.1	3.84839	-0.00005
0.6 ($n = 1$)	2.95550	-1.02196	1/15	3.90328	-0.00001
0.5 ($n = 0$)	0	-6.40000	1/20	3.92882	-0.00002

the scalar case. We note that the asymptotic behaviour sets in very quickly, much like what happened for scalar and electromagnetic perturbations. Typically the formulas yielding the asymptotic behaviour work quite well for $n > 10$. We are now able to prove that for sufficiently high frequencies the scalar and gravitational perturbations are isospectral, a mystery that remained in [77], This is done in section below.

3.5.3.b Even perturbations

Let us now briefly discuss the even modes. As found previously [77, 78] these modes behave very similar to the scalar ones. Yet, the even gravitational modes are stipulated by a more complicated potential, and we have to truncate the series in power of $x - x_+$ at larger N , which makes the whole procedure be more time consuming. That is why when considering small black holes we were restricted only by first seven modes in that case. It is, however, sufficient to see that even gravitational QNMs, similar to other kind of perturbations, tend to arrange into equidistant spectrum under the increasing of n . We show in Tables 3.13-3.16 the numerical results for the QN frequencies of even gravitational perturbations.

(i) **Large black holes** - Results for the QN frequencies of large black holes are shown in Table 3.13. In this regime one finds for $l = 2$ even perturbations

$$\frac{\omega_{\text{even}}}{r_+} = (1.299 - 2.25i)n + 1.88 - 2.66i, \quad (n, r_+) \rightarrow \infty, \quad (3.54)$$

Table 3.13: QNMs corresponding to $l = 2$ even gravitational perturbations of a large Schwarzschild-AdS BH ($r_+ = 100$). For large n , one finds $\frac{\omega_{\text{even}}}{r_+} = (1.299 - 2.25i)n + 0.58 - 0.42i$. The corresponding spacing between consecutive modes seems to be l -independent.

n	Re $[\omega_{QN}]$:	Im $[\omega_{QN}]$:	n	Re $[\omega_{QN}]$:	Im $[\omega_{QN}]$:
0	184.97400	-266.351393	6	966.609780	-1616.695872
1	316.17838	-491.584999	7	1096.56635	-1841.681256
2	446.50884	-716.674054	8	1226.51495	-2066.664293
3	576.62103	-941.70468	9	1356.45821	-2291.645761
4	706.65039	-1166.71147	10	1486.39776	-2516.626168
5	836.64066	-1391.70679	50	6683.51993	-11515.70869

Table 3.14: QNMs corresponding to $l = 2$ even gravitational perturbations of an intermediate Schwarzschild-AdS BH ($r_+ = 1$). Asymptotically for large n one finds approximately $\omega_{\text{even}} \sim (1.96 - 2.35i)n + 2.01 - 1.5i$.

n	Re $[\omega_{QN}]$:	Im $[\omega_{QN}]$:	n	Re $[\omega_{QN}]$:	Im $[\omega_{QN}]$:
0	3.017795	-1.583879	10	21.68949	-24.98271
1	4.559333	-3.810220	11	23.64402	-27.33549
2	6.318337	-6.146587	12	25.60052	-29.68799
3	8.168524	-8.500194	13	27.55860	-32.04026
4	10.061220	-10.85631	14	29.51796	-34.39234
5	11.976813	-13.21224	15	31.47838	-36.74424
6	13.906140	-15.56749	16	33.43969	-39.09600
7	15.844371	-17.92208	17	35.40174	-41.44762
8	17.788721	-20.27609	18	37.36444	-43.79914
9	19.737469	-22.62960	19	39.32769	-46.15057

leading to the spacing

$$\frac{\omega_{\text{even } n+1} - \omega_{\text{even } n}}{r_+} = (1.299 - 2.25i), \quad (n, r_+) \rightarrow \infty, \quad (3.55)$$

which once more turns out to be l -independent! All the results concerning the spacing of frequencies for large black holes have a very good precision, since in this regime it is possible to go very far out in overtone number (typically $n = 300$ is enough to achieve a 0.1% accuracy for the spacing).

(ii) Intermediate black holes - In Table 3.14 we show some of the lowest lying even gravitational QN frequencies for an intermediate black hole with $r_+ = 1$. For a black with this size, one finds again that the spacing does not seem to depend on the angular number l for very high overtone number n . With an error of about 5% the limiting value for the frequency is, for $l = 2$,

$$\omega_{\text{even}} \sim (1.96 - 2.35i)n + 2.01 - 1.5i, \quad n \rightarrow \infty. \quad (3.56)$$

We note that here too the offset in (3.47) does depend on l , but not the asymptotic spacing.

(iii) Small black holes - The behavior for small black holes is shown in Tables 3.15 and 3.16. Our search for the QN frequencies of small black holes, i.e, black holes with $r_+ \ll 1$ revealed

Table 3.15: QNMs corresponding to $l = 2$ even gravitational perturbations of a small Schwarzschild-AdS BH ($r_+ = 0.2$). Asymptotically for large n one finds approximately $\omega_{\text{even}} \sim (1.61 - 0.6i)n + 2.7 + 0.37i$.

n	Re $[\omega_{QN}]$:	Im $[\omega_{QN}]$:	n	Re $[\omega_{QN}]$:	Im $[\omega_{QN}]$:
0	3.56571	-0.01432	3	7.65872	-1.42994
1	4.83170	-0.26470	4	9.20424	-2.04345
2	6.17832	-0.82063	5	10.78800	-2.65360

Table 3.16: The fundamental ($n = 0$) QNMs corresponding to $l = 2$ even gravitational perturbations of a small Schwarzschild-AdS BH for several values of r_+ .

r_+	Re $[\omega_{QN}]$:	Im $[\omega_{QN}]$:	r_+	Re $[\omega_{QN}]$:	Im $[\omega_{QN}]$:
0.8	2.91541	-1.18894	0.3	3.29299	-0.14103
0.7	2.90591	-0.98953	0.2	3.56571	-0.01432
0.6	2.92854	-0.78438	0.1	3.80611	-0.00005
0.5	2.98985	-0.57089	1/15	3.8735	-0.00001
0.4	3.10317	-0.35043	1/20	3.90852	-0.000002

again what was expected on physical grounds: for small black holes, the QN frequencies approach the frequencies of pure AdS spacetime (see Appendix A). In fact we find

$$\omega_{\text{evenAdS}} = 2n + l + 2, r_+ \rightarrow 0. \quad (3.57)$$

In Table 3.15 we show the lowest lying QN frequencies for a small black hole ($r_+ = 0.2$). We stress that the values presented in Table 3.15 (as a matter of fact, all the Tables containing data for small black holes) for the asymptotic spacing between modes may have an error of about 2%. In fact it is extremely difficult to find very high overtones of small black holes, and so it is hard to give a precise estimate of the value they asymptote to. In Table 3.16 we show some the fundamental even QN frequencies for small black holes of decreasing radius, and one can clearly see how the fundamental frequency approaches the pure AdS value given in Appendix A.

3.6 Discussion of the results

3.6.1 On the isospectrality breaking between odd and even perturbations

As is well known [40, 12] in the case of a Schwarzschild black hole in an asymptotically flat space the two potentials V_{even} and V_{odd} give rise to the same QN frequencies (in fact to the same absolute value of the reflection and transmission coefficients). This remarkable property followed from a special relation (the equivalent for asymptotically flat spacetimes of our equation (3.19)) between the potentials and the behavior of W at the boundaries. However, as one can see in the previous tables there is a isospectrality breaking between odd and even perturbations in Schwarzschild anti-de Sitter spacetime.

We shall now treat this problem. The breaking of the isospectrality is intimately related to the behavior of W at infinity. On taking advantage of the machinery developed by Chandrasekhar, we seek a relation between odd and even perturbations of the form

$$Q = p_1 T + q_1 \frac{dT}{dr_*}, \quad (3.58)$$

$$T = p_2 Q + q_2 \frac{dQ}{dr_*}, \quad (3.59)$$

yielding (see [40] for details), $q_1^2 = \frac{1}{\beta - \omega^2}$, $p_1 = qW$, $p_2 = -p_1$ and $q_2 = q_1 = q$. Thus, we obtain

$$Q = qWT + q \frac{dT}{dr_*}, \quad (3.60)$$

$$T = -qWQ + q \frac{dQ}{dr_*}. \quad (3.61)$$

Suppose now that ω is a QNM frequency of T , i.e., one for which

$$T \rightarrow A_{\text{even}} e^{-i\omega r_*}, \quad r \rightarrow r_+, \quad (3.62)$$

$$T \rightarrow 0, \quad r \rightarrow \infty. \quad (3.63)$$

Substituting this into equation (3.61) we see that

$$Q \rightarrow A_{\text{even}} q [W(r_+) - i\omega] e^{-i\omega r_*}, \quad r \rightarrow r_+, \quad (3.64)$$

$$Q \rightarrow q \left(\frac{dQ}{dr_*} \right)_{r=\infty}, \quad r \rightarrow \infty. \quad (3.65)$$

However, from equation (3.28), $\left(\frac{dT}{dr_*} \right)_{r=\infty}$ is in general not zero so that ω will in general fail to be a QNM frequency for Q . Should Q and T be smooth functions of ω , one expects that if q is “almost zero” then ω should “almost” be a QNM frequency for Q . Now, the condition that q is almost zero is that $\beta - \omega^2$ be very large, and one expects this to be true either when ω is very large or else when β is very large. And in fact, as one can see in tables 3, 4 and 5 for very large ω the frequencies are indeed almost identical. On the other hand, for very small black holes (β very large) one expects the frequencies to be exactly the same, since both potentials have the same asymptotic behavior in this regime, as we shall see in the next section. One would be tempted to account for the remarkable resemblances between QNM frequencies of scalar and gravitational perturbations by a similar approach, but the proof is still eluding us. Should such an approach work, it could be of great importance not only to this specific problem, but also to the more general problem of finding the asymptotic distribution of eigenvalues, by studying a different potential with (asymptotically) the same eigenvalues, but more easy to handle.

3.6.2 Why are the scalar and gravitational perturbations isospectral in the large black hole regime?

In the previous subsection, we have showed why the odd and even gravitational perturbations yield the same QN frequencies for large frequencies. The whole approach was based on the fact

that the odd and even gravitational potentials are superpartner potentials [66], i.e., they are related to one another via $V_{\text{odd}} = W^2 + \frac{dW}{dr_*} + \beta$, $V_{\text{even}} = W^2 - \frac{dW}{dr_*} + \beta$, where $\beta = -\frac{\alpha^2 + 2\alpha^3 + \alpha^4}{9M^2}$. The function W is $W = \frac{2M}{r^2} + \frac{-3-2\alpha}{3r} + \frac{3\alpha^2 + 2\alpha^2 + 27M^2}{3\alpha(3M + \alpha r)} - \frac{1}{3} \left(\frac{\alpha}{M} + \frac{\alpha^2}{M} + \frac{9M}{\alpha} \right)$. For more details we refer the reader to [77]. We shall now see that a similar method can be applied to show that in the large black hole regime, scalar and gravitational perturbations are isospectral for large QN frequencies. To begin with, we note that the potentials $V1$ and $V2$ defined by

$$V1 = \tilde{f} \left(\frac{2}{R^2} + \frac{2M}{r^3} \right), \quad (3.66)$$

and

$$V2 = \tilde{f} \left(\frac{a}{r^2} - \frac{6M}{r^3} \right), \quad (3.67)$$

with $\tilde{f} = \frac{r^2}{R^2} + \frac{a}{2} - \frac{2M}{r}$, and a any constant, are superpartner potentials. The superpotential \tilde{W} is in this case is given by

$$\tilde{W} = \frac{r}{R^2} + \frac{a}{2r} - \frac{2M}{r^2}. \quad (3.68)$$

Thus, the two superpartner potentials $V1$ and $V2$ can be expressed in terms of \tilde{W} as

$$V1 = \tilde{W}^2 + \frac{d\tilde{W}}{dr_*}, \quad V2 = \tilde{W}^2 - \frac{d\tilde{W}}{dr_*}. \quad (3.69)$$

Why are these two potentials of any interest? Because in the large r_+ limit, which we shall take to be $r_+ \gg a$, we have $\tilde{f} \sim r^2 - \frac{2M}{r}$. Notice now that in this large r_+ limit the scalar potential (3.37) is $V_s \sim f(2 + \frac{2M}{r^3})$, with $f \sim r^2 - \frac{2M}{r}$, since in this limit and with $r_+ \gg l$, one has $\frac{l(l+1)}{r^2} \ll 2$. Thus, $V1$ reduces to the scalar potential and $V2$ to the gravitational odd potential, provided we take $a = l(l+1)$. It then follows from the analysis in [77] (section IIIC, which is repeated in the previous subsection) that for large black holes these two potentials should yield the same frequencies.

3.6.3 Future directions

The preceding sections have shown that the QNMs of Schwarzschild-AdS black holes have a universal behavior in the asymptotic regime of high overtones. This was verified explicitly and with great accuracy for the large black hole regime, where we showed numerically that the spacing does not depend on the perturbation in question and is equal to

$$\frac{\omega_{n+1} - \omega_n}{r_+} = (1.299 - 2.25i), \quad (n, r_+) \rightarrow \infty. \quad (3.70)$$

We conjecture that the asymptotic behavior is the same for all kinds of perturbations irrespectively of the black hole size, i.e., a fixed horizon radius r_+ Schwarzschild-AdS black hole will have an asymptotic spacing between consecutive QN frequencies which is the same for scalar, electromagnetic and gravitational perturbations. The difficulty in extracting very high overtones for small black holes however, prevents us from having an irrefutable numerical proof of this. It would be extremely valuable to have some kind of analytical scheme for extracting the asymptotic behavior, much as has been done for the asymptotically flat space by Motl

and Neitzke [34, 35]. However it looks quite difficult to make any analytical approximation in asymptotically AdS spaces, although there have been some attempts at this recently (see for example Musiri and Siopsis [75]). We also note that the spacing (3.70) was already found to be true by Berti and Kokkotas [79] for the scalar and gravitational cases for the lowest radiatable multipole, i.e. $l = 0$ and $l = 2$ scalar and gravitational perturbations respectively. We have concluded that, surprisingly, the spacing (3.70) also works for electromagnetic case and for any value of l . It was observed that, despite having such different potentials the scalar, the electromagnetic and gravitational QN frequencies have the same asymptotic behavior. Can one formulate some very general conditions the potentials should obey in order to have the same asymptotic solutions? This is still an open question.

There has been recently an exciting development trying to relate the asymptotic QN frequencies with the Barbero-Immirzi parameter [33, 69]. In fact it was observed, in the Schwarzschild case, that asymptotically for high overtones, the real part of the QN frequencies was a constant, l -independent, and using some (not very clear yet) correspondence between classical and quantum states, was just the right constant to make Loop Quantum Gravity give the correct result for the black hole entropy. Of course it is only natural to ask whether such kind of numerical coincidence holds for other spacetimes. We have seen that apparently we are facing, in AdS space, a universal behavior, i.e., the asymptotic QN frequencies do not depend on the kind of perturbations, and also don't depend on l . However, and in contrast with asymptotically flat space, the real part of the asymptotic QN frequency is not a constant, but rather increases linearly with the mode number n . This is no reason to throw off the initial motivation of seeking some kind of relation between Loop Quantum Gravity and QNMs, after all, there are no predictions for AdS space.

Finally we point out that the asymptotic behavior studied here for the Schwarzschild-AdS black hole will hold also for other black holes in asymptotically AdS. One example of these is the black hole with non-trivial topology [41]. The general line element for this spacetime is [41]:

$$ds^2 = f(r) dt^2 - f(r)^{-1} dr^2 - r^2 (d\theta^2 + d\phi^2) \quad (3.71)$$

where

$$f(r) = \frac{r^2}{R^2} - \frac{4MR}{r}, \quad (3.72)$$

where M is the ADM mass of the black hole, and R is the AdS radius. There is a horizon at $r_+ = (4M)^{1/3}R$. The range of the coordinates θ and ϕ dictates the topology of the black hole spacetime. For a black hole with toroidal topology, a toroidal black hole, the coordinate θ ranges from 0 to 2π , and ϕ ranges from 0 to 2π as well. For the cylindrical black hole, or black string, the coordinate θ has range $-\infty < R\theta < \infty$, and $0 \leq \phi < 2\pi$. For the planar black hole, or black membrane, the coordinate ϕ is further decompactified $-\infty < R\phi < \infty$ [41]. The fundamental QN frequencies for these black holes were computed in [42], where it was verified that they follow the same pattern as for Schwarzschild-AdS black holes. Indeed one easily sees that in the large black hole regime they both should yield the same results as the potentials are equal in this regime (compare the potentials in [42] with the ones in the present work). In particular the asymptotic behavior will be the same.

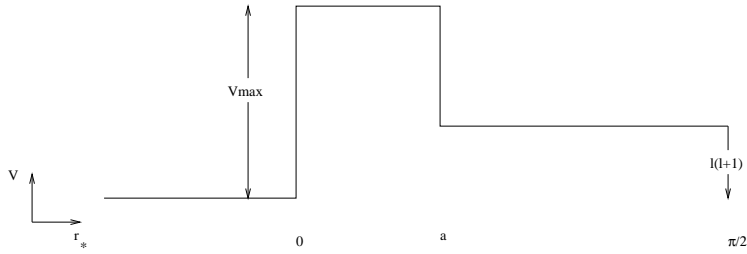


Figure 3.1: The potential for small black holes. $V_{\max} = \frac{4l(l+1)}{27r_+^2}$ and $a \sim 3r_+$.

3.7 The limit $m \rightarrow 0$

Although it is not possible to solve exactly for the QNM frequencies, it is possible to gain some analytical insight in the special case of very small black holes. There has been some discussion about this regime (see [48, 91] and references therein). Here we shall exploit the behavior of QN frequencies in this regime a little further. For very small black holes one can easily see that both potentials (electromagnetic and gravitational) look like, in the r_* coordinate, a barrier with unequal heights:

It is trivial to obtain equations for the QN frequencies in this limit. If Ψ is a general wavefunction then

$$\frac{d\Psi/dr_*}{\Psi} = -i\omega, \quad r_* < 0, \quad (3.73)$$

$$\frac{d\Psi/dr_*}{\Psi} = \frac{ik_1 B e^{ik_1 r_*} - ik_1 C e^{-ik_1 r_*}}{B e^{ik_1 r_*} + C e^{-ik_1 r_*}}, \quad 0 < r_* < a, \quad (3.74)$$

$$\frac{d\Psi/dr_*}{\Psi} = \frac{ik D e^{ik r_*} - ik_1 E e^{-ik r_*}}{D e^{ik r_*} + E e^{-ik r_*}}, \quad r_* > a, \quad (3.75)$$

where $k_1 = (\omega^2 - V_{\max})^{1/2}$, and $k = [\omega^2 - l(l+1)]^{1/2}$. Imposing the continuity of the logarithmic derivative and furthermore that $\Psi = 0$ at infinity ($r_* = \frac{\pi}{2}$), we get

$$k_1 \left[\frac{\frac{k_1 - \omega}{k_1 + \omega} e^{2ik_1 a} - 1}{\frac{k_1 - \omega}{k_1 + \omega} e^{2ik_1 a} + 1} \right] = k \left[\frac{e^{2ik(\frac{\pi}{2} - a)} + 1}{1 - e^{2ik(\frac{\pi}{2} - a)}} \right]. \quad (3.76)$$

In the limit $a \rightarrow 0$, $k_1 \rightarrow \infty$ ($m \rightarrow 0$) we have, supposing that ω stays small, the condition $e^{2ik\frac{\pi}{2}} = 1$ which means that

$$\omega_0^2 = 4n^2 + l(l+1), \quad n = 1, 2, \dots, \quad (3.77)$$

corresponding to a bound state. This gives for the lowest QNM frequencies ($n = 1$): $\omega_0 = 2.45$ for $l = 1$ and $\omega_0 = 3.16$ for $l = 2$. The above are to be compared with those in Tables 1-5. The agreement seems excellent, and we can now go a step further : If we linearize (3.76) around the solution (3.77), i.e, if we write $\omega = \omega_0 + i\delta$ and substitute back in (3.76) we obtain, to third order in δ , the values listed in Table 3.17 .

We have chosen a typical value of $a \sim \frac{3}{h}$, but we can see that, although the real part does not depend very much on a , the imaginary part is strongly sensitive to a . Nevertheless, one can be sure that whatever value of a , the imaginary part goes as $\frac{1}{h^2}$ and is always negative. This question is by now settled, with the numerical work of Konoplya [74]. The imaginary part does indeed go as r_+^2 for scalar perturbations, and for scalar perturbations only.

Table 3.17: The linearized frequency δ for selected values of the angular quantum number l and the potential width a .

	$a = 3/h$	$a = 6/h$
1	δ	δ
1	$-2.1/h - i(1.42/h^2)$	$-1.92/h - i(0.05/h^2)$
2	$-0.859/h - i(0.04/h^2)$	$-0.85/h - i(1.4 \times 10^{-4}/h^2)$

3.8 Conclusion

We have done an extensive search for higher overtones n of the QNMs of Schwarzschild-AdS BH corresponding to scalar, electromagnetic, and gravitational perturbations. We have shown that: (i) No matter what the size of the black hole is, the QN frequencies are evenly spaced, both in the real and in the imaginary component, for high overtone number n ; (ii) The spacing between consecutive modes is independent of the perturbation. This means that scalar, electromagnetic and gravitational perturbations all have, asymptotically, the same spacing between modes. This is one of the major findings in this work, together with the fact that this spacing seems to be also independent of the angular quantum number l ; (iii) We were able to prove that the scalar and gravitational QN frequencies must asymptotically be the same; (iv) The electromagnetic QN frequencies of large black holes have a number of first overtones with pure imaginary parts, and the higher the black hole radius r_+ , the higher the number of these first pure damped, non-oscillating modes; (v) Finally, we have computed analytically the electromagnetic and gravitational pure AdS modes, and we have shown numerically that the QN frequencies of very small black holes asymptote to these pure AdS modes;

3.9 APPENDIX: Pure AdS normal modes for electromagnetic and gravitational perturbations

In this appendix we shall briefly outline how to compute the pure modes of AdS space (no black hole, $M = 0$) for electromagnetic and gravitational perturbations. The scalar case was dealt with by Burgess and Lutken [86]. In pure AdS space the electromagnetic and gravitational potentials (both odd and even) are

$$V = \left(\frac{r^2}{R^2} + 1 \right) \frac{l(l+1)}{r^2}, \quad (3.78)$$

as can be seen by substituting $M = 0$ in (3.5)-(3.17). Also in this case the relation $r(r_*)$ takes the simple form

$$r = R \tan \frac{r_*}{R}, \quad (3.79)$$

and therefore the potential (3.78) takes a simple form in the r_* coordinate, namely

$$V = \frac{l(l+1)}{R^2 \sin\left(\frac{r_*}{R}\right)^2}. \quad (3.80)$$

To proceed, we note that the change of variable $x = \sin\left(\frac{r_*}{R}\right)^2$ leads the wave equation to a hypergeometric equation,

$$\frac{\partial^2 \Psi(x)}{\partial x^2} + \frac{\tilde{\tau}}{\sigma} \frac{\partial \Psi(x)}{\partial x} + \frac{\tilde{\sigma}}{\sigma^2} \Psi(x) = 0, \quad (3.81)$$

with

$$\tilde{\sigma} = 4(\omega R)^2 x(1-x) - 4l(l+1)(1-x), \quad (3.82)$$

$$\sigma = 4x(1-x), \quad (3.83)$$

$$\tilde{\tau} = 2(1-2x). \quad (3.84)$$

To put this in a more standard form, one changes wavefunction by defining

$$\Psi(x) = \sqrt{x-1} x^{\frac{l+1}{2}} Z(x), \quad (3.85)$$

and one gets the following standard hypergeometric differential equation for Z :

$$\sigma \frac{\partial^2 Z(x)}{\partial x^2} + \tau \frac{\partial Z(x)}{\partial x} + \lambda Z(x) = 0, \quad (3.86)$$

with σ defined in (3.83) and

$$\tau = 6 - 4l(x-1) - 12x, \quad (3.87)$$

$$\lambda = -4 - 4l - l^2 + \omega^2. \quad (3.88)$$

By requiring well behaved fields everywhere a simple analysis [63] then shows that the following constraint needs to be satisfied,

$$\omega R = 2n + l + 2. \quad (3.89)$$

These are the pure AdS frequencies for electromagnetic and gravitational perturbations, corresponding to pure AdS normal modes of the corresponding fields. One can compare the frequencies in (3.89) with the scalar frequencies corresponding to pure AdS modes [86], $\omega_s R = 2n + l + 3$.

Chapter 4

Quasinormal modes of the four dimensional toroidal (AdS) black hole

Contents

4.1	Introduction	53
4.2	Scalar, electromagnetic and gravitational perturbations in a toroidal, cylindrical or planar black hole in an AdS background	54
4.3	Quasi-normal modes and some of its properties	59
4.4	Conclusions	62

4.1 Introduction

Black holes in anti-de Sitter (AdS) spacetimes in several dimensions have recently been the object of an intense study. One of the reasons for this intense study is the AdS/CFT conjecture which states that there is a correspondence between string theory in AdS spacetime and a conformal field theory (CFT) on the boundary of that space. For instance, M-theory on $\text{AdS}_4 \times S^7$ is dual to a non-abelian superconformal field theory in three dimensions, and type IIB superstring theory on $\text{AdS}_5 \times S^5$ seems to be equivalent to a super Yang-Mills theory in four dimensions [27] (for a review see [28]).

All dimensions up to eleven are of interest in superstring theory, but experiment singles out four dimensions as the most important. In four-dimensional (4D) general relativity, an effective gravity theory in an appropriate string theory limit, the Kerr-Newman family of four-dimensional black holes can be extended to include a negative cosmological constant [94]. The horizon in this family has the topology of a sphere. There are, however, other families of black holes in general relativity with a negative cosmological constant with horizons having topology different from spherical. Here we want to focus on the family of black holes whose horizon has toroidal, cylindrical or planar topology [41]. We are going to perturb these black holes with scalar, electromagnetic and gravitational fields.

Perturbations of known solutions are very important to perform in order to study their intrinsic properties, such as the natural frequencies of the perturbations, and to test for the

stability of the solutions themselves. For gravitational objects, such as a black hole, the vibrational pattern set by the perturbation obliges the system to emit gravitational waves. Thus, for black holes, the study of perturbations is closely linked to the gravitational wave emission. Due to the dissipative character of the emission of the gravitational waves the vibrational modes do not form a normal set, indeed in the spectrum each frequency is complex whose imaginary part gives the damping timescale. These modes are called quasi-normal modes (QNMs). The QNMs of a black hole appear naturally when one deals with the evolution of some field in the black hole spacetime, and serve as a probe to the dynamics outside its event horizon.

In this chapter we shall study scalar, electromagnetic and gravitational perturbations of the toroidal, cylindrical or planar black holes in an AdS spacetime found in [41]. The motivation to perturb with a scalar field can be seen as follows. If one has, e.g., 11-dimensional M-theory, compactified into a (toroidal BH)₄ × (compact space) the scalar field used to perturb the black hole, can be seen as a type IIB dilaton which couples to a CFT field operator \mathcal{O} . Now, the black hole in the bulk corresponds to a thermal state in the boundary CFT, and thus the bulk scalar perturbation corresponds to a thermal perturbation with nonzero $\langle \mathcal{O} \rangle$ in the CFT. Similar arguments hold for the electromagnetic perturbations since they can be seen as perturbations for some generic gauge field in the low energy limit of 11-dimensional M-theory. On the other hand, gravitational perturbations are always of importance since they belong to the essence of the spacetime itself.

We will find that the QN frequencies for scalar perturbations scale with the horizon radius, at least for large black holes. In the case of electromagnetic perturbations of large black holes, the characteristic QN frequencies have only an imaginary part, and scale with the horizon radius. As for gravitational perturbations, there are two important features. First, contrary to the asymptotically flat spacetime case, odd and even perturbations no longer have the same spectra, although in certain limits one can still prove that the frequencies are almost the same. The second result is that, for odd perturbations, there is a mode with a totally different behavior from that found in the scalar and electromagnetic case: in this mode the frequency scales with $\frac{1}{r_+}$, just as in asymptotically flat Schwarzschild spacetime. These features were also found in our study of Schwarzschild-AdS black holes in the previous chapters. One could have predicted that these features would also appear here, at least for large black holes, because in the large horizon limit the spherical-AdS black holes have the geometry of the cylindrical (planar or toroidal) ones.

4.2 Scalar, electromagnetic and gravitational perturbations in a toroidal, cylindrical or planar black hole in an AdS background

Throughout this paper, we shall deal with the evolution of some perturbation in a spacetime geometry in general relativity with a background metric given by [41]:

$$ds^2 = f(r) dt^2 - f(r)^{-1} dr^2 - r^2 dz^2 - r^2 d\phi^2 \tag{4.1}$$

where

$$f(r) = \frac{r^2}{R^2} - \frac{4MR}{r}, \quad (4.2)$$

M is the ADM mass of the black hole, and R is the AdS lengthscale $R^2 = -\frac{3}{\Lambda}$, Λ being the cosmological constant. There is a horizon at $r_+ = (4M)^{1/3}R$. The range of the coordinates z and ϕ dictates the topology of the black hole spacetime. For a black hole with toroidal topology, a toroidal black hole, the coordinate z is compactified such that z/R ranges from 0 to 2π , and ϕ ranges from 0 to 2π as well. For the cylindrical black hole, or black string, the coordinate z has range $-\infty < z < \infty$, and $0 \leq \phi < 2\pi$. For the planar black hole, or black membrane, the coordinate ϕ is further decompactified $-\infty < R\phi < \infty$ [41]. We will work with the cylindrical topology but the results are not altered for the other two topologies.

According to the AdS/CFT correspondence solution (4.1) ($\times S^7$) is dual to a superconformal field theory in three dimensions with $\mathcal{N} = 8$. These toroidal black holes with Ricci flat horizon we are considering in (4.1) can be seen as the large horizon radius limit, $r_+/R \gg 1$, of the spherical AdS black holes. The large black holes are the ones that matter most to the AdS/CFT correspondence [27]. Perturbations of spherical black holes were studied in the previous chapter. Therefore the results we obtain here should be similar to the results we have obtained in [77] for large black holes. This will be confirmed below. For small black holes we will show that the spherical and toroidal yield different results.

4.2.1 Scalar field perturbations

For scalar perturbations, we are interested in solutions to the minimally coupled scalar wave equation

$$\Phi;^\mu{}_{;\mu} = 0, \quad (4.3)$$

where, a comma stands for ordinary derivative and a semi-colon stands for covariant derivative. We make the following ansatz for the field Φ

$$\Phi = \frac{1}{r} P(r) e^{-i\omega t} e^{ikz} e^{il\phi}, \quad (4.4)$$

where ω , k , and l , are the frequency, the wavenumber and the angular quantum numbers of the perturbation. If one is dealing with the toroidal topology then k should be changed into an angular quantum number \bar{l} , $e^{ikz} \rightarrow e^{i\bar{l}\frac{z}{R}}$. For the planar topology $e^{il\phi} \rightarrow e^{i\bar{k}R\phi}$, where \bar{k} is now a continuous wave number.

It is useful to use the tortoise coordinate r_* defined by the equation $dr_* = dr / (r^2/R^2 - 4MR/r)$. With the ansatz (4.4) and the tortoise coordinate r_* , equation (4.3) is given by,

$$\frac{d^2 P(r)}{dr_*^2} + [\omega^2 - V_{\text{scalar}}(r)] P(r) = 0, \quad (4.5)$$

where,

$$V_{\text{scalar}}(r) = f \left(\frac{l^2}{r^2} + \frac{R^2 k^2}{r^2} + \frac{f'}{r} \right), \quad (4.6)$$

with $r = r(r_*)$ given implicitly and $f' \equiv df/dr$. The rescaling to the radial coordinate $\hat{r} = \frac{r}{R}$ and to the frequency $\hat{\omega} = \omega R$ is equivalent to take $R = 1$ in (4.5) and (4.6), i.e., through this rescaling one measures the frequency and other quantities in terms of the AdS lengthscale R .

4.2.2 Maxwell field perturbations

We consider the evolution of a Maxwell field in a cylindrical-AdS black hole spacetime with a metric given by (4.1). The evolution is governed by Maxwell's equations:

$$F^{\mu\nu}{}_{;\nu} = 0, \quad F_{\mu\nu} = A_{\nu,\mu} - A_{\mu,\nu}. \quad (4.7)$$

One can again separate variables by the ansatz:

$$A_\mu(t, r, \phi, z) = \begin{bmatrix} g^{kl}(r) \\ h^{kl}(r) \\ k^{kl}(r) \\ j^{kl}(r) \end{bmatrix} e^{-i\omega t} e^{ikz} e^{il\phi}, \quad (4.8)$$

When we put this expansion into Maxwell's equations (4.7) we get the 2nd order differential equation for the perturbation:

$$\frac{\partial^2 \Psi(r)}{\partial r_*^2} + [\omega^2 - V_{\text{maxwell}}(r)] \Psi(r) = 0, \quad (4.9)$$

where the wavefunction Ψ is a combination of the functions g^{lm} , h^{lm} , k^{lm} and j^{lm} as appearing in (4.8), and $\Psi = -i\omega h^{lm} - \frac{dg^{lm}}{dr}$ (see [62] for further details). The potential $V_{\text{maxwell}}(r)$ appearing in equation (4.9) is given by

$$V_{\text{maxwell}}(r) = f(r) \left(\frac{l^2}{r^2} + \frac{R^2 k^2}{r^2} \right). \quad (4.10)$$

Again we can take $R = 1$ and measure everything in terms of R .

4.2.3 Gravitational perturbations

In our analysis of gravitational perturbations, we shall adopt a procedure analogous to that of Chandrasekhar [40], generalizing the calculation by the introduction of the cosmological constant $\Lambda = -\frac{3}{R^2}$. The perturbed metric will be taken to be

$$ds^2 = e^{2\nu} dt^2 - e^{2\psi} (d\phi - w dt - q_2 dr - q_3 dz)^2 - e^{2\mu_2} dr^2 - e^{2\mu_3} dz^2. \quad (4.11)$$

where the unperturbed quantities are $e^{2\nu} = \frac{r^2}{R^2} - \frac{4MR}{r}$, $e^{2\psi} = r^2$, $e^{2\mu_2} = \left(\frac{r^2}{R^2} - \frac{4MR}{r}\right)^{-1}$, $e^{2\mu_3} = \frac{r^2}{R^2}$ and all the other unperturbed quantities are zero. By observing the effect of performing $\phi \rightarrow -\phi$, and maintaining the nomenclature of the spherical symmetric case [40], it can be seen that the perturbations fall into two distinct classes: the odd perturbations (also called axial in the spherical case) which are the quantities w , q_2 , and q_3 , and the even perturbations (also called polar in the spherical case) which are small increments $\delta\nu$, $\delta\mu_2$, $\delta\mu_3$ and $\delta\psi$ of the functions ν , μ_2 , μ_3 and ψ , respectively. Note that since z is also an ignorable coordinate, one could, in principle, interchange ϕ with z in the above argument.

In what follows, we shall limit ourselves to axially symmetric perturbations, i.e., to the case in which the quantities listed above do not depend on ϕ . In this case odd and even perturbations decouple, and it is possible to simplify them considerably.

4.2.3.a Odd perturbations

We will deal with odd perturbations first. As we have stated, these are characterized by the non vanishing of w , q_2 and q_3 . The equations governing these quantities are the following Einstein's equations with a cosmological constant

$$G_{12} + \frac{3}{R^2}g_{12} = 0, \quad (4.12)$$

$$G_{23} + \frac{3}{R^2}g_{23} = 0. \quad (4.13)$$

The reduction of these two equations to a one dimensional second order differential equation is well known (see [40]), and we only state the results. By defining

$$Z^-(r) = r \left(\frac{r^2}{R^2} - \frac{4MR}{r} \right) \left(\frac{dq_2}{dz} - \frac{dq_3}{dr} \right), \quad (4.14)$$

One can easily check that $Z^-(r)$ satisfies

$$\frac{\partial^2 Z^-(r)}{\partial r_*^2} + [\omega^2 - V_{\text{odd}}(r)] Z^-(r) = 0, \quad (4.15)$$

where $V_{\text{odd}}(r)$ appearing in equation (4.15) is given by

$$V_{\text{odd}}(r) = f(r) \left(\frac{R^2 k^2}{r^2} - \frac{12MR}{r^3} \right). \quad (4.16)$$

4.2.3.b Even perturbations

Even perturbations are characterized by non-vanishing increments in the metric functions ν , μ_2 , μ_3 and ψ . The equations which they obey are obtained by linearizing $G_{01} + \frac{3}{R^2}g_{01}$, $G_{03} + \frac{3}{R^2}g_{03}$, $G_{13} + \frac{3}{R^2}g_{13}$, $G_{11} + \frac{3}{R^2}g_{11}$ and $G_{22} + \frac{3}{R^2}g_{22}$ about their unperturbed values. Making the ansatz

$$\delta\nu = N(r)e^{ikz}, \quad (4.17)$$

$$\delta\mu_2 = L(r)e^{ikz}, \quad (4.18)$$

$$\delta\mu_3 = T(r)e^{ikz}, \quad (4.19)$$

$$\delta\psi = V(r)e^{ikz}, \quad (4.20)$$

we have from $\delta(G_{03} + \frac{3}{R^2}g_{03}) = 0$ that

$$V(r) = -L(r). \quad (4.21)$$

Inserting this relation and using (4.20) in $\delta(G_{01} + \frac{3}{R^2}g_{01}) = 0$, we have

$$\left(\frac{3}{r} - \frac{f'}{2f} \right) L(r) + \left(\frac{f'}{2f} - \frac{1}{r} \right) T(r) + L(r)_{,r} - T(r)_{,r} = 0. \quad (4.22)$$

From $\delta(G_{13} + \frac{3}{R^2}g_{13}) = 0$ we have

$$\left(\frac{1}{r} + \frac{f'}{2f}\right) L(r) + \left(\frac{1}{r} - \frac{f'}{2f}\right) N(r) - N(r)_{,r} + L(r)_{,r} = 0, \quad (4.23)$$

and from $\delta(G_{11} + \frac{3}{R^2}g_{11}) = 0$ we obtain

$$\begin{aligned} & -\frac{k^2 R^2}{f r^2} N(r) + \left(\frac{k^2 R^2}{f r^2} - \frac{\omega^2}{f^2} - \frac{6}{f}\right) L(r) + \frac{\omega^2}{f^2} T(r) + \\ & \left(\frac{1}{r} + \frac{1}{Rr}\right) N(r)_{,r} + \left(-\frac{f'}{2f} - \frac{1}{Rr}\right) L(r)_{,r} + \left(\frac{f'}{2f} + \frac{1}{r}\right) T(r)_{,r} = 0. \end{aligned} \quad (4.24)$$

Multiplying equation (4.23) by $\frac{2}{r}$ and adding (4.24) we can obtain $N(r)$ and $N(r)_{,r}$ in terms of $L(r)$, $L(r)_{,r}$, $T(r)$ and $T(r)_{,r}$. Using (4.22) and (4.23) we can express $L(r)$, $N(r)$, and up to their second derivatives in terms of $T(r)$, $T(r)_{,r}$ and $T(r)_{,rr}$. Finally, we can look for a function

$$Z^+ = a(r)T(r) + b(r)L(r). \quad (4.25)$$

which satisfies the second order differential equation

$$\frac{\partial^2 Z^+(r)}{\partial r_*^2} + [\omega^2 - V_{\text{even}}(r)] Z^+(r) = 0, \quad (4.26)$$

Substituting (4.25) into (4.26) and expressing $L(r)$ and its derivatives in terms of $T(r)$ and its derivatives, we obtain an equation in $T(r)$, $T(r)_{,r}$ and $T(r)_{,rr}$ whose coefficients must vanish identically. If we now demand that $a(r)$ and $b(r)$ do not depend on the frequency ω we find

$$a(r) = \frac{r}{12Mr + k^2 r^2}, \quad (4.27)$$

$$b(r) = \frac{6M + k^2 r}{72M^2 + 6k^2 Mr}, \quad (4.28)$$

and the potential $V_{\text{even}}(r)$ in (4.26) is

$$V_{\text{even}}(r) = f(r) \left[\frac{576M^3 + 12k^4 Mr^2 + k^6 r^3 + 144M^2 r(k^2 + 2r^2)}{r^3(12M + k^2 r)^2} \right]. \quad (4.29)$$

As a final remark concerning the wave equations obeyed by odd and even gravitational perturbations, we note that it can easily be checked that the two potentials can be expressed in the form

$$V_{\text{even}}^{\text{odd}} = W^2 \pm \frac{dW}{dr_*} + \beta, \quad (4.30)$$

$$W = \frac{96M^2(k^2 + 3r^2)}{2k^2 r^2(12M + k^2 r)} + j, \quad (4.31)$$

where $j = -\frac{k^6 + 288M^2}{24k^2 M}$, and $\beta = -\frac{k^8}{576M^2}$. It is worth of notice that the two potentials can be written in such a simple form (potentials related in this manner are sometimes called superpartner potentials [66]), a fact which seems to have been discovered by Chandrasekhar [12].

Table 4.1: Lowest QN frequencies of scalar perturbations for $l = 0$ and $k = 0$ of the topologically non-trivial black hole [41].

Numerical		
r_+	$-\omega_i$	ω_r
0.1	0.266	0.185
1	2.664	1.849
5	13.319	9.247
10	26.638	18.494
50	133.192	92.471
100	266.373	184.942

4.3 Quasi-normal modes and some of its properties

4.3.0.c Boundary conditions

To solve (4.5), (4.9), (4.15) and (4.26) one must specify boundary conditions, a non-trivial task in AdS spacetimes. Consider first the case of a Schwarzschild black hole in an asymptotically flat spacetime (see [9]). Since the potential now vanishes at both infinity and the horizon, two independent solutions near these points are $\Psi_1 \sim e^{-i\omega r_*}$ and $\Psi_2 \sim e^{i\omega r_*}$, where the r_* coordinate now ranges from $-\infty$ to ∞ . QNMs are defined by the condition that at the horizon there are only ingoing waves, $\Psi_{\text{hor}} \sim e^{-i\omega r_*}$. Furthermore, one wishes to have nothing coming in from infinity (where the potential now vanishes), so one wants a purely outgoing wave at infinity, $\Psi_{\text{infinity}} \sim e^{i\omega r_*}$. Clearly, only a discrete set of frequencies ω meet these requirements.

Consider now our asymptotically AdS spacetime. The first boundary condition stands as it is, so we want that near the horizon $\Psi_{\text{hor}} \sim e^{-i\omega r_*}$. However r_* has a finite range, so the second boundary condition needs to be changed. There have been a number of papers on which boundary conditions to impose at infinity in AdS spacetimes ([84]-[86]). We shall require energy conservation and adopt reflective boundary conditions at infinity [84] which means that the wavefunction is zero at infinity (see however [87]).

4.3.1 Numerical calculation of the QN frequencies

To find the frequencies ω that satisfy the previously stated boundary conditions we follow exactly the same method as outlined in the previous chapter. We shall dwell on this no further.

We present the results in tables 4.1-4.4.

4.3.1.a Scalar:

In table 4.1 we list the numerical values of the lowest ($n = 1$) QN frequencies for the $l = 0$ scalar field and for selected values of r_+ . As discussed in Horowitz and Hubeny (HH) [48] the frequency should be a function of the scales of the problem, R and r_+ . However, they showed and argued that due to additional symmetries in the scalar field case and for large Schwarzschild-AdS black holes the frequency scales as $\omega \propto T$, with the temperature of the

Table 4.2: Lowest QN frequencies of electromagnetic perturbations for $l = 1$ and $k = 0$ of the topologically non-trivial black hole [41].

r_+	Numerical		Highly Damped	
	$-\omega_i$	ω_r	$-\omega_i$	ω_r
0.1	0.104	1.033	–	–
1	1.709	1.336	–	–
5	7.982	~ 0	7.500	~ 0
10	15.220	~ 0	15.000	~ 0
50	75.043	~ 0	75.000	~ 0
100	150.021	~ 0	150.000	~ 0

large black hole given by $T \propto r_+/R^2$, i.e., $\propto r_+$ in our units. This behavior is a totally different behavior from that of asymptotically flat space, in which the frequency scales with $\frac{1}{r_+}$. Now, for cylindrical (planar or toroidal) black holes and scalar fields this symmetry is present for any horizon radius, so $\omega \propto r_+$ always. For these black holes the temperature is also proportional to r_+ , no matter how small the black hole is [41, 96]. Thus, the scalar field QN frequencies are proportional to T , as can be directly seen from table 4.1, $\omega \propto r_+ \propto T$. The imaginary part of the frequency determines how damped the mode is, and according to the AdS/CFT conjecture is a measure of the characteristic time $\tau = \frac{1}{\omega_i}$ of approach to thermal equilibrium in the dual CFT (moreover, the frequencies do not seem to depend on the angular quantum number l , we have performed calculations for higher values of l). In the dual CFT the approach to thermal equilibrium is therefore faster for higher temperatures, i.e., larger black holes. This scaling for all horizon radii with temperature only happens in the scalar field case. For the electromagnetic and some of the gravitational perturbations the frequency scales with the temperature only in the large black hole regime, as we will show.

In table 4.2 we list the numerical values of the lowest ($n = 1$) QN frequencies for $l = 1$ and for selected values of r_+ . For frequencies with no real part, we list the values obtained in the “highly damped approximation” [89, 97]. We can note from table 4.2 that ω is proportional to r_+ and thus to the temperature for large black holes, $r_+ \gtrsim 5$, say.

4.3.1.b Electromagnetic:

In the large black hole regime, both scalar and electromagnetic QN frequencies for this geometry are very similar to those of the Schwarzschild-anti-de Sitter black hole [48, 77, 78]. This is a consequence of the fact that in this regime, the wave equation for the fields become identical in both geometries. Indeed we can compare table 4.1 for the scalar field with table 1 of HH [48] for the same field. We see that for $r_+ = 1$ one has for the toroidal black hole $\omega = 1.849 - 2.664i$, whereas HH find $\omega = 2.798 - 2.671i$. Thus they differ, $r_+ = 1$ is not a large black hole. For $r_+ \gg 1$ one expects to find very similar QN frequencies. For instance, for $r_+ = 100$ we obtain $\omega = 184.942 - 266.373i$ for the toroidal black hole, while HH obtain $\omega = 184.953 - 266.385i$ for the Schwarzschild-anti de Sitter black hole. The same thing happens for electromagnetic perturbations. We can compare table 4.2 for the electromagnetic field with table I of Cardoso and Lemos [77]. For large black holes one can see that the frequencies for toroidal black holes are very similar to the frequencies of the Schwarzschild-

Table 4.3: Lowest and second lowest QN frequencies of gravitational odd perturbations for $k = 2$ of the topologically non-trivial black hole [41].

	lowest QNM		second lowest QNM	
r_+	$-\omega_i$	ω_r	$-\omega_i$	ω_r
1	2.646	~ 0	2.047	2.216
5	0.2703	~ 0	13.288	9.355
10	0.13378	~ 0	26.623	18.549
50	0.02667	~ 0	133.189	92.482
100	0.0134	~ 0	266.384	184.948

Table 4.4: Lowest QN frequencies of gravitational even perturbations for $k = 2$ of the topologically non-trivial black hole [41].

	lowest QNM, $k = 2$	
r_+	$-\omega_i$	ω_r
1	1.552	2.305
5	12.633	9.624
10	26.296	18.696
50	133.124	92.512
100	266.351	184.963

anti-de Sitter black hole. For instance, for $r_+ = 100$ we find $\omega = -150.021i$ for the toroidal black hole, while in [77] we found $\omega = -150.048i$ for the Schwarzschild-anti-de Sitter black hole. We can also see that the QN frequencies in the electromagnetic case are in excellent agreement with the analytical approximation for strongly damped modes.

4.3.1.c Gravitational:

The numerical calculation of the QN frequencies for gravitational perturbations proceeds as outlined previously (the associated differential equation has only regular singularities, so it is possible to use an expansion such as that given in the previous chapter. In tables 4.3 and 4.4 we show the two lowest lying ($n = 1, 2$) QN frequencies for $l = 2$ and $l = 3$ gravitational perturbations.

We first note that there is clearly a distinction between odd and even perturbations: they no longer have the same spectra, contrary to the asymptotically flat space case (see [40]). This problem was studied in some detail by Cardoso and Lemos [77] (the derivation was given in the previous chapter) who showed that it is connected with the behavior of W (see equation (4.31)) at infinity. For odd gravitational QNMs the lowest one scales with $\frac{1}{r_+} \propto \frac{1}{T}$. This is odd, but one can see that it is a reflection of the different behavior of the potential V_{odd} for odd perturbations. For the second lowest odd gravitational QN frequency table 4.3 shows that for large black holes it scales with T . For the lowest even gravitational QN frequency table 4.4 shows that it also scales with T for large black holes. Note further that the scalar, odd second lowest and even gravitational QNMs are very similar in the large black hole regime. Indeed, tables 4.1, 4.3 and 4.4 show a remarkable resemblance even though the potentials are so different. Finally, let us compare tables 4.3 and 4.4 with tables III-V of [77]. We see that

for large black holes the frequencies of toroidal black holes are again very similar to those of the Schwarzschild-anti-de Sitter black hole. For instance, for odd perturbations and $r_+ = 100$ we find from table 3 $\omega = -0.0134i$ for the toroidal black hole, while in [77] we found (table III) $\omega = -0.0132i$ for the Schwarzschild-anti-de Sitter black hole.

4.4 Conclusions

We have computed the scalar, electromagnetic and gravitational QN frequencies of the toroidal, cylindrical or planar black hole in four dimensions. These modes dictate the late time behaviour of a minimally coupled scalar, electromagnetic field and of small gravitational perturbations, respectively. The main conclusion to be drawn from this work is that these black holes are stable with respect to small perturbations. In fact, as one can see, the frequencies all have a negative imaginary part, which means that these perturbations will decay exponentially with time. For odd gravitational perturbations in the large black hole regime, the imaginary part of the frequency goes to zero scaling with $\frac{1}{r_+}$, just as in asymptotically flat space and in the odd gravitational perturbations of Schwarzschild-AdS black hole. In terms of the AdS/CFT correspondence, this implies that the greater the mass, the more time it takes to approach equilibrium, a somewhat puzzling result. Apart from this interesting result, the frequencies all scale with the horizon radius, at least in the large black hole regime, supporting the arguments given in [48]. The QNM for toroidal, cylindrical or planar black holes (in anti-de Sitter space) are quite similar to those of the Schwarzschild-anti-de Sitter black hole [48, 77]. As for the highly damped modes, and as was seen in the previous chapter, we expect them to coincide with those of the Schwarzschild-anti-de Sitter black hole.

Chapter 5

Quasinormal modes of the near extremal four dimensional Schwarzschild-dS black hole

Contents

5.1	Introduction	63
5.2	Equations	64
5.3	Conclusions	67

5.1 Introduction

As we remarked earlier the QNMs have acquired a different importance recently. Following an observation by Hod [31], it has been proposed [33, 70] that the Barbero-Immirzi parameter [98], a factor introduced by hand in order that Loop Quantum Gravity reproduces correctly the black hole entropy, is equal to the real part of the QN frequencies with a large imaginary part. The identification came from what first seemed to be a numerical coincidence, but which has been proved to be exact for Schwarzschild black holes by Motl [34] and Motl and Neitzke [35], assuming the gauge group of the theory to be $SO(3)$.

It is now important to see whether the agreement works only for Schwarzschild black holes, or if it continues to be true in different spacetimes. Anti-de Sitter spacetimes have been tested and it seems, although it is still too early to claim something, that there is a chance of getting a relation between QN frequencies and quantization [67, 37]. It has been conjectured by Kunstatter [70], using Dreyer's [33] arguments that the real part of the QN frequency corresponding to highly damped modes of higher dimensional Schwarzschild black holes should have a particular form [70]. This conjecture has very recently been confirmed by Birmingham [73], following earlier work on quasinormal modes for this spacetime [99, 15]. One of the important black hole spacetimes that has been resisting is the Kerr black hole, which we shall study in the next section, and the Schwarzschild-de Sitter black hole.

We shall take a step further on carrying on this program by computing analytically the QN frequencies of the near extremal Schwarzschild-de Sitter black hole, which is the spacetime for

which the black hole horizon and the cosmological horizon are close to each other, in a manner to be defined later. Sometimes the extreme Schwarzschild-dS black hole is labelled as Nariai black hole. However, we remark that the true Nariai solution is significantly different from the Schwarzschild-dS black hole: it is not a black hole solution, and has a rather different topology. The Nariai solution solves exactly the Einstein equations with $\Lambda > 0$, without or with a Maxwell field, and has been discovered by Nariai in 1951 [100]. It is the direct topological product of $dS_2 \times S^2$, i.e., of a (1+1)-dimensional dS spacetime with a round 2-sphere of fixed radius. Three decades after Nariai's paper, Ginsparg and Perry [101] connected the Nariai solution with the Schwarzschild-dS solution. They showed that the Nariai solution can be generated from a near-extreme dS black hole, through an appropriate non-trivial limiting procedure in which the black hole horizon approaches the cosmological horizon. One of the aims of Ginsparg and Perry was to study the quantum stability of the Nariai and the Schwarzschild-dS solutions [101]. It was shown that the Nariai solution is in general unstable and, once created, decays through a quantum tunnelling process into a slightly non-extreme Schwarzschild-dS black hole (for a complete review and references on this subject see, e.g., Bousso [102] and Dias and Lemos [103]).

For this spacetime, we find that it is possible to solve the field equations exactly in terms of hypergeometric functions, and therefore an exact analytical expression for the QN frequencies of scalar, electromagnetic and gravitational perturbations is also possible. In particular this will give us the QN frequencies with very large imaginary part. We demonstrate why an approach by Moss and Norman [76] based on fitting the potential to the Pöschl-Teller potential works well in the Schwarzschild-de Sitter spacetime. This chapter will follow the work in [106]. This work has been generalized to higher dimensions in [107] and improved to second order in [108]. Very recently, Yoshida and Futamase [111] have taken a completely numerical look at this problem, and solved numerically for the highly damped QNMs. Their conclusion is that while the results we shall present are correct for the low lying QN frequencies, they do not describe the highly damped modes. This means that our results are not correct to all orders in perturbation theory, although they certainly are correct up to second order, as was demonstrated in [108]. For other works related to QNMs in the Schwarzschild-de Sitter spacetime see [109, 110].

5.2 Equations

Our notation will follow that of [104] which we have found convenient. The metric of the Schwarzschild-de Sitter (SdS) spacetime is given by

$$ds^2 = -f dt^2 + f^{-1} dr^2 + r^2(d\theta^2 + \sin^2\theta d\phi^2), \quad (5.1)$$

where

$$f = 1 - \frac{2M}{r} - \frac{r^2}{a^2}, \quad (5.2)$$

with M denoting the black-hole mass, and a^2 is given in terms of the cosmological constant Λ by $a^2 = 3/\Lambda$. The spacetime possesses two horizons: the black-hole horizon is at $r = r_b$ and the cosmological horizon is at $r = r_c$, where $r_c > r_b$. The function f has zeroes at r_b , r_c , and $r_0 = -(r_b + r_c)$. In terms of these quantities, f can be expressed as

$$f = \frac{1}{a^2 r} (r - r_b)(r_c - r)(r - r_0). \quad (5.3)$$

It is useful to regard r_b and r_c as the two fundamental parameters of the SdS spacetime, and to express M and a^2 as functions of these variables. The appropriate relations are

$$a^2 = r_b^2 + r_b r_c + r_c^2 \quad (5.4)$$

and

$$2Ma^2 = r_b r_c (r_b + r_c). \quad (5.5)$$

We also introduce the surface gravity κ_b associated with the black hole horizon $r = r_b$, as defined by the relation $\kappa_b = \frac{1}{2} df/dr_{r=r_b}$. Explicitly, we have

$$\kappa_b = \frac{(r_c - r_b)(r_b - r_0)}{2a^2 r_b}. \quad (5.6)$$

After a Fourier decomposition in frequencies and a multipole expansion, the scalar, electromagnetic and gravitational perturbations all obey a wave equation of the form [37, 77, 42]

$$\frac{\partial^2 \phi(\omega, r)}{\partial r_*^2} + [\omega^2 - V(r)] \phi(\omega, r) = 0, \quad (5.7)$$

where the tortoise coordinate is given by

$$r_* \equiv \int f^{-1} dr, \quad (5.8)$$

and the potential V depends on the kind of field under consideration. Explicitly, for scalar perturbations

$$V_s = f \left[\frac{l(l+1)}{r^2} + \frac{2M}{r^3} - \frac{2}{a^2} \right], \quad (5.9)$$

while for electromagnetic perturbations

$$V_{\text{el}} = f \left[\frac{l(l+1)}{r^2} \right]. \quad (5.10)$$

The gravitational perturbations decompose into two sets [77], the odd and the even parity one. We find however that for this spacetime, they both yield the same QN frequencies, so it is enough to consider one of them, the odd parity ones say, for which the potential is [77]

$$V_{\text{grav}} = f \left[\frac{l(l+1)}{r^2} - \frac{6M}{r^3} \right]. \quad (5.11)$$

In all cases, we denote by l the angular quantum number, that gives the multipolarity of the field. Let us now specialize to the near extremal SdS black hole, which is defined as the spacetime for which the cosmological horizon r_c is very close (in the r coordinate) to the black hole horizon r_b , i.e. $\frac{r_c - r_b}{r_b} \ll 1$. For this spacetime one can make the following approximations

$$r_0 \sim -2r_b^2; \quad a^2 \sim 3r_b^2; \quad M \sim \frac{r_b}{3}; \quad \kappa_b \sim \frac{r_c - r_b}{2r_b^2}. \quad (5.12)$$

Furthermore, and this is the key point, since r is constrained to vary between r_b and r_c , we get $r - r_0 \sim r_b - r_0 \sim 3r_0$ and thus

$$f \sim \frac{(r - r_b)(r_c - r)}{r_b^2}. \quad (5.13)$$

In this limit, one can invert the relation $r_*(r)$ of (5.8) to get

$$r = \frac{r_c e^{2\kappa_b r_*} + r_b}{1 + e^{2\kappa_b r_*}}. \quad (5.14)$$

Substituting this on the expression (5.13) for f we find

$$f = \frac{(r_c - r_b)^2}{4r_b^2 \cosh(\kappa_b r_*)^2}. \quad (5.15)$$

As such, and taking into account the functional form of the potentials (5.9)-(5.11) we see that for the near extremal SdS black hole the wave equation (5.7) is of the form

$$\frac{\partial^2 \phi(\omega, r)}{\partial r_*^2} + \left[\omega^2 - \frac{V_0}{\cosh(\kappa_b r_*)^2} \right] \phi(\omega, r) = 0, \quad (5.16)$$

with

$$V_0 = \begin{cases} \kappa_b^2 l(l+1), & \text{scalar and electromagnetic} \\ & \text{perturbations.} \\ \kappa_b^2 (l+2)(l-1), & \text{gravitational} \\ & \text{perturbations.} \end{cases} \quad (5.17)$$

The potential in (5.16) is the well known Pöshl-Teller potential [105]. The solutions to (5.16) were studied and they are of the hypergeometric type, (for details see Ferrari and Mashhoon [16]). It should be solved under appropriate boundary conditions:

$$\phi \sim e^{-i\omega r_*}, r_* \rightarrow -\infty \quad (5.18)$$

$$\phi \sim e^{i\omega r_*}, r_* \rightarrow \infty. \quad (5.19)$$

These boundary conditions impose a non-trivial condition on ω [16], and those that satisfy both simultaneously are called QN frequencies. For the Pöshl-Teller potential one can show [16] that they are given by

$$\omega = \kappa_b \left[-\left(n + \frac{1}{2}\right)i + \sqrt{\frac{V_0}{\kappa_b^2} - \frac{1}{4}} \right], n = 0, 1, \dots \quad (5.20)$$

Thus, with (5.17) one has

$$\frac{\omega}{\kappa_b} = -\left(n + \frac{1}{2}\right)i + \sqrt{l(l+1) - \frac{1}{4}}, n = 0, 1, \dots \quad (5.21)$$

for scalar and electromagnetic perturbations. And

$$\frac{\omega}{\kappa_b} = -\left(n + \frac{1}{2}\right)i + \sqrt{(l+2)(l-1) - \frac{1}{4}}, n = 0, 1, \dots \quad (5.22)$$

for gravitational perturbations. Our analysis shows that Eqs. (5.21)-(5.22) are correct up to terms of order $O(r_c - r_b)$ or higher. Moss and Norman [76] have studied the QN frequencies in the SdS geometry numerically and also analytically, by fitting the potential to a Pöshl-Teller potential. Their analytical results (see their Figs 1 and 2) were in excellent agreement

with their numerical results, and this agreement was even more remarkable for near extremal black holes and for high values of the angular quantum number l . We can now understand why: for near extremal black holes the true potential is indeed given by the Pöshl-Teller potential! Furthermore for near extremal SdS black holes and for high l our formula (5.22) is approximately equal to formula (19) of Moss and Norman [76]. With their analytical method of fitting the potential one can never be sure if the results obtained will continue to be good as one increases the mode number n . But we have now proved that if one is in the near extremal SdS black hole, the Pöshl-Teller is the true potential, and so Eq. (5.21)-(5.22) is exact. For example, Moss and Norman obtain numerically, and for gravitational perturbations with $l = 2$ of nearly extreme SdS black holes, the result

$$\frac{\omega_{\text{num}}}{\kappa_b} = 1.93648 - i\left(n + \frac{1}{2}\right), \quad (5.23)$$

and we obtain, from (5.22)

$$\frac{\omega}{\kappa_b} = 1.936492 - i\left(n + \frac{1}{2}\right). \quad (5.24)$$

For $l = 3$ Moss and Norman [76] obtain

$$\frac{\omega_{\text{num}}}{\kappa_b} = 3.12249 - i\left(n + \frac{1}{2}\right), \quad (5.25)$$

and we obtain, from (5.22)

$$\frac{\omega}{\kappa_b} = 3.122499 - i\left(n + \frac{1}{2}\right). \quad (5.26)$$

So this remarkable agreement allows us to be sure that (5.21)-(5.22) are indeed correct.

5.3 Conclusions

We have found for the first time an analytical expression for the QNMs and frequencies of a nearly extreme schwarzschild-de Sitter black hole. This expression, Eqs. (5.21)-(5.22) are correct up to terms of order $O(r_c - r_b)$ or higher for all n . We should stress however that our results may not be correct to all orders in $(r_c - r_b)$ (although they are indeed correct for terms up to second order [108]), and as such it is not guaranteed that our results give the correct behaviour of the highly damped QNMs. As a matter of fact it would be strange indeed if they described correctly highly damped modes. In that case there would be an l -dependent quantization scheme, which does not fit easily into the existing framework. Some recent work [111] seems indeed to confirm what we said: for the lowest lying modes our expressions (5.21)-(5.22) are correct. However, the highly damped modes show a different behaviour.

Chapter 6

Quasinormal modes of Schwarzschild black holes in four and higher dimensions

Contents

6.1	Introduction	69
6.2	QN frequencies of the four-dimensional Schwarzschild black hole	72
6.3	QN frequencies of D -dimensional Schwarzschild black holes	77
6.4	Discussion of results and future directions	87

6.1 Introduction

The study of quasinormal modes of black holes began more than thirty years ago, when Vishveshwara [1] noticed that the signal from a perturbed black hole is, for most of the time, an exponentially decaying ringing signal. It turns out that the ringing frequency and damping timescale are characteristic of the black hole, depending only on its parameters (like the mass and angular momentum). We call these characteristic oscillations the quasinormal modes (QNMs) and the associated frequencies are termed quasinormal frequencies (QN frequencies), because they are really not stationary perturbations. Not surprisingly, QNMs play an important role in the dynamics of black holes, and consequently in gravitational wave physics. In fact, it is possible [23, 24] to extract the parameters of the black hole simply by observing these QN frequencies, using for example gravitational wave detectors. The discovery that QNMs dominate the answer of a black hole to almost any exterior perturbation was followed by a great effort to find, numerically and analytically, the QN frequencies. For excellent reviews on the status of QNMs, prior to 2000, we refer the reader to Kokkotas and Schmidt [9] and Nollert [10]. It is important to note that on the astrophysical aspect, the most important QN frequencies are the lowest ones, i.e., frequencies with smaller imaginary part, and the most important spacetimes are the asymptotically flat and perhaps now the asymptotically de Sitter. However, three years ago Horowitz and Hubeny [48] pointed out that QNMs of black holes in anti-de Sitter space have a different importance. According to the AdS/CFT

correspondence [27], a black hole in anti-de Sitter space may be viewed as a thermal state in the dual theory. Perturbing this black hole corresponds to perturbing the thermal state, and therefore the typical timescale of approach to thermal equilibrium (which is hard to compute directly in the dual theory) should as well be governed by the lowest QN frequencies. That this is indeed the case was proved by Birmigham, Sachs and Solodukhin [53] for the BTZ black hole, taking advantage that this is one of the few spacetimes where one can compute exactly its QN frequencies, as showed by Cardoso and Lemos [37]. A similar study was made by Kurita and Sakagami [112] for the D-3 brane. This interpretation for the imaginary part of the QN frequencies in terms of timescales of approach to thermal equilibrium in the dual conformal field theory has motivated a generalized search for the quasinormal modes of different black holes in anti-de Sitter spacetime, over the last three years [48, 37, 75].

Recently, the motivation for studying QN modes of black holes has grown enormously with the conjectures [31, 33, 70, 113] relating the highly damped QNMs (i.e., QN frequencies with large imaginary parts) to black hole area quantization and to the Barbero Immirzi parameter appearing in Loop Quantum Gravity. The seeds of that idea were planted some time ago by Bekenstein [29]. A semi-classical reasoning of the conjecture [32] that the black hole area spectrum is quantized leads to

$$A_n = \gamma l_P^2 n, \quad n = 1, 2, \dots \quad (6.1)$$

Here l_P is the Planck length and γ is an undetermined constant. However, statistical physics arguments impose a constraint on γ [32]:

$$\gamma = 4 \log k, \quad (6.2)$$

where k is an integer. The integer k was left undetermined (although there were some suggestions for it [32]), until Hod [31], supported by some of Bekenstein's ideas, put forward the proposal to determine k via a version of Bohr's correspondence principle, in which one admits that the real part of QN frequencies with a large imaginary part plays a fundamental role. It was seen numerically by Nollert [10, 18] that QN frequencies with a large imaginary part behave, in the Schwarzschild geometry as

$$\omega M = 0.0437123 + \frac{i}{8} (2n + 1), \quad (6.3)$$

where M is the black hole mass, and n the mode number. Hod first realized that $0.0437123 \sim \frac{\ln 3}{8\pi}$, and went on to say that, if one supposes that the emission of a quantum with frequency $\frac{\ln 3}{8\pi}$ corresponds to the least possible energy a black hole can emit, then the change in surface area will be (using $A = 16\pi M^2$)

$$\Delta A = 32\pi M dM = 32\pi M \hbar \omega = 4\hbar \ln 3. \quad (6.4)$$

Comparing with (6.1) we then get $k = 3$ and therefore the area spectrum is fixed to

$$A_n = 4 \ln 3 l_P^2 n; \quad n = 1, 2, \dots \quad (6.5)$$

It was certainly a daring proposal to map 0.0437123 to $\ln 3$, and even more to use the QN frequencies to quantize the black hole area, by appealing to ‘‘Bohr's correspondence principle’’. The risk paid off: recently, Dreyer [33] put forward the hypothesis that if one uses such a

correspondence it is possible to fix a formerly free parameter, the Barbero-Immirzi parameter, appearing in Loop Quantum Gravity. This fixing of the Barbero-Immirzi parameter was made at the expense of changing the gauge group from $SU(2)$, which is the most natural one, to $SO(3)$. It may be possible however to keep $SU(2)$ as gauge group, as Ling and Zhang [113] recently remarked, by considering the supersymmetric extension of Loop Quantum Gravity.

All of these proposals and conjectures could be useless if one could not prove that the real part of the QN frequencies do approach $\frac{\ln 3}{8\pi}$, i.e., that the number 0.0437123 in Nollert's paper was exactly $\frac{\ln 3}{8\pi}$. This was accomplished by Motl [34] some months ago, using an ingenious technique, working with the continued fraction representation of the wave equation. Subsequently, Motl and Neitzke [35] used a more flexible and powerful approach, called the monodromy method, and were not only able to rederive the four dimensional Schwarzschild value $\frac{\ln 3}{8\pi}$, but also to compute the asymptotic value for generic D -dimensional Schwarzschild black holes thereby confirming a previous conjecture by Kunstatter [70]. They have also predicted the form of the asymptotic QN frequencies for the Reissner-Nordström geometry, a prediction which was verified by Berti and Kokkotas [71].

It is interesting to speculate why, in thirty years investigating QNMs and QN frequencies, no one has ever been able to deduce analytically the asymptotic value of the QN frequencies, nor even for the Schwarzschild geometry, which is the simplest case. In our opinion, there are three important facts that may help explain this: first, the concern was mostly with the lowest QN frequencies, the ones with smaller imaginary part, since they are the most important in the astrophysical context where QNMs were inserted until three years ago. In fact, most of the techniques to find QN frequencies, and there were many, have been devised to compute the lowest QN frequencies (see [9, 10] for a review). Secondly, there was no suggestion for the asymptotic $\ln 3$ value. To know this value serves as a strong stimulation. The third reason is obvious: this was a very difficult technical problem.

It is thus satisfying that Motl and Neitzke have proved exactly that the limit is $\ln 3$. In addition, Van den Brink [72] used a somewhat different approach to rederive the $\frac{\ln 3}{8\pi}$ value, and at the same time computed the first order correction to gravitational QN frequencies, confirming analytically Nollert's [18] numerical results. However, Motl and Neitzke's monodromy method is more flexible and powerful: it has been easily adapted to other spacetimes. For example, Castello-Branco and Abdalla [116] have generalized the results to the Schwarzschild-de Sitter geometry, while Schiappa, Natário and Cardoso [117] have used it to compute the asymptotic values in the D -dimensional Reissner-Nordström geometry. Moreover the first order corrections are also easily obtained, as has been showed by Musiri and Siopsis [114] for the four dimensional Schwarzschild geometry. Here we shall also generalize these first order corrections so that they can encompass a general D -dimensional Schwarzschild black hole. A body of work has been growing on the subject of computing highly damped QNMs, both in asymptotically flat and in de Sitter or anti-de Sitter spacetimes (see the references in [120]).

As an aside, we note that one of the most intriguing features of Motl and Neitzke's technique is that the region beyond the event horizon, which never enters in the definition of quasinormal modes, plays an extremely important role. In particular, the singularity at $r = 0$ is decisive for the computation. At the singularity the effective potential for wave propagation blows up. Somehow, the equation, or the singularity, knows what we are seeking! It is also worth of note the following: for high frequencies, or at least frequencies with a large imaginary part, the important region is therefore $r = 0$ where the potential blows up, whereas for low frequencies, of interest for late-time tails [240], it is the other limit, $r \rightarrow \infty$ which is

important.

The purpose of this work is two-fold: first we want to enlarge and settle the results for the four dimensional Schwarzschild black hole. We shall first numerically confirm Nollert's results for the gravitational case, and Berti and Kokkotas'[71] results for the scalar case, and see that the match between these and the analytical prediction is quite good. Then we shall fill-in a gap left behind in these two studies: the electromagnetic asymptotic QN frequencies, for which there are no numerical results, but a lot of analytical predictions. This will put the monodromy method on a firmer ground. One might say that in the present context (of black hole quantization and relation with Loop Quantum Gravity) electromagnetic perturbations are not relevant, only the gravitational ones are. This is not true though, because when considering the Reissner-Nordström case gravitational and electromagnetic perturbations are coupled [40] and it is therefore of great theoretical interest to study each one separately, in the case they do decouple, i.e., the Schwarzschild geometry. We find that all the analytical predictions are correct: scalar and gravitational QN frequencies asymptote to $\frac{\omega}{T_H} = \ln 3 + i(2n+1)\pi$ with $\frac{1}{\sqrt{n}}$ corrections, where $T_H = \frac{1}{8\pi M}$ is the Hawking temperature. The corrections are well described by the existing analytical formulas. On the other hand, electromagnetic QN frequencies asymptote to $\frac{\omega}{T_H} = 0 + i2n\pi$ with no $\frac{1}{\sqrt{n}}$ corrections, as predicted by Musiri and Siopsis [114]. Indeed we find that the corrections seem to appear only at the $\frac{1}{n^{3/2}}$ level.

The second aim of this paper is to establish numerically the validity of the monodromy method by extending the numerical calculation to higher dimensional Schwarzschild black holes, in particular to the five dimensional one. We obtain numerically in the five dimensional case the asymptotic value of the QN frequencies, which turns out to be $\ln 3 + i(2n+1)\pi$ (in units of the black hole temperature), for scalar, gravitational tensor and gravitational vector perturbations. Equally important, is that the first order corrections appear as $\frac{1}{n^{2/3}}$ for these cases. We shall generalize Musiri and Siopsis' method to higher dimensions and find that (i) the agreement with the numerical data is very good (ii) In generic D dimensions the corrections appear at the $\frac{1}{n^{(D-3)/(D-2)}}$ level. Electromagnetic perturbations in five dimensions seem to be special: according to the analytical prediction by Motl and Neitzke, they should not have any asymptotic QN frequencies. Our numerics seem not to go higher enough in mode number to prove or disprove this. They indicate that the real part approaches zero, as the mode number increases, but we have not been able to follow the QN frequencies for very high overtone number. We also give complete tables for the lowest lying QN frequencies of the five dimensional black holes, and confirm previous results [99, 15, 115, 118] for the fundamental QN frequencies obtained using WKB-like methods. We find no purely imaginary QN frequencies for the gravitational QNMs, which may be related to the fact that the potentials are no longer superpartners. This chapter will follow [120].

6.2 QN frequencies of the four-dimensional Schwarzschild black hole

The first computation of QN frequencies of four-dimensional Schwarzschild black holes was carried out by Chandrasekhar and Detweiler [12]. They were only able to compute the lowest lying modes, as it was and still is quite hard to find numerically QN frequencies with a very large imaginary part. After this pioneering work, a number of analytical, semi-analytical and

numerical techniques were devised with the purpose of computing higher order QNMs and to establish the low-lying ones using different methods [9, 10]. The most successful numerical method to study QNMs of black holes was proposed by Leaver [17]. In a few words his method amounts to reducing the problem to a continued fraction, rather easy to implement numerically. Using this method Leaver was able to determine the first 60 modes of the Schwarzschild black hole, which at that time was about an order of magnitude better than anyone had ever gone before. The values of the QN frequencies he determined, and we note he only computed gravitational ones, suggested that there is an infinite number of QN modes, that the real part of the QN frequencies approach a finite value, while the imaginary part grows without bound. That the real part of the QN frequencies approach a finite value was however opened to debate [119]: it seemed one still had to go higher in mode number in order to ascertain the true asymptotic behaviour. Nollert [18] showed a way out of these problems: he was able to improve Leaver's method in a very simple fashion so as to go very much higher in mode number: he was able to compute more than 2000 modes of the gravitational QNMs. His results were clear: the real part of the gravitational QN frequencies approaches a constant value $\sim 0.0437123/M$, and this value is independent of l . The imaginary part grows without bound as $(2n + 1)/8$ where n is any large integer. These asymptotic behaviours have both leading corrections, which were also determined by Nollert. He found that to leading order the asymptotic behaviour of the gravitational QN frequencies of a Schwarzschild black hole is given by Eq. (6.3) plus a leading correction, namely,

$$\omega M = 0.0437123 + \frac{i}{8}(2n + 1) + \frac{a}{\sqrt{n}}, \quad (6.6)$$

where the correction term a depends on l . About ten years later, Motl [34] proved analytically that this is indeed the correct asymptotic behaviour. To be precise he proved that

$$\frac{\omega}{T_H} = \ln 3 + i(2n + 1)\pi + \text{corrections}. \quad (6.7)$$

Since the Hawking temperature T_H is $T_H = \frac{1}{8\pi M}$, Nollert's result follows. He also proved that this same result also holds for scalar QN frequencies, whereas electromagnetic QN frequencies asymptote to a zero real part. Motl and Neitzke [35] using a completely different approach, have rederived this result whereas Van den Brink [72] was able to find the leading asymptotic correction term a in (6.6) for the gravitational case. Very recently, Musiri and Siopsis [114], leaning on Motl and Neitzke's technique, have found the leading correction term for any field, scalar, electromagnetic and gravitational. This correction term is presented in section 6.3.2, where we also generalize to higher dimensional black holes. In particular, for electromagnetic perturbations they find that the first order corrections are zero.

Here we use Nollert's method to compute scalar, electromagnetic and gravitational QN frequencies of the four-dimensional Schwarzschild black hole. The details on the implementation of this method in four dimensions are well known and we shall not dwell on it here any more. We refer the reader to the original references [18, 17].

Our results are summarized in Figures 6.1-6.2, and Tables 6.1- 6.2. In Fig. 6.1 we show the behaviour of the 500 lowest QN frequencies for the lowest radiatable multipole of each field (we actually have computed the first 5000 QN frequencies, but for a better visualization we do not show them all): $l = 0$ for scalar, $l = 1$ for electromagnetic and $l = 2$ gravitational. Note that in Fig. 6.1, as well as in all other plots in this work, the dots indicate the QN

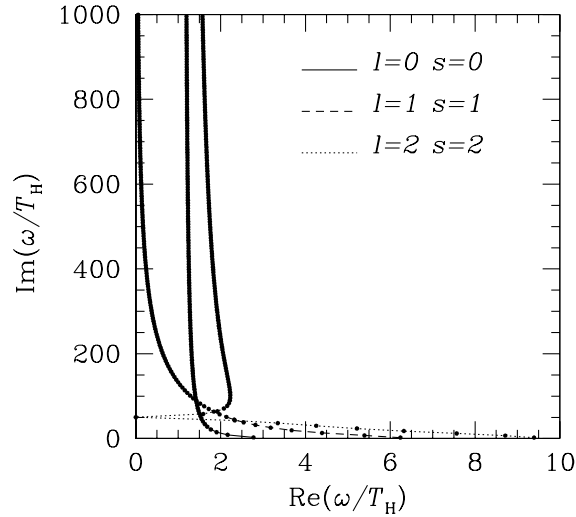


Figure 6.1: Scalar ($s = 0$), electromagnetic ($s = 1$) and gravitational ($s = 2$) QN frequencies of a four-dimensional Schwarzschild black hole. Note that the dots indicate the QN frequencies there, and the lines connecting the dots only help to figure out to which multipole (l, s) they belong to. We show the lowest 500 modes for the lowest radiatable multipoles of each field, i.e., $l = 0$ for the scalar field, $l = 1$ for the electromagnetic and $l = 2$ for gravitational. However, the asymptotic behaviour is l -independent. It is quite clear from this plot that highly damped electromagnetic QN frequencies have a completely different behaviour from that of scalar or gravitational highly damped QN frequencies. In fact, the electromagnetic ones asymptote to $\frac{\omega}{T_H} \rightarrow i(2n+1)\pi$, $n \rightarrow \infty$, as predicted by Motl [34] and Motl and Neitzke [35]. The scalar and gravitational ones asymptote to $\frac{\omega}{T_H} \rightarrow \ln 3 + i\pi(2n+1)$, $n \rightarrow \infty$.

Table 6.1: The correction coefficients for the four-dimensional Schwarzschild black hole, both numerical, here labeled as “Corr₄^N” and analytical, labeled as “Corr₄^A”. These results refer to scalar perturbations. The analytical results are extracted from [114] (see also formula (6.29 below). Notice the very good agreement between the numerically extracted results and the analytical prediction. These values were obtained using the first 5000 modes.

$s = 0$		
l	Corr ₄ ^N :	Corr ₄ ^A
0	1.20-1.20i	1.2190-1.2190i
1	8.52- 8.52i	8.5332-8.5332i
2	23.15-23.15i	23.1614-23.1614i
3	44.99-44.99i	45.1039-45.1039i
4	74.34-74.34i	74.3604-74.3605i

frequencies there, and the lines connecting the dots only help to figure out to which multipole (l, s) they belong to. In what concerns the asymptotic behaviour, our numerics show it is not dependent on l , and that formula (6.6) holds. The results for the scalar and gravitational QN frequencies are not new: the gravitational ones have been obtained by Nollert [18], as we previously remarked, and the scalar ones have been recently arrived at by Berti and Kokkotas [71]. Here we have verified both. Both scalar and gravitational QN frequencies have a real part asymptoting to $\ln 3 \times T_H$. Electromagnetic QN frequencies, on the other hand, have a real part asymptoting to 0. This is clearly seen in Fig. 6.1. For gravitational perturbations Nollert found, and we confirm, that the correction term a in (6.6) is

$$\begin{aligned} a &= 0.4850, \quad l = 2 \\ a &= 1.067, \quad l = 3 \end{aligned} \tag{6.8}$$

We have also computed the correction terms for the scalar case, and we have obtained results in agreement with Berti and Kokkotas’ ones [71]. Our results are summarized in Tables 6.1-6.2, where we also show the analytical prediction [114] (see section 6.3.2). To fix the conventions adopted throughout the rest of the paper, we write

$$\frac{\omega}{T_H} = \ln 3 + i(2n + 1)\pi + \frac{\text{Corr}}{\sqrt{n}}. \tag{6.9}$$

Thus, the correction term a in (6.6) is related to Corr by $a = \text{Corr} \times T_H$.

As for the electromagnetic correction terms, we found it was not very easy to determine them. In fact, it is hard, even using Nollert’s method, to go very high in mode number for these perturbations (we have made it to $n = 5000$). The reason is tied to the fact that these frequencies asymptote to zero, and it is hard to determine QN frequencies with a vanishingly small real part. Nevertheless, there are some features one can be sure of. We have fitted the electromagnetic data to the following form $\frac{\omega}{T_H} = \ln 3 + (2n + 1)i + \frac{b}{\sqrt{n}}$, and found that this gave very poor results. Thus one saw numerically that the first order correction term is absent, as predicted in [114] (see also section 6.3.2 where we rederive these corrections, generalizing them to arbitrary dimension). Our data seems to indicate that the leading correction term is of the form $\frac{b}{n^{3/2}}$. This is more clearly seen in Fig. 6.2 where we plot the first electromagnetic

Table 6.2: The correction coefficients for the four-dimensional Schwarzschild black hole, both numerical, here labeled as “Corr₄^N” and analytical, labeled as “Corr₄^A”. These results refer to gravitational perturbations. The analytical results are extracted from [114] (see also formula (6.29) below). Notice the very good agreement between the numerically extracted results and the analytical prediction. These values were obtained using the first 5000 modes.

$s = 2$		
l	Corr ₄ ^N :	Corr ₄ ^A
2	6.08-6.08i	6.0951-6.0951i
3	13.39-13.39i	13.4092-13.4092i
4	23.14-23.14i	23.1614-23.1614i
5	35.33-35.33i	35.3517-35.3517i
6	48.90-48.90i	49.9799-49.9799i

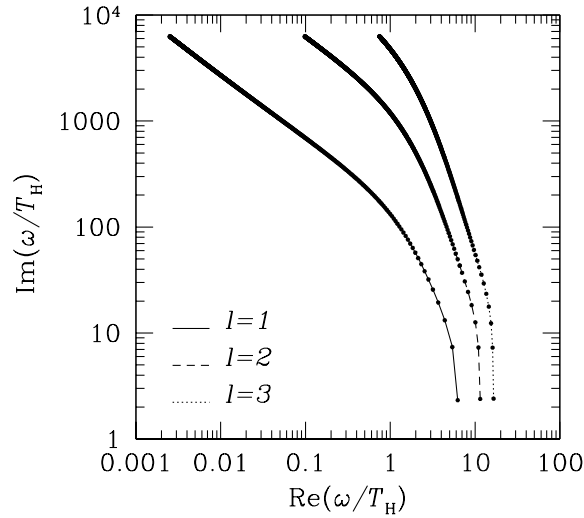


Figure 6.2: Electromagnetic QN frequencies of a four-dimensional Schwarzschild black hole.

QN frequencies on a \ln plot. For frequencies with a large imaginary part, the slope is about $-2/3$ as it should if the asymptotic behaviour is of the form

$$\frac{\omega}{T_H} = \ln 3 + (2n + 1)i + \frac{b}{n^{3/2}}. \quad (6.10)$$

Our numerics indicate that b has an l -dependence going like

$$b \sim c_1 l(l + 1) + c_2 [l(l + 1)]^2 + c_3 [l(l + 1)]^3, \quad (6.11)$$

where c_1 , c_2 , and c_3 are constants. This is also the expected behaviour, since a $\frac{1}{n^{3/2}}$ dependence means we have to go to third order perturbation theory, where we get corrections of the form (6.11) as one can easily convince oneself.

6.3 QN frequencies of D -dimensional Schwarzschild black holes

6.3.1 Equations and conventions

The metric of the D -dimensional Schwarzschild black hole in $(t, r, \theta_1, \theta_2, \dots, \theta_{D-2})$ coordinates is [154, 155]

$$ds^2 = -f dt^2 + f^{-1} dr^2 + r^2 d\Omega_{D-2}^2, \quad (6.12)$$

with

$$f = 1 - \frac{m}{r^{D-3}}. \quad (6.13)$$

The mass of the black hole is given by $M = \frac{(D-2)\Omega_{D-2}m}{16\pi\mathcal{G}}$, where $\Omega_{D-2} = \frac{2\pi^{(D-1)/2}}{\Gamma[(D-1)/2]}$ is the area of a unit $(D-2)$ sphere, $d\Omega_{D-2}^2$ is the line element on the unit sphere S^{D-2} , and \mathcal{G} is Newton's constant in D -dimensions. In the following it will prove more useful to rescale variables so that the form of the metric is (6.12) but with $f = 1 - \frac{1}{r^{D-3}}$, i.e., we shall choose $m = 1$, following the current fashion. We will only consider the linearized approximation, which means that we are considering wave fields outside this geometry that are so weak they do not alter this background. The evolution equation for a massless scalar field follows directly from the Klein-Gordon equation (see [224] for details). The gravitational evolution equations have recently been derived by Kodama and Ishibashi [126]. There are three kinds of gravitational perturbations, according to Kodama and Ishibashi's terminology: the scalar gravitational, the vector gravitational and the tensor gravitational perturbations. The first two already have their counterparts in $D = 4$, which were first derived by Regge and Wheeler [38] and by Zerilli [219]. The tensor type is a new kind appearing in higher dimensions. However, it obeys exactly the same equation as massless scalar fields, as can easily be seen. Due to the complex form of the gravitational scalar potential, we shall not deal with it. Instead, we shall only consider the tensor and vector type of gravitational perturbations. In any case, if the analytic results are correct, then the gravitational scalar QN frequencies should have the same asymptotic form as the gravitational vector and tensor QN frequencies. The evolution equation for the electromagnetic field in the higher dimensional Schwarzschild geometry was arrived at for the first time by Crispino, Higuchi and Matsas [121]. It has recently been rederived by Kodama and Ishibashi, in a wider context of charged black hole perturbations.

We shall follow Kodama and Ishibashi's terminology. According to them, there are two kinds of electromagnetic perturbations: the vector and scalar type. If one makes the charge of the black hole $Q = 0$ in Kodama and Ishibashi's equations one recovers the equations by Crispino, Higuchi and Matsas, although this seems to have been overlooked in the literature. The evolution equation for all kinds of fields (scalar, gravitational and electromagnetic) can be reduced to the second order differential equation

$$\frac{d^2\Psi}{dr_*^2} + (\omega^2 - V)\Psi = 0, \quad (6.14)$$

where r is a function of the tortoise coordinate r_* , defined through $\frac{\partial r}{\partial r_*} = f(r)$, and the potential can be written in compact form as

$$V = f(r) \left[\frac{l(l+D-3)}{r^2} + \frac{(D-2)(D-4)}{4r^2} + \frac{(1-j^2)(D-2)^2}{4r^{D-1}} \right]. \quad (6.15)$$

The constant j depends on what kind of field one is studying:

$$j = \begin{cases} 0, & \text{scalar and gravitational tensor} \\ & \text{perturbations.} \\ 1, & \text{gravitational vector} \\ & \text{perturbations.} \\ \frac{2}{D-2}, & \text{electromagnetic vector} \\ & \text{perturbations.} \\ 2 - \frac{2}{D-2}, & \text{electromagnetic scalar} \\ & \text{perturbations.} \end{cases} \quad (6.16)$$

Notice that in four dimensions, j reduces to the usual values given by Motl and Neitzke [35]. According to our conventions, the Hawking temperature of a D -dimensional Schwarzschild black hole is

$$T_H = \frac{D-3}{4\pi} \quad (6.17)$$

Our purpose here is to investigate the QN frequencies of higher dimensional black holes. Of course one cannot study every D . We shall therefore focus on one particular dimension, five, and make a complete analysis of its QN frequencies. The results should be representative. In particular, one feature that distinguishes an arbitrary D from the four dimensional case is that the correction terms come with a different power, i.e., whereas in four dimensions the correction is of the form $\frac{1}{\sqrt{n}}$ we shall find that in generic D it is of the form $\frac{1}{n^{(D-3)/(D-2)}}$. Thus, if one verifies this for $D = 5$ for example, one can ascertain it will hold for arbitrary D . We shall now briefly sketch our numerical procedure for finding QN frequencies of a five dimensional black hole. This is just Leaver's and Nollert's technique with minor modifications.

The QNMs of the higher-dimensional Schwarzschild black hole are characterized by the boundary conditions of incoming waves at the black hole horizon and outgoing waves at spatial infinity, written as

$$\Psi(r) \rightarrow \begin{cases} e^{-i\omega r_*} & \text{as } r_* \rightarrow \infty \\ e^{i\omega r_*} & \text{as } r_* \rightarrow -\infty, \end{cases} \quad (6.18)$$

where the time dependence of perturbations has been assumed to be $e^{i\omega t}$.

6.3.2 Perturbative calculation of QNMs of D -dimensional Schwarzschild BHs

In this section we shall outline the procedure for computing the first order corrections to the asymptotic value of the QN frequencies of a D -dimensional Schwarzschild black hole. This will be a generalization of Musiri and Siopsis' method [114], so we adopt all of their notation, and we refer the reader to their paper for further details. The computations are however rather tedious and the final expressions are too cumbersome, so we shall refrain from giving explicit expressions for the final result.

We start with the expansion of the potential V near the singularity $r = 0$. One can easily show that near this point the potential (6.15) may be approximated as

$$V \sim -\frac{\omega^2}{4z^2} \left[1 - j^2 + \frac{A}{(-z\omega)^{(D-3)/(D-2)}} \right], \quad (6.19)$$

where we adopted the conventions in [114] and therefore $z = \omega r_*$. The constant A is given by

$$A = \frac{4l(l + D - 3) + (D - 2)(D - 4) - (D - 2)^2(1 - j^2)}{(D - 2)^{(D-1)/(D-2)}} + \frac{2(1 - j^2)(D - 2)^{(2D-5)/(D-2)}}{2D - 5}. \quad (6.20)$$

In $D = 4$ this reduces to the usual expression [114, 127] for the potential near $r = 0$. Expression (6.19) is a formal expansion in $\frac{1}{\omega^{(D-3)/(D-2)}}$, so we may anticipate that indeed the first order corrections will appear in the form $\frac{1}{\omega^{(D-3)/(D-2)}}$. So now we may proceed in a direct manner: we expand the wavefunction to first order in $\frac{1}{\omega^{(D-3)/(D-2)}}$ as

$$\Psi = \Psi^{(0)} + \frac{1}{\omega^{(D-3)/(D-2)}} \Psi^{(1)}, \quad (6.21)$$

and find that the first-order correction obeys the equation

$$\frac{d^2 \Psi^{(1)}}{dz^2} + \left(\frac{1 - j^2}{4z^2} + 1 \right) \Psi^{(1)} = \omega^{(D-3)/(D-2)} \delta V \Psi^{(0)}, \quad (6.22)$$

with

$$\delta V = -\frac{A}{\omega^{(D-3)/(D-2)} (-z)^{(D-1)/(D-2)}}. \quad (6.23)$$

All of Musiri and Siopsis' expressions follow directly to the D -dimensional case, if one makes the replacement $\sqrt{-\omega r_0} \rightarrow \omega^{(D-3)/(D-2)}$ in all their expressions. For example, the general solution of (6.22) is

$$\Psi_{\pm}^{(1)} = \mathcal{C} \Psi_{+}^{(0)} \int_0^z \Psi_{-}^{(0)} \delta V \Psi_{\pm}^{(0)} - \mathcal{C} \Psi_{-}^{(0)} \int_0^z \Psi_{+}^{(0)} \delta V \Psi_{\pm}^{(0)}, \quad (6.24)$$

where

$$\mathcal{C} = \frac{\omega^{(D-3)/(D-2)}}{\sin j\pi/2}, \quad (6.25)$$

and the wavefunctions $\Psi_{\pm}^{(0)}$ are

$$\Psi_{\pm}^{(0)} = \sqrt{\frac{\pi z}{2}} J_{\pm j/2}(z). \quad (6.26)$$

The only minor modification is their formula (30). In D -dimensions, it follows that

$$\Psi_{\pm}^{(1)} = z^{1 \pm j/2 + k} G_{\pm}(z), \quad (6.27)$$

where $k = \frac{D-4}{2(D-2)}$, and G_{\pm} are even analytic functions of z . So we have all the ingredients to construct the first order corrections in the D -dimensional Schwarzschild geometry. Unfortunately the final expressions turn out to be quite cumbersome, and we have not managed to simplify them. We have worked with the symbolic manipulator *Mathematica*. It is possible to obtain simple expression for any particular D , but apparently not for a generic D . For generic D we write

$$\frac{\omega}{T_H} = \ln(1 + 2 \cos \pi j) + i(2n + 1)\pi + \frac{\text{Corr}_D}{\omega^{(D-3)/(D-2)}} \quad (6.28)$$

So the leading term is $\frac{\omega}{T_H} = \ln 3 + i(2n + 1)\pi$, for scalar, gravitational tensor and gravitational tensor perturbations (and the same holds for gravitational scalar). However, for electromagnetic perturbations (vector or scalar) in $D = 5$, $1 + 2 \cos \pi j = 1 + 2 \cos \frac{2\pi}{3} = 0$. So there seem to be no QN frequencies as argued by Motl and Neitzke [35]. We obtained for $D = 4$ the following result for the correction coefficient in (6.28),

$$\text{Corr}_4 = -\frac{(1 - i)\pi^{3/2}(-1 + j^2 - 3l(l + 1))\frac{\cos j\pi}{2}\Gamma[1/4]}{3(1 + 2 \cos j\pi)\Gamma[3/4]\Gamma[3/4 - j/2]\Gamma[3/4 + j/2]}, \quad (6.29)$$

which reduces to Musiri and Siopsis' expression. For $D = 5$ it is possible also to find a simple expression for the corrections:

$$\begin{aligned} \text{Corr}_5 &= \frac{i(9j^2 - (24 + 20l(l + 2)))\pi^{3/2}}{120 \times 3^{1/3}\Gamma[2/3]\Gamma[2/3 - j/2]\Gamma[2/3 + j/2]} \\ &\times \Gamma[1/6] \frac{\frac{e^{ij\pi}}{\sin((1/3+j/2)\pi)} - \frac{1}{\sin((2/3+j/2)\pi)}}{-1 + e^{ij\pi}}. \end{aligned} \quad (6.30)$$

The limits $j \rightarrow 0, 2$ are well defined and yield

$$\text{Corr}_5^{j=0} = \frac{(1 - i\sqrt{3})(6 + 10l + 5l^2)\pi^{3/2}\Gamma[1/6]}{45 \times 3^{1/3}\Gamma[2/3]^3}, \quad (6.31)$$

$$\text{Corr}_5^{j=2} = \frac{(-1 + i\sqrt{3})(-3 + 10l + 5l^2)\pi^{3/2}\Gamma[1/6]}{45 \times 3^{1/3}\Gamma[-1/3]\Gamma[2/3]\Gamma[5/3]}, \quad (6.32)$$

We list in Tables 6.6-6.7 some values of this five dimensional correction for some values of the parameter j and l and compare them with the results extracted numerically. The agreement is quite good. The code for extracting the generic D -dimensional corrections is available from the authors upon request. It should not come as a surprise that for $j = 2/3$ the correction term blows up: indeed already the zeroth order term is not well defined.

6.3.3 Numerical procedure and results

6.3.3.a Numerical procedure

In order to numerically obtain the QN frequencies, in the present investigation, we make use of Nollert's method [10], since asymptotic behaviors of QNMs in the limit of large imaginary frequencies are prime concern in the present study.

In our numerical study, we only consider the QNMs of the Schwarzschild black hole in the five dimensional spacetime, namely the $D = 5$ case. As we have remarked, this should be representative. The tortoise coordinate is then reduced to

$$r_* = x^{-1} + \frac{1}{2x_1} \ln(x - x_1) - \frac{1}{2x_1} \ln(x + x_1), \quad (6.33)$$

where $x = r^{-1}$ and $x_1 = r_h^{-1}$. Here, r_h stands for the horizon radius of the black hole. The perturbation function Ψ may be expanded around the horizon as

$$\Psi = e^{-i\omega x^{-1}} (x - x_1)^\rho (x + x_1)^\rho \sum_{k=0}^{\infty} a_k \begin{pmatrix} x - x_1 \\ -x_1 \end{pmatrix}^k, \quad (6.34)$$

where $\rho = i\omega/2x_1$ and a_0 is taken to be $a_0 = 1$. The expansion coefficients a_k in equation (6.34) are determined via the four-term recurrence relation (it's just a matter of substituting expression (6.34) in the wave equation (6.14)), given by

$$\begin{aligned} \alpha_0 a_1 + \beta_0 a_0 &= 0, \\ \alpha_1 a_2 + \beta_1 a_1 + \gamma_1 a_0 &= 0, \\ \alpha_k a_{k+1} + \beta_k a_k + \gamma_k a_{k-1} + \delta_k a_{k-2} &= 0, \quad k = 2, 3, \dots, \end{aligned} \quad (6.35)$$

where

$$\begin{aligned} \alpha_k &= 2(2\rho + k + 1)(k + 1), \\ \beta_k &= -5(2\rho + k)(2\rho + k + 1) - l(l + 2) - \frac{3}{4} \\ &\quad - \frac{9}{4}(1 - j^2), \\ \gamma_k &= 4(2\rho + k - 1)(2\rho + k + 1) + \frac{9}{2}(1 - j^2), \\ \delta_k &= -(2\rho + k - 2)(2\rho + k + 1) - \frac{9}{4}(1 - j^2). \end{aligned}$$

It is seen that since the asymptotic form of the perturbations as $r_* \rightarrow \infty$ is written in terms of the variable x as

$$e^{-i\omega r_*} = e^{-i\omega x^{-1}} (x - x_1)^{-\rho} (x + x_1)^\rho, \quad (6.36)$$

the expanded perturbation function Ψ defined by equation (6.34) automatically satisfy the QNM boundary conditions (6.18) if the power series converges for $0 \leq x \leq x_1$. Making use of a Gaussian elimination [123], we can reduce the four-term recurrence relation to the three-term one, given by

$$\begin{aligned} \alpha'_0 a_1 + \beta'_0 a_0 &= 0, \\ \alpha'_k a_{k+1} + \beta'_k a_k + \gamma'_k a_{k-1} &= 0, \quad k = 1, 2, \dots, \end{aligned} \quad (6.37)$$

where α'_k , β'_k , and γ'_k are given in terms of α_k , β_k , γ_k and δ_k by

$$\alpha'_k = \alpha_k, \quad \beta'_k = \beta_k, \quad \gamma'_k = \gamma_k, \quad \text{for } k = 0, 1, \quad (6.38)$$

and

$$\begin{aligned} \alpha'_k &= \alpha_k, \\ \beta'_k &= \beta_k - \alpha'_{k-1} \delta_k / \gamma'_{k-1}, \\ \gamma'_k &= \gamma_k - \beta'_{k-1} \delta_k / \gamma'_{k-1}, \quad \text{for } k \geq 2. \end{aligned} \quad (6.39)$$

Now that we have the three-term recurrence relation for determining the expansion coefficients a_k , the convergence condition for the expansion (6.34), namely the QNM conditions, can be written in terms of the continued fraction as [124, 17]

$$\beta'_0 - \frac{\alpha'_0 \gamma'_1}{\beta'_1 - \frac{\alpha'_1 \gamma'_2}{\beta'_2 - \frac{\alpha'_2 \gamma'_3}{\beta'_3 - \dots}}} \equiv \beta'_0 - \frac{\alpha'_0 \gamma'_1}{\beta'_1 - \frac{\alpha'_1 \gamma'_2}{\beta'_2 - \frac{\alpha'_2 \gamma'_3}{\beta'_3 - \dots}}} = 0, \quad (6.40)$$

where the first equality is a notational definition commonly used in the literature for infinite continued fractions. Here we shall adopt such a convention. In order to use Nollert's method, with which relatively high-order QNM with large imaginary frequencies can be obtained, we have to know the asymptotic behaviors of a_{k+1}/a_k in the limit of $k \rightarrow \infty$. According to a similar consideration as that by Leaver [123], it is found that

$$\frac{a_{k+1}}{a_k} = 1 \pm 2\sqrt{\rho} k^{-1/2} + \left(2\rho - \frac{3}{4}\right) k^{-1} + \dots, \quad (6.41)$$

where the sign for the second term in the right-hand side is chosen so as to be

$$\text{Re}(\pm 2\sqrt{\rho}) < 0. \quad (6.42)$$

In actual numerical computations, it is convenient to solve the k -th inversion of the continue fraction equation (6.40), given by

$$\begin{aligned} &\beta'_k - \frac{\alpha'_{k-1} \gamma'_k}{\beta'_{k-1} - \frac{\alpha'_{k-2} \gamma'_{k-1}}{\beta'_{k-2} - \dots}} \dots \frac{\alpha'_0 \gamma'_1}{\beta'_0} \\ &= \frac{\alpha'_k \gamma'_{k+1}}{\beta'_{k+1} - \frac{\alpha'_{k+1} \gamma'_{k+2}}{\beta'_{k+2} - \dots}} \dots \end{aligned} \quad (6.43)$$

The asymptotic form (6.41) plays an important role in Nollert's method when the infinite continued fraction in the right-hand side of equation (6.43) is evaluated [10].

6.3.3.b Numerical results

Using the numerical technique described in section 6.3.3.a we have extracted the 5000 lowest lying QN frequencies for the five dimensional Schwarzschild black hole, in the case of scalar, gravitational tensor and gravitational vector perturbations. For electromagnetic vector perturbations the situation is different: the real part rapidly approaches zero, and we have not been able to compute more than the first 30 modes.

Table 6.3: The first lowest QN frequencies for scalar and gravitational tensor ($j = 0$) perturbations of the five dimensional Schwarzschild black hole. The frequencies are normalized in units of black hole temperature, so the Table really shows $\frac{\omega}{T_H}$, where T_H is the Hawking temperature of the black hole.

$j = 0$			
n	$l = 0:$	$l = 1:$	$l = 2$
0	3.3539+2.4089i	6.3837+2.2764i	9.4914+2.2462i
1	2.3367+8.3101i	5.3809+7.2734i	8.7506+6.9404i
2	1.8868+14.786i	4.1683+13.252i	7.5009+12.225i
3	1.6927+21.219i	3.4011+19.708i	6.2479+18.214i
4	1.5839+27.607i	2.9544+26.215i	5.3149+24.597i

Table 6.4: The first lowest QN frequencies for gravitational vector ($j = 2$) perturbations of the five dimensional Schwarzschild black hole. The frequencies are normalized in units of black hole temperature, so the Table really shows $\frac{\omega}{T_H}$, where T_H is the Hawking temperature of the black hole.

$j = 2$			
n	$l = 2:$	$l = 3:$	$l = 4$
0	7.1251+2.0579i	10.8408+2.0976i	14.3287+2.1364i
1	5.9528+6.4217i	8.8819+1.0929i	12.8506+1.0574i
2	3.4113+12.0929i	7.2160+16.3979i	11.5069+16.0274i
3	2.7375+19.6094i	5.5278+22.3321i	9.99894+21.5009i
4	2.5106+26.2625i	3.9426+28.6569i	8.56386+27.4339i

(i) *Low-lying modes*

Low lying modes are important since they govern the intermediate-time evolution of any black hole perturbation. As such they may play a role in TeV-scale gravity scenarios [151], and higher dimensional black hole formation [99, 158]. For example, it is known [99, 159, 160, 161, 162, 122] that if one forms black holes through the high energy collision of particles, then the fundamental quasinormal frequencies serve effectively as a cutoff in the energy spectra of the gravitational energy radiated away. In Tables 6.3-6.5 we list the five lowest lying QN frequencies for some values of the multipole index l . The fundamental modes are in excellent agreement with the ones presented by Konoplya [15, 115] using a high-order WKB approach. Notice he uses a different convention so one has to be careful when comparing the results. For example, in our units Konoplya obtains for scalar and tensorial perturbations ($j = 0$) with $l = 2$ a fundamental QN frequency $\omega_0/T_H = 9.49089 + 2.24721i$, whereas we get, from Table 6.3 the number $9.4914 + 2.2462i$ so the WKB approach does indeed yield good results, at least for low-lying modes, since it is known it fails for high-order ones.

In the four dimensional case, and for gravitational vector perturbations, there is for is each l , a purely imaginary QN frequency, which had been coined an “algebraically special frequency” by Chandrasekhar [40]. For further properties of this special frequencies we refer the reader to [132, 133]. The existence of these purely imaginary frequencies translates, in the four dimensional case, a relation between the two gravitational wavefunctions (i.e., between

Table 6.5: The first lowest QN frequencies for electromagnetic vector ($j = 2/3$) perturbations of the five dimensional Schwarzschild black hole. The frequencies are normalized in units of black hole temperature, so the Table really shows $\frac{\omega}{T_H}$, where T_H is the Hawking temperature of the black hole.

$j = 2$			
n	$l = 1:$	$l = 2:$	$l = 3$
0	5.9862+2.2038i	9.2271+2.2144i	12.4184+2.2177i
1	4.9360+7.0676i	8.4728+6.8459i	11.8412+6.7660i
2	3.6588+12.9581i	7.1966+12.0804i	10.7694+11.6626i
3	2.8362+19.3422i	5.9190+18.0343i	9.4316+17.1019i
4	2.3322+25.7861i	4.9682+24.3832i	8.1521+23.0769i

the Regge-Wheeler and the Zerilli wavefunction, or between the gravitational vector and gravitational scalar wavefunctions, respectively). It is possible to show for example that the associated potentials are related through supersymmetry. Among other consequences, this relation allows one to prove that the QN frequencies of both potentials are exactly the same [40].

We have not spotted any purely imaginary QN frequency for this five-dimensional black hole. In fact the QN frequency with the lowest real part is a gravitational vector QN frequency with $l = 4$ and overtone number $n = 13$, $\omega = 8.7560 \times 10^{-2} + 6.9934i$. This may indicate that in five dimensions, there is no relation between the wavefunctions, or put another way, that the potentials are no longer superpartner potentials. This was in fact already observed by Kodama and Ishibashi [126] for any dimension greater than four. It translates also in Tables 6.3-6.4, which yield different values for the QN frequencies. Although we have not worked out the gravitational scalar QN frequencies, a WKB approach can be used for the low-lying QN frequencies, and also yields different values [15, 115].

(ii) Highly damped modes

Our numerical results for the highly damped modes, i.e., QN frequencies with a very large imaginary part, are summarized in Figures 6.3-6.5 and in Tables 6.6-6.7.

In Fig. 6.3 we show our results for scalar, gravitational tensor ($j = 0$), gravitational vector ($j = 2$) and electromagnetic vector ($j = 2/3$) QN frequencies. For $j = 0, 2$ the real part approaches $\ln 3$ in units of the black hole temperature, a result consistent with the analytical result in [35] (see also section 6.3.2). Electromagnetic vector ($j = 2/3$) QN frequencies behave differently: the real part rapidly approaches zero, and this makes it very difficult to compute the higher modes. In fact, the same kind of problem appears in the Kerr geometry [43], and this a major obstacle to a definitive numerical characterization of the highly damped QNMs in this geometry. We have only been able to compute the first 30 modes with accuracy. The prediction of [35] for this case (see section 6.3.2) is that there are no asymptotic QN frequencies. It is left as an open question whether this is true or not. Our results indicate that the real part rapidly approaches zero, but we cannot say whether the modes die there or not, or even if they perform some kind of oscillation. The imaginary part behaves in the usual manner, growing linearly with mode number.

Let us now take a more detailed look at our numerical data for scalar and gravitational

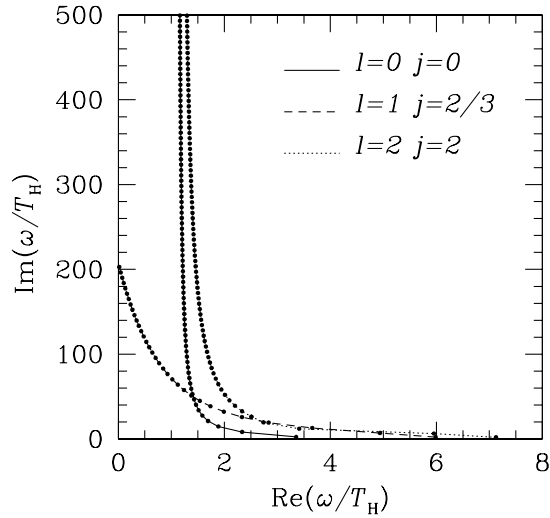


Figure 6.3: The QN frequencies of scalar ($j = 0$), gravitational vector ($j = 2$) and electromagnetic vector ($j = 2/3$) perturbations of a five-dimensional Schwarzschild black hole. We only show the lowest radiatable multipoles, but the asymptotic behaviour is l -independent.

QN frequencies. In Fig. 6.4 we show in a ln plot our results for scalar and gravitational tensor ($j = 0$) QN frequencies.

Our numerical results are very clear: asymptotically the QN frequencies for scalar and gravitational tensor perturbations ($j = 0$) behave as

$$\frac{\omega}{T_H} = \ln 3 + i(2n + 1)\pi + \frac{\text{Corr}_5}{n^{2/3}}, \quad (6.44)$$

So the leading terms $\ln 3 + (2n + 1)i$ are indeed the ones predicted in [35]. Interestingly, the first corrections do not appear as $\frac{1}{\sqrt{n}}$, but as $\frac{1}{n^{2/3}}$. This was shown to be the expected analytical result in section 6.3.2, where we generalized Musiri and Siopsis’ [114] results to

Table 6.6: The correction coefficients for the five-dimensional Schwarzschild black hole, both numerical, here labeled as “Corr₅^N” and analytical, labeled as “Corr₅^A”. These results refer to scalar or gravitational tensor perturbations ($j = 0$). The analytical results are extracted from the analytical formula (6.31). Notice the very good agreement, to within 0.5% or less, between the numerically extracted results and the analytical prediction.

$j = 0$		
l	Corr ₅ ^N :	Corr ₅ ^A
0	1.155 - 1.993i	1.15404-1.99886i
1	4.058 - 6.956i	4.03915-6.99601i
2	8.894 - 15.26i	8.84765-15.3246i
3	15.64 - 26.79i	15.5796-26.9847i
4	24.33 - 41.67i	24.2349-41.9761i

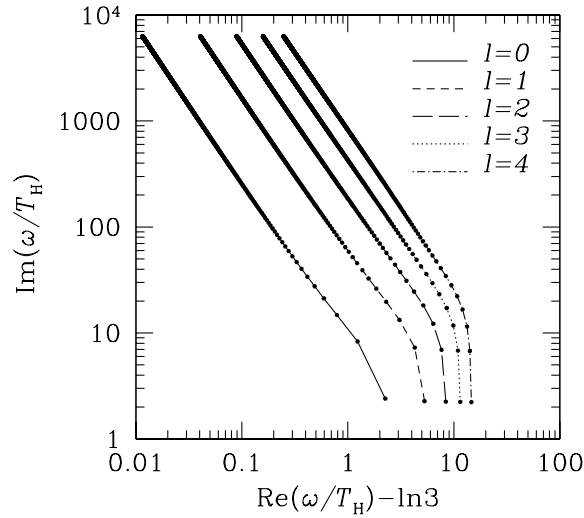


Figure 6.4: The QN frequencies of scalar and gravitational tensor perturbations ($j = 0$) of a five-dimensional Schwarzschild black hole. Notice that for frequencies with a large imaginary part the slope is l -independent and equals $3/2$.

Table 6.7: The correction coefficients for the five-dimensional Schwarzschild black hole, both numerical, here labeled as “ Corr_5^{N} ” and analytical, labeled as “ Corr_5^{A} ”, for gravitational vector perturbations ($j = 2$). The analytical results are extracted from the analytical formula (6.32). Notice the very good agreement, to within 0.5% or less, between the numerically extracted results and the analytical prediction.

$j = 2$		
l	Corr_5^{N} :	Corr_5^{A} :
2	3.568 - 6.139i	3.5583 - 6.16316i
3	6.947 - 11.94i	6.92425 - 11.9932i
4	11.29 - 19.38 i	11.2519 - 19.4889i

higher dimensions. In table 6.6 we show the coefficient Corr_5 extracted numerically along with the predicted coefficient (see expression (6.31)). The table is very clear: the numerical values match the analytical ones. Another confirmation that the corrections appear as $\frac{1}{n^{2/3}}$ is provided by Fig. 6.4. In this figure the QN frequencies are plotted in a ln plot for an easier interpretation. One sees that for large imaginary parts of the QN frequencies, the slope of the plot is approximately $-3/2$, as it should be if the corrections are of the order $\frac{1}{n^{2/3}}$.

In Fig. 6.5 we show in a ln plot our results for gravitational vector ($j = 2$) QN frequencies. Again, vector QN frequencies have the asymptotic behaviour given by expression (6.44), with a different correction term Corr_5 . Again, the $\frac{1}{n^{2/3}}$ corrections show themselves in the ln plot of Fig. 6.5: for very large imaginary parts, the slope is $-3/2$, as it should. The numerically extracted coefficient Corr_5 for $j = 2$ perturbations is listed in Table 6.7, along with the analytically predicted value (see section 6.3.2). the agreement is very good.

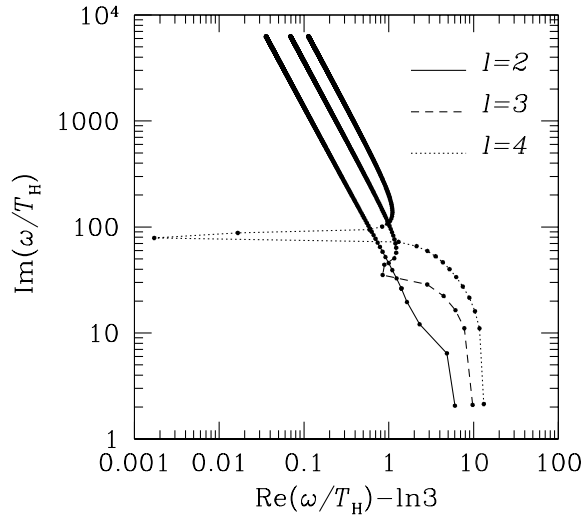


Figure 6.5: The QN frequencies of gravitational vector perturbations ($j = 2$) of a five-dimensional Schwarzschild black hole.

6.4 Discussion of results and future directions

We have made an extensive survey of the QNMs of the four and five dimensional Schwarzschild black hole. The investigation presented here makes a more complete characterization of the highly damped QNMs in the Schwarzschild geometry. In the four-dimensional case, we confirmed previous numerical results regarding the scalar and gravitational asymptotic QN frequencies. We found that both the leading behaviour and the first order corrections for the scalar and gravitational perturbations agree extremely well with existing analytical formulas. We have presented new numerical results concerning electromagnetic QN frequencies of the four-dimensional Schwarzschild geometry. In particular, this is the first work dealing with highly damped electromagnetic QNMs. Again, we find that the leading behaviour and the first order corrections agree with the analytical calculations. The first order corrections appear at the $\frac{1}{n^{3/2}}$ level. In the five-dimensional case this represents the first study on highly damped QNMs. We have seen numerically that the asymptotic behaviour is very well described by $\frac{\omega}{T_H} = \ln 3 + \pi i(2n + 1)$ for scalar and gravitational perturbations, and agrees with the predicted formula. Moreover the first order corrections appear at the level $\frac{1}{n^{2/3}}$, which is also very well described by the analytical calculations, providing one more consistency check on the theoretical framework. In generic D dimensions the corrections appear at the $\frac{1}{n^{(D-3)/(D-2)}}$ level. We have not been able to prove or disprove the analytic result for electromagnetic QN frequencies in five dimensions ($j = 2/3$). Other conclusions that can be taken from our work are: the monodromy method by Motl and Neitzke is correct. It is important to test it numerically, as we did, since there are some ambiguous assumptions in that method. Moreover, their method is highly flexible, since it allows an easy computation of the correction terms, as shown by Musiri and Siopsis, and generalized here for the higher dimensional Schwarzschild black hole. We have basically showed numerically that the monodromy method by Motl and Neitzke [35], and its extension by Musiri and Siopsis [114] to include for correction terms in

overtone number, are excellent techniques to investigate the highly damped QNMs of black holes.

Highly damped QNMs of black holes are the bed rocks that the recent conjectures [31, 33, 113] are built on, relating these to black hole area quantization. However, to put on solid ground the conjecture that QNMs can actually be of any use to black hole area quantization, one has to do much better than one has been able to do up to now. In particular, it is crucial to have a deeper understanding of the Kerr and Reissner-Nordström QNMs. These are, next to the Schwarzschild, the simpler asymptotically flat geometries. If these conjectures hold, they must do also for these spacetimes. Despite the fact that there are convincing numerical results for the Kerr geometry [43], there seems to be for the moment no serious analytical investigation of the highly damped QNMs for this spacetime. Moreover, even though we are in possession of an analytical formula for the highly damped QNMs of the Reissner-Nordström geometry [35], and this has been numerically tested already [71], we have no idea what it means! In particular, can one use it to quantize the black hole area? In this case the electromagnetic perturbations are coupled to the gravitational ones. How do we proceed with the analysis, that was so simple in the Schwarzschild geometry? Is the assumption of equally spaced eigenvalues a correct one, in this case? Can these ideas on black hole area quantization be translated to non-asymptotically flat spacetimes, as the de Sitter or anti-de Sitter spacetime? These are the fundamental issues that remain to be solved in this field. Should any of them be solved satisfactorily, then these conjectures would gain a whole new meaning. As they stand, it may just be a numerical coincidence that the real part of the QN frequency goes to $\ln 3$.

Chapter 7

Quasinormal modes of the four dimensional Kerr black hole

Contents

7.1	Introduction	89
7.2	Numerical method	91
7.3	Gravitational perturbations	92
7.4	Scalar and electromagnetic perturbations	97
7.5	The asymptotic behaviour of the modes' imaginary part	98
7.6	Algebraically special modes	99
7.7	Conclusions	102

7.1 Introduction

The study of linearized perturbations of black hole solutions in general relativity has a long history [40]. The development of the relevant formalism, initially motivated by the need of a formal proof of black hole stability, gave birth to a whole new research field. A major role in this field has been played by the concept of QNMs: oscillations having purely ingoing wave conditions at the black hole horizon and purely outgoing wave conditions at infinity. These modes determine the late-time evolution of perturbing fields in the black hole exterior. Numerical simulations of stellar collapse and black hole collisions in the “full” (non-linearized) theory have shown that in the final stage of such processes (“ringdown”) QNM’s dominate the black hole response to any kind of perturbation. Since their frequencies are uniquely determined by the black hole parameters (mass, charge and angular momentum), QNM’s are likely to play a major role in the nascent field of gravitational wave astronomy, providing unique means to “identify” black holes [9, 10].

An early attempt at relating classical black hole oscillations to the quantum properties of black holes was carried out by York [68]. More recently Hod made an interesting proposal [31], which has been described in the previous chapter. In light of these exciting new results,

Hod’s conjecture seems to be a very promising candidate to shed light on quantum properties of black holes. However, it is natural to ask whether the conjecture applies to more general (charged and/or rotating) black holes. If asymptotic frequencies for “generic” black holes depend (as they do) on the hole’s charge, angular momentum, or on the presence of a cosmological constant, should Hod’s proposal be modified in some way? And what is the correct modification? The hint for an answer necessarily comes from analytical or numerical calculations of highly damped QNM’s for charged and rotating black holes, or for black holes in non-asymptotically flat spacetimes. Some calculations in this direction have now been performed, revealing unexpected and puzzling features [71, 35, 106, 108, 129, 78].

In particular, the technique originally developed by Nollert to study highly damped modes of Schwarzschild black holes has recently been extended to the RN case [79], showing that highly damped RN QNM’s show a peculiar spiralling behaviour in the complex- ω plane as the black hole charge is increased. Independently, Motl and Neitzke obtained an analytic formula for the asymptotic frequencies of scalar and electromagnetic-gravitational perturbations of a RN black hole whose predictions show an excellent agreement (at least for large values of the charge) with the numerical results [35]. For computational convenience, Motl and Neitzke fixed their units in a somewhat unconventional way: they introduced a parameter k related to the black hole charge and mass by $Q/M = 2\sqrt{k}/(1+k)$, so that $\beta = 4\pi/(1-k) = 1/T_H$ is the inverse black hole Hawking temperature and $\beta_I = -k^2\beta$ is the inverse Hawking temperature of the inner horizon. Their result is an implicit formula for the QNM frequencies,

$$e^{\beta\omega} + 2 + 3e^{-\beta_I\omega} = 0, \quad (7.1)$$

and has now been confirmed by independent calculations [130]. However, its interpretation in terms of the suggested correspondence is still unclear. QN frequencies of a charged black hole, according to formula (7.1), depend not only on the black hole’s Hawking temperature, but also on the Hawking temperature of the (causally disconnected) inner horizon. Perhaps more worrying is the fact that the asymptotic formula does not yield the correct Schwarzschild limit as the black hole charge Q tends to zero. However this may well be due to higher-order corrections in $\omega_I^{-1/2}$; as we shall see, the numerical study of Kerr modes we present in this chapter (first presented in [43], but see also the more recent developments in [44]) seems to support such a conjecture. Finally and most importantly, it is not at all clear which are the implications of the non-periodic behaviour of asymptotic RN modes for the Hod conjecture. Maybe the complicated behaviour we observe is an effect of the electromagnetic-gravitational coupling, and we should only consider *pure gravitational perturbations* for a first understanding of black hole quantization based on Hod’s conjecture. The latter suggestion may possibly be ruled out on the basis of two simple observations: first of all, in the large damping limit “electromagnetic” and “gravitational” perturbations seem to be isospectral [35]; secondly, Kerr modes having $m = 0$ show a very similar spiralling behaviour, which is clearly *not* due to any form of electromagnetic-gravitational coupling.

The available numerical calculations for highly damped modes of black holes in non-asymptotically flat spacetimes are as puzzling as those for RN black holes in flat spacetime. Cardoso and Lemos [106] have studied the asymptotic spectrum of Schwarzschild black holes in a de Sitter background. They found that, when the black hole radius is comparable to the cosmological radius, the asymptotic spectrum depends not only on the hole’s parameters, but also on the angular separation index l . Quite worryingly the universality of the formula, that does not depend on dimensionality and gives the same limit for “scalar” and “gravitational”

modes (loosely using the standard four dimensional terminology; see [126, 73] for a more precise formulation in higher dimensions) seems to be lost when the cosmological constant is non-zero. This study has recently been generalized to higher dimensional Schwarzschild-de Sitter black holes in [107]. Higher-order corrections to the behaviour predicted in [106] have been found by Van den Brink [108]. The issue is not settled yet however, and the asymptotics may be different from what was predicted in [106]. Indeed, recent numerical calculations [111] seem to suggest that the analytical result in [106] is correct only when the overtone index n satisfies $nk \ll 1$, where k is the surface gravity at the Schwarzschild-de Sitter black hole horizon. For higher overtones, the behaviour seems to be different. One still needs a complete numerical verification, as it seems difficult to extract QNM frequencies for $nk > 1$ [111]. Calculations of QNM's for Schwarzschild-anti-de Sitter black holes were performed in various papers [75], showing that the nature of the QNM spectrum in this case is remarkably different (basically due to the “potential barrier” arising because of the cosmological constant, and to the changing QNM boundary conditions at infinity). Those calculations were recently extended to encompass asymptotic modes [78]. The basic result is that consecutive highly damped modes (whose real part goes to infinity as the imaginary part increases) have a uniform *spacing* in both the real and the imaginary part; this spacing is apparently independent of the kind of perturbation considered and of the angular separation index l .

The aim of this chapter is to study in depth the behaviour of highly damped Kerr QNM's, complementing and clarifying results that were presented in previous works [71, 131]. The plan of the chapter is as follows, and is based on the work presented in [43]. In section 7.2 we briefly introduce our numerical method. In section 7.3 we discuss some results presented in [71] and show a more comprehensive calculation of gravitational QNM's, considering generic values of m and higher multipoles (namely, $l = 3$). In section 7.4 we display some results for scalar and electromagnetic perturbations, showing that the asymptotic behaviour we observe for $l = m = 2$ gravitational perturbations seems to be very special. In section 7.5 we briefly summarize our results and we discuss the asymptotic behaviour of the modes' imaginary part. Finally, in section 7.6 we turn our attention to a different open problem concerning Kerr perturbations. Motivated by some recent, surprising developments arising from the study of the branch cut in the Schwarzschild problem [132] and by older conjectures steaming from analytical calculations of the properties of algebraically special modes [133], we turn our attention to Kerr QNM's in the vicinity of the Schwarzschild algebraically special frequencies. As the black hole is set into rotation, we find for the first time that a QNM multiplet appears close to the algebraically special Schwarzschild modes. A summary, conclusions and an overlook on possible future research directions follow.

7.2 Numerical method

A first numerical study of Kerr QNM's was carried out many years ago by Detweiler [134]. Finding highly damped modes through a straightforward integration of the perturbation equations is particularly difficult even for non-rotating black holes [9, 10]. In the Kerr case the situation is even worse, because, due to the non-spherical symmetry of the background, the perturbation problem does not reduce to a single ordinary differential equation for the radial part of the perturbations, but rather to a couple of differential equations (one for the angular

part of the perturbations, the other for the radial part).

A method to find the eigenfrequencies without resorting to integrations of the differential equations was developed by Leaver, and has been extensively discussed in the literature [17, 131, 71]. In this chapter we will apply exactly the same method. Following Leaver, we will choose units such that $2M = 1$. Then the perturbation equations depend on a parameter s denoting the spin of the perturbing field ($s = 0, -1, -2$ for scalar, electromagnetic and gravitational perturbations respectively), on the Kerr rotation parameter a ($0 < a < 1/2$), and on an angular separation constant A_{lm} . In the Schwarzschild limit the angular separation constant can be determined analytically, and is given by the relation $A_{lm} = l(l+1) - s(s+1)$. The basic idea in Leaver's method is the following. Boundary conditions for the radial and angular equations translate into convergence conditions for the series expansions of the corresponding eigenfunctions. In turn, these convergence conditions can be expressed as two equations involving continued fractions. Finding QNM frequencies is a two-step procedure: for assigned values of a , ℓ , m and ω , first find the angular separation constant $A_{lm}(\omega)$ looking for zeros of the *angular* continued fraction equation; then replace the corresponding eigenvalue into the *radial* continued fraction equation, and look for its zeros as a function of ω . Leaver's method is relatively well convergent and numerically stable for highly damped modes, when compared to other techniques [135]. We mention that an alternative, approximate method to find Kerr QN frequencies, that has the advantage of highlighting some physical features of the problem, has recently been presented [136].

In the next sections we will use Leaver's technique to complement numerical studies of Kerr QN overtones carried out by some of us in the past [131, 71]. As we just said, the method we use for our analysis is the one described in those papers. However, since we are pushing our numerics to their limits, we have systematically cross-checked all the results we present here using two independent codes. As we shall see, our study will uncover a plethora of interesting new features.

7.3 Gravitational perturbations

7.3.1 Modes having $l = m = 2$: a more extensive discussion

Let us consider rotating black holes, having angular momentum per unit mass $a = J/M$. The black hole's (event and inner) horizons are given in terms of the black hole parameters by $r_{\pm} = M \pm \sqrt{M^2 - a^2}$. The hole's temperature $T_H = (r_+ - r_-)/A$ where $A = 8\pi M r_+$ is the hole's surface area, related to its entropy S by the relation $A = S/4$. Introducing the angular velocity of the horizon $\Omega = 4\pi a/A$, applying the first law of black hole thermodynamics,

$$\Delta M = T_H \Delta S + \Omega \Delta J, \quad (7.2)$$

and assuming that the formula for the area spectrum derived for a Schwarzschild black hole still holds in this case, Hod conjectured that the real parts of the asymptotic frequencies for rotating black holes are given by:

$$\omega_R = \tilde{\omega}_R = T_H \ln 3 + m\Omega, \quad (7.3)$$

where m is the azimuthal eigenvalue of the field [31]. Hod later used a systematic exploration of moderately damped Kerr black hole QNM's carried out a few years ago by one of us [131]

to lend support to formula (7.3), at least for modes having $l = m$ [137]. His conclusions were shown to be in contrast with the observed behaviour of modes having stronger damping in [71]: the deviations between the numerics and formula (7.3) were indeed shown to *grow* as the mode order grows (see figure 7 in [71]). Hod even used (7.2), *without including the term due to variations of the black hole charge ΔQ* , to conjecture that (7.3) holds for Kerr–Newman black holes as well [31]. This second step now definitely looks as a bold extrapolation. Not only does formula (7.3) disagree with the observed numerical behaviour for perturbations of Kerr black holes having $l = m = 2$ [71] (not to mention other values of m , as we shall see in the following); by now, analytical and numerical calculations have now shown that RN QNM’s have a much more rich and complicated behaviour [71, 35, 127]. Summarizing, there is now compelling evidence that the conjectured formula (7.3) must be wrong. However it turns out [71], quite surprisingly, that an extremely good fit to the numerical data for $l = m = 2$ is provided by an even simpler relation, not involving the black hole temperature:

$$\omega_R = m\Omega. \tag{7.4}$$

Is this just a coincidence? After all, this formula does not yield the correct Schwarzschild limit; why should we trust it when it is only based on numerical evidence? A convincing argument in favour of formula (7.4) is given in figure 7.1. There we show the real part of modes having $l = m = 2$ as a function of n at fixed a , for some selected values of a (namely, $a = 0.00, 0.05, ..0.45$). The convergence to the limiting value $\omega_R = 2\Omega$ (horizontal lines in the plot) is evident. Furthermore, the convergence is much faster for holes spinning closer to the extremal limit, and becomes slower for black holes which are slowly rotating. In our opinion, this lends support to the idea that the Schwarzschild limit may not be recovered straightforwardly as $a \rightarrow 0$, and that some order-of-limits issues may be at work, as recently claimed in [127] to justify the incorrect behaviour of formula (7.1) as the black hole charge $Q \rightarrow 0$.

Is formula (7.4) just an approximation to the “true” asymptotic behaviour, for example a lowest–order expansion in powers of Ω ? To answer this questions we can try and replace (7.4) by some alternative relation. Since in the Schwarzschild limit (7.4) doesn’t give the desired “ $\ln 3$ ” behaviour, we would like a higher–order correction that *does* reproduce the non–rotating limit, while giving a good fit to the numerical data. Therefore, in addition to formulas (7.3) and (7.4), we tried out the following fitting relations:

$$\omega_R = 4\pi T_H^2 \ln 3 + m\Omega = T_H \ln 3(1 - \Omega^2) + m\Omega, \tag{7.5}$$

$$\omega_R = T_H \ln 3(1 - m^2\Omega^2) + m\Omega. \tag{7.6}$$

Formula (7.5) enforces the correct asymptotic limit at $a = 0$, and can be seen as an Ω^2 –correction of Hod’s relation. Since numerical results suggest a dependence on $m\Omega$ we also used the slight modification given by formula (7.6), hoping it could turn out to fit better our numerical data. The relative errors of the various fitting formulas with respect to the numerical computation for a the $n = 40$ QNM are given in figure 7.2. Once again, formula (7.4) is clearly the one which performs better. All relations are seen to fail quite badly for small rotation rate, but this apparent failure is only due to the onset of the asymptotic behaviour occurring *later* (that is, when $n > 40$) for small values of a .

We think that the excellent fitting properties and the convergence plot, when combined together, are very good evidence in favour of formula (7.4). Therefore, let us assume (7.4) is the correct formula (at least for $l = m = 2$, and maybe for large enough a), and let's look at its consequences in computing the area spectrum for Kerr black holes. Modes having $l = m$ may be the relevant ones to make a connection with quantum gravity, as recently claimed in [137]. The proportionality of these modes to the black hole's angular velocity Ω seems to suggest that something deep is at work in this particular case.

In the following, we will essentially repeat the calculation carried out by Abdalla *et al.* [129] for extremal ($a = M$) Kerr black holes. We will argue that the conclusion of their calculation may in fact be wrong, since those authors did not take into account the (then unknown) functional behaviour of $\omega_R(a)$, but rather assumed $\omega_R = m/2M$ (=constant) in the vicinity of the extremal limit. In following the steps traced out in [129] we will restore for clarity all factors of M . This means, for example, that the asymptotic frequency for $m > 0$ in the extremal limit is $\omega = m/2M$. Let us also define $x = a/M$. The black hole inner and outer horizons are $r_{\pm} = M [1 \pm \sqrt{1 - x^2}]$. The black hole temperature is

$$T = \frac{r_+ - r_-}{A} = \frac{1}{4\pi M} \frac{\sqrt{1 - x^2}}{1 + \sqrt{1 - x^2}}, \quad (7.7)$$

where

$$A = 8\pi M r_+ = 8\pi M^2 \left[1 + \sqrt{1 - x^2}\right] \quad (7.8)$$

is the hole's surface area, related to its entropy S by the relation $A = S/4$. The hole's rotational frequency is

$$\Omega = \frac{4\pi a}{A} = \frac{a}{2Mr_+} = \frac{1}{2M} \frac{x}{1 + \sqrt{1 - x^2}}. \quad (7.9)$$

Let us now apply the first law of black hole thermodynamics and the area-entropy relation to find

$$\Delta A = \frac{4}{T} (\Delta M - \Omega \Delta J). \quad (7.10)$$

The authors of [129] focused on the extremal limit. They used $\Delta J = \hbar m$ and $\Delta M = \hbar \omega_R(x = 1) = \hbar m/2M$ to deduce that

$$\Delta A = 4\hbar m \left[\frac{1/2M - \Omega}{T} \right] = \hbar m \mathcal{A}. \quad (7.11)$$

where \mathcal{A} is the area quantum. Now, the square parenthesis is undefined, since $\Omega \rightarrow 1/2M$ when $x \rightarrow 1$. Taking the limit $x \rightarrow 1$ and keeping $\Delta M = \hbar m/2M$ constant leads to

$$\mathcal{A} = 8\pi \left(1 + \sqrt{\frac{1-x}{2}} \right) \simeq 8\pi, \quad (7.12)$$

which is the final result in [129]. The fundamental assumption in this argument is that the asymptotic frequency $\omega_R = m/2M$, which is true only for $x = 1$. However one has to consider how the QNM frequency changes with x , and our numerical QNM calculations show that assuming it is constant ($\omega_R = m/2M$) is not justified. What is the effect of assuming

$\omega_R = m\Omega$ on the area spectrum? The calculation is exactly the same, but the equation $\Delta M = \hbar m/2M$ is replaced by $\Delta M = \hbar m\Omega$, and we conclude

$$\Delta A = 0. \tag{7.13}$$

The area variation is *zero* at any black hole rotation rate. At first sight, this result may look surprising. It is not, and it follows from fundamental properties of black holes. Indeed, we are looking at reversible black hole transformations. It is well known that the gain in energy ΔE and the gain in angular momentum ΔJ resulting from a particle with negative energy $-E$ and angular momentum $-L_z$ arriving at the event horizon of a Kerr black hole is subject to the inequality

$$\Delta M \geq \Omega \Delta J; \tag{7.14}$$

see, for example, formula (352) on page 373 in [40] and the related discussion. This inequality is equivalent to the statement that the irreducible mass $M_{irr} \equiv (Mr_+/2)^{1/2}$ of the black hole can only increase [138], or that by no continuous infinitesimal process involving a single Kerr black hole can the surface area of the black hole be decreased (Hawking's area theorem). Assuming the validity of Hod's conjecture, and using the result (7.4) for asymptotic QNM's, we are saturating the inequality (7.14); in other words, we are in presence of a *reversible* process, in which the area (or the irreducible mass, which is the same) is conserved. This is indeed the content of equation (7.13).

The result (7.13) can either mean that using modes having $l = m$ in Hod's conjecture is wrong, or that we cannot use Bohr's correspondence principle to deduce the area spectrum for Kerr. A speculative suggestion may be to *modify Bohr's correspondence principle as introduced by Hod*. For example, if we do not interpret the asymptotic frequencies as a change in *mass* ($\Delta M = \hbar\omega_R$) but rather impose $T\Delta S = \hbar\omega_R$ (this is of course equivalent to Hod's original proposal when $a = 0$), the asymptotic formula would imply, using the first law of black hole mechanics, that the minimum possible variation in mass is $\Delta M = 2m\hbar\Omega$.

7.3.2 Modes having $l = 2, l \neq m$

From the discussion in the previous paragraph we feel quite confident that the real part of modes having $l = m = 2$ approaches the limit $\omega_R = m\Omega$ as the mode damping tends to infinity. What about modes having $l \neq m$? In [71] it was shown that modes having $m = 0$ show a drastically different behaviour. As the damping increases, modes show more and more loops; pushing the calculation to very high dampings is not easy, but the trend strongly suggests a spiralling asymptotic behaviour, reminiscent of RN modes. In this section we present results for the cases not considered in [71], concentrating on the real parts of modes having $l = 2$ and $m = 1, -1, -2$.

Modes having $l = 2, m = 1$ are displayed in figure 7.3. They do not seem to approach the limit one could naively expect, that is, $\omega_R = \Omega$. The real part of the frequency shows instead a minimum as a function of a , and approaches the limit $\omega_R = m$ as $a \rightarrow 1/2$. The fact that the real part of modes having $l = 2$ and $m = 1$ approaches $\omega_R = m = 1$ as $a \rightarrow 1/2$ has not been observed before, to our knowledge. We will see later that this behaviour is characteristic of QNM's due to perturbation fields having arbitrary spin as long as $m > 0$.

The real parts of modes having $l = 2, m < 0$ as functions of a (for some selected values of n) are displayed in figure 7.4. From the left panel, displaying the real part of modes having

$m = -1$, we infer an interesting conclusion: the frequencies tend to approach a constant (presumably a -independent) limiting value, with a convergence rate which is faster for large a , as in the $l = m = 2$ case. The limiting value is approximately given by 0.12. A similar result holds for modes having $l = 2$, $m = -2$ (right panel). Once again the frequencies seem to asymptotically approach a (roughly) constant value, with a convergence rate which is faster for large a . The limiting value is now approximately given by $\omega_R = 0.24$, about twice the value we got for $m = -1$. Concluding, an extremely interesting result emerges from our calculations: the real part of modes having $m < 0$ seems to asymptotically approach the limit

$$\omega_R = -m\varpi, \quad (7.15)$$

where $\varpi \simeq 0.12$ is to a good approximation independent of a . We have not yet been able to obtain this result analytically, but an analytical calculation is definitely needed. It may offer some insight on the physical interpretation of the result, and help explain the surprising qualitative difference in the asymptotic behaviour of modes having different values of m .

7.3.3 Modes having $l = 3$

Results for a few highly-damped modes having $l = 3$, $m = 0$ were shown in [71]. Those modes exhibit the usual “spiralling” behaviour in the complex plane as the damping increases. In this paragraph we present a more complete calculation of modes having $l = 3$. Unfortunately we did not manage to push the calculation to values of n larger than about 50. The algebraically special frequency separating the lower QNM branch from the upper branch corresponds to $n = 41$ when $l = 3$, so we cannot be completely sure that our calculations are indicative of the asymptotic behaviour.

However, some prominent features emerge from the general behaviour of the real part of the modes, as displayed in the different panels of figure 7.5. First of all, contrary to our expectations, neither the branch of modes having $m = 3$ nor the branch having $m = 2$ seem to approach the limit $m\Omega$. These modes show a behaviour which is more closely reminiscent of modes having $l = 2$, $m = 1$: the modes’ real part “bends” towards the zero-frequency axis, shows a minimum as a function of a , and tends to $\omega_R = m$ as $a \rightarrow 1/2$. We stress that the observed behaviour should not be taken as the final word on the problem, since we should probably look at modes having $n \gtrsim 100$ to observe the true asymptotic behaviour. However, should not the qualitative features of the modes at larger n drastically change, we would face a puzzling situation. Indeed, gravitational modes with $l = m = 2$ would have a rather unique asymptotic behaviour, that would require more physical understanding to be motivated.

Another prominent feature is that, whenever $m > 0$, there seems to be an infinity of modes approaching the limit $\omega_R = m$ as the hole becomes extremal. This behaviour confirms the general trend we observed for $l = 2$, $m > 0$.

Finally, our calculations of modes having $m < 0$ show, once again, that these modes tend to approach $\omega_R = -m\varpi$, where $\varpi \simeq 0.12$. We display, as an example, modes having $l = 3$ and $m = -1$ in the bottom right panel of figure 7.5.

7.4 Scalar and electromagnetic perturbations

The calculations we have performed for $l = 3$ hint at the possibility that modes having $l = m = 2$ are the only ones approaching the limit $\omega_R = m\Omega$. However, as we have explained, reaching the asymptotic regime for modes having $l > 2$ is difficult. The reason is quite simple to understand. The (pure imaginary) Schwarzschild algebraically special mode, located at

$$\tilde{\Omega}_l = \frac{-i(l-1)l(l+1)(l+2)}{6} \quad (7.16)$$

and marking the onset of the asymptotic regime moves quickly downwards in the complex plane as l increases. Therefore, calculations in the asymptotic regime rapidly become impracticable as l grows.

This technical difficulty is a hindrance if we want to test whether the observed behaviour of gravitational modes having $l = m = 2$ is in some sense “unique”. An alternative idea to check this “uniqueness” is to look, not at gravitational modes having different l ’s, but at perturbations due to fields having different spin and $l \leq 2$. In particular, here we show some results we obtained extending our calculation to scalar ($s = 0$) and electromagnetic ($s = -1$) modes. Results for Kerr scalar modes, to our knowledge, have only been published in [136]; some highly damped electromagnetic modes were previously computed in [131].

7.4.1 Scalar modes

In figure 7.6 we show a few scalar modes having $l = m = 0$. As we could expect from existing calculations [71, 136] the modes show the typical spiralling behaviour; the surprise here is that this spiralling behaviour sets in very quickly, and is particularly pronounced even if we look at the first overtone ($n = 2$). As the mode order grows, the number of spirals grows, and the centre of the spiral (corresponding to extremal Kerr holes) moves towards the pure imaginary axis, at least for $n \lesssim 10$.

In figure 7.7 we show the trajectories of some scalar modes for $l = 2$. As can be seen in the top left panel, rotation removes the degeneracy of modes having different values of m . If we follow modes having $m = 0$ we see the usual spiralling behaviour, essentially confirming results obtained in [136] using the Prüfer method. However our numerical technique seems to be more accurate than Prüfer’s method, which is intrinsically approximate, and we are able to follow the modes up to larger values of the rotation parameter (compare the bottom right panel in our figure 7 to figure 6 in [136], remembering that their numerical values must be multiplied by a factor 2 due to the different choice of units). On the basis of our numerical results, it is quite likely that the asymptotic behaviour of scalar modes having $l = m = 0$ is described by a formula similar to (7.1). However, at present, no such formula has been analytically derived.

In figure 7.8 we show the real part of scalar modes having $l = m = 1$ and $l = m = 2$ as a function of a for increasing values of the mode index. In both cases modes do not show a tendency to approach the $\omega_R = m\Omega$ limit suggested by gravitational modes with $l = m = 2$. Once again (as we observed for modes having $l = 3$ and $m > 0$) the behaviour is more similar to that of gravitational modes with $l = 2$ and $m = 1$. This may be considered further evidence that gravitational perturbations having $l = m = 2$ are indeed a very special case.

7.4.2 Electromagnetic modes

The calculation of highly damped electromagnetic QNM's basically confirms the picture we obtained from the computation of scalar QNM's presented in the previous section. We show some selected results in figure 7.9. The top left panel of figure 7.9 shows that the real part of electromagnetic QNM's having $m > 0$ tend, for large damping, to show a local minimum and approach the limit $\omega_R = m$ as $a \rightarrow 1/2$. The top right panel shows that the real parts of modes having $l = 1$ and $m = 0$ quickly start oscillating (that is, QNM's display spirals in the complex- ω plane). Finally, the bottom plots show the behaviour of modes having $l = 1$, $m = -1$ (left) and $l = 2$, $m = -2$ (right). Once again, modes seem to approach a roughly constant value $\omega \simeq -m\varpi$. However, our computations probably break down too early to draw any final conclusion on this.

7.5 The asymptotic behaviour of the modes' imaginary part

The evidence for a universality of behaviour emerging from the calculations we have presented in the previous sections is suggestive. Calling for some caution, due to the fact that we may not always be in the asymptotic regime when our numerical codes become unreliable, we can still try and draw some conclusions. Our results suggest that, whatever the kind of perturbation (scalar, electromagnetic or gravitational) that we consider, asymptotic modes belong to one of three classes:

1) Modes having $m > 0$: their real part probably approaches the limit $\omega_R = m\Omega$ only for gravitational modes having $l = m$ (our calculation for $l = m = 3$ is not conclusive in this respect, since we are not yet in the asymptotic regime). For other kinds of perturbations, or for $m \neq l$, ω_R apparently shows a minimum as a function of a . This may be a real feature of asymptotic modes, but it may as well be due to the asymptotic behaviour emerging only for larger values of n . To choose between the two alternatives we would either require better numerical methods or the development of analytical techniques. A “universal” feature is that, whatever the spin of the perturbing field, QNM frequencies approach the limiting value $\omega_R = m$ as $a \rightarrow 1/2$.

2) Modes having $m = 0$: these modes show a spiraling behaviour in the complex plane, reminiscent of RN QNM's.

3) Modes having $m < 0$: their real part seems to asymptotically approach a constant (or weakly a -dependent) limit $\omega_R \simeq -m\varpi$, where $\varpi \simeq 0.12$, whatever the value of l and the spin of the perturbing field. Maybe this limit is not exactly independent of a , but on the basis of our numerical data we are quite confident that highly damped modes with $m < 0$ tend to a universal limit $\omega_R \simeq -m\varpi_{ext}$, where ϖ_{ext} has some value between 0.11 and 0.12, as $a \rightarrow 1/2$.

What about the modes' imaginary part? In [71] we observed that the following formula holds for gravitational modes having $l = m = 2$:

$$\omega_{l=m=2}^{Kerr} = 2\Omega + i2\pi T_H n. \quad (7.17)$$

Our numerical data show that, in general, all modes having $m > 0$, *whatever the kind of perturbation* (scalar, electromagnetic or gravitational) we consider, have an asymptotic separation equal to $2\pi T_H$ if $m > 0$. For $m = 0$ the imaginary part oscillates, and this beautiful,

general result does not hold. It turns out that it doesn't hold as well for modes having $m < 0$. An analysis of our numerical data did not lead us, up to now, to any conclusion on the asymptotic separation of modes having $m < 0$. This may hint at the fact that for $m < 0$ our calculations are not yet indicative of the asymptotic regime. Therefore, some care is required in drawing conclusions on asymptotic modes from our results for $m < 0$.

7.6 Algebraically special modes

7.6.1 An introduction to the problem

Algebraically special modes of Schwarzschild black holes have been studied for a long time, but only recently their understanding has reached a satisfactory level. Among the early studies rank those of Wald [139] and of Chandrasekhar [140], who gave the exact solution of the Regge–Wheeler, Zerilli and Teukolsky equations at the algebraically special frequency. The nature of the QNM boundary conditions at the Schwarzschild algebraically special frequency is extremely subtle, and has been studied in detail by Van den Brink [133]. Black hole oscillation modes belong to three categories:

- 1) “standard” QNM’s, which have outgoing wave boundary conditions at both sides (that is, they are outgoing at infinity and “outgoing into the horizon”, using Van den Brink’s “observer-centered definition” of the boundary conditions);
- 2) total transmission modes from the left ($T\text{TM}_L$ ’s) are modes incoming from the left and outgoing to the other side;
- 3) total transmission modes from the right ($T\text{TM}_R$ ’s) are modes incoming from the right and outgoing to the other side.

In our units, the Schwarzschild “algebraically special” frequency is given by formula (7.16), and has been traditionally associated with TTM’s. However, when Chandrasekhar found the exact solution of the perturbation equations at the algebraically special frequency he did not check that these solutions satisfy TTM boundary conditions. In [133] it was shown that, in general, they don’t. An important conclusion reached in [133] is that the Regge–Wheeler equation and the Zerilli equation (which are known to yield the same QNM spectrum, being related by a supersymmetry transformation) have to be treated on different footing at $\tilde{\Omega}_l$, since the supersymmetry transformation leading to the proof of isospectrality is singular there. In particular, the Regge-Wheeler equation has *no modes at all* at $\tilde{\Omega}_l$, while the Zerilli equation has *both a QNM and a $T\text{TM}_L$* .

Numerical calculations of algebraically special modes have yielded some puzzling results. Leaver [17] (studying the Regge-Wheeler equation, that should have no QNM’s at all according to Van den Brink’s analysis, and not the Zerilli equation) found a QNM which is very close, but not exactly located *at*, the algebraically special frequency. Namely, he found QNM’s at frequencies $\tilde{\Omega}'_l$ such that

$$\tilde{\Omega}'_2 = 0.000000 - 3.998000i, \quad \tilde{\Omega}'_3 = -0.000259 - 20.015653i. \quad (7.18)$$

Notice that the “special” QNM’s $\tilde{\Omega}'_l$ are such that $\Re i\tilde{\Omega}'_2 < |\tilde{\Omega}_2|$, $\Re i\tilde{\Omega}'_3 > |\tilde{\Omega}_3|$, and that the real part of $\tilde{\Omega}'_3$ is not zero. Van den Brink [133] speculated that the numerical calculation may be inaccurate and the last three digits may not be significant, so that no conclusion can be drawn on the coincidence of $\tilde{\Omega}_l$ and $\tilde{\Omega}'_l$, “if the latter does exist at all”.

An independent calculation was carried out by Andersson [141]. Using a phase–integral method, he found that the Regge–Wheeler equation has pure imaginary TTM_R 's which are very close to $\tilde{\Omega}_l$ for $2 \leq l \leq 6$. He therefore suggested that the modes he found coincide with $\tilde{\Omega}_l$, which would then be a TTM. Van den Brink [133] observed that, if all figures in the computed modes are significant, the coincidence of TTM's and QNM's is not confirmed by this calculation, since $\tilde{\Omega}'_l$ and $\tilde{\Omega}_l$ are numerically (slightly) different.

Onozawa [131] showed that the Kerr mode having $n = 9$ tends to $\tilde{\Omega}_l$ as $a \rightarrow 0$, but suggested that modes approaching $\tilde{\Omega}_l$ from the left and the right may cancel each other at $a = 0$, leaving only the special (TTM) mode. He also calculated this (TTM) special mode for Kerr black holes, solving the relevant condition that the Starobinsky constant should be zero and finding the angular separation constant by a continued fraction method; his results improved upon the accuracy of those previously obtained in [140].

The analytical approach adopted in [133] clarified many aspects of the problem for Schwarzschild black holes, but the situation concerning Kerr modes branching from the algebraically special Schwarzschild mode is still far from clear. In [133] Van den Brink, using slow–rotation expansions of the perturbation equations, drew two basic conclusions on these modes. The first is that, for $a > 0$, the so–called Kerr special modes (that is, solutions to the condition that the Starobinsky constant should be zero [140, 131]) are all TTM's (left or right, depending on the sign of the spin). The TTM_R 's cannot survive as $a \rightarrow 0$, since they do not exist in the Schwarzschild limit; this is related to the limit $a \rightarrow 0$ being a very tricky one. In particular, in this limit, the special Kerr mode becomes a TTM_L for $s = -2$; furthermore, the special mode and the TTM_R cancel each other for $s = 2$. Studying the limit $a \rightarrow 0$ in detail, Van den Brink reaches a second important conclusion: the Schwarzschild special frequency $\tilde{\Omega}_l$ is a limit point for a multiplet of “standard” Kerr QNM's, which for small a are well approximated by

$$\omega = -4i - \frac{33078176}{700009}ma + \frac{3492608}{41177}ia^2 + \mathcal{O}(ma^2) + \mathcal{O}(a^4) \quad (7.19)$$

when $l = 2$, and by a more complicated formula – his equation (7.33) – when $l > 2$. We will see in the next section that, unfortunately, none of the QNM's we numerically found seems to approach this limit when the rotation rate a is small.

Van den Brink suggested (see note [46] in [133]) that QNM's corresponding to the algebraically special frequency and having $m > 0$ may have one of the following three behaviours in the Schwarzschild limit: they may merge with those having $m < 0$ at a frequency $\tilde{\Omega}'_l$ such that $|\tilde{\Omega}'_l| < |\tilde{\Omega}_l|$ (but $|\tilde{\Omega}'_l| > |\tilde{\Omega}_l|$ for $l \geq 4$) and disappear, as suggested by Onozawa [131]; they may terminate at some (finite) small a ; or, finally, they may disappear towards $\omega = -i\infty$. Recently Van den Brink *et al.* [132] put forward another possibility: studying the branch cut on the imaginary axis, they found that in the Schwarzschild case a pair of “unconventional damped modes” should exist. For $l = 2$, these modes are identified by a fitting procedure to be located at

$$\omega_{\pm} = \mp 0.027 + (0.0033 - 4)i. \quad (7.20)$$

An approximate analytical calculation confirms the presence of these modes, yielding

$$\omega_+ \simeq -0.03248 + (0.003436 - 4)i, \quad (7.21)$$

in reasonable agreement with (7.20). If their prediction is true, an *additional* QNM multiplet should emerge, as a increases, near $\tilde{\Omega}_l$; this multiplet “*may well be due to ω_{\pm} splitting (since*

spherical symmetry is broken) and moving through the negative imaginary axis as a is tuned” [132]. In the following paragraph we will show that a careful numerical search reveals, indeed, the emergence of such multiplets, but these do not seem to behave exactly as predicted in [132].

7.6.2 Numerical search and QNM multiplets

As we have summarized in the previous paragraph, the situation for Kerr modes branching from the algebraically special Schwarzschild mode is still unclear. Is a multiplet of modes emerging from the algebraically special frequency when $a > 0$? Can QNM’s be matched by the analytical prediction (7.19) at small values of a ? If a doublet does indeed appear, as recently suggested in [132], does it tend to the algebraically special frequency $\tilde{\Omega}_2 = -4i$ as $a \rightarrow 0$, does it tend to the values predicted by formula (7.20), or does it go to some other limit?

After carrying out an extensive numerical search with both of our numerical codes, we have indeed found some surprises. Our main new result is shown in the left panel of figure 7.10. There we show the trajectories in the complex plane of QNM’s having $l = 2$ and $m > 0$: a *doublet* of modes does indeed appear close to the algebraically special frequency. Both modes in the doublet tend to the usual limit ($\tilde{\Omega}_2 = m$) as $a \rightarrow 1/2$. We have tried to match these “twin” modes with the predictions of the analytical formula (7.19). Unfortunately, none of the two branches we find seems to agree with (7.19) at small a . Our searches succeeded in finding a mode doublet only when $m > 0$. For $m \leq 0$ the behaviour of the modes is, in a way, more conventional. For example, in the right panel of figure 7.10 we see the $l = 2$, $m = 0$ mode coming out of the standard algebraically special frequency $\tilde{\Omega}_2$ and finally describing the “usual” spirals as a increases.

In the top left panel of figure 7.11 we see that the real part of all modes having $m \geq 0$ does indeed go to zero as $a \rightarrow 0$, with an m -dependent slope. However, the top right panel in the same figure shows that the imaginary part of the modes does *not* tend to -4 as $a \rightarrow 0$. This behaviour agrees quite well, at least qualitatively, with that predicted by formula (7.20). Extrapolating our numerical data to the limit $a \rightarrow 0$ yields, however, slightly different numerical values; our extrapolated values for $l = 2$ are $\omega = (-4 - 0.10)i$ and $\omega = (-4 + 0.09)i$.

At present, we have no explanation for the appearance of the doublet only when $m > 0$. A numerical confirmation of this behaviour comes from numerical searches we have carried out close to the algebraically special frequency $\tilde{\Omega}_3$. There we observed a similar behaviour: a multiplet of modes appears only when $m > 0$. In particular, we see the appearance of a doublet that behaves quite similarly to the modes shown in the left panel of figure 7.10. Extrapolating the numerical data for the $l = 3$ doublet yields the values $\omega = (-20 - 0.19)i$ and $\omega = (-20 + 0.24)i$ as $a \rightarrow 0$.

A more careful search around the algebraically special frequency $\tilde{\Omega}_3$ surprisingly revealed the existence of other QNM’s. However, we don’t trust our numerics enough to present our findings in this chapter. The additional modes we find may well be “spurious” modes due to numerical inaccuracies, since we are pushing our method to its limits of validity (very high dampings and very small imaginary parts). Our numerical data will be made available on request to those who may be interested.

7.7 Conclusions

In this chapter we have numerically investigated the behaviour of highly damped QNM's for Kerr black holes, using two independent numerical codes to check the reliability of our results. Our findings do not agree with the simple behaviour conjectured by Hod's for the real part of the frequency [31, 137] as given in formula (7.3). We did not limit our attention to gravitational modes, thus filling some gaps in the existing literature.

Our main results concerning highly damped modes can be summarized as follows. Scalar, electromagnetic and gravitational modes show a remarkable universality of behaviour in the high damping limit. The asymptotic behaviour crucially depends, for any kind of perturbation, on whether $m > 0$, $m = 0$ or $m < 0$. As already observed in [71], the frequency of gravitational modes having $l = m = 2$ tends to $\omega_R = 2\Omega$, Ω being the angular velocity of the black hole horizon. We showed that, if Hod's conjecture is valid, this asymptotic behaviour is related to *reversible black hole transformations*, that is, transformations for which the black hole irreducible mass (and its surface area) does not change. Other (gravitational and non-gravitational) modes having $m > 0$ do *not* show a similar asymptotic behaviour in the range of n allowed by our numerical method. In particular, in the high-damping limit, the real part of (gravitational and non-gravitational) modes having $m > 0$ typically shows a minimum as a function of the rotation parameter a , and then approaches the limit $\omega_R = m$ as the black hole becomes extremal. At present we cannot exclude the possibility that our calculations actually break down *before* we reach the asymptotic regime. Better numerical methods or analytical techniques are needed to give a final answer concerning the asymptotic behaviour of modes having $m > 0$.

An interesting new finding of this chapter is that for all values of $m > 0$, and for any kind of perturbing field, there seems to be an infinity of modes tending to the critical frequency for superradiance, $\omega_R = m$, in the extremal limit. This finding generalizes a well-known analytical result by Detweiler for QNM's having $l = m$ [134, 136]. It would be interesting to generalize Detweiler's proof, which only holds for $l = m$, to confirm our conjecture that for *any* $m > 0$ there is an infinity of QNM's tending to $\omega_R = m$ as $a \rightarrow 1/2$.

The real part of modes having $l = 2$ and *negative* m asymptotically approaches a value $\omega_R \simeq -m\varpi$, $\varpi \simeq 0.12$ being (almost) independent of a . Maybe this limit is not exactly independent of a , but on the basis of our numerical data we feel quite confident that highly damped modes with $m < 0$ do tend to a universal limit $\omega_R \simeq -m\varpi_{ext}$ (where ϖ_{ext} has some value between 0.11 and 0.12) as $a \rightarrow 1/2$.

This is an interesting prediction, and it would again be extremely useful to confirm it using analytical techniques. Up to now, we have not been able to find any simple explanation for this limiting value. For example, we have tentatively explored a possible connection between ϖ and the frequencies of marginally stable counterrotating photon orbits, but we could not find any obvious correlation between the two.

Both for gravitational and for non-gravitational perturbations, the trajectories in the complex plane of modes having $m = 0$ show a spiralling behaviour, strongly reminiscent of the one observed for Reissner-Nordström (RN) black holes, and probably well approximated in the high damping limit by a formula similar to (7.1).

Last but not least, an important result concerning highly damped modes is that, for any perturbing field, the asymptotic separation in the imaginary part of consecutive modes having $m > 0$ is given by $2\pi T_H$ (T_H being the black hole temperature). This is presumably related

to the fact that QNM's determine the position of the poles of a Green's function on the black hole background, and that the Euclidean black hole solution converges to a thermal circle at infinity having temperature T_H ; so it is not surprising that the spacing in asymptotic QNM's coincides with the spacing, $2\pi iT_H$, expected for a thermal Green's function [35]. This simple relation concerning the mode spacing does not seem to hold when $m \leq 0$.

Finally, we studied numerically in some detail modes branching from the so-called "algebraically special frequency" of Schwarzschild black holes. We found numerically for the first time that QNM *multiplets* emerge from the algebraically special modes as the black hole rotation increases, confirming a recent speculation [132]. However, we found some quantitative disagreement with the analytical predictions presented in [133, 132], that deserves further investigation.

Our numerical results will hopefully serve as an important guide in the analytical search for asymptotic QNM's of Kerr black holes. Although one can in principle apply Motl and Neitzke's [35] method in the present case, the Kerr geometry has some special features that complicate the analysis. The Teukolsky equation describing the field's evolution no longer has the Regge-Wheeler-Zerilli (Schrödinger-like) form; however, it can be reduced to that form by a suitable transformation of the radial coordinate. The main technical difficulty concerns the fact that the angular separation constant A_{lm} is not given analytically in terms of l , as it is in the Schwarzschild or RN geometry; even worse, it depends on the frequency ω in a non linear way. Therefore, an analytical understanding of the problem must encompass also an understanding of the asymptotic properties of the separation constant. The scalar case is well studied, both analytically and numerically [142], but a similar investigation for the electromagnetic and gravitational perturbations is still lacking. An idea we plan to exploit in the future is to use a numerical analysis of the angular equation as a guideline to find the asymptotic behaviour of A_{lm} . Once the asymptotic behaviour of A_{lm} is determined, the analysis of the radial equation may proceed along the lines traced in [35].

Table 7.1: Caption of the table.

r_+	Scalar ($l = 0$)		Axial ($l = 2$)		Polar ($l = 2$)	
r_+	min	max	min	max	min	max
100	0.366	0.474	0.366	0.474	0.366	0.474
50	0.366	0.474	0.366	0.474	0.366	0.474
10	0.367	0.475	0.368	0.476	0.369	0.477
5	0.372	0.480	0.376	0.483	0.376	0.488
1	0.468	0.571	-	-	0.503	-

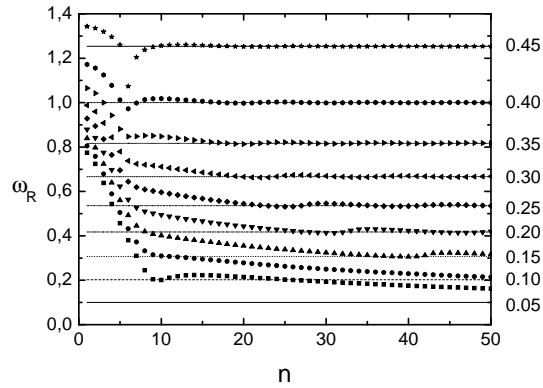


Figure 7.1: Each different symbol corresponds to the (numerically computed) value of ω_R as a function of the mode index n , at different selected values of the rotation parameter a . The selected values of a are indicated on the right of the plot. Horizontal lines correspond to the predicted asymptotic frequencies 2Ω at the given values of a . Convergence to the asymptotic value is clearly faster for larger a . In the range of n allowed by our numerical method ($n \lesssim 50$) convergence is not yet achieved for $a \lesssim 0.1$.

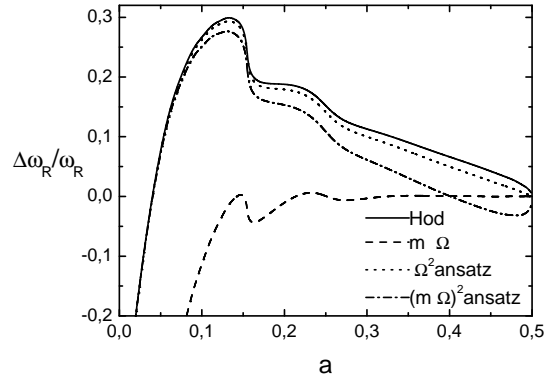


Figure 7.2: Relative difference between various fit functions and numerical results for the mode having index $n = 40$. From top to bottom in the legend, the lines correspond to the relative errors for formulas (7.3), (7.4), (7.5) and (7.6).

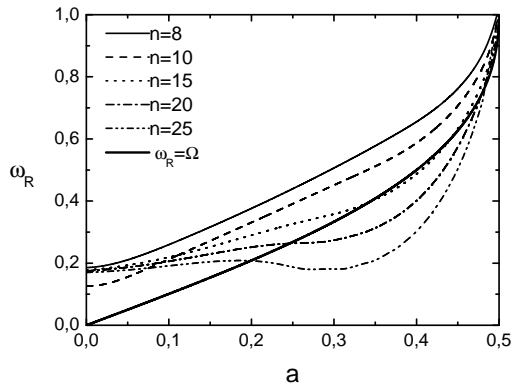


Figure 7.3: Real part of the frequency for modes with $l = 2$, $m = 1$. The modes “bend” downwards as n increases; the bold solid line is $\omega_R = \Omega$. Mode frequencies tend to $\omega_R = m = 1$ in the extremal limit.

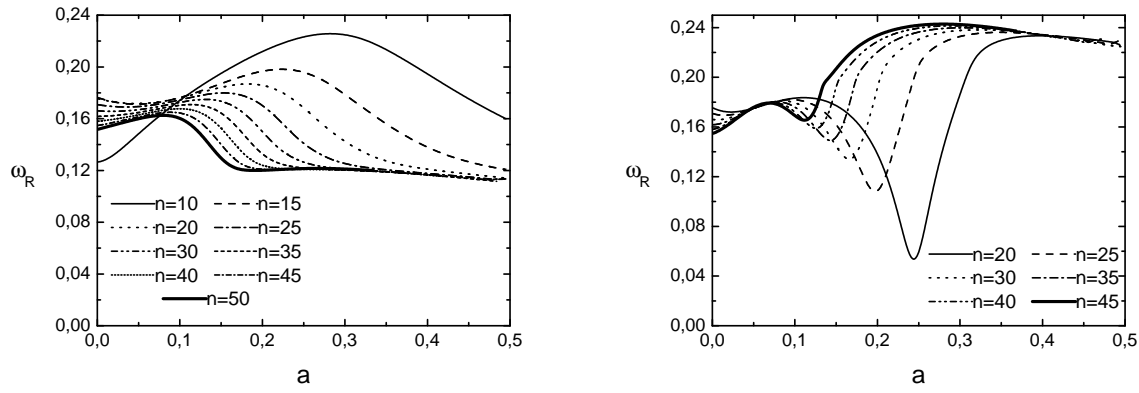


Figure 7.4: Real part of the first few modes with $l = 2$ and $m < 0$. Modes having $m = -1$ are shown in the left panel, modes having $m = -2$ in the right panel. As the mode order n increases, ω_R seems to approach a (roughly) constant value $\omega_R = -m\varpi$, where $\varpi \simeq 0.12$. Convergence to this limiting value is faster for large values of the rotation parameter a (compare figure 7.1).

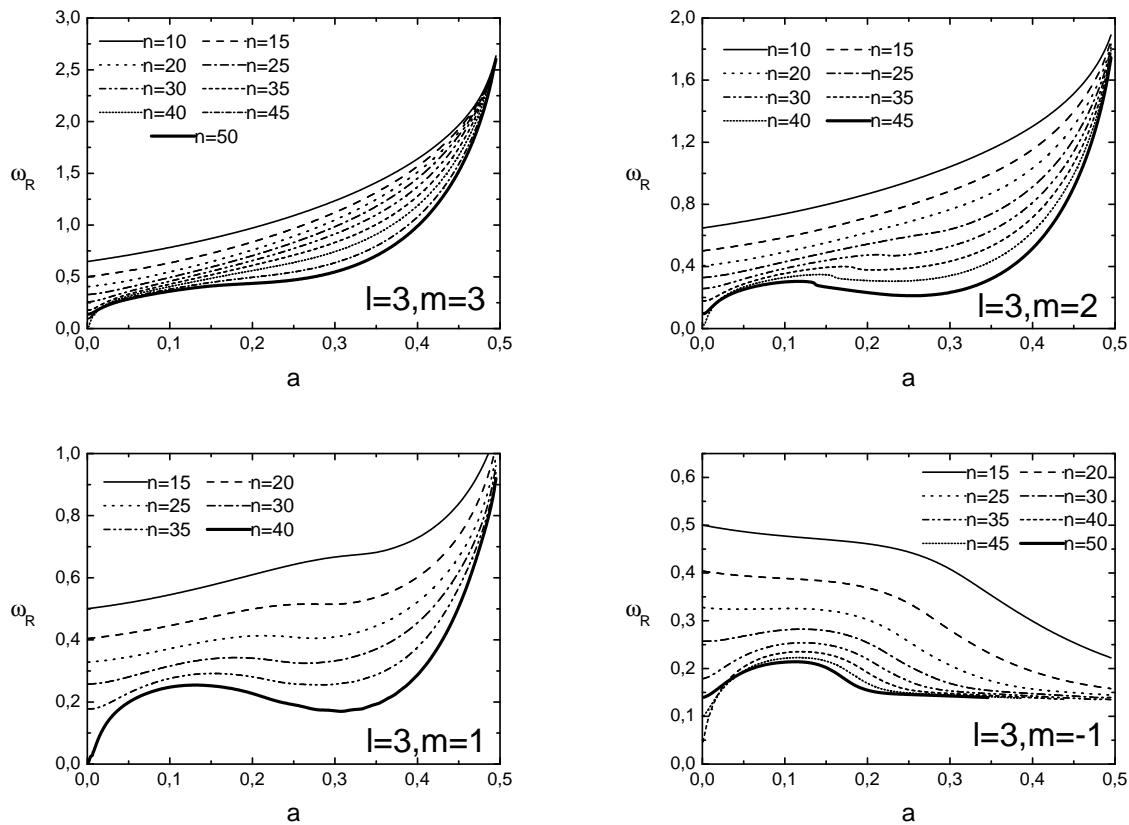


Figure 7.5: Real parts of some modes having $l = 3$ and different values of m (indicated in the plots). When $m > 0$, the observed behaviour is reminiscent of modes having $l = 2$, $m = 1$ (see figure 7.3). Modes having $m < 0$ approach a (roughly) constant value $\omega_R = -m\varpi$ (we only show modes having $m = -1$), as they do for $l = 2$ (see figure 7.4).

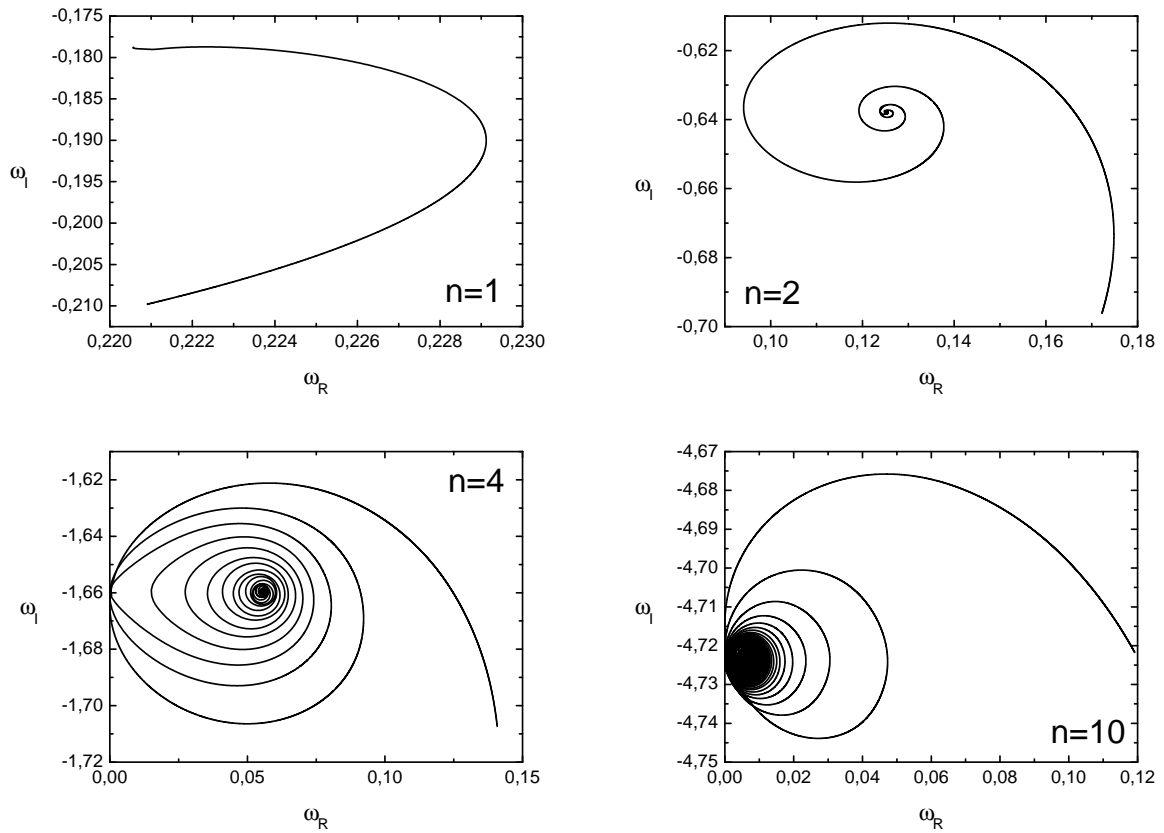


Figure 7.6: Trajectories of a few scalar modes having $l = m = 0$. The different panels correspond to the fundamental mode (top left), showing no spiralling behaviour, and to modes having overtone indices $n = 2, 4, 10$.

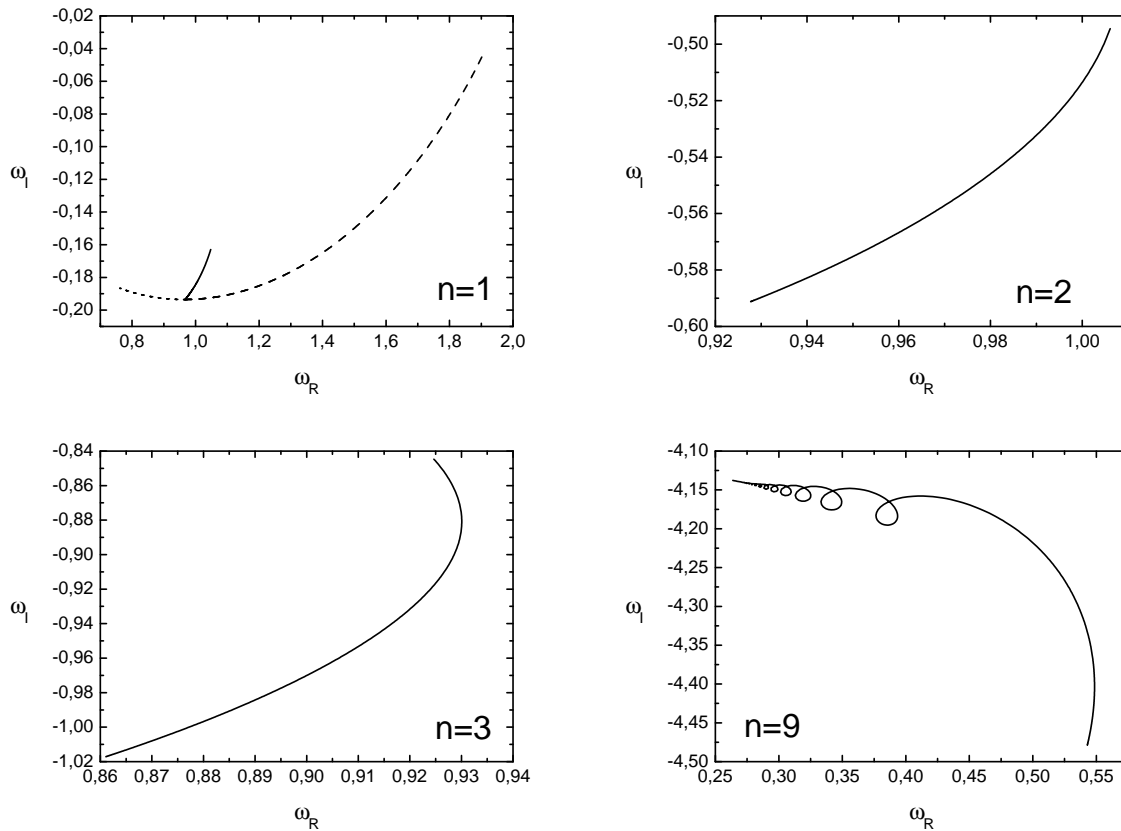


Figure 7.7: Trajectories of a few scalar modes for $l = 2$. In the top left panel we show how rotation removes the degeneracy of modes having different m 's, displaying three branches (corresponding to $m = 2, 0, -2$) “coming out of the Schwarzschild limit” for the fundamental mode ($n = 1$). In the top right and bottom left panel we show the progressive “bending” of the trajectory of the $m = 0$ branch for the first two overtones ($n = 2, 3$). Finally, in the bottom right panel we show the typical spiralling behaviour for a mode with $m = 0$ and $n = 9$. This plot can be compared to figure 6 in [136] (notice that their scales have to be multiplied by two to switch to our units). The continued fraction method allows us to compute modes for larger values of a (and is presumably more accurate) than the Prüfer method.

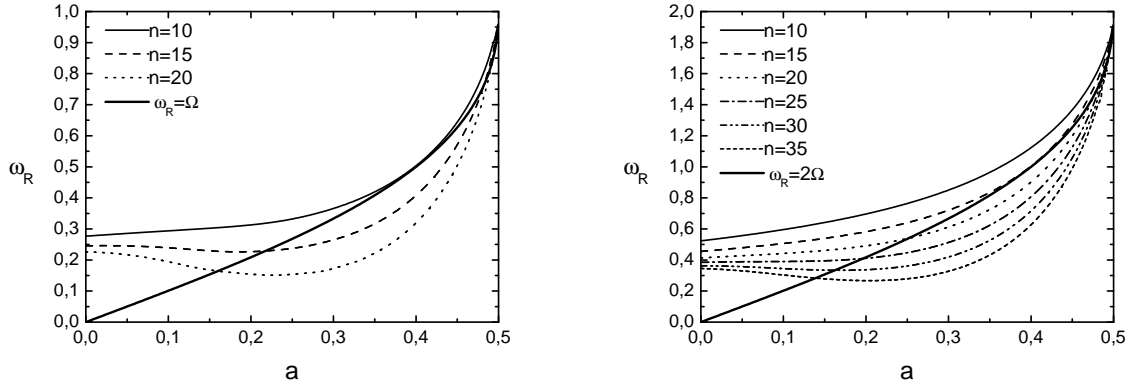


Figure 7.8: Real parts of the scalar modes having $l = m = 1$, $l = m = 2$. The observed behaviour is reminiscent of figures 7.3 and 7.5.

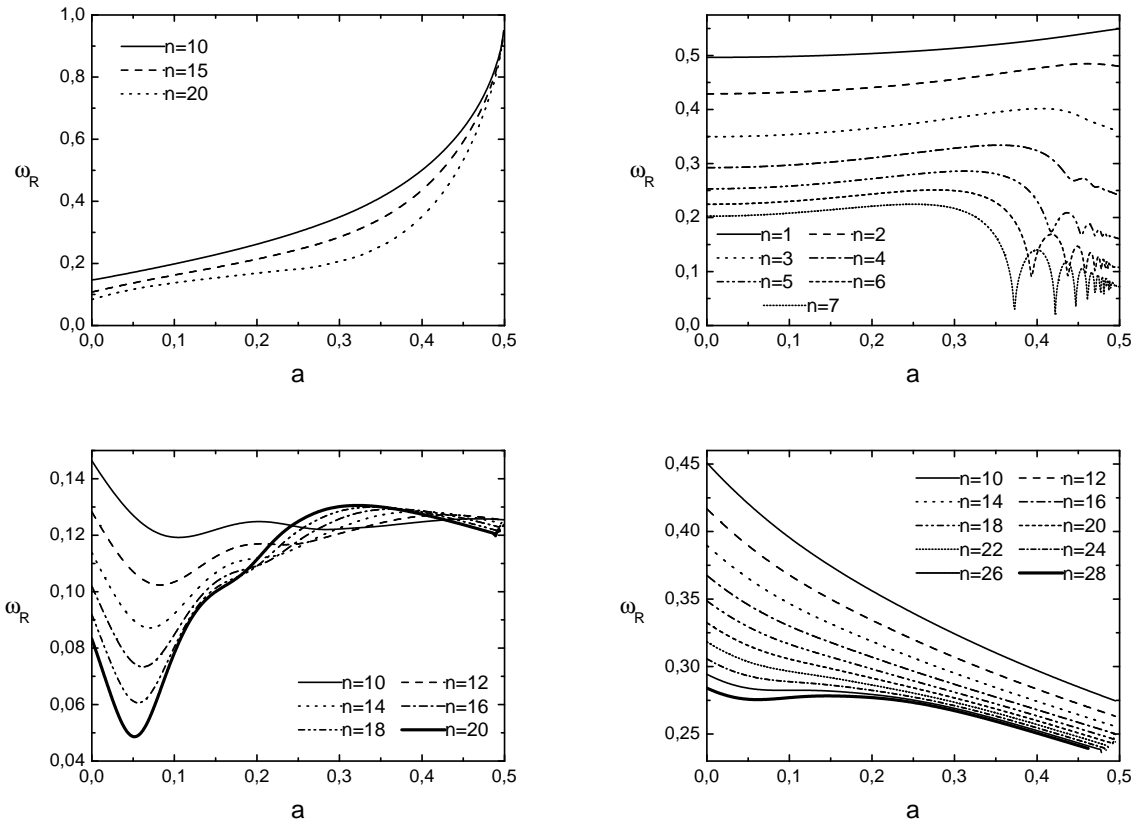


Figure 7.9: Real part of electromagnetic modes having $l = m = 1$ (top left), $l = 1, m = 0$ (top right), $l = 1, m = -1$ (bottom left) and $l = 2, m = -2$ (bottom right) as a function of the rotation parameter a , for increasing values of the mode index.

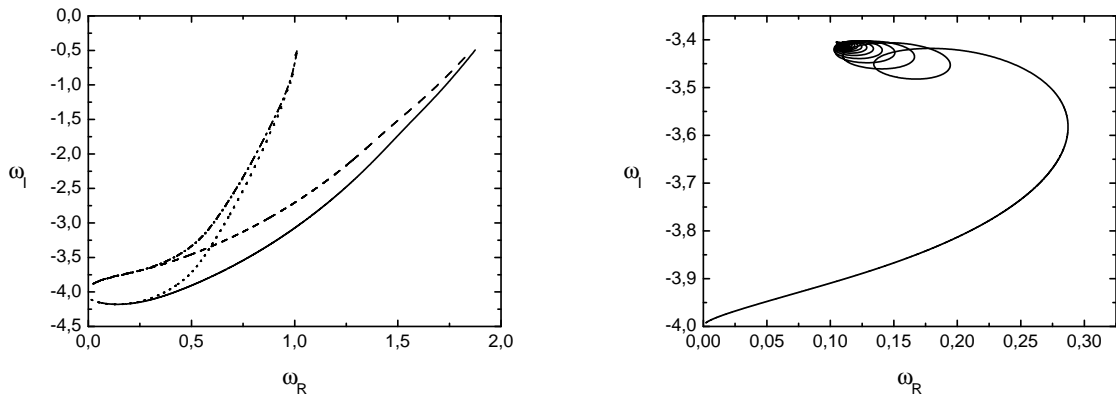


Figure 7.10: The left panel shows the trajectories described in the complex- ω plane by the doublets emerging close to the Schwarzschild algebraically special frequency ($\tilde{\Omega}_2 = -4i$) when $m > 0$ and $l = 2$. Notice that the real part of modes having $m > 0$ tends to $\omega_R = m$ as $a \rightarrow 1/2$. The right panel shows the spiralling trajectory of the mode having $m = 0$.

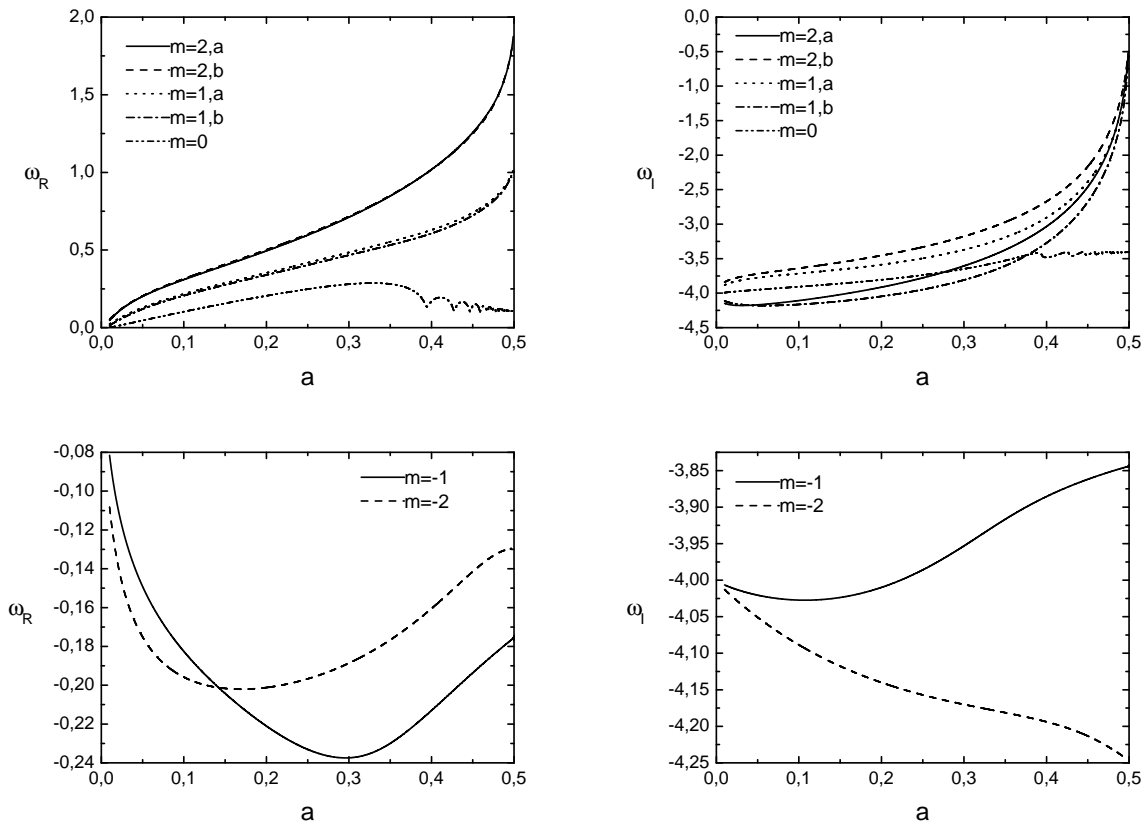


Figure 7.11: The top row shows the real and imaginary parts (left and right, respectively) of the “doublet” of QNMs emerging from the algebraically special frequency as functions of a . The doublets only appear when $m > 0$. We also overplot the real and imaginary parts of the mode having $l = 2$, $m = 0$ (showing the usual oscillatory behaviour). The bottom row shows, for completeness, the real and imaginary parts (left and right, respectively) of modes having negative m and branching from the algebraically special frequency.

Part II

**Encounters of black holes with
particles in four and higher
dimensions: quasinormal modes,
gravitational and scalar radiation**

Chapter 8

Gravitational radiation: an introduction

Contents

8.1	Introduction	113
8.2	Astronomical sources of gravitational waves	114
8.3	Microscopic sources of gravitational waves	116
8.4	Outline of Part II	119

8.1 Introduction

The existence of electromagnetic waves was predicted by Maxwell in the 1860's, and verified experimentally by Hertz less than two decades later. The usefulness of electromagnetic waves for our understanding of the Universe is enormous, in fact, most of our knowledge is due to their existence. Each time one opened a new electromagnetic window for our telescopes, for example the radio band or the X-ray band, some revolution occurred. Take for example the discovery of cosmic radio waves in the 1930's and their detailed study in the 1940's, 50's and 60's. Previously, the Universe, as seen by visible light, was very serene and quiescent. It was, so it seemed, composed in the vast majority by stars revolving smoothly in their orbits, and evolving on timescales of millions or billions of years. The radio window showed us a completely new aspect of the Universe, a violent one: galaxies were colliding, jets thrown away from galactic nuclei, quasars with luminosities far greater than our galaxy evolving on timescales of hours, pulsars with gigantic radio beams rotating many times per second, and many others. The history of gravitational waves is not as glamorous, but we are witnessing a dramatic turning of events. Gravitational waves were theoretically predicted by Einstein in 1916, soon after the formulation of general relativity. However, a series of failed attempts to analyze theoretically radiation reaction in some systems in the late 1940's and 1950's shook physicist's faith in the ability of the waves to carry off energy. It required a clever thought experiment by Bondi [143] to restore faith in the energy of the waves. By now, we have a soundly based theory of gravitational waves, an account of which may be found in the review papers by Thorne [144] and Damour [145]. Gravitational waves have not been experimentally

detected directly, however there has been an indirect verification, in the form of the observed inspiral of a binary pulsar due to gravitational radiation reaction [146]). We are still trying to detect them directly, an effort that began 40 years ago with Weber's pioneering work [147], and that continues nowadays with more modern gravitational wave detectors, such as GEO [20], LIGO [21] or VIRGO [22]. The reason for the difficulty in detecting gravitational waves is that gravity is about 10^{40} times weaker than electromagnetism. This number comes from comparing the gravitational and electromagnetic forces between a proton and an electron. This extreme feebleness is the major obstacle to the technological manipulation of gravity and almost certainly means that the study of gravitational radiation will have to rely on powerful natural sources in the Universe. Unfortunately, the same feebleness that inhibits the generation of gravitational waves also afflicts their detection, so that even a flux of gravitational energy at the Earth's surface comparable to the heat and light of the Sun is unlikely to be detected by present terrestrial equipment. So weak is the interaction between gravitational waves and matter that only one graviton in 10^{23} registers on a typical detector. This means that enormously powerful processes are necessary to render any practical interest to the subject of gravitational waves. But these processes do exist, and the payoff may be extremely high. I shall now describe briefly some of these processes, and the information they may give us regarding the nature of our Universe. It is likely this information may be collected in forthcoming years, since our gravitational wave detectors are already quite sensible.

We have talked about astrophysical sources. There is yet another process of producing gravitational waves and indirectly detect them. It has been proposed that the Universe may have large extra dimensions. If this is so, one consequence may be the production of black holes from collisions with center of mass energy of about $1TeV$. Thus, the Large Hadron Collider (LHC) at CERN might be a black hole factory. An enormous fraction (maybe about 25% or more) of the center of mass energy is expected to be radiated as gravitational radiation during the black hole production. This will appear as a missing energy, and thus one can indirectly observe gravitational waves at accelerators. In the following I will describe both sources of gravitational waves, astronomical and microscopic, in more detail.

8.2 Astronomical sources of gravitational waves

Among the sources that can be detected using present day technology, some of the most promising are (see the review papers by Schutz [148] and by Hughes [149]).

Supernovae and gravitational collapse. Supernovae are triggered by the gravitational collapse of the interior degenerate core of an evolved star. According to current theory the final outcome should be a neutron star or a black hole. The collapse releases an enormous amount of energy, about $0.15M_{\odot}c^2$, most of which is carried away by neutrinos. An uncertain fraction is carried by gravitational waves. It is ironic that, although detecting supernovae was the initial goal of detector development when it started 4 decades ago, little more is known today about what to expect than scientists knew then. The problem with gravitational collapse is that perfectly spherical motions do not emit gravitational waves, and it is still not possible to estimate in a reliable way the amount of asymmetry in gravitational collapse.

Binary systems. These systems have provided us with the best proof, up to the moment, of the existence of gravitational waves. This has been an indirect proof, through the decrease of the orbital period due to the emission of gravitational radiation. For example, for the

famous binary pulsar PSR 1916+16, discovered by Hulse and Taylor in 1974, the observed value is $2.4 \times 10^{-12} s/s$. The theoretical prediction is $2.38 \times 10^{-12} s/s$, which is in agreement within the measurement errors. Detection of gravitational waves from these systems seems however impossible using the current detectors, since the frequency of the radiation is too low to be detected on Earth.

Chirping binary systems. When a binary loses enough energy so that its orbit shrinks by an observable amount during an observation, it is said to *chirp*. As the orbit shrinks, the frequency and amplitude go up. Chirping binary systems are more easily detected than gravitational collapse events because one can model with great accuracy the gravitational waveform during the inspiral phase. There will be radiation, probably with considerable energy, during the poorly understood plunge phase (when the objects reach the last stable circular orbit and fall rapidly toward one another) and during the merger event, but the detectability of such systems rests on tracking their orbital emissions.

Big Bang. Quantum fluctuations in the spacetime metric are parametrically amplified during inflation to relatively high amplitudes.

There are many other important astrophysical sources of gravitational waves, the reader can find a more complete account of them in [148, 149].

A certain fraction of such systems could contain black holes instead of neutron stars. Astronomers now recognize that there is an abundance of black holes in the Universe. Observations of various kinds have located black holes in X-ray binary systems in the galaxy and in the centers of galaxies. These two classes of black holes have very different masses, stellar black holes typically have masses of around $10M_{\odot}$, and are thought to have been formed by the gravitational collapse of the center of a large, evolved red giant star, perhaps in a supernova explosion. Massive black holes in galactic centers seem to have masses between 10^6M_{\odot} and $10^{10}M_{\odot}$, but their history and method of formation are not yet understood. It was generally believed these were the only two kinds of black holes in the Universe. In the last few years, however, evidence has accumulated for an intermediate-mass class of black holes, with hundreds to thousands of solar masses. If such objects exist they have important implications for the dynamics of stellar clusters, the formation of supermassive black holes, and the production and detection of gravitational waves. We refer the reader to [150] for a review on the observational evidence of such black holes, and the implications their existence may have for our knowledge of the Universe.

Radiation from stellar black holes is expected mainly from coalescing binary systems, when one or both of the components is a black hole. Gravitational radiation is expected from supermassive black holes in two ways. In one scenario, two massive black holes spiral together in a powerful version of the coalescence we have discussed. A second scenario for the production of radiation by massive black holes is the swallowing of a stellar mass black hole or a neutron star by the large hole. Such captures emit a gravitational wave signal that may be approximated by studying the motion of a point mass near a black hole. This process is well understood theoretically, and will be revisited in this thesis. (As an aside, and as expected from Part I of this thesis, this process is also dominated by a quasinormal ringing at intermediate times).

What can we gain from gravitational wave observations? First, the weakness with which gravitational waves interact with matter is a great advantage for astronomy. It means that gravitational waves arriving at Earth have not been corrupted by any matter they may have encountered since their generation. As such they carry clean information about their birth

place.

Gravitational waves are emitted by motions of their sources as a whole, not by individual atoms or electrons, as is normally the case for electromagnetic waves. Astrophysical electromagnetic radiation typically arises from the incoherent superposition of many emitters. This radiation directly probes the thermodynamic state of a system or an environment. On the other hand, gravitational waves are coherent superpositions arising from the bulk dynamics of a dense source of mass-energy. These waves directly probe the dynamical state of a system.

The direct observable of gravitational radiation is the waveform h , a quantity that falls off with distance as $\frac{1}{r}$. Most electromagnetic observables are related to the energy flux, and so fall off with a $\frac{1}{r^2}$ law. This means that a small improvement in the gravitational wave detector's sensitivity can have a large impact on their science: doubling the sensitivity of a detector doubles the distance to which sources can be detected (and this increases the volume of the Universe to which sources are measurable by a factor of 8).

Black holes can emit gravitational waves, and indeed gravitational waves provide the only way to make direct observation of these objects. Since there is now strong indirect evidence that giant black holes inhabit the centers of many, or most, galaxies and since smaller ones are common in the galaxy (and not to mention intermediate ones, which also seem to be abundant, as has recently been recognized [150]), there is great interest in making direct observations of them.

Gravitational waves can come from extraordinarily early in the history of the Universe. Gravitational waves, if they can be detected, would picture the Universe when it was only perhaps 10^{-24} seconds old, just at the end of Inflation.

Gravitational radiation is the last fundamental prediction of Einstein's general relativity that has not yet been directly verified. If another theory of gravity is correct, then differences could in principle show up in the properties of gravitational waves, such as their polarization.

8.3 Microscopic sources of gravitational waves

Studying highly relativistic collisions between astrophysical objects is not interesting: it is highly unlikely we will ever observe such event. However, a new scenario, described below, as been recently proposed in which the gravitational radiation generated during highly relativistic is extremely interesting.

Another mechanism by which gravitational waves may be indirectly detected is provided by the TeV-scale gravity scenario. This scenario tries to solve some problems in high energy physics, namely the hierarchy problem, by postulating the existence of large extra dimensions in our Universe.

Traditionally, high energy physics seeks the nature of the strong and weak subnuclear interactions, which can be understood through the Standard Model. However, the foundations of the Standard Model are still mysterious. Over the last two decades, one of the greatest driving forces for the construction of theories beyond the Standard Model has been trying to explain the huge difference between the two fundamental energy scales in nature: the electroweak scale $m_{EW} \sim 300 \text{ GeV}$ and the Planck scale $M_{Pl} \sim 10^{19} \text{ GeV}$. This is the so called hierarchy problem. There is an important difference in these two scales, though [151]: while electroweak interactions have been probed at distances $\sim m_{EW}^{-1} = 10^{-16} \text{ cm}$, gravitational forces have not been probed at distances $\sim M_{Pl}^{-1} = 10^{-33} \text{ cm}$. For instance,

from $e^+e^- \rightarrow e^+e^-$ at LEP200, we know that the electromagnetic interactions are $\frac{1}{r}$ down to 5×10^{-17} cm. However, gravity has only been accurately measured in the ~ 0.01 cm range [152]. Thus, the view that $M_{\text{Pl}} = 10^{19}$ GeV is a fundamental energy scale is based solely on the belief that gravity stays unmodified over the 31 orders of magnitude going from 10^{-33} cm to ~ 0.01 cm, where it is measured. One can thus conceive ways to solve the hierarchy problem, if gravity gets indeed modified at scales smaller than 1 mm. As a simple realization of this, suppose our world is $(4+n)$ -dimensional. The n extra dimensions must be compact, otherwise gravity would not behave as $\frac{1}{r}$ at large distances, as we know it does. Consider therefore that each of these n extra dimensions have typical length $\sim R$. Two test masses m_1, m_2 placed within a distance $r \ll R$ will feel a gravitational potential dictated by Gauss's law in $(4+n)$ dimensions,

$$V(r) = G_{4+n} \frac{m_1 m_2}{r^{n+1}}, \quad r \ll R. \quad (8.1)$$

Here, G_{4+n} is Newton's constant in the $(4+n)$ dimensional world. On the other hand, if the masses are placed at distances $r \gg R$, their gravitational flux lines can not continue to penetrate in the extra dimensions, and the usual $\frac{1}{r}$ potential is recovered [151]

$$V(r) = \frac{G_{4+n}}{R^n} \frac{m_1 m_2}{r}, \quad r \gg R. \quad (8.2)$$

In order to have the usual strength at large distances, one must impose

$$\frac{G_{4+n}}{R^n} = G_4, \quad (8.3)$$

where G_4 is our usual four dimensional Newton's constant. Let's now see what happens to the Planck scale. The Planck mass can be obtained by equating the Schwarzschild radius and the Compton wavelength of an object of mass m . In general $(4+n)$ dimensions, the Schwarzschild radius r_+ of that object is

$$r_+ = \left[\frac{16\pi G_{4+n} m}{2(n+2)\pi^{(n+2)/2}} \Gamma[(n+3)/2] \right]^{1/(n+1)} \sim (G_{4+n} m)^{1/(n+1)}, \quad (8.4)$$

and the Compton wavelength is

$$\lambda = \frac{1}{m}, \quad (8.5)$$

where we have set both Planck's constant h and the velocity of light c equal to 1. Equating (8.4) with (8.5) for a mass m equal to the Planck mass M_{Pl} we get

$$M_{\text{Pl}}^{2+n} = \frac{1}{G_{4+n}}. \quad (8.6)$$

But in view of (8.3), and keeping in mind that the four dimensional Planck scale is simply $M_{4\text{Pl}}^2 = \frac{1}{G_4}$, it means that the fundamental $(4+n)$ Planck scale M_{Pl} is related to the effective 4 dimensional Planck scale $M_{4\text{Pl}}$ as

$$M_{4\text{Pl}}^2 \sim M_{\text{Pl}}^{2+n} R^n. \quad (8.7)$$

It is now very easy to solve the hierarchy problem: just make it go away, by imposing equal scales, i.e., $m_{\text{EW}} = M_{\text{Pl}}$. This constraints the typical sizes R of the extra dimensions to be

$$R \sim 10^{30/n-17} \text{cm} \left(\frac{1 \text{TeV}}{m_{\text{EW}}} \right)^{1+2/n}. \quad (8.8)$$

If $n = 1$ this gives $R \sim 10^{13}$ cm, which is excluded empirically, since this would imply deviations from Newtonian gravity over solar system distances. However any $n \geq 2$ gives modifications of Newtonian gravity at distances smaller than those currently probed by experiment.

On the other hand, Standard Model gauge forces have been accurately measured at weak scale distances, as we remarked earlier. This means that Standard Model particles cannot freely propagate in the n extra dimensions, but must, somehow, be localized to a 4 dimensional submanifold. An important question is the mechanism by which the Standard Model fields are localized to the brane, which has several resolutions, see [151].

An exciting consequence of TeV-scale gravity is the possibility of production of black holes at the LHC and beyond [158]. To understand how this comes about, let's consider the formation of a black hole with horizon radius r_+ much smaller than the typical size R of the extra dimensions. When the Schwarzschild radius of a black hole is much smaller than the radius R of the compactified dimensions, it should be insensitive to the brane and the boundary conditions in the n transverse directions, and so is well approximated by a $(4 + n)$ -dimensional Schwarzschild black hole [154, 155]. The Schwarzschild radius of a non-rotating $(4 + n)$ -dimensional black hole is

$$r_+ = \frac{1}{\sqrt{\pi} M_{\text{Pl}}} \left[\frac{M}{M_{\text{Pl}}} \frac{8\Gamma\left(\frac{n+3}{2}\right)}{n+2} \right]^{1/(n+1)}, \quad (8.9)$$

where M is the black hole mass. To estimate the parton-level cross section, consider partons scattering at center of mass energy \sqrt{s} and impact parameter b . A conjecture in general relativity is Thorne's hoop conjecture [156], which states that horizons form when and only when a mass M is compacted into a region whose circumference in every direction is less than $2\pi r_+$. This conjecture implies that the cross section for black hole production is

$$\sigma \sim \pi r_+^2 = \frac{1}{M_{\text{Pl}}^2} \left[\frac{M}{M_{\text{Pl}}} \frac{8\Gamma\left(\frac{n+3}{2}\right)}{n+2} \right]^{2/(n+1)}. \quad (8.10)$$

It is important to note that this is only correct if the black hole is larger than the colliding particles. Since these partons have no internal structure, at least up to ~ 1 TeV, then we can assume they are indeed pointlike in such calculation. A simple estimate gives an impressive result: for $M_{\text{Pl}} \sim 1$ TeV, the LHC will produce one black hole per second with mass $> 5M_{\text{Pl}}$. If this is true it will turn LHC into a black hole factory.

After the black hole forms, it will start to decay. First, it will radiate all the excess multipole moments, because when the black hole is born, it has an highly asymmetric shape and thus will settle down to a stationary shape (which in four dimensions must be a Kerr-Newman black hole, by the uniqueness theorem). One calls this the balding stage. After this phase we are left, in general, with a spinning black hole. It will then start to lose angular momentum through the Hawking process: as Page [157] as shown, a spinning black hole Hawking radiates mainly along the equatorial plane, and the Hawking radiation carries away most of the black hole's angular momentum. This is the spin-down phase. After this we have a non-spinning black hole Hawking radiating. This is the Schwarzschild phase. When the black hole finally reaches the Planck size, we lose track of what will happen: current physics is not able to go that deep. This second part of the thesis will try to give an account of the balding phase, as we shall explain below.

8.4 Outline of Part II

In this second part of the thesis we will begin, in Chapter 9 by refining the calculation of the gravitational radiation released when a high energy particle collides with a black hole. This study shows three highly interesting aspects: first, it is in amazingly agreement with a similar, but flat space calculation by Weinberg. Second, the total result for the radiation, when one takes the limit of equal mass particles, gives an answer quite similar to that coming from a completely different formalism, but also studying the high energy collision of two black holes. Finally this study shows clearly that the fundamental QN frequencies act as a cutoff in the energy spectra. The main advantage of the technique used here is that it allows for an important generalization, which does not seem feasible using the other formalism: it is easy to study the collision between rotating black holes, as i shall also do in Chapter 10, and allows to study the collision of higher dimensional black holes, a work which is now being carried by some authors.

In Chapter 11 we shall begin the study of radiation in non-asymptotically flat spacetimes. We shall focus on scalar radiation in asymptotically anti-de Sitter background, and consider the radial infall of massive particles into Schwarzschild-anti-de Sitter black holes. As expected, and as very often remarked in Chapter 1, the waveform is dominated by the quasinormal ringing. The work presented in this chapter is the first showing that in fact QNMs dominate the answer even for non-asymptotically flat spacetimes. The infalling particle and consequent scalar radiation have an interpretation in terms of the AdS/CFT: if one recognizes that a black hole corresponds to a thermal state. then the infalling particle corresponds to some perturbation of this thermal state. Again, the typical timescale of approach to equilibrium is therefore dictated by the lowest QN frequency, since the signal is dominated by QN ringing.

Chapter 9

Gravitational radiation in a curved asymptotically flat four dimensional background: high energy encounters of non-rotating black holes with particles

Contents

9.1	Introduction	121
9.2	Basic Formalism	122
9.3	Numerical Results	124

9.1 Introduction

The study of gravitational wave emission by astrophysical objects has been for the last decades one of the most fascinating topics in General Relativity. This enthusiasm is of course partly due to the possibility of detecting gravitational waves by projects such as GEO600 [20], LIGO [21] or VIRGO [22], already operating. Since gravity couples very weakly to matter, one needs to have powerful sources of in order to hope for the detection of the gravitational waves. Of the candidate sources, black holes stand out naturally, as they provide huge warehouses of energy, a fraction of which may be converted into gravitational waves, by processes such as collisions between two black holes. As it often happens, the most interesting processes are the most difficult to handle, and events such as black hole-black hole collisions are no exception. An efficient description of such events requires the use of the full non linear Einstein's equations, which only begin to be manageable by numerical methods, and state-of-the-art computing. In recent years we have witnessed serious progress in this field [4], and we are now able to evolve numerically the collision of two black holes, provided their initial separation is not much larger than a few Schwarzschild radius. At the same time these numerical results have been supplemented with results from first and second order perturbation theory [5], which simultaneously served as guidance into the numerical codes. The agreement between the two methods is not only reassuring, but it is also in fact impressive that a linearization

of Einstein's equations yield such good results (as Smarr [7] puts it, "the agreement is so remarkable that something deep must be at work"). In connection with this kind of events, the use of perturbation methods goes back as far as 1970, when Zerilli [219] and Davis et al [2] first computed the gravitational energy radiated away during the infall from rest at infinity of a small test particle of mass m_0 , into a Schwarzschild black hole with mass M . Later, Ruffini [62] generalized these results to allow for an initial velocity of the test particle (this problem has recently been the subject of further study [163], in order to investigate the question of choosing appropriate initial data for black hole collisions). Soon after, one began to realize that the limit $m_0 \rightarrow M$ describing the collision of two black holes did predict reasonable results, still within perturbation theory, thereby making perturbation theory an inexpensive tool to study important phenomena.

In this paper we shall extend the results of Davis et al [2] and Ruffini [62] by considering a massless test particle falling in from infinity through a radial geodesic. This process describes the collision of an infalling test particle in the limit that the initial velocity goes to the speed of light, thereby extending the range of Ruffini's results into larger Lorentz boost parameters γ s. If then one continues to rely on the agreement between perturbation theory and the fully numerical outputs, these results presumably describe the collision of two black holes near the speed of light, these events have been extensively studied through matching techniques by D'Eath (a good review can be found in his book [164]), and have also been studied in [222]. The extension is straightforward, the mathematics involved are quite standard, but the process has never been studied. Again supposing that these results hold for the head on collision of two black holes travelling towards each other at the speed of light, we have a very simple and tractable problem which can serve as a guide and supplement the results obtained by Smarr and by D'Eath. Another strong motivation for this work comes from the possibility of black hole formation in TeV-scale gravity [151]. Previous estimates on how this process develops, in particular the final mass of the black hole formed by the collision of relativistic particles have relied heavily upon the computations of D'Eath and Payne [165]. A fresher look at the problem is therefore recommended, and a comparison between our results with results obtained years ago [164, 222] and with recent results [158] are in order.

The fully relativistic results we will present here show an impressive agreement with results by Smarr [222] for collisions of massive particles near the speed of light, namely a flat spectrum, with a zero frequency limit (ZFL) $(\frac{dE}{d\omega})_{\omega=0} = 0.4244m_0^2\gamma^2$. We also show that Smarr underestimated the total energy radiated to infinity, which we estimate to be $\Delta E = 0.26m_0^2\gamma^2/M$, with M the black hole mass. The quadrupole part of the perturbation carries less than 50% of this energy. When applied to the head on collision of two black holes moving at the speed of light, we obtain an efficiency for gravitational wave generation of 13%, quite close to D'Eath and Payne's result of 16% [164, 165]. This chapter will follow closely the analysis in [159]

9.2 Basic Formalism

Since the mathematical formalism for this problem has been thoroughly exploited over the years, we will just outline the procedure. Treating the massless particle as a perturbation, we write the metric functions for this spacetime, black hole + infalling particle, as

$$g_{ab}(x^\nu) = g_{ab}^{(0)}(x^\nu) + h_{ab}(x^\nu), \quad (9.1)$$

where the metric $g_{ab}^{(0)}(x^\nu)$ is the background metric, (given by some known solution of Einstein's equations), which we now specialize to the Schwarzschild metric

$$ds^2 = -f(r)dt^2 + \frac{dr^2}{f(r)} + r^2(d\theta^2 + \sin^2\theta d\phi^2), \quad (9.2)$$

where $f(r) = 1 - 2M/r$. Also, $h_{ab}(x^\nu)$ is a small perturbation, induced by the massless test particle, which is described by the stress energy tensor

$$T^{\mu\nu} = -\frac{p_0}{(-g)^{1/2}} \int d\lambda \delta^4(x - z(\lambda)) \dot{z}^\mu \dot{z}^\nu. \quad (9.3)$$

Here, z^ν is the trajectory of the particle along the world-line, parametrized by an affine parameter λ (the proper time in the case of a massive particle), and p_0 is the momentum of the particle. To proceed, we decompose Einstein's equations $G_{ab} = 8\pi T_{ab}$ in tensorial spherical harmonics and specialize to the Regge-Wheeler [38] gauge. For our case, in which the particle falls straight in, only even parity perturbations survive. Finally, following Zerilli's [39] prescription, we arrive at a wavefunction (a function of the time t and radial r coordinates only) whose evolution can be followed by the wave equation

$$\frac{\partial^2 \tilde{\mathbf{Z}}(\omega, r)}{\partial r_*^2} + [\omega^2 - V(r)] \tilde{\mathbf{Z}}(\omega, r) = (1 - 2M/r)S, \quad (9.4)$$

Here, the l -dependent potential V is given by

$$V(r) = \frac{f(r) [2\sigma^2(\sigma + 1)r^3 + 6\sigma^2 r^2 M + 18\sigma r M^2 + 18M^3]}{r^3(3M + \sigma r)^2}, \quad (9.5)$$

where $\sigma = \frac{(l-1)(l+2)}{2}$ and the tortoise coordinate r_* is defined as $\frac{\partial r}{\partial r_*} = f(r)$. The passage from the time variable t to the frequency ω has been achieved through a Fourier transform, $\tilde{\mathbf{Z}}(\omega, r) = \frac{1}{(2\pi)^{1/2}} \int_{-\infty}^{\infty} e^{i\omega t} Z(t, r) dt$. The source S depends entirely on the stress energy tensor of the particle and on whether or not it is massive. The difference between massive and massless particles lies on the geodesics they follow. The radial geodesics for massive particles are:

$$\frac{dT}{dr} = -\frac{E}{f(r)(E^2 - 1 + 2M/r)^{1/2}}; \quad \frac{dt}{d\tau} = \frac{E}{f(r)}, \quad (9.6)$$

where E is a conserved energy parameter: For example, if the particle has velocity v_∞ at infinity then $E = \frac{1}{(1-v_\infty^2)^{1/2}} \equiv \gamma$. On the other hand, the radial geodesics for massless particles are described by

$$\frac{dT}{dr} = -\frac{1}{f(r)}; \quad \frac{dt}{d\tau} = \frac{\epsilon_0}{f(r)}, \quad (9.7)$$

where again ϵ_0 is a conserved energy parameter, which in relativistic units is simply p_0 . We shall however keep ϵ_0 for future use, to see more directly the connection between massless particles and massive ones traveling close to the speed of light. One can see that, on putting $p_0 \rightarrow m_0$, $\epsilon_0 \rightarrow \gamma$ and $\gamma \rightarrow \infty$, the radial null geodesics reduce to radial timelike geodesics, so that all the results we shall obtain in this paper can be carried over to the case of ultrarelativistic (massive) test particles falling into a Schwarzschild black hole. For massless particles the source term S is

$$S = \frac{4ip_0 e^{-i\omega r_*} \epsilon_0 (4l + 2)^{1/2} \sigma}{w(3M + \sigma r)^2}. \quad (9.8)$$

To get the energy spectra, we use

$$\frac{dE}{d\omega} = \frac{1}{32\pi} \frac{(l+2)!}{(l-2)!} \omega^2 |\tilde{\mathbf{Z}}(\omega, r)|^2, \quad (9.9)$$

and to reconstruct the wavefunction $Z(t, r)$ one uses the inverse Fourier transform

$$Z(t, r) = \frac{1}{(2\pi)^{1/2}} \int_{-\infty}^{\infty} e^{-i\omega t} \tilde{\mathbf{Z}}(\omega, r) d\omega. \quad (9.10)$$

Now we have to find $\tilde{\mathbf{Z}}(\omega, r)$ from the differential equation (9.4). This is accomplished by a Green's function technique. Imposing the usual boundary conditions, i.e., only ingoing waves at the horizon and outgoing waves at infinity, we get that, near infinity,

$$\tilde{\mathbf{Z}} = \frac{1}{W} \int_{r_+}^{\infty} z_L S dr. \quad (9.11)$$

Here, z_L is a homogeneous solution of (9.4) which asymptotically behaves as

$$z_L \sim e^{-i\omega r_*}, r_* \rightarrow -\infty \quad (9.12)$$

$$z_L \sim B(\omega) e^{i\omega r_*} + C(\omega) e^{-i\omega r_*}, r_* \rightarrow +\infty. \quad (9.13)$$

W is the wronskian of the homogeneous solutions of (9.4). These solutions are, z_L which has just been defined, and z_R which behaves as $z_R \sim e^{i\omega r_*}, r_* \rightarrow +\infty$. From this follows that $W = 2i\omega C(\omega)$. We find $C(\omega)$ by solving (9.4) with the right hand side set to zero, and with the starting condition $z_L = e^{-i\omega r_*}$ imposed at a large negative value of r_* . For computational purposes good accuracy is hard to achieve with the form (9.13), so we used an asymptotic solution one order higher in $1/(\omega r)$:

$$\begin{aligned} z_L = & B(\omega) \left(1 + \frac{i(\sigma+1)}{\omega r}\right) e^{i\omega r_*} + \\ & + C(\omega) \left(1 - \frac{i(\sigma+1)}{\omega r}\right) e^{-i\omega r_*}, r_* \rightarrow +\infty. \end{aligned} \quad (9.14)$$

In the numerical work, we chose to adopt r as the independent variable, thereby avoiding the numerical inversion of $r_*(r)$. A fourth order Runge-Kutta routine started the integration of z_L near the horizon, at $r = r_i = 2M + 2M\epsilon$, with typically $\epsilon = 10^{-5}$. It then integrated out to large values of r , where one matches z_L extracted numerically with the asymptotic solution (9.14), in order to find $C(\omega)$. To find $Z(t, r)$ the integral in (9.10) is done by Simpson's rule. For both routines Richardson extrapolation is used.

9.3 Numerical Results

The results for the wavefunction $Z(t, r)$ as a function of the retarded time $u \equiv t - r_*$ are shown in Figure 9.1, for the three lowest radiatable multipoles, $l = 2, 3$ and 4. As expected from the work of Ruffini [62] and Ferrari and Ruffini [16], the wavefunction is not zero at very early times, reflecting the fact that the particle begins to fall with non zero velocity. At late times, the $l = 2$ (for example) signal is dominated by quasinormal ringing with frequency $\omega \sim 0.35/M$, the lowest quasinormal frequency for this spacetime [40]. The energy spectra is

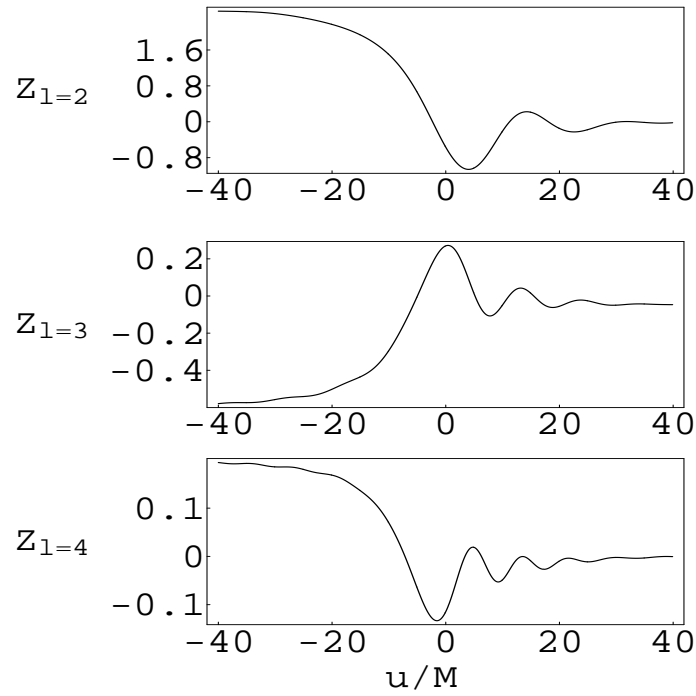


Figure 9.1: Waveforms for the three lowest radiatable multipoles, for a massless particle falling from infinity into a Schwarzschild black hole. Here, the wavefunction Z is measured in units of $\epsilon_0 p_0$.

Table 9.1: The zero frequency limit (ZFL) for the ten lowest radiatable multipoles.

l	ZFL($\times \frac{1}{\epsilon_0^2 p_0^2}$)	l	ZFL($\times \frac{1}{\epsilon_0^2 p_0^2}$)
2	0.265	7	0.0068
3	0.075	8	0.0043
4	0.032	9	0.003
5	0.0166	10	0.0023
6	0.01	11	0.0017

shown in Figure 9.2, for the four lowest radiatable multipoles. First, as expected from Smarr's work [222], the spectra is flat, up to a certain critical value of the frequency, after which it rapidly decreases to zero. This (l -dependent) critical frequency is well approximated, for each l -pole, by the fundamental quasinormal frequency. In Table 9.1, we list the zero frequency limit (ZFL) for the first ten lowest radiatable multipoles.

For high values of the angular quantum number l , a good fit to our numerical data is

$$\left(\frac{dE_l}{d\omega}\right)_{\omega=0} = \frac{2.25}{l^3} \epsilon_0^2 p_0^2 \quad (9.15)$$

We therefore estimate the zero ZFL as

$$\begin{aligned} \left(\frac{dE_l}{d\omega}\right)_{\omega=0} &= \left[\sum_{l=2}^{l=11} \left(\frac{dE_l}{d\omega}\right)_{\omega=0}\right] + \frac{1}{2} \frac{2.25}{12^2} \epsilon_0^2 p_0^2 \\ &= 0.4244 \epsilon_0^2 p_0^2. \end{aligned} \quad (9.16)$$

To calculate the total energy radiated to infinity, we proceed as follows: as we said, the spectra goes as $2.25/l^3$ as long as $\omega < \omega_{lQN}$, where ω_{lQN} is the lowest quasinormal frequency for that l -pole. For $\omega > \omega_{lQN}$, $dE/d\omega \sim 0$ (In fact, our numerical data shows that $dE/d\omega \sim e^{-27\alpha\omega M}$, with α a factor of order unity, for $\omega > \omega_{lQN}$). Now, from the work of Ferrari and Mashhoon [167] and Schutz and Will [13], one knows that for large l , $\omega_{lQN} \sim \frac{l+1/2}{3^{3/2}M}$. Therefore, for large l the energy radiated to infinity in each multipole is

$$\Delta E_l = \frac{2.25(l+1/2)}{3^{3/2}l^3} \frac{\epsilon_0^2 p_0^2}{M}, \quad (9.17)$$

and an estimate to the total energy radiated is then

$$\Delta E = \sum_l \Delta E_l = 0.262 \frac{\epsilon_0^2 p_0^2}{M} \quad (9.18)$$

Let us now make the bridge between these results and previous results on collisions between massive particles at nearly the speed of light [62, 164, 222]. As we mentioned, putting $p_0 \rightarrow m_0$ and $\epsilon_0 \rightarrow \gamma$ does the trick. So for ultrarelativistic test particles with mass m_0 falling into a Schwarzschild black hole, one should have $(dE/d\omega)_{\omega=0} = 0.4244 m_0^2 \gamma^2$ and $\Delta E = 0.262 \frac{m_0^2 \gamma^2}{M}$. Smarr [222] obtains

$$\begin{aligned} \left(\frac{dE}{d\omega}\right)_{\omega=0}^{\text{Smarr}} &= \frac{8}{6\pi} m_0^2 \gamma^2 \sim 0.4244 m_0^2 \gamma^2, \\ \Delta E_{\text{Smarr}} &= 0.2 \frac{m_0^2 \gamma^2}{M}. \end{aligned} \quad (9.19)$$

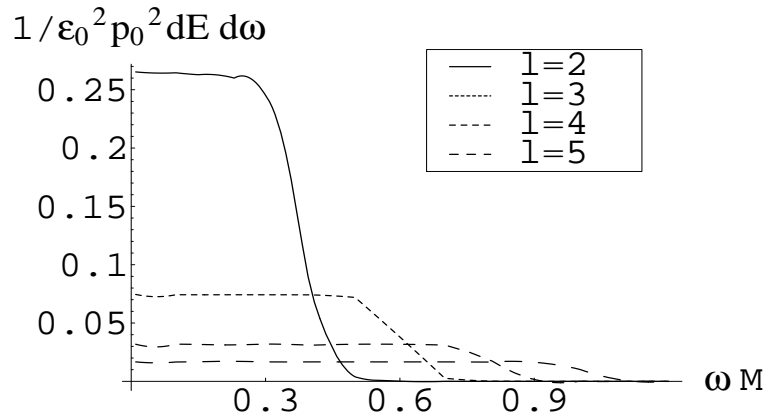


Figure 9.2: The energy spectra for the four lowest radiatable multipoles, for a massless particle falling from infinity into a Schwarzschild black hole.

So Smarr's result for the ZFL is in excellent agreement with ours, while his result for the total energy radiated is seen to be an underestimate. As we know from the work of Davis et al [2] for a particle falling from infinity with $v_\infty = 0$ most of the radiation is carried by the $l = 2$ mode. Not so here, in fact in our case less than 50% is carried in the quadrupole mode (we obtain $\Delta E_{l=2} = 0.1 \frac{\epsilon_0^2 p_0^2}{M}$, $\Delta E_{l=3} = 0.0447 \frac{\epsilon_0^2 p_0^2}{M}$). This is reflected in the angular distribution of the radiated energy (power per solid angle)

$$\frac{dE}{d\Omega} = \Delta E_l \frac{(l-2)!}{(l+2)!} \left[2 \frac{\partial^2}{\partial \theta^2} Y_{l0} + l(l+1) Y_{l0} \right]^2, \quad (9.20)$$

which we plot in Figure 9.3. Compare with figure 5 of [222]. If, as Smarr, we continue to assume that something deep is at work, and that these results can be carried over to the case of two equal mass black holes flying towards each other at (close to) the speed of light, we obtain a wave generation efficiency of 13 %. This is in close agreement with results by D'Eath and Payne [164, 165], who obtain a 16% efficiency (Smarr's results cannot be trusted in this regime, as shown by Payne [168]). Now, D'Eath and Payne's results were achieved by cutting an infinite series for the news function at the second term, so one has to take those results with some care. However, the agreement we find between ours and their results lead us to believe that once again perturbation theory has a much more wider realm of validity. To our knowledge, this is the first alternative to D'Eath and Payne's method of computing the energy release in such events.

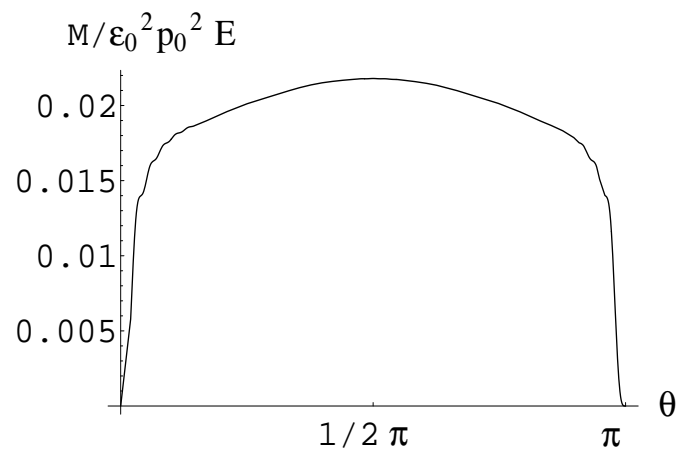


Figure 9.3: The energy radiated per solid angle as a function of θ .

Chapter 10

Gravitational radiation in a curved asymptotically flat four dimensional background: high energy encounters of Kerr black holes with particles

Contents

10.1 Introduction	129
10.2 The Teukolsky and Sasaki-Nakamura formalism	131
10.3 The Sasaki-Nakamura equations for a point particle falling along a geodesic of the Kerr black hole spacetime	133
10.4 Implementing a numerical solution	134
10.5 Numerical Results and Conclusions	135

10.1 Introduction

In the previous chapter we have studied the collision at the speed of light between a point particle and a Schwarzschild black hole [159]. This analyses can describe several phenomena, such as, the collision between small and massive black holes [13], the collision between stars and massive black holes, or the collision between highly relativistic particles like cosmic and gamma rays colliding with black holes [169], to name a few. We have argued in [159, 160] that these studies could give valuable quantitative answers for the collision at the speed of light between equal mass black holes, although we only work with perturbation theory *à la* Regge-Wheeler-Zerilli-Teukolsky-Sasaki-Nakamura, which formally does not describe this process. In fact, extrapolating for two equal mass, Schwarzschild black holes we obtained [159] results which were in very good agreement with results [165] obtained through different methods. For equal mass black holes, we found that the collision at the speed of light between a Schwarzschild black hole and a Kerr black hole along the symmetry axis gave similar results to those in [159]. In particular, we found that 15.5% of the total energy gets converted into

gravitational waves (for two non-rotating holes the amount is slightly less, 13%). There are as yet no numerical results for rotating black holes, so there is no clue as to the correctness of our results for rotating holes. However, should these results give radiated energies larger than that allowed by the cosmic censorship, and therefore by the area theorem, we would run into problems, and we would know that the extrapolation to equal masses is strictly forbidden. Our previous results do not violate the area theorem, but the mere possibility brings us to the study of the collision of a non-rotating black hole with a rotating one, along the equatorial plane, both approaching each other at nearly the speed of light. Sasaki, Nakamura and co-workers [170] have studied the infall of particles, at rest at infinity into Kerr black holes, along the equatorial plane and along the axis. They found that the energy radiated for radial infall along the equatorial plane was about 2.6 times larger than for radial along the axis, for extreme holes. Accordingly, we expect the energy for highly relativistic collisions along the equatorial plane to be larger than that along the symmetry axis, but how larger? If the ratio $\frac{\Delta E_{\text{equator}}}{\Delta E_{\text{axis}}}$ should still be the same, 2.6, then the energy released in the collision along the equatorial plane of a Kerr hole and a non-rotating hole at the speed of light would be $\sim 40\%$ of the total energy. But this is slightly more than the upper bound on the efficiency allowed by the area theorem, which is $\sim 38.7\%$. Motivated mainly by this scenario, we shall study here the collision at nearly the speed of light between a point particle and a Kerr black hole, along its equatorial plane. We will then perform a boost in the Kerr black hole, and extrapolate for two equal mass objects, one rotating, the other non-rotating.

Another point of interest to study this process is the hypothesis that black holes could be produced at the Large Hadron Collider (LHC) at CERN, which has recently been put forward [158] in the so called TeV-scale gravity scenarios. In such scenarios, the hierarchy problem is solved by postulating the existence of n extra dimensions, sub-millimeter sized, such that the $4+n$ Planck scale is equal to the weak scale $\sim 1\text{TeV}$. The Standard Model lives on a 4-dimensional sub-manifold, the brane, whereas gravity propagates in all dimensions. If TeV-scale gravity is correct, then one could manufacture black holes at the LHC. The ability to produce black holes would change the status of black hole collisions from a rare event into a human controlled one. This calls for accurate predictions of gravitational wave spectra and gravitational energy emitted during black hole formation from the high speed encounter of two particles. This investigation was first carried out by D'Eath and Payne [165] by doing a perturbation expansion around the Aichelburg-Sexl metric, describing a boosted Schwarzschild black hole. Their computation was only valid for non-rotating black holes and it seems quite difficult to extend their methods to include for spinning black holes. Our approach however allows one to also study spinning black holes, which is of great importance, since if one forms black holes at the LHC, they will most probably be rotating ones, the chance for having a zero impact parameter being vanishingly small.

Suppose therefore one can produce black holes at LHC. The first thing that should happen is a release of the hole's hair, in a phase termed "balding" [158]. The total amount of energy released in such a phase is not well known, and is based mostly in D'Eath and Payne's results. With our results one can predict the total gravitational energy radiated in the balding phase when the resulting holes are rotating, a process which, as we shall see, radiates a tremendous amount of energy. This means that there will be a "missing" energy during the formation of a black hole, this energy being carried away by gravitational waves, and undetected, at least by any realistic present technology. Our results suggest that at most 35% of the center of mass energy can be leaking away as gravitational waves, and therefore one should have at most

35% missing energy. Strictly speaking, these values are only valid for a head-on collision, i.e. a collision with zero impact parameter, along the equatorial plane. One expects the total energy to decrease if the collision is taken along a different plane, or specially with non-zero impact parameter.

10.2 The Teukolsky and Sasaki-Nakamura formalism

In this section, we give a very brief account of the Teukolsky equation, and of the Sasaki-Nakamura equation. Details about the Teukolsky formalism may be found in the original literature [171], and also in [172]. For a good account of the Sasaki-Nakamura formalism we refer the reader to [170, 173, 174].

We start from the Kerr background geometry, written in Boyer-Lindquist (t, r, θ, ϕ) coordinates:

$$ds^2 = -\left(1 - \frac{2Mr}{\Sigma}\right)dt^2 - \frac{4Mar}{\Sigma} \sin^2 \theta dt d\phi + \frac{\Sigma}{\Delta} dr^2 + \Sigma d\theta^2 + \frac{A \sin^2 \theta}{\Sigma} d\phi^2, \quad (10.1)$$

Here, M is the mass of the black hole, and a its angular momentum per unit mass. Also $\Sigma = r^2 + a^2 \cos^2 \theta$; $\Delta = r^2 + a^2 - 2Mr$; $A = (r^2 + a^2)^2 - \Delta a^2 \sin^2 \theta$.

Working with Kinnersley's null tetrad, one can show [171] that the equations for the Newman-Penrose quantities decouple and separate, giving rise to the Teukolsky equation,

$$\Delta^{-s} \frac{d}{dr} (\Delta^{s+1} \frac{d}{dr} {}_s R) - {}_s V {}_s R = - {}_s T. \quad (10.2)$$

Here,

$${}_s V = \frac{-K^2}{\Delta} + \frac{isK\Delta'}{\Delta} - \frac{2isK'}{\Delta} - 2isK' + {}_s \lambda \quad (10.3)$$

$$K = (r^2 + a^2)\omega - am, \quad (10.4)$$

and a prime denotes derivative with respect to r . The quantity s denotes the spin weight (or helicity) of the field under consideration (see for example [175]) and m is an azimuthal quantum number. We are interested in gravitational perturbations, which have spin-weight $s = -2, +2$. Solutions with $s = -2$ are related to those with $s = 2$ via the Teukolsky-Starobinsky identities, so we need only worry about a specific one. For definiteness, and because that was the choice adopted by Sasaki and others [170], we work with $s = -2$. The constants $m, {}_s \lambda$ (${}_s \lambda$ depends non-linearly on ω) are separation constants arising from the azimuthal function $e^{im\phi}$ and the angular eigenfunction ${}_s Z_{lm}^{a\omega}(\theta, \phi)$, respectively. ${}_s Z_{lm}^{a\omega}(\theta, \phi)$ is the spin-weighted spheroidal harmonic, ${}_s Z_{lm}^{a\omega}(\theta, \phi) = \frac{1}{(2\pi)^{1/2}} {}_s S_{lm}^{a\omega}(\theta) e^{im\phi}$, and in turn, ${}_s S_{lm}^{a\omega}(\theta)$ satisfies

$$\frac{1}{\sin \theta} \frac{d}{d\theta} \left(\sin \theta \frac{d}{d\theta} S \right) + \left(a^2 \cos^2 \theta - \frac{m^2}{\sin^2 \theta} + 4a\omega \cos \theta + \frac{4m \cos \theta}{\sin^2 \theta} - 4 \cot^2 \theta + c \right) S = 0, \quad (10.5)$$

where $c = \lambda - 2 - a^2\omega^2 + 2am\omega$. The spheroidal functions are normalized according to $\int d\Omega |{}_s Z_{lm}^{a\omega}(\theta, \phi)|^2 = 1$. These functions have not been thoroughly exploited as far as we know, but the essentials, together with tables for the eigenvalues λ for $s = -2$ can be found in

[176, 177]. The source term ${}_sT$ appearing in (10.2) may be found in [172], and depends on the stress-energy tensor of the perturbation under consideration. We note that, for a test particle falling in from infinity with zero velocity, for example, $T \sim r^{7/2}$ and V is always long-range. This means that when we try to solve the Teukolsky equation (10.2) numerically we will run into problems, since usually the numerical solution is accomplished by integrating the source term times certain homogeneous solutions. At infinity this integral will not be well defined since the source term explodes there, and also because since the potential is long range, the homogeneous solution will also explode at infinity. We can remedy this long-range nature of the potential and at the same time regularize the source term in the Sasaki-Nakamura formalism. After a set of transformations, the Teukolsky equation (10.2) may be brought to the Sasaki-Nakamura form [173]:

$$\frac{d^2}{dr_*^2}X(\omega, r) - \mathcal{F}\frac{d}{dr_*}X(\omega, r) - \mathcal{U}X(\omega, r) = \mathcal{L}. \quad (10.6)$$

The functions \mathcal{F} and \mathcal{U} can be found in the original literature [170, 173]. The source term \mathcal{L} is given by

$$\mathcal{L} = \frac{\gamma_0\Delta}{r^2(r^2 + a^2)^{3/2}}We^{-i\int K/\Delta dr_*}, \quad (10.7)$$

and W satisfies

$$W'' = -\frac{r^2}{\Delta}Te^{i\int K/\Delta dr_*}. \quad (10.8)$$

The tortoise r_* coordinate is defined by $dr_*/dr = (r^2 + a^2)/\Delta$, and ranges from $-\infty$ at the horizon to $+\infty$ at spatial infinity. The Sasaki-Nakamura equation (10.6) is to be solved under the “only outgoing radiation at infinity” boundary condition (see section 4.2), meaning

$$X(\omega, r) = X^{\text{out}}e^{i\omega r_*}, r_* \rightarrow \infty. \quad (10.9)$$

The two independent polarization modes of the metric, h_+ and h_\times , are given by

$$h_+ + ih_\times = \frac{8}{r\sqrt{2\pi}} \int_{-\infty}^{+\infty} d\omega \sum_{l,m} e^{i\omega(r_*-t)} \frac{X^{\text{out}}S_{lm}^{a\omega}(\theta)}{\lambda(\lambda+2) - 12i\omega - 12a^2\omega^2} e^{im\phi}, \quad (10.10)$$

and the power per frequency per unit solid angle is

$$\frac{d^2E}{d\Omega d\omega} = \frac{4\omega^2}{\pi} \left| \sum_{l,m} \frac{X^{\text{out}}}{\lambda(\lambda+2) - 12i\omega - 12a^2\omega^2} S_{lm}^{a\omega} \right|^2. \quad (10.11)$$

Following Nakamura and Sasaki [170] the multipolar structure is given by

$$h_+ + ih_\times = -\frac{(2\pi)^{1/2}}{r} \int_{-\infty}^{+\infty} d\omega \sum_{l,m} e^{i\omega(r_*-t)} [h^{lm}(\omega) {}_{-2}Y_{lm}] e^{im\phi}, \quad (10.12)$$

which defines h^{lm} implicitly. Moreover,

$$\Delta E = \frac{\pi}{4} \int_0^\infty \sum_{lm} |h^{lm}(\omega)|^2 + |h^{lm}(-\omega)|^2. \quad (10.13)$$

Here, ${}_{-2}Y_{lm}(\theta)$ are spin-weighted spherical harmonics (basically ${}_2S_{lm}^{a\omega=0}(\theta)$), whose properties are described by Newman and Penrose [175] and Goldberg et al [178].

For the benefit of comparison, the general relation between Sasaki and Nakamura's $X(\omega, r)$ function and Teukolsky's $R(\omega, r)$ function is given in [170] in terms of some complicated expressions. One finds however that near infinity, which is the region we are interested in, this relation simplifies enormously. In fact, when $r_* \rightarrow \infty$, the relation is

$$R = R^{\text{out}} r^3 e^{i\omega r_*} \quad (10.14)$$

where,

$$R^{\text{out}} \equiv -\frac{4\omega^2 X^{\text{out}}}{\lambda(\lambda + 2) - 12i\omega - 12a^2\omega^2}. \quad (10.15)$$

10.3 The Sasaki-Nakamura equations for a point particle falling along a geodesic of the Kerr black hole spacetime

The dependence of the emitted gravitational wave power on the trajectory of the particle comes entirely from the source \mathcal{L} in eqs. (10.6)-(10.7), which in turn through (10.8) depends on the source term T in Teukolsky's equation (10.2). To compute the explicit dependence, one would have to consider the general expression for the geodesics in the Kerr geometry [40], which in general gives an end result not very amenable to work with. However we find that by working in the highly relativistic regime, the equations simplify enormously, and in particular for radial infall (along the symmetry axis or along the equator) it is possible to find a closed analytic and simple expression for W in (10.7)-(10.8). Accordingly, we shall in the following give the closed expressions for \mathcal{L} in these two special situations: radial infall along the symmetry axis and radial infall along the equator of an highly energetic particle.

10.3.1 The Sasaki-Nakamura equations for an highly relativistic point particle falling along the symmetry axis of the Kerr black hole

We now specialize then all the previous equations to the case under study. We suppose the particle to be falling radially along the symmetry axis of the Kerr hole, in which case all the equations simplify enormously. In this case the geodesics, written in Boyer-Lindquist coordinates, are

$$\frac{dt}{d\tau} = \frac{\epsilon_0(r^2 + a^2)}{\Delta}; \quad \left(\frac{dr}{d\tau}\right)^2 = \epsilon_0^2 - \frac{\Delta}{r^2 + a^2}; \quad \frac{d\phi}{d\tau} = \frac{a\epsilon_0}{\Delta}, \quad (10.16)$$

where the parameter ϵ_0 is the energy per unit rest mass of the infalling particle. On considering highly relativistic particles, $\epsilon_0 \rightarrow \infty$, we find that the term \mathcal{L} takes the simple form (compare with the source term in [159, 160]) :

$$\mathcal{L} = -\frac{\mu C \epsilon_0 \gamma_0 \Delta}{2\omega^2 r^2 (r^2 + a^2)^{3/2}} e^{-i\omega r_*}. \quad (10.17)$$

Here, $C = \left[\frac{8Z_{l0}^{a\omega}}{\sin^2\theta} \right]_{\theta=0}$, the function $\gamma_0 = \gamma_0(r)$ can be found in [170], while μ is the mass of the particle.

10.3.2 The Sasaki-Nakamura equations for an highly relativistic point particle falling along the equatorial plane of the Kerr black hole

We now suppose the particle is falling radially along the equator of the Kerr hole, where radially is defined in the sense of Chandrasekhar [40], meaning that $L = a\epsilon_0$, where L is the conserved angular momentum. In this case the geodesics, written in Boyer-Lindquist coordinates, are

$$\frac{dt}{d\tau} = \frac{\epsilon_0(r^2 + a^2)}{\Delta}; \quad r^2\left(\frac{dr}{d\tau}\right)^2 = \epsilon_0^2 r^2 - \Delta; \quad \frac{d\phi}{d\tau} = \frac{a\epsilon_0}{\Delta}. \quad (10.18)$$

On considering highly relativistic particles, $\epsilon_0 \rightarrow \infty$, we find that the source term takes again a very simple form (compare with the source term in [159, 160]):

$$\mathcal{L} = -\frac{\mu \hat{S} \epsilon_0 \gamma_0 \Delta}{\omega^2 r^2 (r^2 + a^2)^{3/2}} e^{-i \int \frac{\kappa}{\Delta} dr}, \quad (10.19)$$

where

$$\hat{S} = \left[\frac{\lambda}{2} - (m - a\omega)^2 \right] Z_{lm}(\theta = \frac{\pi}{2}) + [(m - a\omega)] Z'_{lm}(\theta = \frac{\pi}{2}) \quad (10.20)$$

Once X^{out} is known, we can get the Teukolsky wavefunction near infinity from (10.14), and the waveform and energy spectra from (10.10)-(10.13).

10.4 Implementing a numerical solution

To compute the spin-weighted spheroidal functions, one would have to compute the eigenvalues λ , for each ω , using a shooting method [179] or any other numerical scheme one chooses [170, 174]. We have chosen to lean ourselves on work already done by Press and Teukolsky [176] and to verify at each step the correctness of their results (we found no discrepancies). Press and Teukolsky have found, for each (l, m) , a sixth-order polynomial (in $a\omega$) which approximates the eigenvalue λ , to within five decimal places (see their Table 1). This is a good approximation as long as $a\omega < 3$, which is within our demands for $l < 6$. The computation of the spheroidal function then follows trivially, by numerically integrating (10.5).

The next step is to determine $X(\omega, r)$ from the Sasaki-Nakamura differential equation (10.6). This is accomplished by a Green's function technique, constructed so as to satisfy the usual boundary conditions, i.e., only ingoing waves at the horizon ($X \sim e^{-i\omega r_*}, r_* \rightarrow -\infty$) and outgoing waves at infinity ($X \sim e^{i\omega r_*}, r_* \rightarrow \infty$). We get that, near infinity, and for infall along the equator (we are interested in knowing the wavefunction in this region),

$$X = X^\infty \int \frac{X^H \mathcal{S}}{\text{Wr}} dr_*; \quad X^{\text{out}} = \int \frac{X^H \mathcal{S}}{\text{Wr}} dr_*. \quad (10.21)$$

The similar expression for infall along the symmetry axis is given in [160]. Here, X^∞ and X^H are two linearly independent homogeneous solutions of (10.6) which asymptotically behave as

$$X^H \sim A(\omega)e^{i\omega r_*} + B(\omega)e^{-i\omega r_*}, r_* \rightarrow \infty \quad (10.22)$$

$$X^H \sim e^{-i\omega r_*}, r_* \rightarrow -\infty \quad (10.23)$$

$$X^\infty \sim e^{i\omega r_*}, r_* \rightarrow \infty \quad (10.24)$$

$$X^\infty \sim C(\omega)e^{i\omega r_*} + D(\omega)e^{-i\omega r_*}, r_* \rightarrow -\infty, \quad (10.25)$$

and W is the wronskian of these two solutions. Expression (10.21) can be further simplified in the case of infall along the equator to

$$X^{\text{out}} = -\frac{\mu\epsilon_0 c_0 \hat{S}}{2i\omega^3 B} \int \frac{e^{-i\int \frac{K}{\Delta} dr} X^H}{r^2(r^2 + a^2)^{1/2}} dr. \quad (10.26)$$

To implement a numerical solution, we first have to determine $B(\omega)$. We find $B(\omega)$ by solving (10.6) with the right hand side set to zero, and with the starting condition $X^H = e^{-i\omega r_*}$ imposed at a large negative value of r_* . For computational purposes good accuracy is hard to achieve with the form (10.22), so we used an asymptotic solution one order higher in $1/(\omega r)$:

$$X^H = A(\omega)\left(1 + \frac{i(\lambda+2+2am\omega-2i\omega P)}{2\omega r}\right)e^{i\omega r_*} + B(\omega)\left(1 - \frac{i(\lambda+2+2am\omega-2i\omega P)}{2\omega r}\right)e^{-i\omega r_*}, r_* \rightarrow +\infty. \quad (10.27)$$

Here, $P = \frac{8ai(-m\lambda+a\omega(\lambda-3))}{12a^2\omega^2+12iM\omega-\lambda^2-2\lambda-12am\omega}$. These expressions all refer to the case of infall along the equator. For analogous expressions for infall along the symmetry axis see [160].

In the numerical work, we chose to adopt r as the independent variable, thereby avoiding the numerical inversion of $r_*(r)$. A fourth order Runge-Kutta routine started the integration of X^H near the horizon, at $r = r_+ + r_+\epsilon$ (the horizon radius r_+ is $r_+ = M + (M^2 - a^2)^{1/2}$), with typically $\epsilon = 10^{-5}$. It then integrated out to large values of r , where one matches X^H extracted numerically with the asymptotic solution (10.27), in order to find $B(\omega)$. To find ΔE the integral in (10.13) is done by Simpson's rule. For both routines Richardson extrapolation is used.

10.5 Numerical Results and Conclusions

Recent studies [159, 160] on high energy collisions of point particles with black holes point to the existence of some characteristic features of these processes, namely: (i) the spectrum and waveform largely depend upon the lowest quasinormal frequency of the spacetime under consideration; (ii) there is a non-vanishing zero frequency limit (ZFL) for the spectra, $\frac{dE}{d\omega} \omega \rightarrow 0$, and it seems to be independent of the spin of the colliding particles whereas for low-energy collisions the ZFL is zero; (iii) the energy radiated in each multipole has a power-law dependence rather than exponential for low-energy collisions.

The present study reinforces all these aspects. In Fig. 10.1 we show, for an almost extreme Kerr hole with $a = 0.999M$, the energy spectra for the four lowest values of l , when the particle collides along the equatorial plane. In Fig. 10.2 we show the same values but for a collision along the symmetry axis. The existence of a non-vanishing ZFL is evident, but the

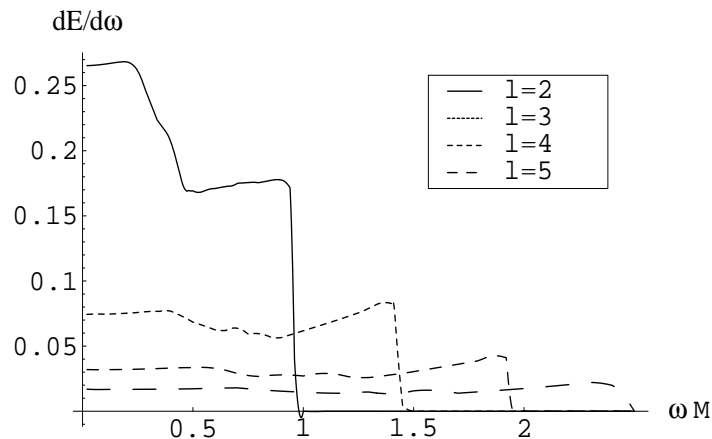


Figure 10.1: The energy spectra for a point particle moving at nearly the speed of light and colliding, along the equatorial plane, with an extreme ($a=0.999M$) Kerr black hole. The energy is normalized in units of $\mu^2\epsilon_0^2$. Notice that the spectra is almost flat (for large l), the ZFL is non-vanishing and that the quadrupole carries less than half of the total radiated energy.

Table 10.1: The zero frequency limit (ZFL) for the ten lowest radiatable multipoles.

l	ZFL($\times \frac{1}{\mu^2\epsilon_0^2}$)	l	ZFL($\times \frac{1}{\mu^2\epsilon_0^2}$)
2	0.265	7	0.0068
3	0.075	8	0.0043
4	0.032	9	0.003
5	0.0166	10	0.0023
6	0.01	11	0.0017

most important in this regard is that the ZFL is exactly the same, whether the black hole is spinning or not, or whether the particle is falling along the equator or along the symmetry axis. In fact, our numerical results show that, up to the numerical error of about 1% the ZFL is given by Table 10.1 (see also [159] and the exact value given by Smarr [222]), and this holds for highly relativistic particles falling along the equator (present work), along the symmetry axis [159, 160], or falling into a Schwarzschild black hole [159].

The l -dependence of the energy radiated is a power-law; in fact for large l we find for infall along the equator

$$\Delta E_l = 0.61 \frac{\mu^2 \epsilon_0^2}{M^{1.666}} , \quad a = 0.999M. \quad (10.28)$$

Such a power-law dependence seems to be universal for high energy collisions. Together with the universality of the ZFL this is one of the most important results borne out of our numerical studies. The exponent of l in (10.28) depends on the rotation parameter. As a decreases, the exponent increases monotonically, until it reaches the Schwarzschild value of 2 ($\Delta E_l \sim \frac{1}{l^2}$) which was also found for particles falling along the symmetry axis of a Kerr hole. In Table 10.2 we show the values of the exponent, as well as the total energy radiated, for some values of the rotation parameter a .

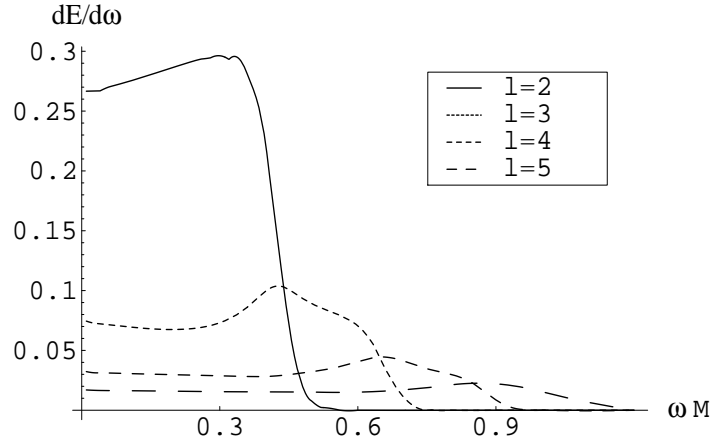


Figure 10.2: The energy spectra for a point particle moving at nearly the speed of light and colliding, along the symmetry axis, with an extreme ($a=0.999M$) Kerr black hole. The energy is normalized in units of $\mu^2\epsilon_0^2$. Notice that the spectra is almost flat (for large l), the ZFL is non-vanishing and that the quadrupole carries less than half of the total radiated energy.

Table 10.2: Power-law dependence of the energy radiated in each multipole l , here shown for some values of a , the rotation parameter. We write $\Delta E_l = \frac{c}{l^b}$ for the energy emitted for each l and ΔE_{tot} for the total energy radiated away. The collision happens along the equatorial plane.

$\Delta E_l = cl^{-b}$			
$\frac{a}{M}$	c	b	$\Delta E_{\text{tot}} \frac{M}{\mu^2\epsilon_0^2}$
0.999	0.61	1.666	0.69
0.8	0.446	1.856	0.36
0.5	0.375	1.88	0.29
0	0.4	2	0.26

This power-law dependence and our numerical results allow us to infer that the total energy radiated for a collision along the equator is

$$\Delta E_{\text{tot}} = 0.69 \frac{\mu^2\epsilon_0^2}{M}, \quad a = 0.999M. \quad (10.29)$$

This represents a considerable enhancement of the total radiated energy, in relation to the Schwarzschild case [159] or even to the infall along the symmetry axis [160]. Again, the energy carried by the $l = 2$ mode ($\Delta E_{l=2} = 0.2 \frac{\mu^2\epsilon_0^2}{M}$, $a = 0.999M$) is much less than the total radiated energy. In Fig. 10.3 we show, for $l = 2$, the energy spectra as a function of m , which allows us to see clearly the influence of the quasinormal modes. Indeed, one can see that the energy radiated for $m = 2$ is much higher than for $m = -2$, and this is due to the behaviour of the quasinormal frequency for different azimuthal numbers m [180], as emphasized by different authors [170]. A peculiar aspect is that the energy radiated for $m + l = \text{odd}$ is about two orders of magnitude lower than for $m + l = \text{even}$, and that is why the spectra for $m = -1, 1$ is not plotted in Fig. 10.3. Notice that the ZFL is the same for

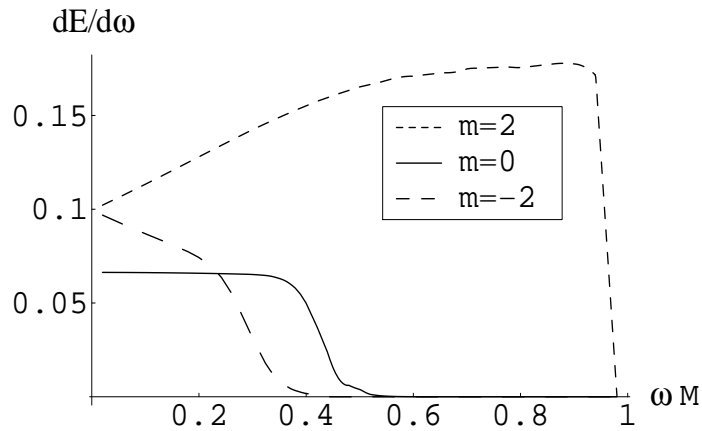


Figure 10.3: The energy spectra as a function of m for $l = 2$ and for an highly relativistic particle falling along the equatorial plane of a Kerr black hole. The energy is normalized in units of $\mu^2 \epsilon_0^2$.

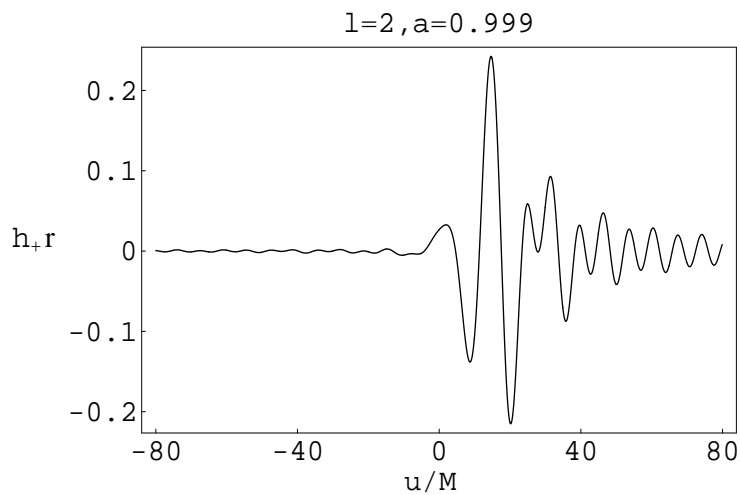


Figure 10.4: The $l = 2$ waveform as defined by (10.12) for an highly relativistic particle falling along the equatorial plane of an extreme ($a=0.999$) Kerr black hole. The waveform is normalized in units of $\mu \epsilon_0$.

$m = 2$ and for $m = -2$ both conspiring to make the ZFL universal. In Fig. 10.4 we show the $l = 2$ waveform for $a = 0.999M$ as seen in $\phi = 0, \theta = \pi/2$. By symmetry, $h_{\times} = 0$.

Up to now, we dealt only with the head-on collision between a particle and a black hole. What can we say about collisions with non-zero impact parameter, and along the equator? As is clear from our results, the fact that the quasinormal modes are excited is fundamental in obtaining those high values for the total energy radiated. Previous studies [180] show that the quasinormal modes are still strongly excited if the impact parameter is less than $2M$. We are therefore tempted to speculate that as long as the impact parameter is less than $2M$ the total energy radiated is still given by Table 10.2. For larger values of the impact parameter, one expects the total energy to decrease rapidly. Moreover, for large impact parameters, Smarr's calculation [222] should apply (but see also other work cited in [222]). On the other hand, if the collision is not along the equatorial plane, we do expect the total energy to decrease. For example, if the collision is along the symmetry axis, we know [160] that the total energy is $0.31 \frac{\mu^2 \epsilon_0^2}{M}$ for $a = 0.999M$. So we expect that as the angle between the collision axis and the equator is varied between 0 and $\pi/2$ the total energy will be a monotonic function decreasing from $0.69 \frac{\mu^2 \epsilon_0^2}{M}$ to $0.31 \frac{\mu^2 \epsilon_0^2}{M}$. Still, more work is necessary to confirm this. Let us now consider, using these results, the collision at nearly the speed of light between a Schwarzschild and a Kerr black hole, along the equatorial plane. We have argued in previous papers [159, 160] that the naive extrapolation $\mu \rightarrow M$ may give sensible results, so let's pursue that idea here. We obtain an efficiency of 34.5% for gravitational wave generation, a remarkable increase relative to the Schwarzschild-Schwarzschild collision. Now, the area theorem gives an upper limit of 38.7% so we may conclude with two remarks: (a) these perturbative methods pass the area theorem test; (b) we are facing the most energetic events in the Universe, with the amazing fraction of 34.5% of the rest mass being converted into gravitational waves.

Chapter 11

Radiation in asymptotically anti-de Sitter in three, four and higher dimensional spacetimes

Contents

11.1 Introduction	141
11.2 Scalar radiation from infall of a particle into a BTZ black hole	143
11.3 Scalar radiation from infall of a particle into a D -dimensional Schwarzschild-anti-de Sitter black hole	149
11.4 Conclusions	159

11.1 Introduction

Anti-de Sitter (AdS) spacetime has been considered of fundamental meaning within high energy elementary particle physics, specially in supersymmetric theories of gravity such as 11-dimensional supergravity and M-theory (or string theory). The dimension D of AdS spacetime is a parameter which can have values from two to eleven, and where the other spare dimensions either are joined as a compact manifold \mathcal{M} into the whole spacetime to yield $\text{AdS}_d \times \mathcal{M}^{11-D}$ or receive a Kaluza-Klein treatment. AdS spacetime appears as the background for black holes solutions and it also plays a further crucial role since it is the near-horizon geometry, separated by a (soft) boundary from an otherwise asymptotically flat spacetime, of some black solutions [181]. In addition, by taking low energy limits at strong coupling and through group theoretic analysis, Maldacena conjectured a correspondence between the bulk of AdS spacetime and a dual conformal field gauge theory (CFT) on the spacetime boundary itself [27]. A concrete method to implement this correspondence is to identify the extremum of the classical string theory action I for the dilaton field φ , say, at the boundary of AdS, with the generating functional W of the Green's correlation functions in the CFT for the operator \mathcal{O} that corresponds to φ [182], $I_{\varphi_0(x^\mu)} = W[\varphi_0(x^\mu)]$, where φ_0 is the value of φ at the AdS boundary and the x^μ label the coordinates of the boundary. The motivation for this

proposal can be seen in the reviews [183, 28]. In its strongest form the conjecture requires that the spacetime be asymptotically AdS, the interior could be full of gravitons or containing a black hole. The correspondence realizes the holographic principle, since the bulk is effectively encoded in the boundary, and is also a strong/weak duality, it can be used to study issues of strong gravity using weak CFT or CFT issues at strong coupling using classical gravity in the bulk.

A particular important AdS dimension is three. In AdS₃ Einstein gravity is simple, the group of isometries is given by two copies of $SL(2, R)$, it has no propagating degrees of freedom, is renormalizable, it allows for the analytical computation of many physical processes extremely difficult or even impossible in higher dimensions, it belongs to the full string theory compactification scheme [183, 28], the dual CFT₂ is the low-energy field theory of a D1-D5-brane system which can be thought of as living on a cylinder (the boundary of AdS₃) [184], and it contains the BTZ black hole. The BTZ black hole is of considerable interest, not only because it can yield exact results, but also because one hopes that the results can qualitatively be carried through to higher dimensions. Several results related to the BTZ black hole itself and to the AdS/CFT correspondence have been obtained [185, 186, 187, 188]. The AdS/CFT mapping implies that a black hole in the bulk corresponds to a thermal state in the gauge theory [189]. Perturbing the black hole corresponds to perturbing the thermal state and the decaying of the perturbation is equivalent to the return to the thermal state. Particles initially far from the black hole correspond to a blob (a localized excitation) in the CFT, as the IR/UV duality teaches [190]. The evolution towards the black hole represents a growing size of the blob with the blob turning into a bubble traveling close to the speed of light [186].

In this chapter we will extend some of the previous results and we begin by studying in detail the collision between a BTZ black hole and a scalar particle. This will follow closely [195] (see also [196]). Generically, a charged particle falling towards a black hole emits radiation of the corresponding field. In higher dimensions it also emits gravitational waves, but since in three dimensions there is no gravitational propagation in the BTZ case there is no emission.

Thus, a scalar particle falling into a BTZ black hole emits scalar waves. This collision process is important from the points of view of three-dimensional dynamics and of the AdS/CFT conjecture. Furthermore, one can compare this process with previous works, since there are exact results for the quasinormal mode (QNM) spectrum of scalar perturbations which are known to govern their decay at intermediate and late times [48, 37, 196, 78, 42, 77].

The phenomenon of radiation emission generated from an infalling particle in asymptotically flat spacetimes has been studied by several authors [2, 3, 4, 5] and most recently in [163], where the results are to be compared to full scale numerical computations for strong gravitational wave emission of astrophysical events [191] which will be observed by the GEO600, LIGO and VIRGO projects. A scalar infalling particle as a model for calculating radiation reaction in flat spacetimes has been considered in [192]. Many of the techniques have been developed in connection to such spacetimes. Such an analysis has not been carried to non-asymptotically flat spacetimes, which could deepen our understanding of these kind of events, and of Einstein's equations. In this respect, for the mentioned reasons, AdS spacetimes are the most promising candidates. As asymptotically flat spacetimes they provide well defined conserved charges and positive energy theorems, which makes them a good testing ground if one wants to go beyond flatness. However, due to different boundary conditions it raises new problems. The first one is that since the natural boundary conditions are boxy-like all of the generated radiation will eventually fall into the black hole, thus infinity has no special

meaning in this problem, it is as good a place as any other, i.e., one can calculate the radiation passing at any radius r , for instance near the horizon. Second, in contrast to asymptotically flat spacetimes, here one cannot put a particle at infinity (it needs an infinite amount of energy) and thus the particle has to start from finite r . This has been posed in [163] but was not fully solved when applied to AdS spacetimes.

We shall then extend the analysis, and compute in detail the collision between a black hole and a scalar particle in general dimensions [224]. This collision process is interesting from the point of view of the dynamics itself in relation to the possibility of manufacturing black holes at LHC within the brane world scenario [151, 158], and from the point of view of the AdS/CFT conjecture, since the scalar field can represent the string theory dilaton, and 4, 5, 7 (besides 3) are dimensions of interest for the AdS/CFT correspondence [28, 48]. In addition, one can compare this process with previous works, since there are results for the quasinormal modes of scalar, and electromagnetic perturbations which are known to govern the decay of the perturbations, at intermediate and late times [77, 78, 48, 195, 75].

Some general comments can be made about the mapping AdS/CFT when it involves a black hole. A black hole in the bulk corresponds to a thermal state in the gauge theory [189]. Perturbing the black hole corresponds to perturbing the thermal state and the decaying of the perturbation is equivalent to the return to the thermal state. So one obtains a prediction for the thermal time scale in the strongly coupled CFT. Particles initially far from the black hole correspond to a blob (a localized excitation) in the CFT, as the IR/UV duality teaches (a position in the bulk is equivalent to size of an object) [190]. The evolution toward the black hole represents a growing size of the blob with the blob turning into a bubble travelling close to the speed of light [186]. For other processes in anti-de Sitter spacetime, we refer the reader to [197] and references therein.

11.2 Scalar radiation from infall of a particle into a BTZ black hole

11.2.1 Formulation of the problem and basic equations

We consider a small test particle of mass m_0 and charge q_0 , coupled to a massless scalar field φ , moving along a radial timelike geodesic outside a BTZ black hole of mass M . The metric outside the BTZ black hole is

$$ds^2 = f(r)dt^2 - \frac{dr^2}{f(r)} - r^2d\theta^2, \quad (11.1)$$

where, $f(r) = (-M + \frac{r^2}{l^2})$, l is the AdS radius ($G=1/8$; $c=1$). The horizon radius is given by $r_+ = M^{1/2}l$. We treat the scalar field as a perturbation, so we shall neglect the back reaction of the field's stress tensor on the metric (this does not introduce large errors [5]). If we represent the particle's worldline by $x^\mu = x_p^\mu(\tau)$, with τ the proper time along a geodesic,

then the interaction action \mathcal{I} is

$$\mathcal{I} = -\frac{1}{8\pi} \int g^{1/2} \varphi_{;a} \varphi^{;a} d^3y - m_0 \int (1 + q_0 \varphi) (-g_{ab} \dot{x}^a \dot{x}^b)^{1/2} d\tau, \quad (11.2)$$

and thus the scalar field satisfies the inhomogeneous wave equation $\square\varphi = -4\pi m_0 q_0 \int \delta^3(x^\mu - x_p^\mu(\tau)) (-g)^{-1/2} d\tau$, where g is the metric determinant and \square denotes the covariant wave operator. As the particle moves on a timelike geodesic, we have

$$\dot{t}_p = \frac{\mathcal{E}}{f(r_p)}, \quad \dot{r}_p = -(\mathcal{E}^2 - f(r_p))^{1/2}, \quad (11.3)$$

where $\dot{} \equiv d/d\tau$, and \mathcal{E} is a conserved energy parameter. We shall be considering the test particle initially at rest at a distance r_0 (where $\mathcal{E}^2 = f(r_0)$) and at $\theta_p = 0$. Expanding the field as

$$\varphi(t, r, \theta) = \frac{1}{r^{1/2}} \phi(t, r) \sum_m e^{im\theta}, \quad (11.4)$$

where m is the angular momentum quantum number, the wave equation is given by (after an integration in θ)

$$\begin{aligned} \frac{\partial^2 \phi(t, r)}{\partial r_*^2} - \frac{\partial^2 \phi(t, r)}{\partial t^2} - V(r) \phi(t, r) = \\ - \frac{2q_0 m_0 f}{r^{1/2}} \left(\frac{dt}{d\tau}\right)^{-1} \delta(r - r_p), \end{aligned} \quad (11.5)$$

with $V(r) = \frac{3r^2}{4l^4} - \frac{M}{2l^2} - \frac{M^2}{4r^2} + \frac{m^2}{l^2} - \frac{Mm^2}{r^2}$, and $r_* = -M^{-1/2} \operatorname{arccoth}(r M^{-1/2})$.

11.2.2 The initial data and boundary conditions

In the case we study, and in contrast to asymptotically flat spacetimes where initial data can be pushed to infinity [2, 3, 4, 5], initial data must be provided. Accordingly, we take the Laplace transform $\Phi(\omega, r)$ of $\phi(t, r)$ to be

$$\Phi(\omega, r) = \frac{1}{(2\pi)^{1/2}} \int_0^\infty e^{i\omega t} \phi(t, r) dt. \quad (11.6)$$

Then, equation (11.5) may be written as

$$\frac{\partial^2 \Phi(r)}{\partial r_*^2} + [\omega^2 - V(r)] \Phi(r) = S + \frac{i\omega \phi_0}{(2\pi)^{1/2}}, \quad (11.7)$$

with, $S = -\frac{f}{r^{1/2}} \left(\frac{2}{\pi}\right)^{1/2} \frac{1}{\dot{r}_p} e^{i\omega t}$ being the source function, and ϕ_0 is the initial value of $\phi(t, r)$ satisfying $\frac{\partial^2 \phi_0(r, m)}{\partial r_*^2} - V(r) \phi_0(r, m) = -\frac{2f}{r^{1/2}} \left(\frac{dt}{d\tau}\right)^{-1} \delta(r - r_p)$. We have rescaled r , $r \rightarrow \frac{r}{l}$, and measure everything in terms of l , i.e., ϕ , r_+ and ω are to be read, $\frac{1}{l^{1/2} q_0 m_0} \phi$, $\frac{r_+}{l}$ and ωl , respectively. One can numerically solve the equation for the initial data ϕ_0 by demanding regularity at both the horizon and infinity (for a similar problem see [193]). In Fig. 11.1, we show the form of ϕ_0 for a typical case $r_+ = 0.1$, $r_0 = 1$, and for three different values of m , $m = 0, 1, 2$. Other cases like $r_+ = 1, 10, \dots$ and several values of r_0 can be computed. Large

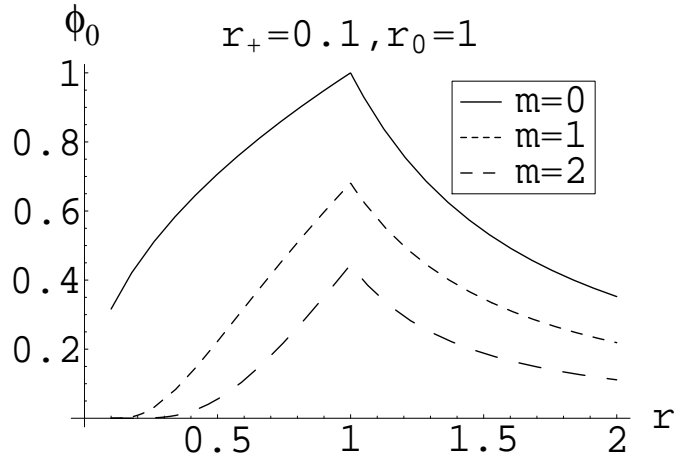


Figure 11.1: Initial data ϕ_0 for a BTZ black hole with $r_+ = 0.1$, and with the particle at $r_0 = 1$, for several values of m , the angular quantum number.

black holes have a direct interpretation in the AdS/CFT conjecture. The results for large or small black holes are nevertheless similar, as we have checked. As a test for the numerical evaluation of ϕ_0 , we have checked that as $r_0 \rightarrow r_+$, all the multipoles fade away, i.e., $\phi_0 \rightarrow 0$, supporting the no-hair conjecture (that all the multipoles go to zero).

To solve equation (11.7) one has to impose physically sensible boundary conditions, appropriate to AdS spacetimes. In our case the potential diverges at infinity, where ϕ_0 vanishes, so we impose reflective boundary conditions [84] there, i.e., $\Phi = 0$ at infinity. It has been common practice to set $\Phi \sim F(\omega)e^{-i\omega r_*}$ near the horizon, meaning ingoing waves there. This is an allowed boundary condition as long as ϕ_0 vanishes there. However, if ϕ_0 does not vanish there, one has to be careful in defining boundary conditions at the horizon. When dealing with AdS spacetimes this detail is crucial to extract the correct information, and it has been overlooked when one deals with asymptotically flat spacetimes as in [163]. Equation (11.7) together with the source term S allow us to conclude that near the horizon $\Phi \sim G(\omega)e^{i\omega r_*} + F(\omega)e^{-i\omega r_*} + \frac{i\phi_0}{(2\pi)^{1/2}\omega}$. Since we want waves going down the black hole, we shall require

$$\Phi \sim F(\omega)e^{-i\omega r_*} + \frac{i\phi_0}{(2\pi)^{1/2}\omega}, r \rightarrow r_+ \quad (11.8)$$

11.2.3 Green's function solution

To proceed we must find a solution to equation (11.7) through a Green's function analysis. A standard treatment [163] invokes contour integration to calculate the integrals near the horizon. There is no need for this here, by demanding regularized integrals the correct boundary conditions appear in a natural way (see [194] for a regularization of the Teukolsky equation). Let Φ^∞ and Φ^H be two independent solutions of the homogeneous form of (11.7), satisfying: $\Phi^H \sim e^{-i\omega r_*}, r \rightarrow r_+$; $\Phi^H \sim A(\omega)r^{1/2} + B(\omega)r^{-3/2}, r \rightarrow \infty$; $\Phi^\infty \sim C(\omega)e^{i\omega r_*} + D(\omega)e^{-i\omega r_*}, r \rightarrow r_+$; $\Phi^\infty \sim 1/r^{3/2}, r \rightarrow \infty$. Define h^H through $dh^H/dr_* = -\Phi^H$

and h^∞ through $dh^\infty/dr_* = -\Phi^\infty$. We can then show that Φ given by

$$\begin{aligned} \Phi = & \frac{1}{W} \left[\Phi^\infty \int_{-\infty}^r \Phi^H S dr_* + \Phi^H \int_r^\infty \Phi^\infty S dr_* \right] + \\ & \frac{i\omega}{(2\pi)^{1/2} W} \left[\Phi^\infty \int_{-\infty}^r h^H \frac{d\phi_0}{dr_*} dr_* + \right. \\ & \quad \left. \Phi^H \int_r^\infty h^\infty \frac{d\phi_0}{dr_*} dr_* + \right. \\ & \quad \left. (h^\infty \phi_0 \Phi^H - h^H \phi_0 \Phi^\infty)(r) \right], \end{aligned} \quad (11.9)$$

is a solution to (11.7) and satisfies the boundary conditions. The Wronskian $W = 2i\omega C(\omega)$ is a constant. Near infinity, we get from (11.9) that

$$\begin{aligned} \Phi(r \rightarrow \infty) = & \frac{1}{W} \left[\Phi_{(r \rightarrow \infty)}^\infty \int_{-\infty}^\infty \Phi^H S dr_* \right] + \\ & \frac{i\omega}{(2\pi)^{1/2} W} \left[\Phi_{(r \rightarrow \infty)}^\infty \int_{-\infty}^\infty h^H \frac{d\phi_0}{dr_*} dr_* + \right. \\ & \quad \left. (h^\infty \phi_0 \Phi^H - h^H \phi_0 \Phi^\infty)(r \rightarrow \infty) \right]. \end{aligned} \quad (11.10)$$

Now, in our case, this is just zero, as it should, because both $\Phi^\infty, \phi_0 \rightarrow 0$, as $r \rightarrow \infty$. However, if one is working with asymptotically flat space, as in [163], where $\Phi^\infty \rightarrow e^{i\omega r_*}$ at infinity, we get (recalling that $\phi_0 \rightarrow 0$):

$$\begin{aligned} \Phi(r \rightarrow \infty) = & \frac{1}{W} \left[\Phi_{(r \rightarrow \infty)}^\infty \int_{-\infty}^\infty \Phi^H S dr_* \right] + \\ & \frac{i\omega}{(2\pi)^{1/2} W} \Phi_{(r \rightarrow \infty)}^\infty \int_{-\infty}^\infty h^H \frac{d\phi_0}{dr_*} dr_*, \end{aligned} \quad (11.11)$$

and where each integral is well defined. In particular, integrating by parts the second integral can be put in the form

$$\begin{aligned} \int_{-\infty}^\infty h^H \frac{d\phi_0}{dr_*} dr_* = & [h^H \phi_0]_{-\infty}^\infty + \int_{-\infty}^\infty \Phi^H \phi_0 dr_* \\ = & \frac{i\phi_0 e^{-i\omega r_*}}{\omega}(r \rightarrow -\infty) + \int_{-\infty}^\infty \Phi^H \phi_0 dr_*. \end{aligned} \quad (11.12)$$

Here, the final sum converges, but not each term in it. Expression (11.12) is just expression (3.15) in [163], although it was obtained imposing incorrect boundary conditions and not well defined regularization schemes. Due to the fact that the initial data vanishes at infinity, the results in [163] are left unchanged. In this work, we are interested in computing the wavefunction $\Phi(r, \omega)$ near the horizon ($r \rightarrow r_+$). In this limit we have

$$\begin{aligned} \Phi(r \sim r_+) = & \frac{1}{W} \left[\Phi^H \int_{r_+}^\infty \Phi^\infty S dr_* \right] + \\ & \frac{i\omega}{(2\pi)^{1/2} W} \Phi^H \left[\int_{r_+}^\infty \Phi^\infty \phi_0 dr_* - (h^\infty \phi_0)(r_+) \right] + \\ & \quad + \frac{i\phi_0(r_+)}{(2\pi)^{1/2} \omega}, \end{aligned} \quad (11.13)$$

where an integration by parts has been used. Fortunately, one can obtain an exact expression for Φ^∞ in terms of hypergeometric functions [195]. The results for Φ^∞ and W are

$$\Phi^\infty = \frac{1}{r^{3/2}(1 - M/r^2)^{\frac{i\omega}{2M^{1/2}}}} F\left(a, b, 2, \frac{M}{r^2}\right), \quad (11.14)$$

$$W = 2i\omega \frac{2^{i\omega} M^{1/2} \Gamma(2) \Gamma(-\frac{i\omega}{M^{1/2}})}{M^{3/4} \Gamma(1 + i\frac{m-\omega}{2\sqrt{M}}) \Gamma(1 - i\frac{m+\omega}{2\sqrt{M}})}. \quad (11.15)$$

Here, $a = 1 + i\frac{m-\omega}{2\sqrt{M}}$ and $b = 1 - i\frac{m+\omega}{2\sqrt{M}}$. So, to find Φ we only have to numerically integrate (11.13). We have also determined Φ^∞ numerically by imposing the boundary conditions above. The agreement between the numerical computed Φ^∞ and (11.14) was excellent. To find $\phi(t, r)$ one must apply the inverse Laplace transformation to $\Phi(\omega, r)$. Integrating the wave equation in this spacetime is simpler than in asymptotically flat space, in the sense that, due to the boundary conditions at infinity the solution is more stable, and less effort is needed to achieve the same accuracy. Using a similar method to that in [163], we estimate the error in our results to be limited from above by 0.5%.

11.2.4 Numerical results for the waveforms and spectra

To better understand the numerical results, we first point out that the QNM frequencies for this geometry, calculated by Cardoso and Lemos [37] (see also [53] for a precise relation between these QNM frequencies and the poles of the correlation functions on the CFT side) are

$$\omega_{\text{QNM}} = \pm m - 2iM^{1/2}(n + 1). \quad (11.16)$$

In Fig. 11.2 we show the waveforms for the $r_+ = 0.1$, $r_0 = 1$ black hole, as a function of the advanced null-coordinate $v = t + r_*$. This illustrates in a beautiful way that QNMs govern the late time behavior of the waveform.

For example, for $m = 0$, $\omega_{\text{QNM}} = -0.2i(n + 1)$, one expects to find a purely decaying perturbation. This is evident from Fig. 11.2. For $m = 1$, $\omega_{\text{QNM}} = 1 - 0.2i(n + 1)$, so the signal should ring (at late times) with frequency one. This is also clearly seen from Fig 11.2. For $m = 2$ we have the same kind of behavior. For large negative v and fixed t one has large negative r_* , so one is near the horizon. Thus $\phi(v \rightarrow -\infty)$ in Fig. 11.2 should give the same values as ϕ_0 at r_+ in Fig. 11.1, which is the case. The energy spectra peaks at higher ω when compared to the fundamental ω_{QNM} as is evident from Fig. 11.3, which means that higher modes are excited. The total radiated energy as a function of m goes to zero slower than $1/m$ implying that the total radiated energy diverges. However, this divergence can be normalized by taking a minimum size L for the particle with a cut off given by $m_{\text{max}} \sim \frac{\pi r_+}{2L}$ [2, 3, 4, 5]. We have calculated for $r_+ = 0.1$ the total energy for the cases $m = 0, 1, 2$, yielding $E_{m=0} \simeq 26$, $E_{m=1} \simeq 12$, $E_{m=2} \simeq 6$. An estimation of the total energy for a particle with $m_{\text{max}} \simeq 1000$ yields $E_{\text{total}} \simeq 80$ (the energy is measured in units of $q_0^2 m_0^2$).

We have also computed the radiated energy for several values of r_0 and verified that is not a monotonic function of r_0 . For small values of r_0 the energy radiated is a linear function of $(r_0 - r_+)$, for intermediate r_0 it has several peaks, and it grows monotonically for large r_0 . The zero frequency limit (ZFL), depends only on the initial data and one can prove that it is given by $(\frac{dE}{d\omega})_{\omega \rightarrow 0} = \phi_0^2$. This is to be contrasted to the ZFL for outgoing gravitational radiation in asymptotically flat spacetimes [222] where it depends only on the initial velocity of the test particle.

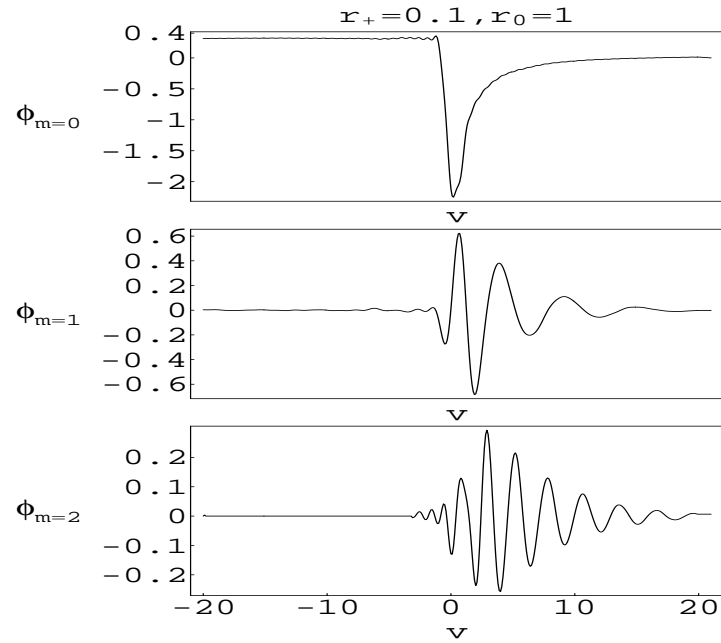


Figure 11.2: Waveforms $\phi(v)$ for a $r_+ = 0.1$, $r_0 = 1$ BTZ black hole, for the three lowest values of m .

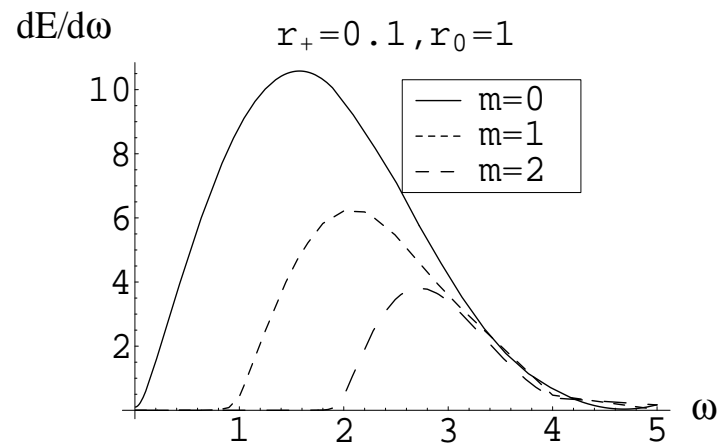


Figure 11.3: Typical energy spectra, here shown for $r_+ = 0.1$, and $r_0 = 1$.

11.3 Scalar radiation from infall of a particle into a D -dimensional Schwarzschild-anti-de Sitter black hole

11.3.1 The Problem, the Equations and the Laplace transform, and the initial and boundary conditions for D -dimensions

11.3.1.a The problem

In this paper we shall present the results of the following process: the radial infall of a small particle coupled to a massless scalar field, into a d -dimensional Schwarzschild-AdS black hole. We will consider that both the mass m_0 and the scalar charge q_s of the particle are a perturbation on the background spacetime, i.e., $m_0, q_s \ll M, R$, where M is the mass of the black hole and R is the AdS radius. In this approximation the background metric is not affected by the scalar field, and is given by

$$ds^2 = f(r) dt^2 - \frac{dr^2}{f(r)} - r^2 d\Omega_{D-2}^2, \quad (11.17)$$

where, $f(r) = \left(\frac{r^2}{R^2} + 1 - \frac{16\pi M}{(D-2)A_{D-2}} \frac{1}{r^{D-3}}\right)$, A_{D-2} is the area of a unit $(D-2)$ sphere, $A_{D-2} = \frac{2\pi^{\frac{D-1}{2}}}{\Gamma(\frac{D-1}{2})}$, and $d\Omega_{D-2}^2$ is the line element on the unit sphere S^{D-2} . The action for the scalar field ϕ and particle is given by a sum of three parts, the action for the scalar field itself, the action for the particle and an interaction piece,

$$\mathcal{I} = -\frac{1}{8\pi} \int \phi_{;a} \phi^{;a} \sqrt{-g} d^D x - m_0 \int (1 + q_s \phi) (-g_{ab} \dot{z}^a \dot{z}^b)^{\frac{1}{2}} d\lambda, \quad (11.18)$$

where g_{ab} is the background metric, g its determinant, and $z^a(\lambda)$ represents the worldline of the particle as a function of an affine parameter λ .

11.3.1.b The equations and the Laplace transform

We now specialize to the radial infall case. In the usual (asymptotically flat) Schwarzschild geometry, one can for example let a particle fall in from infinity with zero velocity there [2, 3, 4, 5]. The peculiar properties of AdS spacetime do not allow a particle at rest at infinity [195] (we would need an infinite amount of energy for that) so we consider the mass m_0 to be held at rest at a given distance r_0 in Schwarzschild coordinates. At $t = 0$ the particle starts falling into the black hole. As the background is spherically symmetric, Laplace's equation separates into the usual spherical harmonics $Y(\theta, \varphi_1, \dots, \varphi_{D-3})$ defined over the $(D-2)$ unit sphere [199], where θ is the polar angle and $\varphi_1, \dots, \varphi_{D-3}$ are going to be considered azimuthal

angles of the problem. In fact, since we are considering radial infall, the situation is symmetric with respect to a $(d - 3)$ sphere. We can thus decompose the scalar field as

$$\phi(t, r, \theta, \varphi_1, \dots, \varphi_{D-3}) = \frac{1}{r^{\frac{D-2}{2}}} \sum_l Z_l(t, r) Y_{l0..0}(\theta). \quad (11.19)$$

The polar angle θ carries all the angular information, and l is the angular quantum number associated with θ . From now on, instead of $Y_{l0..0}(\theta)$, we shall simply write $Y_l(\theta)$ for the spherical harmonics over the $(D - 2)$ unit sphere. In fact $Y_l(\theta)$ is, apart from normalizations, just a Gegenbauer polynomial $C_l^{\frac{D-3}{2}}(\cos \theta)$ [199]. Upon varying the action (11.18), integrating over the $(D - 2)$ sphere and using the orthonormality properties of the spherical harmonics we obtain the following equation for $Z_l(t, r)$

$$\frac{\partial^2 Z_l(t, r)}{\partial r_*^2} - \frac{\partial^2 Z_l(t, r)}{\partial t^2} - V(r) Z_l(t, r) = \frac{4\pi q_s m_0 f}{r^{\frac{D-2}{2}}} \left(\frac{dt}{d\tau}\right)^{-1} \delta(r - r_p(t)) Y_l(0). \quad (11.20)$$

The potential $V(r)$ appearing in equation (11.20) is given by

$$V(r) = f(r) \left[\frac{a}{r^2} + \frac{(D-2)(D-4)f(r)}{4r^2} + \frac{(D-2)f'(r)}{2r} \right], \quad (11.21)$$

where $a = l(l + D - 3)$ is the eigenvalue of the Laplacian on S^{D-2} , and the tortoise coordinate r_* is defined as $\frac{\partial r}{\partial r_*} = f(r)$. By defining the Laplace transform $\tilde{\mathbf{Z}}_l(\omega, r)$ of $Z_l(t, r)$ as

$$\tilde{\mathbf{Z}}(\omega, r) = \frac{1}{(2\pi)^{1/2}} \int_0^\infty e^{i\omega t} Z_l(t, r) dt. \quad (11.22)$$

Then, equation (11.20) transforms into

$$\frac{\partial^2 \tilde{\mathbf{Z}}(\omega, r)}{\partial r_*^2} + [\omega^2 - V(r)] \tilde{\mathbf{Z}}(\omega, r) = S_l(\omega, r) + \frac{i\omega}{(2\pi)^{1/2}} Z_{0l}(r), \quad (11.23)$$

with the source term $S_l(\omega, r)$ given by,

$$S_l(\omega, r) = \frac{2(2\pi)^{1/2} q_s m_0 f Y_l(0)}{r^{(D-2)/2} (E^2 - f)^{1/2}} e^{i\omega T(r)}. \quad (11.24)$$

Note that $Z_{0l}(r)$ is the initial value of $Z(t, r)$, i.e., $Z_{0l}(r) = Z(t = 0, r)$, satisfying

$$\frac{\partial^2 Z_{0l}(r)}{\partial r_*^2} - V(r) Z_{0l}(r) = -\frac{4\pi q_s m_0 f(r) Y_l(0)}{r^{(D-2)/2}} \left(\frac{dt}{d\tau}\right)_{r_0}^{-1} \delta(r - r_0), \quad (11.25)$$

where $r_0 = r_p(t = 0)$. We have represented the particle's worldline by $z^\mu = z_p^\mu(\tau)$, with τ the proper time along a geodesic. Here, $t = T(r)$ describes the particle's radial trajectory giving the time as a function of radius along the geodesic

$$\frac{dT(r)}{dr} = -\frac{E}{f(E^2 - f)^{1/2}} \quad (11.26)$$

with initial conditions $T(r_0) = 0$, and $E^2 = f(r_0)$.

We have rescaled r , $r \rightarrow \frac{r}{R}$, and measure everything in terms of R , i.e., ω is to be read ωR , Ψ is to be read $\frac{R}{q_s m_0} \Psi$ and r_+ , the horizon radius is to be read $\frac{r_+}{R}$.

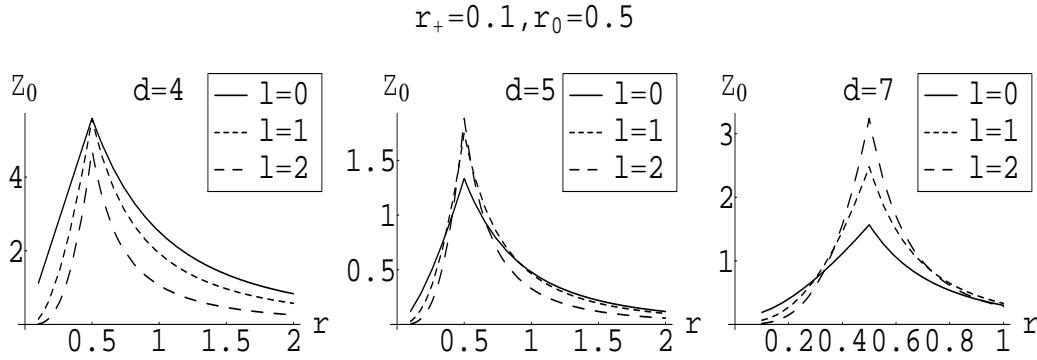


Figure 11.4: Initial data Z_{0l} for a small black hole with $r_+ = 0.1$, for $D = 4, 5$ and 7 (from left to right respectively). The small scalar particle is located at $r_0 = 0.5$. The results are shown for the lowest values of the angular quantum number l .

11.3.1.c The initial data

We can obtain $Z_{0l}(r)$, the initial value of $Z(t, r)$, by solving numerically equation (11.25), demanding regularity at both the horizon and infinity (for a similar problem, see for example [193, 192, 62]). To present the initial data and the results we divide the problem into two categories: (i) small black holes with $r_+ \ll 1$, and (ii) intermediate and large black holes with $r_+ \gtrsim 1$.

(i): Initial data for small black holes, $r_+ = 0.1$

In Fig. 11.4 we present initial data for small black holes with $r_+ = 0.1$ in the dimensions of interest ($d = 4, 5$ and 7). In this case, the fall starts at $r_0 = 0.5$. Results referring to initial data in $d = 3$ (BTZ black hole) are given in [195]. We show a typical form of Z_{0l} for $r_+ = 0.1$ and $r_0 = 0.5$, and for different values of l . As a test for the numerical evaluation of Z_{0l} , we have checked that as $r_0 \rightarrow r_+$, all the multipoles fade away, i.e., $Z_{0l} \rightarrow 0$, supporting the No Hair Conjecture. Note that Z_{0l} has to be small. We are plotting $\frac{Z_{0l}}{q_s m_0 / R}$. Since $q_s m_0 / R \ll 1$ in our approximation one has from Figs. 11.4-11.6 that indeed $Z_{0l} \ll 1$.

(ii): Initial data for intermediate and large black holes, $r_+ = 1$

In Figs. 11.5 and 11.6 we show initial data for an intermediate to large black hole, $r_+ = 1$. In Fig.11.5 the fall starts at $r_0 = 5$. We show a typical form of Z_{0l} for $r_+ = 1$ and $r_0 = 5$, and for different values of l . In Fig. 11.6 it starts further down at $r_0 = 1.5$. We show a typical form of Z_{0l} for $r_+ = 1$ and $r_0 = 1.5$, and for different values of l . Again, we have checked that as $r_0 \rightarrow r_+$, all the multipoles fade away, i.e., $Z_{0l} \rightarrow 0$, supporting the No Hair Conjecture.

Two important remarks are in order: first, it is apparent from Figs. 11.4-11.6 that the field (sum over the multipoles) is divergent at the particle's position r_0 . This is to be expected, as the particle is assumed to be point-like; second, one is led to believe from Figs. 11.4-11.6 (but especially from Figs.11.5 -11.6) that Z_{0l} increases with l . This is not true however, as this behavior is only valid for small values of the angular quantum number l . For large l , Z_{0l} decreases with l , in such a manner as to make $\phi(t, r)$ in (11.19) convergent and finite. For example, for $r_+ = 1, r_0 = 5$ and $D = 4$, we have at $r = 6$, $Z_{0l=20} = 0.781$ and $Z_{0l=40} = 0.3118$.

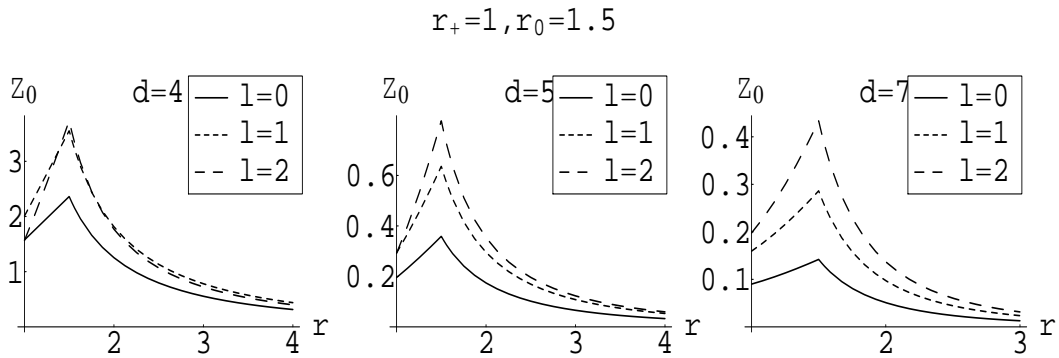


Figure 11.5: Initial data Z_{0l} for a black hole with $r_+ = 1$, and with the particle at $r_0 = 1.5$, for some values of l the angular quantum number. Again, we show the results for $D = 4, 5$ and 7 from left to right respectively.

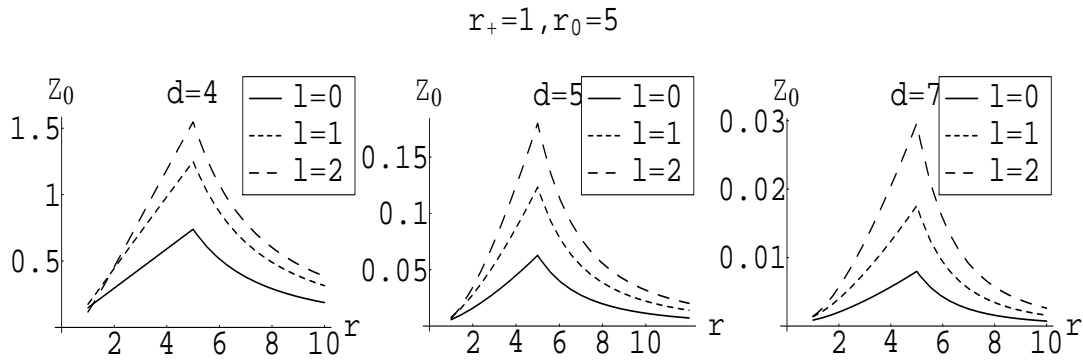


Figure 11.6: Initial data Z_{0l} for a black hole with $r_+ = 1$, and with the particle at $r_0 = 5$, for some values of l the angular quantum number. Again, we show the results for $D = 4, 5$ and 7 from left to right respectively.

11.3.1.d Boundary conditions and the Green's function

Equation (11.23) is to be solved with the boundary conditions appropriate to AdS spacetimes, but special attention must be paid to the initial data [195]: ingoing waves at the horizon,

$$\tilde{\mathbf{Z}} \sim F(\omega)e^{-i\omega r_*} + \frac{iZ_{0l}}{(2\pi)^{1/2}\omega}, r \rightarrow r_+, \quad (11.27)$$

and since the potential diverges at infinity we impose reflective boundary conditions ($\tilde{\mathbf{Z}} = 0$) there [84]. Naturally, given these boundary conditions, all the energy eventually sinks into the black hole. To implement a numerical solution, we note that two independent solutions $\tilde{\mathbf{Z}}^H$ and $\tilde{\mathbf{Z}}^\infty$ of (11.23), with the source term set to zero, have the behavior:

$$\tilde{\mathbf{Z}}^H \sim e^{-i\omega r_*} \quad r \rightarrow r_+, \quad (11.28)$$

$$\tilde{\mathbf{Z}}^H \sim Ar^{D/2-1} + Br^{-D/2} \quad r \rightarrow \infty, \quad (11.29)$$

$$\tilde{\mathbf{Z}}^\infty \sim Ce^{i\omega r_*} + De^{-i\omega r_*} \quad r \rightarrow r_+, \quad (11.30)$$

$$\tilde{\mathbf{Z}}^\infty \sim r^{-D/2} \quad r \rightarrow \infty, \quad (11.31)$$

$$(11.32)$$

Here, the wronskian W of these two solutions is a constant, $W = 2Ci\omega$. Define as in [195] h^H through $dh^H/dr_* = -\tilde{\mathbf{Z}}^H$ and h^∞ through $dh^\infty/dr_* = -\tilde{\mathbf{Z}}^\infty$. We can then show that $\tilde{\mathbf{Z}}$ given by

$$\begin{aligned} \tilde{\mathbf{Z}} = \frac{1}{W} & \left[\tilde{\mathbf{Z}}^\infty \int_{-\infty}^r \tilde{\mathbf{Z}}^H S dr_* + \tilde{\mathbf{Z}}^H \int_r^\infty \tilde{\mathbf{Z}}^\infty S dr_* \right] + \frac{i\omega}{(2\pi)^{1/2}W} \left[\tilde{\mathbf{Z}}^\infty \int_{-\infty}^r h^H \frac{dZ_{0l}}{dr_*} dr_* + \right. \\ & \left. \tilde{\mathbf{Z}}^H \int_r^\infty h^\infty \frac{dZ_{0l}}{dr_*} dr_* + (h^\infty Z_{0l} \tilde{\mathbf{Z}}^H - h^H Z_{0l} \tilde{\mathbf{Z}}^\infty)(r) \right], \end{aligned} \quad (11.33)$$

is a solution to (11.23) and satisfies the boundary conditions. In this work, we are interested in computing the wavefunction $\tilde{\mathbf{Z}}(\omega, r)$ near the horizon ($r \rightarrow r_+$). In this limit we have

$$\begin{aligned} \tilde{\mathbf{Z}}(r \sim r_+) = \frac{1}{W} & \left[\tilde{\mathbf{Z}}^H \int_{r_+}^\infty \tilde{\mathbf{Z}}^\infty S dr_* \right] + \\ & \frac{i\omega}{(2\pi)^{1/2}W} \tilde{\mathbf{Z}}^H \left[\int_{r_+}^\infty \tilde{\mathbf{Z}}^\infty Z_{0l} dr_* - (h^\infty Z_{0l})(r_+) \right] + \frac{iZ_{0l}(r_+)}{(2\pi)^{1/2}\omega}, \end{aligned} \quad (11.34)$$

where an integration by parts has been used.

All we need to do is to find a solution $\tilde{\mathbf{Z}}_2$ of the corresponding homogeneous equation satisfying the above mentioned boundary conditions (11.32), and then numerically integrate it in (11.34). In the numerical work, we chose to adopt r as the independent variable, therefore avoiding the numerical inversion of $r_*(r)$. To find $\tilde{\mathbf{Z}}_2$, the integration (of the homogeneous form of (11.23)) was started at a large value of $r = r_i$, which was $r_i = 10^5$ typically. Equation (11.32) was used to infer the boundary conditions $\tilde{\mathbf{Z}}_2(r_i)$ and $\tilde{\mathbf{Z}}_2'(r_i)$. We then integrated inward from $r = r_i$ in to typically $r = r_+ + 10^{-6}r_+$. Equation (11.32) was then used to get C .

11.3.2 Results

11.3.2.a Numerical results

Our numerical evolution for the field showed that some drastic changes occur when the size of the black hole varies, so we have chosen to divide the results in (i) small black holes and

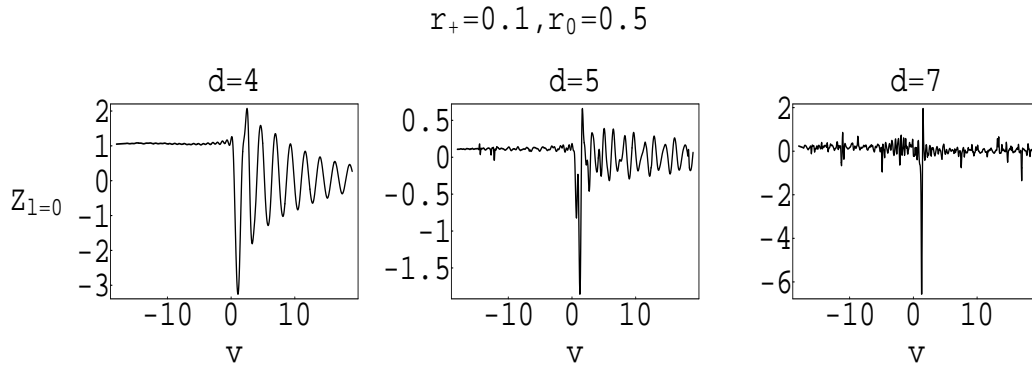


Figure 11.7: The spherically symmetric ($l = 0$) waveform for the case of a particle falling from $r_0 = 0.5$ into a $r_+ = 0.1$ black hole. The results are displayed for $D = 4, 5$ and 7 from left to right respectively. The coordinate $v = t + r_*$ is the usual Eddington coordinate.

(ii) intermediate and large black holes . We will see that the behavior of these two classes is indeed strikingly different.

(i): Wave forms and spectra for small black holes, $r_+ = 0.1$

We plot the waveforms and the spectra. Figs. 11.7-11.10 are typical plots for small black holes of waveforms and spectra for $l = 0$ and $l = 1$ (for $l = 2$ and higher the conclusions are not altered). They show the first interesting aspect of our numerical results: for small black holes the $l = 0$ signal is clearly dominated by quasinormal, exponentially decaying, ringing modes with a frequency $\omega \sim D - 1$ (scalar quasinormal frequencies of Schwarzschild-AdS black holes can be found in [48, 78]). This particular limit is a pure AdS mode [86, 74]. For example, Fig. 11.7 gives, for $D = 4$, $\omega = 2\pi/T \sim 2\pi/(10/4.5) \sim 2.7$. This yields a value near the pure AdS mode for $d = 4$, $\omega = 3$. Likewise, Fig. 11.7 gives $\omega \sim 4$ when $d = 5$, the pure AdS mode for $D = 5$. All these features can be more clearly seen in the energy spectra plots, Fig.11.9 , where one can observe the intense peak at $\omega \sim D - 1$. The conclusion is straightforward: spacetimes with small black holes behave as if the black hole was not there at all. This can be checked in yet another way by lowering the mass of the black hole. We have done that, and the results we have obtained show that as one lowers the mass of the hole, the ringing frequency goes to $\omega \sim 3$ (for $D = 4$) and the imaginary part of the frequency, which gives us the damping scale for the mode, decreases as r_+ decreases. In this limit, the spacetime effectively behaves as a bounding box in which the modes propagate “freely”, and are not absorbed by the black hole.

Not shown is the spectra for higher values of the angular quantum number l . The total energy going down the hole increases slightly with l . This would lead us to believe that an infinite amount of energy goes down the hole. However, as first noted in [3], this divergence results from treating the incoming object as a point particle. Taking a minimum size L for the particle implies a cutoff in l given by $l_{\max} \sim \frac{\pi r_+}{2L}$, and this problem is solved.

(ii): Wave forms and spectra for intermediate and large black holes, $r_+ = 1$

We plot the waveforms and the spectra. As we mentioned, intermediate and large black holes (which are of more direct interest to the AdS/CFT) behave differently. The signal is dominated by a sharp precursor near $v = r_{*0}$ and there is no ringing: the waveform

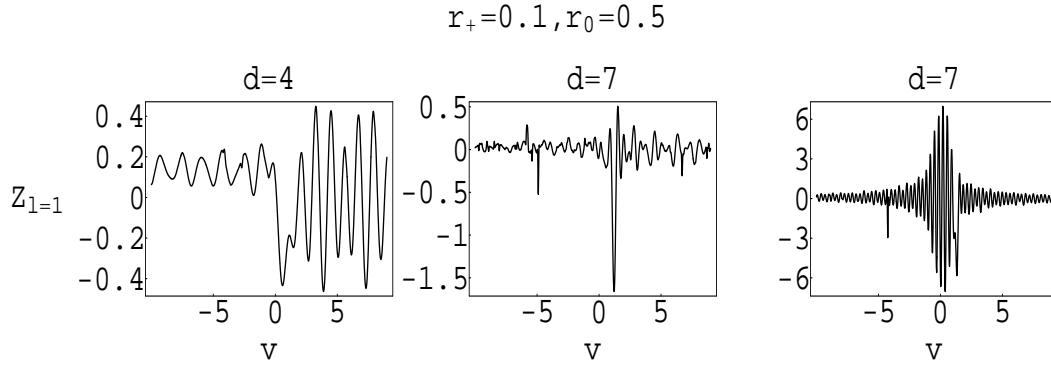


Figure 11.8: The $l = 1$ waveform for the case of a particle falling from $r_0 = 0.5$ into a $r_+ = 0.1$ black hole. The results are displayed for $D = 4, 5$ and 7 from left to right respectively.

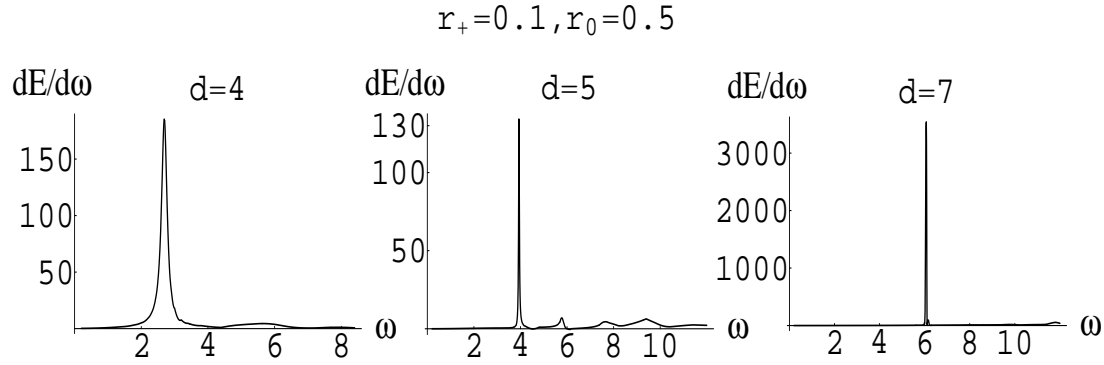


Figure 11.9: Typical energy spectra for the spherically symmetric part of the perturbation ($l = 0$), here shown for $r_+ = 0.1$, and $r_0 = 0.5$, and for $D = 4, 5$ and 7 . Total energy in this mode: for $d=4$ we have $E_{l=0,d=4} \sim 75$. For $D = 5$, we have $E_{l=0,D=5} \sim 34$. For $D = 7$, we have $E_{l=0,D=7} \sim 1500$.

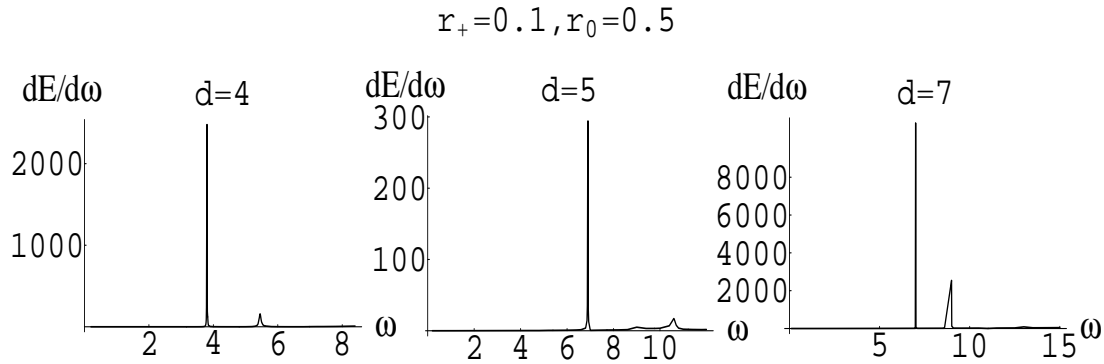


Figure 11.10: Typical energy spectra (for $l = 1$), here shown for $r_+ = 0.1$, and $r_0 = 0.5$.

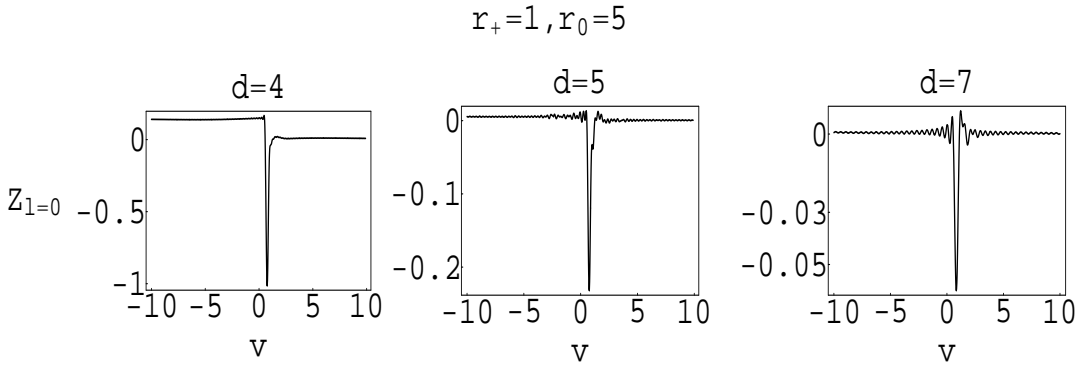


Figure 11.11: The spherically symmetric ($l = 0$) waveform for the case of a particle falling from $r_0 = 5$ into a $r_+ = 1$ black hole. The results are displayed for $D = 4, 5$ and 7 from left to right respectively.

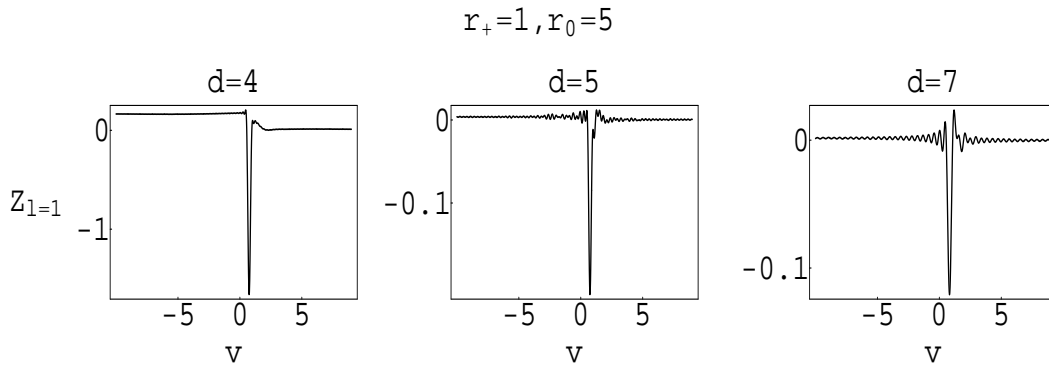


Figure 11.12: The $l = 1$ waveform for the case of a particle falling from $r_0 = 5$ into a $r_+ = 1$ black hole.

quickly settles down to the final zero value in a pure decaying fashion. The timescale of this exponential decay is, to high accuracy, given the inverse of the imaginary part of the quasinormal frequency for the mode. The total energy is not a monotonic function of r_0 and still diverges if one naively sums over all the multipoles. In either case, there seem to be no power-law tails, as was expected from the work of Ching et. al. [88]. Note that E is given in terms of $E/(q_s m_0/r)^2$. Since $q_s m_0/r \ll 1$ the total energy radiated is small in accord with our approximation.

The value attained by $\tilde{\mathbf{Z}}$ for large negative v - Fig. 11.15 - is the initial data, and this can be most easily seen by looking at the value of Z_0 near the horizon in Fig. 11.6 (see also [195]). This happens for small black holes also, which is only natural, since large negative v means very early times, and at early times one can only see the initial data, since no information has arrived to tell that the particle has started to fall. The spectra in general does not peak at the lowest quasinormal frequency (cf Figs. 11.13-11.16), as it did in flat spacetime [2]. (Scalar quasinormal frequencies of Schwarzschild-AdS black holes can be found in [48, 78]). Most importantly, the location of the peak seems to have a strong dependence on r_0 (compare Figs. 11.13 and 11.16). This discrepancy has its roots in the behavior of the quasinormal frequencies. In fact, whereas in (asymptotically) flat spacetime the real part of the frequency

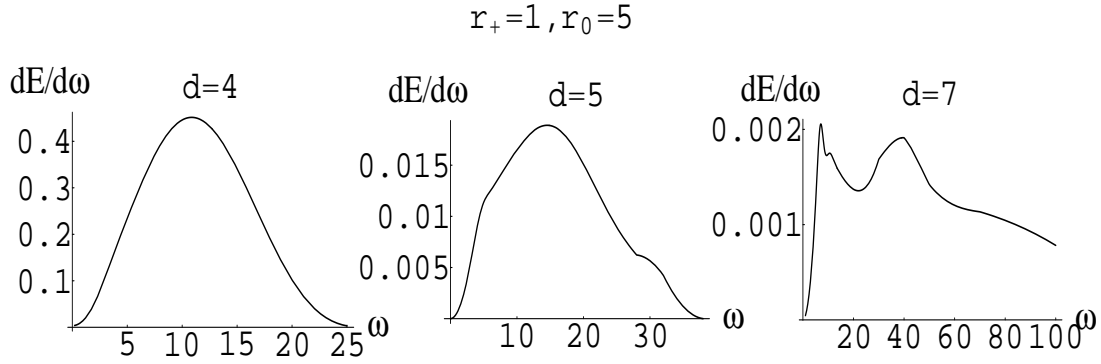


Figure 11.13: Typical energy spectra for the spherically symmetric part of the perturbation ($l = 0$), here shown for $r_+ = 1$, and $r_0 = 5$, and for $D = 4, 5$ and 7 .

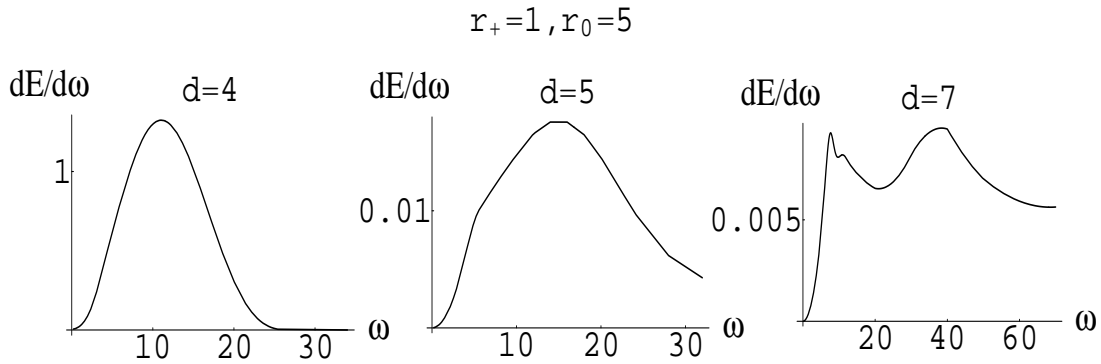


Figure 11.14: Typical energy spectra (for $l = 1$), here shown for $r_+ = 1$, and $r_0 = 5$.

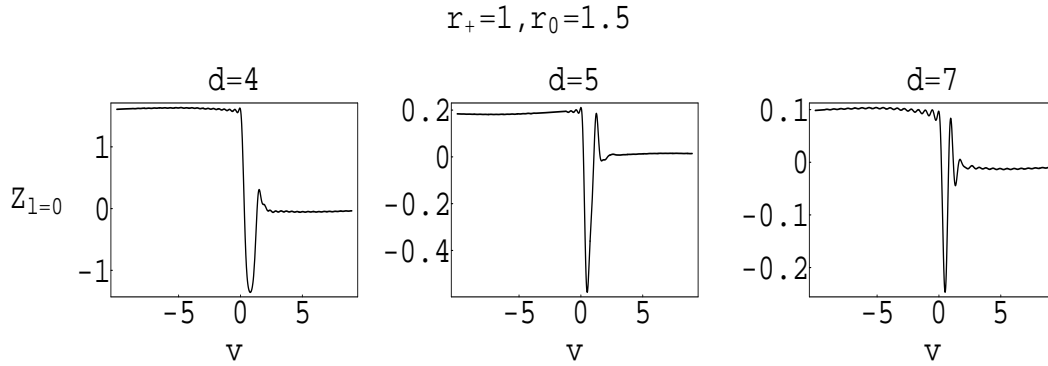


Figure 11.15: The $l = 0$ waveform for the case of a particle falling from $r_0 = 1.5$ into a $r_+ = 1$ black hole.

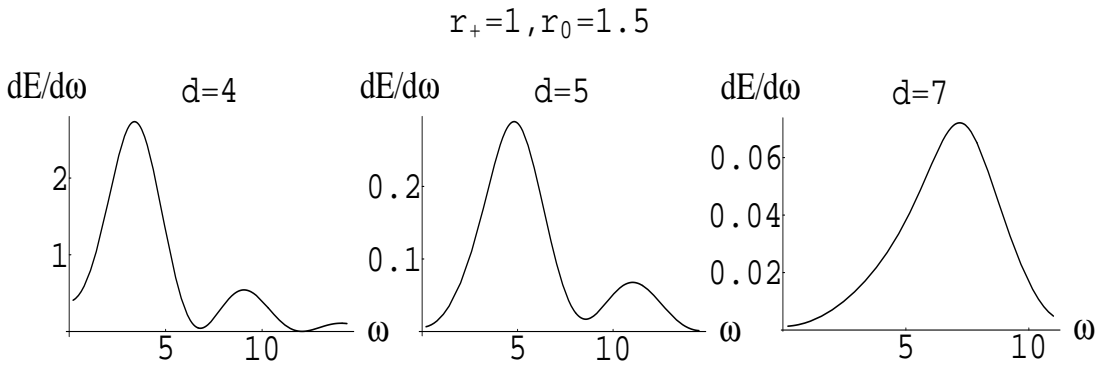


Figure 11.16: Typical energy spectra (for $l = 0$), here shown for $r_+ = 1$, and $r_0 = 1.5$.

is bounded and seems to go to a constant [10, 18, 125], in AdS spacetime it grows without bound as a function of the principal quantum number n [48, 78]. Increasing the distance r_0 at which the particle begins to fall has the effect of increasing this effect, so higher modes seem to be excited at larger distances.

11.3.2.b Discussion of results

Two important remarks regarding these results can be made:

(i) the total energy radiated depends on the size of the infalling object, and the smaller the object is, the more energy it will radiate. This is a kind of a scalar analog in AdS space of a well known result for gravitational radiation in flat space [200].

(ii) the fact that the radiation emitted in each multipole is high even for high multipoles leads us to another important point, first posed by Horowitz and Hubeny [48]. While we are not able to guarantee that the damping time scale stays bounded away from infinity (as it seems), it is apparent from the numerical data that the damping time scale increases with increasing l . Thus it looks like the late time behavior of these kind of perturbations will be dominated by the largest l -mode ($L_{\max} \sim \frac{r_+}{\text{size of object}}$), and this answers the question posed in [48]. Thus a perturbation in $\langle F^2 \rangle$ in the CFT] with given angular dependence Y_l on S^3 will decay exponentially with a time scale given by the imaginary part of the lowest quasinormal

mode with *that* value of l .

11.4 Conclusions

We have computed the scalar energy emitted by a point test particle falling from rest into a Schwarzschild-AdS black hole. From the point of view of the AdS/CFT conjecture, where the (large) black hole corresponds on the CFT side to a thermal state, the infalling scalar particle corresponds to a specific perturbation of this state (an expanding bubble), while the scalar radiation is interpreted as particles decaying into bosons of the associated operator of the gauge theory. Previous works [48, 78] have shown that a general perturbation should have a timescale directly related to the inverse of the imaginary part of the quasinormal frequency, which means that the approach to thermal equilibrium on the CFT should be governed by this timescale. We have shown through a specific important problem that this is in fact correct, but that it is not the whole story, since some important features of the waveforms highly depend on r_0 .

Overall, we expect to find the same type of features, at least qualitatively, in the gravitational or electromagnetic radiation by test particles falling into a Schwarzschild-AdS black hole. For example, if the black hole is small, we expect to find in the gravitational radiation spectra a strong peak located at $\omega^2 = 4n^2 + l(l + 1)$, $n = 1, 2, \dots$. Moreover, some major results in perturbation theory and numerical relativity [4, 5], studying the collision of two black holes, with masses of the same order of magnitude, allow us to infer that evolving the collision of two black holes in AdS spacetime, should not bring major differences in relation to our results (though it is of course a much more difficult task, even in perturbation theory). In particular, in the small black hole regime, the spectra and waveforms should be dominated by quasinormal ringing.

Part III

Gravitational waves in higher dimensions

Chapter 12

Gravitational waves in higher dimensions

Contents

12.1 Introduction	163
12.2 Outline of Part III	165

12.1 Introduction

One expects to finally detect gravitational waves in the forthcoming years. If this happens, and if the observed waveforms match the predicted templates, General Relativity will have pass a crucial test. Moreover, if one manages to cleanly separate gravitational waveforms, we will open a new and exciting window to the Universe, a window from which one can look directly into the heart of matter, as gravitational waves are weakly scattered by matter. A big effort has been spent in the last years trying to build gravitational wave detectors, and a new era will begin with gravitational wave astronomy [148, 149]. What makes gravitational wave astronomy attractive, the weakness with which gravitational waves are scattered by matter, is also the major source of technical difficulties when trying to develop an apparatus which interacts with them. Nevertheless, some of these highly non-trivial technical difficulties have been surmounted, and we have detectors already operating [20, 21, 22]. Another effort is being dedicated by theoreticians trying to obtain accurate templates for the various physical processes that may give rise to the waves impinging on the detector. We now have a well established theory of wave generation and propagation, which started with Einstein and his quadrupole formula. The quadrupole formula expresses the energy lost to gravitational waves by a system moving at low velocities, in terms of its energy content. The quadrupole formalism is the most famous example of slow motion techniques to compute wave generation. All these techniques break Einstein's equations non-linearity by imposing a power series in some small quantity and keeping only the lowest or the lowest few order terms. The quadrupole formalism starts from a flat background and expands the relevant quantities in R/λ , where R is the size of source and λ the wavelength of waves. Perturbation formalisms on the other hand, start from some non-radiative background, whose metric is known exactly, for example the

Schwarzschild metric, and expand in deviations from that background metric. For a catalog of the various methods and their description we refer the reader to the review works by Thorne [144] and Damour [145]. The necessity to develop all such methods was driven of course by the lack of exact radiative solutions to Einstein's equations (although there are some worthy exceptions, like the C-metric [201]), and by the fact that even nowadays solving the full set of Einstein's equations numerically is a monumental task, and has been done only for the more tractable physical situations. All the existing methods seem to agree with each other when it comes down to the computation of waveforms and energies radiated during physical situations, and also agree with the few available results from a fully numerical evolution of Einstein's equations.

We extend some of these results to higher dimensional spacetimes. There are several reasons why one should now try to do it. It seems impossible to formulate in four dimensions a consistent theory which unifies gravity with the other forces in nature. Thus, most efforts in this direction have considered a higher dimensional arena for our universe, one example being string theories which have recently made some remarkable achievements. Moreover, recent investigations [151] propose the existence of extra dimensions in our Universe in order to solve the hierarchy problem, i.e., the huge difference between the electroweak and the Planck scale, $m_{EW}/M_{Pl} \sim 10^{-17}$. The fields of standard model would inhabit a 4-dimensional submanifold, the brane, whereas the gravitational degrees of freedom would propagate throughout all dimensions. One of the most spectacular consequences of this scenario would be the production of black holes at the Large Hadron Collider at CERN [158] (for recent relevant work related to this topic we refer the reader to [202, 159, 160, 161, 162]). Now, one of the experimental signatures of black hole production will be a missing energy, perhaps a large fraction of the center of mass energy [161]. This will happen because when the partons collide to form a black hole, some of the initial energy will be converted to gravitational waves, and due to the small amplitudes involved, there is no gravitational wave detector capable of detecting them, so they will appear as missing. Thus, the collider could in fact indirectly serve as a gravitational wave detector. This calls for the calculation of the energy given away as gravitational waves when two high energy particles collide to form a black hole, which lives in all the dimensions. The work done so far on this subject [203, 204] in higher dimensions, is mostly geometric, and generalizes a construction by Penrose to find trapped surfaces on the union of two shock waves, describing boosted Schwarzschild black holes. On the other hand, there are clues [159, 160, 161] indicating that a formalism described by Weinberg [205] to compute the gravitational energy radiated in the collision of two point particles, gives results correct to a order of magnitude when applied to the collision of two black holes. This formalism assumes a hard collision, i.e., a collision lasting zero seconds. It would be important to apply this formalism in higher dimensions, trying to see if there is agreement between both results. This will be one of the topics discussed here. The other topic we study is the quadrupole formula in higher dimensions. Due to the difficulties in handling the wave tails in odd dimensions we concentrate our study in even dimensions. We shall also see, in Chapter 14 that in odd dimensional spacetimes there are tails associated with wave propagation, even if the spacetime is flat. On the other hand, for even dimensional spacetimes, this tail only appears if the spacetime is curved, by including for example a black hole.

12.2 Outline of Part III

In this third part of the thesis we will begin, in Chapter 13, by reviewing our understanding of linearized gravitational waves in a flat background. As there is now a great interest in physics in higher dimensions, due to the TeV-scale gravity scenario, I shall extend all of the results we have in four dimensional spacetimes to D dimensional spacetimes. This is a non-trivial extension, mainly because the Green's function for the wave equation in D -dimensions no longer has the simple structure that we know so well when $D = 4$. In fact, whereas for even D there is still propagation on the light cone (this means Huygens principle still holds), for odd D this propagation on the light cone is lost (this shows up clearly in the Green's function expression). Due to difficulties in handling the wave tails that arise in odd dimensional spacetimes, we will therefore focus on even-dimensional spacetimes (even D). We will compute the D -dimensional quadrupole formula, thereby extending Einstein's formula to general dimension, and we shall also compute the gravitational radiation when a high energy particle collides with a black hole. It is unnecessary to write the importance this may have, should the TeV-scale scenario be correct, but we shall do it nonetheless. If this scenario is correct, we may be lucky enough to produce black holes at the LHC, as we remarked earlier. If this happens, one needs desperately some estimates for the gravitational radiation released during the balding phase, the first stage of black hole formation. So, the computation of gravitational radiation when black holes collide in higher dimensions is extremely important. Finally I shall compute, for the first time, the gravitational radiation released during the quantum process of black hole pair creation. The quantum process of black hole pair creation as a process for gravitational wave generation seems to have been overlooked over the years. We show it may well be a strong generator of gravitational waves.

In Chapter 14 we shall conclude this thesis by continuing the program of gravitational wave physics in higher dimensional spacetimes. We consider higher dimensional Schwarzschild black holes. Supporting what has been said about (flat space) Green's function in higher dimensions, we show that if the spacetime has odd number of dimensions then the appearance of tails is inevitable, even if there is no black hole. We also show that the late time behaviour of any field is dictated by $\Psi \sim t^{-(2l+D-2)}$, where l is the angular index determining the angular dependence of the field. One can show directly from the flat space Green's function that such a power-law is indeed expected in flat odd dimensional spacetimes, and it is amusing to note that the same conclusion can be reached directly from an independent analysis, as I shall do. For even dimensional spacetimes we find also a power-law decay at late times, but with a much more rapid decay, $\Psi \sim t^{-(2l+3D-8)}$. For even D , this power-law tail is entirely due to the black hole, as opposed to the situation in odd D . These results are strictly valid for $D > 4$. Four dimensional Schwarzschild geometry is special, having the well known power-law tail $\Psi \sim t^{-(2l+3)}$.

Chapter 13

Gravitational waves in a flat higher dimensional background

Contents

13.1 Introduction	167
13.2 Linearized D -dimensional Einstein's equations	168
13.3 The even D -dimensional quadrupole formula	173
13.4 Instantaneous collisions in even D -dimensions	177
13.5 Summary and discussion	183

13.1 Introduction

This chapter is organized as follows, and is based on [99]: In section II we linearize Einstein's equations in a flat D -dimensional background and arrive at an inhomogeneous wave equation for the metric perturbations. The source free equations are analyzed in terms of plane waves, and then the general solution to the homogeneous equation is deduced in terms of the D -dimensional retarded Green's function. In section III we compute the D -dimensional quadrupole formula (assuming slowly moving sources), expressing the metric and the radiated energy in terms of the time-time component of the energy-momentum tensor. We then apply the quadrupole formula to two cases: a particle in circular motion in a generic background, and a particle falling into a D -dimensional Schwarzschild black hole. In section IV we consider the hard collision between two particles, i.e., the collision takes zero seconds, and introduce a cutoff frequency necessary to have meaningful results. We then apply to the case where one of the colliding particles is a black hole. We propose that this cutoff should be related to the gravitational quasinormal frequency of the black hole, and compute some values of the scalar quasinormal frequencies for higher dimensional Schwarzschild black holes, expecting that the gravitational quasinormal frequencies will behave in the same manner. Finally, we apply this formalism to compute the generation of gravitational radiation during black hole pair creation in four and higher dimensions, a result that has never been worked out, even for $D = 4$. In our presentation we shall mostly follow Weinberg's [205] exposition.

13.2 Linearized D -dimensional Einstein's equations

Due to the non-linearity of Einstein's equations, the treatment of the gravitational radiation problem is not an easy one since the energy-momentum tensor of the gravitational wave contributes to its own gravitational field. To overcome this difficulty it is a standard procedure to work only with the weak radiative solution, in the sense that the energy-momentum content of the gravitational wave is small enough in order to allow us to neglect its contribution to its own propagation. This approach is justified in practice since we expect the detected gravitational radiation to be of low intensity. For some non-linear effects in gravitational wave physics, we refer the reader to [206] and references therein.

13.2.1 The inhomogeneous wave equation

We begin this subsection by introducing the general background formalism (whose details can be found, e.g., in [205]) that will be needed in later sections. Then we obtain the linearized inhomogeneous wave equation.

Greek indices vary as $0, 1, \dots, D-1$ and latin indices as $1, \dots, D-1$ and our units are such that $c \equiv 1$. We work on a D -dimensional spacetime described by a metric $g_{\mu\nu}$ that approaches asymptotically the D -dimensional Minkowski metric $\eta_{\mu\nu} = \text{diag}(-1, +1, \dots, +1)$, and thus we can write

$$g_{\mu\nu} = \eta_{\mu\nu} + h_{\mu\nu} \quad \mu, \nu = 0, 1, \dots, D-1, \quad (13.1)$$

where $h_{\mu\nu}$ is small, i.e., $|h_{\mu\nu}| \ll 1$, so that it represents small corrections to the flat background. The exact Einstein field equations, $G_{\mu\nu} = 8\pi\mathcal{G}T_{\mu\nu}$ (with \mathcal{G} being the usual Newton constant), can then be written as

$$R^{(1)}_{\mu\nu} - \frac{1}{2}\eta_{\mu\nu}R^{(1)\alpha}_{\alpha} = 8\pi\mathcal{G}\tau_{\mu\nu}, \quad (13.2)$$

with

$$\tau^{\mu\nu} \equiv \eta^{\mu\alpha}\eta^{\nu\beta}(T_{\alpha\beta} + t_{\alpha\beta}). \quad (13.3)$$

Here $R^{(1)}_{\mu\nu}$ is the part of the Ricci tensor linear in $h_{\mu\nu}$, $R^{(1)\alpha}_{\alpha} = \eta^{\alpha\beta}R^{(1)}_{\beta\alpha}$, and $\tau_{\mu\nu}$ is the effective energy-momentum tensor, containing contributions from $T_{\mu\nu}$, the energy-momentum tensor of the matter source, and $t_{\mu\nu}$ which represents the gravitational contribution. The pseudo-tensor $t_{\mu\nu}$ contains the difference between the exact Ricci terms and the Ricci terms linear in $h_{\mu\nu}$,

$$t_{\mu\nu} = \frac{1}{8\pi\mathcal{G}} \left[R_{\mu\nu} - \frac{1}{2}g_{\mu\nu}R^{\alpha}_{\alpha} - R^{(1)}_{\mu\nu} + \frac{1}{2}\eta_{\mu\nu}R^{(1)\alpha}_{\alpha} \right]. \quad (13.4)$$

The Bianchi identities imply that $\tau_{\mu\nu}$ is locally conserved,

$$\partial_{\mu}\tau^{\mu\nu} = 0. \quad (13.5)$$

Introducing the cartesian coordinates $x^{\alpha} = (t, \mathbf{x})$ with $\mathbf{x} = x^i$, and considering a $D-1$ volume V with a boundary spacelike surface S with dimension $D-2$ whose unit exterior normal is \mathbf{n} , eq. (13.5) yields

$$\frac{d}{dt} \int_V d^{D-1}\mathbf{x} \tau^{0\nu} = - \int_S d^{D-2}\mathbf{x} n_i \tau^{i\nu}. \quad (13.6)$$

This means that one may interpret

$$p^\nu \equiv \int_V d^{D-1}\mathbf{x} \tau^{0\nu} \quad (13.7)$$

as the total energy-momentum (pseudo)vector of the system, including matter and gravitation, and $\tau^{i\nu}$ as the corresponding flux. Since the matter contribution is contained in $t^{\mu\nu}$, the flux of gravitational radiation is

$$\text{Flux} = \int_S d^{D-2}\mathbf{x} n_i t^{i\nu}. \quad (13.8)$$

In this context of linearized general relativity, we neglect terms of order higher than the first in $h_{\mu\nu}$ and all the indices are raised and lowered using $\eta^{\mu\nu}$. We also neglect the contribution of the gravitational energy-momentum tensor $t_{\mu\nu}$ (i.e., $|t_{\mu\nu}| \ll |T_{\mu\nu}|$) since from (13.4) we see that $t_{\mu\nu}$ is of higher order in $h_{\mu\nu}$. Then, the conservation equations (13.5) yield

$$\partial_\mu T^{\mu\nu} = 0. \quad (13.9)$$

In this setting and choosing the convenient coordinate system that obeys the harmonic (also called Lorentz) gauge conditions,

$$2\partial_\mu h^\mu{}_\nu = \partial_\nu h^\alpha{}_\alpha \quad (13.10)$$

(where $\partial_\mu = \partial/\partial x^\mu$), the first order Einstein field equations (13.2) yield

$$\square h_{\mu\nu} = -16\pi\mathcal{G}S_{\mu\nu}, \quad (13.11)$$

$$S_{\mu\nu} = T_{\mu\nu} - \frac{1}{D-2}\eta_{\mu\nu}T^\alpha{}_\alpha, \quad (13.12)$$

where $\square = \eta^{\mu\nu}\partial_\mu\partial_\nu$ is the D -dimensional Laplacian, and $S_{\mu\nu}$ will be called the modified energy-momentum tensor of the matter source. Eqs. (13.11) and (13.12) subject to (13.10) allow us to find the gravitational radiation produced by a matter source $S_{\mu\nu}$.

13.2.2 The plane wave solutions

In vacuum, the linearized equations for the gravitational field are $R^{(1)}{}_{\mu\nu} = 0$ or, equivalently, the homogeneous equations $\square h_{\mu\nu} = 0$, subjected to the harmonic gauge conditions (13.10). The solutions of these equations, the plane wave solutions, are important since the general solutions of the inhomogeneous equations (13.10) and (13.11) approach the plane wave solutions at large distances from the source. Setting $k_\alpha = (-\omega, \mathbf{k})$ with ω and \mathbf{k} being respectively the frequency and wave vector, the plane wave solutions can be written as a linear superposition of solutions of the kind

$$h_{\mu\nu}(t, \mathbf{x}) = e_{\mu\nu} e^{ik_\alpha x^\alpha} + e_{\mu\nu}^* e^{-ik_\alpha x^\alpha}, \quad (13.13)$$

where $e_{\mu\nu} = e_{\nu\mu}$ is called the polarization tensor and * means the complex conjugate. These solutions satisfy eq. (13.11) with $S_{\mu\nu} = 0$ if $k_\alpha k^\alpha = 0$, and obey the harmonic gauge conditions (13.10) if $2k_\mu e^\mu{}_\nu = k_\nu e^\mu{}_\mu$.

An important issue that must be addressed is the number of different polarizations that a gravitational wave in D dimensions can have. The polarization tensor $e_{\mu\nu}$, being symmetric, has in general $D(D+1)/2$ independent components. However, these components are subjected to the D harmonic gauge conditions that reduce by D the number of independent components. In addition, under the infinitesimal change of coordinates $x'^{\mu} = x^{\mu} + \xi^{\mu}(x)$, the polarization tensor transforms into $e'_{\mu\nu} = e_{\mu\nu} - \partial_{\nu}\xi_{\mu} - \partial_{\mu}\xi_{\nu}$. Now, $e'_{\mu\nu}$ and $e_{\mu\nu}$ describe the same physical system for arbitrary values of the D parameters $\xi^{\mu}(x)$. Therefore, the number of independent components of $e_{\mu\nu}$, i.e., the number of polarization states of a gravitational wave in D dimensions is $D(D+1)/2 - D - D = D(D-3)/2$. From this computation we can also see that gravitational waves are present only when $D > 3$. Therefore, from now on we assume $D > 3$ whenever we refer to D . In what concerns the helicity of the gravitational waves, for arbitrary D the gravitons are always spin 2 particles.

To end this subsection on gravitational plane wave solutions, we present the average gravitational energy-momentum tensor of a plane wave, a quantity that will be needed later. Notice that in vacuum, since the matter contribution is zero ($T_{\mu\nu} = 0$), we cannot neglect the contribution of the gravitational energy-momentum tensor $t_{\mu\nu}$. From eq. (13.4), and neglecting terms of order higher than h^2 , the gravitational energy-momentum tensor of a plane wave is given by

$$t_{\mu\nu} \simeq \frac{1}{8\pi\mathcal{G}} \left[R^{(2)}_{\mu\nu} - \frac{1}{2}\eta_{\mu\nu}R^{(2)\alpha}_{\alpha} \right], \quad (13.14)$$

and through a straightforward calculation (see e.g. [205] for details) we get the average gravitational energy-momentum tensor of a plane wave,

$$\langle t_{\mu\nu} \rangle = \frac{k_{\mu}k_{\nu}}{16\pi\mathcal{G}} \left[e^{\alpha\beta}e_{\alpha\beta}^* - \frac{1}{2}|e^{\alpha}_{\alpha}|^2 \right]. \quad (13.15)$$

13.2.3 The D -dimensional retarded Green's function

The general solution to the inhomogeneous differential equation (13.11) may be found in the usual way in terms of a Green's function as

$$h_{\mu\nu}(t, \mathbf{x}) = -16\pi\mathcal{G} \int dt' \int d^{D-1}\mathbf{x}' S_{\mu\nu}(t', \mathbf{x}') G(t-t', \mathbf{x}-\mathbf{x}') + \text{homogeneous solutions}, \quad (13.16)$$

where the Green's function $G(t-t', \mathbf{x}-\mathbf{x}')$ satisfies

$$\eta^{\mu\nu}\partial_{\mu}\partial_{\nu}G(t-t', \mathbf{x}-\mathbf{x}') = \delta(t-t')\delta(\mathbf{x}-\mathbf{x}'), \quad (13.17)$$

where $\delta(z)$ is the Dirac delta function. In the momentum representation this reads

$$G(t, \mathbf{x}) = -\frac{1}{(2\pi)^D} \int d^{D-1}\mathbf{k} e^{i\mathbf{k}\cdot\mathbf{x}} \int d\omega \frac{e^{-i\omega t}}{\omega^2 - k^2}, \quad (13.18)$$

where $k^2 = k_1^2 + k_2^2 + \dots + k_{D-1}^2$. To evaluate this, it is convenient to perform the k -integral by using spherical coordinates in the $(D-1)$ -dimensional k -space. The required transformation, along with some useful formulas which shall be used later on, is given in Appendix 13.4.3. The result for the retarded Green's function in those spherical coordinates is

$$G^{\text{ret}}(t, \mathbf{x}) = -\frac{\Theta(t)}{(2\pi)^{(D-1)/2}} \times \frac{1}{r^{(D-3)/2}} \int k^{(D-3)/2} J_{(D-3)/2}(kr) \sin(kt) dk, \quad (13.19)$$

where $r^2 = x_1^2 + x_2^2 + \dots + x_{D-1}^2$, and $\Theta(t)$ is the Heaviside function defined as

$$\Theta(t) = \begin{cases} 1 & \text{if } t > 0 \\ 0 & \text{if } t < 0. \end{cases} \quad (13.20)$$

The function $J_{(D-3)/2}(kr)$ is a Bessel function [207, 208]. The structure of the retarded Green's function will depend on the parity of D , as we shall see. This dependence on the parity, which implies major differences between even and odd spacetime dimensions, is connected to the structure of the Bessel function. For even D , the index of the Bessel function is semi-integer and then the Bessel function is expressible in terms of elementary functions, while for odd D this does not happen. A concise explanation of the difference between retarded Green's function in even and odd D , and the physical consequences that entails is presented in [209] (see also [210, 211, 212]). A complete derivation of the Green's function in higher dimensional spaces may be found in Hassani [213]. The result is

$$G^{\text{ret}}(t, \mathbf{x}) = \frac{1}{4\pi} \left[-\frac{\partial}{2\pi r \partial r} \right]^{(D-4)/2} \left[\frac{\delta(t-r)}{r} \right], \quad D \text{ even.} \quad (13.21)$$

$$G^{\text{ret}}(t, \mathbf{x}) = \frac{\Theta(t)}{2\pi} \left[-\frac{\partial}{2\pi r \partial r} \right]^{(D-3)/2} \left[\frac{1}{\sqrt{t^2 - r^2}} \right], \quad D \text{ odd.} \quad (13.22)$$

It is sometimes convenient to work with the Fourier transform (in the time coordinate) of the Green's function. One finds [213] an analytical result independent of the parity of D

$$G^{\text{ret}}(\omega, \mathbf{x}) = \frac{i^D \pi}{2(2\pi)^{(D-1)/2}} \left(\frac{\omega}{r} \right)^{(D-3)/2} H_{(D-3)/2}^1(\omega r), \quad (13.23)$$

where $H_\nu^1(z)$ is a modified Bessel function [208, 207]. Of course, the different structure of the Green's function for different D is again embodied in these Bessel functions. Equations (13.21) and (13.23), are one of the most important results we shall use in this paper. For $D = 4$ (13.21) obviously reproduce well known results [213]. Now, one sees from eq. (13.21) that although there are delta function derivatives on the even- D Green's function, the localization of the Green's function on the light cone is preserved. However, eq. (13.22) tells us that the retarded Green's function for odd dimensions is non-zero inside the light cone. The consequence, as has been emphasized by different authors [209, 212, 214], is that for odd D the Huygens principle does not hold: the fact that the retarded Green's function support extends to the interior of the light cone implies the appearance of radiative tails in (13.16). In other words, we still have a propagation phenomenon for the wave equation in odd dimensional spacetimes, in so far as a localized initial state requires a certain time to reach a point in space. Huygens principle no longer holds, because the effect of the initial state is not sharply limited in time: once the signal has reached a point in space, it persists there indefinitely as a reverberation.

This fact coupled to the analytic structure of the Green's function in odd dimensions make it hard to get a grip on radiation generation in odd dimensional spacetimes. Therefore, from now on we shall focus on even dimensions, for which the retarded Green's function is given by eq. (13.21).

13.2.4 The even D -dimensional retarded solution in the wave zone

The retarded solution for the metric perturbation $h_{\mu\nu}$, obtained by using the retarded Green's function (13.21) and discarding the homogeneous solution in (13.16) will be given by

$$h_{\mu\nu}(t, \mathbf{x}) = 16\pi\mathcal{G} \int dt' \int d^{D-1}\mathbf{x}' S_{\mu\nu}(t', \mathbf{x}') G^{\text{ret}}(t - t', \mathbf{x} - \mathbf{x}'), \quad (13.24)$$

with $G^{\text{ret}}(t - t', \mathbf{x} - \mathbf{x}')$ as in eq. (13.21). For $D = 4$ for example one has

$$G^{\text{ret}}(t, \mathbf{x}) = \frac{1}{4\pi} \frac{\delta(t - r)}{r}, \quad D = 4, \quad (13.25)$$

which is the well known result. For $D = 6$, we have

$$G^{\text{ret}}(t, \mathbf{x}) = \frac{1}{8\pi^2} \left(\frac{\delta'(t - r)}{r^2} + \frac{\delta(t - r)}{r^3} \right), \quad D = 6, \quad (13.26)$$

where the $\delta'(t - r)$ means derivative of the Dirac delta function with respect to its argument. For $D = 8$, we have

$$G^{\text{ret}}(t, \mathbf{x}) = \frac{1}{16\pi^3} \left(\frac{\delta''(t - r)}{r^3} + 3\frac{\delta'(t - r)}{r^4} + 3\frac{\delta(t - r)}{r^5} \right), \quad D = 8. \quad (13.27)$$

We see that in general even- D dimensions the Green's function consists of inverse integer powers in r , spanning all values between $\frac{1}{r^{(D-2)/2}}$ and $\frac{1}{r^{D-3}}$, including these ones. Now, the retarded solution is given by eq. (13.24) as a product of the Green's function times the modified energy-momentum tensor $S_{\mu\nu}$. The net result of having derivatives on the delta functions is to transfer these derivatives to the energy-momentum tensor as time derivatives (this can be seen by integrating (13.24) by parts in the t -integral).

A close inspection then shows that the retarded field possesses a kind of peeling property in that it consists of terms with different fall off at infinity. Explicitly, this means that the retarded field will consist of a sum of terms possessing all integer inverse powers in r between $\frac{D-2}{2}$ and $D - 3$. The term that dies off more quickly at infinity is the $\frac{1}{r^{D-3}}$, typically a static term, since it comes from the Laplacian. As a matter of fact this term was already observed in the higher dimensional black hole by Tangherlini [154] (see also Myers and Perry [155]). We will see that the term falling more slowly, the one that goes like $\frac{1}{r^{(D-2)/2}}$, gives rise to gravitational radiation. It is well defined, in the sense that the power crossing sufficiently large hyperspheres with different radius is the same, because the volume element goes as r^{D-2} and the energy as $|h|^2 \sim \frac{1}{r^{D-2}}$.

In radiation problems, one is interested in finding out the field at large distances from the source, $r \gg \lambda$, where λ is the wavelength of the waves, and also much larger than the source's dimensions R . This is defined as the wave zone. In the wave zone, one may neglect all terms in the Green's function that decay faster than $\frac{1}{r^{(D-2)/2}}$. So, in the wave zone, we find

$$h_{\mu\nu}(t, \mathbf{x}) = -8\pi\mathcal{G} \frac{1}{(2\pi r)^{(D-2)/2}} \partial_t^{(\frac{D-4}{2})} \left[\int d^{D-1}\mathbf{x}' S_{\mu\nu}(t - |\mathbf{x} - \mathbf{x}'|, \mathbf{x}') \right], \quad (13.28)$$

where $\partial_t^{(\frac{D-4}{2})}$ stands for the $\frac{D-4}{2}$ th derivative with respect to time. For $D = 4$ eq. (13.28) yields the standard result [205]:

$$h_{\mu\nu}(t, \mathbf{x}) = -\frac{4\mathcal{G}}{r} \int d^{D-1}\mathbf{x}' S_{\mu\nu}(t - |\mathbf{x} - \mathbf{x}'|, \mathbf{x}'), \quad D = 4. \quad (13.29)$$

To find the Fourier transform of the metric, one uses the representation (13.23) for the Green's function. Now, in the wave zone, the Green's function may be simplified using the asymptotic expansion for the Bessel function [208]

$$H_{(D-3)/2}^1(\omega r) \sim \sqrt{\frac{2}{\pi(\omega r)}} e^{i[\omega r - \frac{\pi}{4}(D-2)]}, \quad \omega r \rightarrow \infty. \quad (13.30)$$

This yields

$$h_{\mu\nu}(\omega, \mathbf{x}) = -\frac{8\pi\mathcal{G}}{(2\pi r)^{(D-2)/2}} \omega^{(D-4)/2} e^{i\omega r} \int d^{D-1}\mathbf{x}' S_{\mu\nu}(\omega, \mathbf{x}'). \quad (13.31)$$

This could also have been arrived at directly from (13.28), using the rule time derivative $\rightarrow -i\omega$ for Fourier transforms. Equations (13.28) and (13.31) are one of the most important results derived in this paper, and will be the basis for all the subsequent section. Similar equations, but not as general as the ones presented here, were given by Chen, Li and Lin [215] in the context of gravitational radiation by a rolling tachyon.

To get the energy spectrum, we use (13.12) yielding

$$\frac{d^2 E}{d\omega d\Omega} = 2\mathcal{G} \frac{\omega^{D-2}}{(2\pi)^{D-4}} \left(T^{\mu\nu}(\omega, \mathbf{k}) T_{\mu\nu}^*(\omega, \mathbf{k}) - \frac{1}{D-2} |T^\lambda{}_\lambda(\omega, \mathbf{k})|^2 \right). \quad (13.32)$$

13.3 The even D -dimensional quadrupole formula

13.3.1 Derivation of the even D -dimensional quadrupole formula

When the velocities of the sources that generate the gravitational waves are small, it is sufficient to know the T^{00} component of the gravitational energy-momentum tensor in order to have a good estimate of the energy they radiate. In this subsection, we will deduce the D -dimensional quadrupole formula and in the next subsection we will apply it to (1) a particle in circular orbit and (2) a particle in free fall into a D -dimensional Schwarzschild black hole.

We start by recalling that the Fourier transform of the energy-momentum tensor is

$$T_{\mu\nu}(\omega, \mathbf{k}) = \int d^{D-1}\mathbf{x}' e^{-i\mathbf{k}\cdot\mathbf{x}'} \int dt e^{i\omega t} T^{\mu\nu}(t, \mathbf{x}) + \text{c.c.}, \quad (13.33)$$

where c.c. means the complex conjugate of the preceding term. Then, the conservation equations (13.9) for $T^{\mu\nu}(t, \mathbf{x})$ applied to eq. (13.33) yield $k^\mu T_{\mu\nu}(\omega, \mathbf{k}) = 0$. Using this last result we obtain $T_{00}(\omega, \mathbf{k}) = \hat{k}^j \hat{k}^i T_{ji}(\omega, \mathbf{k})$ and $T_{0i}(\omega, \mathbf{k}) = -\hat{k}^j T_{ji}(\omega, \mathbf{k})$, where $\hat{\mathbf{k}} = \mathbf{k}/\omega$. We can then write the energy spectrum, eq. (13.32), as a function only of the spacelike components of $T^{\mu\nu}(\omega, \mathbf{k})$,

$$\frac{d^2 E}{d\omega d\Omega} = 2\mathcal{G} \frac{\omega^{D-2}}{(2\pi)^{D-4}} \Lambda_{ij,lm}(\hat{k}) T^{*ij}(\omega, \mathbf{k}) T^{ij}(\omega, \mathbf{k}), \quad (13.34)$$

where

$$\Lambda_{ij,lm}(\hat{k}) = \delta_{il}\delta_{jm} - 2\hat{k}_j\hat{k}_m\delta_{il} + \frac{1}{D-2} \left(-\delta_{ij}\delta_{lm} + \hat{k}_l\hat{k}_m\delta_{ij} + \hat{k}_i\hat{k}_j\delta_{lm} \right) + \frac{D-3}{D-2} \hat{k}_i\hat{k}_j\hat{k}_l\hat{k}_m. \quad (13.35)$$

At this point, we make a new approximation (in addition to the wave zone approximation) and assume that $\omega R \ll 1$, where R is the source's radius. In other words, we assume that the internal velocities of the sources are small and thus the source's radius is much smaller than the characteristic wavelength $\sim 1/\omega$ of the emitted gravitational waves. Within this approximation, one can set $e^{-i\mathbf{k}\cdot\mathbf{x}'} \sim 1$ in eq. (13.33) (since $R = |\mathbf{x}'|_{\max}$). Moreover, after a straightforward calculation, one can also set in eq. (13.34) the approximation $T^{ij}(\omega, \mathbf{k}) \simeq -(\omega^2/2)D_{ij}(\omega)$, where

$$D_{ij}(\omega) = \int d^{D-1}\mathbf{x} x^i x^j T^{00}(\omega, \mathbf{x}). \quad (13.36)$$

Finally, using

$$\begin{aligned} \int d\Omega_{D-2} \hat{k}_i \hat{k}_j &= \frac{\Omega_{D-2}}{D-1} \delta_{ij}, \\ \int d\Omega_{D-2} \hat{k}_i \hat{k}_j \hat{k}_l \hat{k}_m &= \frac{3\Omega_{D-2}}{D^2-1} (\delta_{ij}\delta_{lm} + \delta_{il}\delta_{jm} + \delta_{im}\delta_{jl}), \end{aligned} \quad (13.37)$$

where Ω_{D-2} is the $(D-2)$ -dimensional solid angle defined in (13.71), we obtain the D -dimensional quadrupole formula

$$\frac{dE}{d\omega} = \frac{2^{2-D}\pi^{-(D-5)/2}\mathcal{G}(D-3)D}{\Gamma[(D-1)/2](D^2-1)(D-2)} \omega^{D+2} \left[(D-1)D_{ij}^*(\omega)D_{ij}(\omega) - |D_{ii}(\omega)|^2 \right], \quad (13.38)$$

where the Gamma function $\Gamma[z]$ is defined in Appendix 13.4.3. As the dimension D grows it is seen that the rate of gravitational energy radiated increases as ω^{D+2} . Sometimes it will be more useful to have the time rate of emitted energy

$$\frac{dE}{dt} = \frac{2^{2-D}\pi^{-(D-5)/2}\mathcal{G}(D-3)D}{\Gamma[(D-1)/2](D^2-1)(D-2)} \left[(D-1)\partial_t^{(D+2)/2} D_{ij}^*(t)\partial_t^{(D+2)/2} D_{ij}(t) - |\partial_t^{(D+2)/2} D_{ii}(t)|^2 \right]. \quad (13.39)$$

For $D=4$, eq. (13.39) yields the well known result [205]

$$\frac{dE}{dt} = \frac{\mathcal{G}}{5} \left[\partial_t^3 D_{ij}^*(t)\partial_t^3 D_{ij}(t) - \frac{1}{3}|\partial_t^3 D_{ii}(t)|^2 \right]. \quad (13.40)$$

13.3.2 Applications of the quadrupole formula: test particles in a background geometry

The quadrupole formula has been used successfully in almost all kind of problems involving gravitational wave generation. By successful we mean that it agrees with other more accurate methods. Its simplicity and the fact that it gives results correct to within a few percent, makes it an invaluable tool in estimating gravitational radiation emission. We shall in the following present two important examples of the application of the quadrupole formula.

13.3.2.a A particle in circular orbit

The radiation generated by particles in circular motion was perhaps the first situation to be considered in the analysis of gravitational wave generation. For orbits with low frequency, the quadrupole formula yields excellent results. As expected it is difficult to find in nature a

system with perfect circular orbits, they will in general be elliptic. In this case the agreement is also remarkable, and one finds that the quadrupole formalism can account with precision for the increase in period of the pulsar PSR 1913+16, due to gravitational wave emission [216]. In four dimensions the full treatment of elliptic orbital motion is discussed by Peters [217]. In dimensions higher than four, it has been shown [154] that there are no stable geodesic circular orbits, and so geodesic circular motion is not as interesting for higher D . For this reason, and also because we only want to put in evidence the differences that arise in gravitational wave emission as one varies the spacetime dimension D , we will just analyze the simple circular, not necessarily geodesic motion, to see whether the results are non-trivially changed as one increases D . Consider then two bodies of equal mass m in circular orbits a distance l apart. Suppose they revolve around the center of mass, which is at $l/2$ from both masses, and that they orbit with frequency ω in the $x - y$ plane. A simple calculation [217, 218] yields

$$D_{xx} = \frac{ml^2}{4} \cos(2\omega t) + \text{const} , \quad (13.41)$$

$$D_{yy} = -D_{xx} , \quad (13.42)$$

$$D_{xy} = \frac{ml^2}{4} \sin(2\omega t) + \text{const} , \quad (13.43)$$

independently of the dimension in which they are imbedded and with all other components being zero. We therefore get from eq. (13.39)

$$\frac{dE}{dt} = \frac{2\mathcal{G}D(D-3)}{\pi^{(D-5)/2}\Gamma[(D-1)/2](D+1)(D-2)} m^2 l^4 \omega^{D+2} . \quad (13.44)$$

For $D = 4$ one gets

$$\frac{dE}{dt} = \frac{8\mathcal{G}}{5} m^2 l^4 \omega^6 , \quad (13.45)$$

which agrees with known results [217, 218]. Eq. (13.44) is telling us that as one climbs up in dimension number D , the frequency effects gets more pronounced.

13.3.2.b A particle falling radially into a higher dimensional Schwarzschild black hole

As yet another example of the use of the quadrupole formula eq. (13.39) we now calculate the energy given away as gravitational waves when a point particle, with mass m falls into a D -dimensional Schwarzschild black hole, a metric first given in [154]. Historically, the case of a particle falling into a $D = 4$ Schwarzschild black hole was one of the first to be studied [219, 2] in connection with gravitational wave generation, and later served as a model calculation when one wanted to evolve Einstein's equations fully numerically [7, 5]. This process was first studied [2] by solving numerically Zerilli's [219] wave equation for a particle at rest at infinity and then falling into a Schwarzschild black hole. Davis et al [2] found numerically that the amount of energy radiated to infinity as gravitational waves was $\Delta E_{\text{num}} = 0.01 \frac{m^2}{M}$, where m is the mass of the particle falling in and M is the mass of the black hole. It is found that the $D = 4$ quadrupole formula yields [220] $\Delta E_{\text{quad}} = 0.019 \frac{m^2}{M}$, so it is of the order of magnitude as that given by fully relativistic numerical results. Despite the fact that the quadrupole formula fails somewhere near the black hole (the motion is not slow, and the background is certainly not flat), it looks like one can get an idea of how much radiation will be released with the help

of this formula. Based on this good agreement, we shall now consider this process but for higher dimensional spacetimes. The metric for the D -dimensional Schwarzschild black hole in $(t, r, \theta_1, \theta_2, \dots, \theta_{D-2})$ coordinates (see Appendix 13.4.3) is

$$ds^2 = - \left(1 - \frac{16\pi\mathcal{G}M}{(D-2)\Omega_{D-2}r^{D-3}} \right) dt^2 + \left(1 - \frac{16\pi\mathcal{G}M}{(D-2)\Omega_{D-2}r^{D-3}} \right)^{-1} dr^2 + r^{D-2}d\Omega_{D-2}^2. \quad (13.46)$$

Consider a particle falling along a radial geodesic, and at rest at infinity. Then, the geodesic equations give

$$\frac{dr}{dt} \sim \frac{16\pi\mathcal{G}M}{(D-2)\Omega_{D-2}r^{D-3}}, \quad (13.47)$$

where we make the flat space approximation $t = \tau$. We then have, in these coordinates, $D_{11} = r^2$, and all other components vanish. From (13.39) we get the energy radiated per second, which yields

$$\frac{dE}{dt} = \frac{2^{2-D}\pi^{-(D-5)/2}\mathcal{G}(D-3)}{\Gamma[(D-1)/2](D^2-1)} D |\partial_t^{(D+2)/2} D_{11}|^2, \quad (13.48)$$

We can perform the derivatives and integrate to get the total energy radiated. There is a slight problem though, where do we stop the integration? The expression for the energy diverges at $r = 0$ but this is no problem, as we know that as the particle approaches the horizon, the radiation will be infinitely red-shifted. Moreover, the standard picture [220] is that of a particle falling in, and in the last stages being frozen near the horizon. With this in mind we integrate from $r = \infty$ to some point near the horizon, say $r = b \times r_+$, where r_+ is the horizon radius and b is some number larger than unit, and we get

$$\Delta E = A \frac{D(D-2)\pi}{2^{2D-4}} \times b^{(9-D^2)/2} \times \frac{m^2}{M}, \quad (13.49)$$

where

$$A = \frac{(3-D)^2(5-D)^2(7-3D)^2(8-4D)^2(9-5D)^2 \dots (D/2+4-D^2/2)^2}{\Gamma[(D-1)/2]^2(D-1)(D+1)(D+3)} \quad (13.50)$$

To understand the effect of both the dimension number D and the parameter b on the total energy radiated according to the quadrupole formula, we list in Table 13.1 some values ΔE for different dimensions, and b between 1 and 1.3.

The parameter b is in fact a measure of our ignorance of what goes on near the black hole horizon, so if the energy radiated doesn't vary much with b it means that our lack of knowledge doesn't affect the results very much. For $D = 4$ that happens indeed. Putting $b = 1$ gives only an energy 2.6 times larger than with $b = 1.3$, and still very close to the fully relativistic numerical result of $0.01 \frac{m^2}{M}$. However as we increase D , the effect of b increases dramatically. For $D = 12$ for example, we can see that a change in b from 1 to 1.3 gives a corresponding change in ΔE of 3×10^6 to 0.0665. This is 8 orders of magnitude lower! Since there is as yet no Regge-Wheeler-Zerilli [219, 38] treatment of this process for higher dimensional Schwarzschild black holes, there are no fully relativistic numerical results to compare our results with. Thus $D = 4$ is just the perfect dimension to predict, through the quadrupole formula, the gravitational energy coming from collisions between particles and black holes,

Table 13.1: The energy radiated by a particle falling from rest into a higher dimensional Schwarzschild black hole, as a function of dimension. The integration is stopped at $b \times r_+$ where r_+ is the horizon radius.

	$\Delta E \times \frac{M}{m^2}$		
D	$b = 1:$	$b = 1.2:$	$b = 1.3:$
4	0.019	0.01	0.0076
6	0.576	0.05	0.0167
8	180	1.19	0.13
10	24567	6.13	0.16
12	3.3×10^6	14.77	0.0665

or between small and massive black holes. It is not a problem related to the quadrupole formalism, but rather one related to D . A small change in parameters translates itself, for high D , in a large variation in the final result. Thus, as the dimension D grows, the knowledge of the cutoff radius $b \times r_+$ becomes essential to compute accurately the energy released. We note however that a decomposition of gravitational perturbations in higher dimensions has recently become available, with the work of Kodama and Ishibashi [126]. We hope their work allows the computation in a perturbation framework of the gravitational radiation generated by the infall of particles into higher dimensional Schwarzschild black holes.

13.4 Instantaneous collisions in even D -dimensions

In general, whenever two bodies collide or scatter there will be gravitational energy released due to the changes in momentum involved in the process. If the collision is hard meaning that the incoming and outgoing trajectories have constant velocities, there is a method first envisaged by Weinberg [205, 221], later explored in [222] by Smarr to compute exactly the metric perturbation and energy released. The method is valid for arbitrary velocities (one will still be working in the linear approximation, so energies have to be low). Basically, it assumes a collision lasting for zero seconds. It was found that in this case the resulting spectra were flat, precisely what one would expect based on one's experience with electromagnetism [223], and so to give a meaning to the total energy, a cutoff frequency is needed. This cutoff frequency depends upon some physical cutoff in the particular problem. We shall now generalize this construction for arbitrary dimensions.

13.4.1 Derivation of the radiation formula in terms of a cutoff for a head-on collision

Consider therefore a system of freely moving particles with D -momenta P_i^μ , energies E_i and $(D - 1)$ -velocities \mathbf{v} , which due to the collision change abruptly at $t = 0$, to corresponding primed quantities. For such a system, the energy-momentum tensor is

$$T^{\mu\nu}(t, \mathbf{v}) = \sum \frac{P_i^\mu P_i^\nu}{E_i} \delta^{D-1}(\mathbf{x} - \mathbf{v}t) \Theta(-t) + \frac{P_i'^\mu P_i'^\nu}{E_i'} \delta^{D-1}(\mathbf{x}' - \mathbf{v}'t) \Theta(t), \quad (13.51)$$

from which, using eqs. (13.31) and (13.32) one can get the quantities $h_{\mu\nu}$ and also the radiation emitted. Let us consider the particular case in which one has a head-on collision of two particles, particle 1 with mass m_1 and Lorentz factor γ_1 , and particle 2 with mass $m = m_2$ with Lorentz factor γ_2 , colliding to form a particle at rest. Without loss of generality, one may orient the axis so that the motion is in the (x_{D-1}, x_D) plane, and the x_D axis is the radiation direction (see Appendix 13.4.3). We then have

$$P_1 = \gamma_1 m_1 (1, 0, 0, \dots, v_1 \sin \theta_1, v_1 \cos \theta_1); \quad P'_1 = (E'_1, 0, 0, \dots, 0, 0) \quad (13.52)$$

$$P_2 = \gamma_2 m_2 (1, 0, 0, \dots, -v_2 \sin \theta_1, -v_2 \cos \theta_1); \quad P'_2 = (E'_2, 0, 0, \dots, 0, 0). \quad (13.53)$$

Momentum conservation leads to the additional relation $\gamma_1 m_1 v_1 = \gamma_2 m_2 v_2$. Replacing (13.52) and (13.53) in the energy-momentum tensor (13.51) and using (13.32) we find

$$\frac{d^2 E}{d\omega d\Omega} = \frac{2\mathcal{G}}{(2\pi)^{D-2}} \frac{D-3}{D-2} \frac{\gamma_1^2 m_1^2 v_1^2 (v_1 + v_2)^2 \sin^4 \theta_1}{(1 - v_1 \cos \theta_1)^2 (1 + v_2 \cos \theta_1)^2} \times \omega^{D-4}. \quad (13.54)$$

We see that the for arbitrary (even) D the spectrum is not flat. Flatness happens only for $D = 4$. For any D the total energy, integrated over all frequencies would diverge so one needs a cutoff frequency which shall depend on the particular problem under consideration. Integrating (13.54) from $\omega = 0$ to the cutoff frequency ω_c we have

$$\frac{dE}{d\Omega} = \frac{2\mathcal{G}}{(2\pi)^{D-2}} \frac{1}{D-2} \frac{\gamma_1^2 m_1^2 v_1^2 (v_1 + v_2)^2 \sin^4 \theta_1}{(1 - v_1 \cos \theta_1)^2 (1 + v_2 \cos \theta_1)^2} \times \omega_c^{D-3}. \quad (13.55)$$

Two limiting cases are of interest here, namely (i) the collision between identical particles and (ii) the collision between a light particle and a very massive one. In case (i) replacing $m_1 = m_2 = m$, $v_1 = v_2 = v$, eq. (13.55) gives

$$\frac{dE}{d\Omega} = \frac{8\mathcal{G}}{(2\pi)^{D-2}} \frac{1}{D-2} \frac{\gamma^2 m^2 v^4 \sin^4 \theta_1}{(1 - v^2 \cos^2 \theta_1)^2} \times \omega_c^{D-3}. \quad (13.56)$$

In case (ii) considering $m_1 \gamma_1 \equiv m\gamma \ll m_2 \gamma_2$, $v_1 \equiv v \gg v_2$, eq. (13.55) yields

$$\frac{dE}{d\Omega} = \frac{2\mathcal{G}}{(2\pi)^{D-2}} \frac{1}{D-2} \frac{\gamma^2 m^2 v^4 \sin^4 \theta_1}{(1 - v \cos \theta_1)^2} \times \omega_c^{D-3}. \quad (13.57)$$

Notice that the technique just described is expected to break down if the velocities involved are very low, since then the collision would not be instantaneous. In fact a condition for this method to work would can be stated

Indeed, one can see from eq. (13.55) that if $v \rightarrow 0$, $\frac{dE}{d\omega} \rightarrow 0$, even though we know (see Subsection (13.4.1)) that $\Delta E \neq 0$. In any case, if the velocities are small one can use the quadrupole formula instead.

13.4.2 Applications: the cutoff frequency when one of the particles is a black hole and radiation from black hole pair creation

13.4.2.a The cutoff frequency when one of the head-on colliding particles is a black hole

We shall now restrict ourselves to the case (ii) of last subsection, in which at least one of the particles participating in the collision is a massive black hole, with mass $M \gg m$ (where we

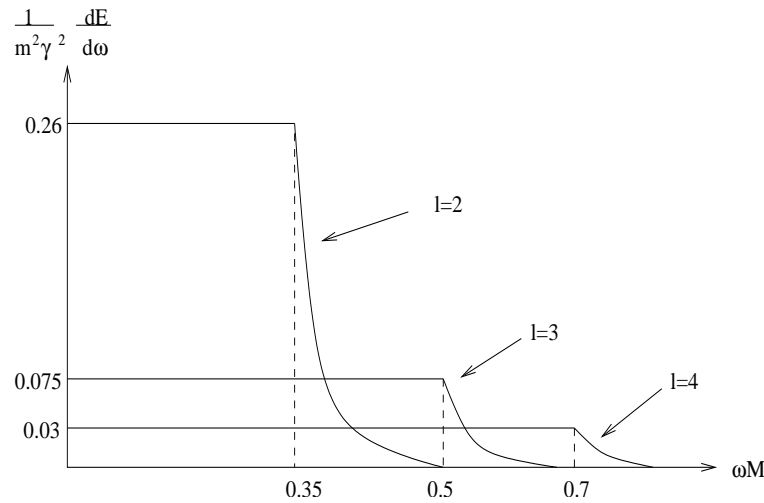


Figure 13.1: The energy spectra as a function of the angular number l , for a highly relativistic particle falling into a $D = 4$ Schwarzschild black hole [159]. The particle begins to fall with a Lorentz factor γ . Notice that for each l there is a cutoff frequency ω_{c_l} which is equal to the quasinormal frequency ω_{QN} after which the spectrum decays exponentially. So it is clearly seen that ω_{QN} works as a cutoff frequency. The total energy radiated is a given by a sum over l , which is the same as saying that the effective cutoff frequency is given by a weighted average of the various ω_{c_l} .

have put $m_1 = m$ and $m_2 = M$). Formulas (13.55)- (13.57) are useless unless one is able to determine the cutoff frequency ω_c present in the particular problem under consideration. In the situation where one has a small particle colliding at high velocities with a black hole, it has been suggested by Smarr [222] that the cutoff frequency should be $\omega_c \sim 1/2M$, presumably because the characteristic collision time is dictated by the large black hole whose radius is $2M$. Using this cutoff he finds

$$\Delta E_{\text{Smarr}} \sim 0.2\gamma^2 \frac{m^2}{M}. \quad (13.58)$$

The exact result, using a relativistic perturbation approach which reduces to the numerical integration of a second order differential equation (the Zerilli wavefunction), has been given by Cardoso and Lemos [159], as

$$\Delta E_{\text{exact}} = 0.26\gamma^2 \frac{m^2}{M}. \quad (13.59)$$

This is equivalent to saying that $\omega_c = \frac{0.613}{M} \sim \frac{1}{1.63M}$, and so it looks like the cutoff is indeed the inverse of the horizon radius. However, in the numerical work by Cardoso and Lemos, it was found that it was not the presence of an horizon that contributed to this cutoff, but the presence of a potential barrier V outside the horizon. By decomposing the field in tensorial spherical harmonics with index l standing for the angular quantum number, we found that for each l , the spectrum is indeed flat (as predicted by eq. (13.55) for $D = 4$), until a cutoff frequency ω_{c_l} which was numerically equal to the lowest gravitational quasinormal frequency ω_{QN} . For $\omega > \omega_{c_l}$ the spectrum decays exponentially. This behavior is illustrated in Fig. 13.1. The quasinormal frequencies [9] are those frequencies that correspond to only outgoing waves at infinity and only ingoing waves near the horizon. As such the gravitational

quasinormal frequencies will in general have a real and an imaginary part, the latter denoting gravitational wave emission and therefore a decay in the perturbation. There have been a wealth of works dwelling on quasinormal modes on asymptotically flat spacetimes [9], due to its close connection with gravitational wave emission, and also on non-asymptotically flat spacetimes, like asymptotically anti-de Sitter [75] or asymptotically de Sitter [83, 76, 106, 107, 108, 109, 110, 111] spacetimes, mainly due to the AdS/CFT and dS/CFT [27] correspondence conjecture. We argue here that it is indeed the quasinormal frequency that dictates the cutoff, and not the horizon radius. For $D = 4$ it so happens that the weighted average of ω_{c_l} is $\frac{0.613}{M}$, which, as we said, is quite similar to $r_+ = \frac{1}{2M}$. The reason for the cutoff being dictated by the quasinormal frequency can be understood using some WKB intuition. The presence of a potential barrier outside the horizon means that waves with some frequencies get reflected back on the barrier while others can cross. Frequencies such that ω^2 is lower than the maximum barrier height V_{\max} will be reflected back to infinity where they will be detected. However, frequencies ω^2 larger than the maximum barrier height cross the barrier and enter the black hole, thereby being absorbed and not contributing to the energy detected at infinity. So only frequencies ω^2 lower than this maximum barrier height are detected at infinity. It has been shown [13] that the gravitational quasinormal frequencies are to first order equal to the square root of the maximum barrier height. In view of this picture, and considering the physical meaning of the cutoff frequency, it seems quite natural to say that the cutoff frequency is equal to the quasinormal frequency. If the frequencies are higher than the barrier height, they don't get reflected back to infinity. This discussion is very important to understand how the total energy varies with the number D of dimensions. In fact, if we set $\omega_c \sim \frac{1}{r_+}$, we find that the total energy radiated decreases rapidly with the dimension number, because r_+ increases rapidly with the dimension. This conflicts with recent results [203, 204], which using shock waves that describe boosted Schwarzschild black holes, and searching for apparent horizons, indicate an increase with D . So, we need the gravitational quasinormal frequencies for higher dimensional Schwarzschild black holes. To arrive at an wave equation for gravitational perturbations of higher dimensional Schwarzschild black holes, and therefore to compute its gravitational quasinormal frequencies, one needs to decompose Einstein's equations in D -dimensional tensorial harmonics, which would lead to some quite complex expressions (this has recently been carried through in [126]). It is not necessary to go that far though, because one can get an idea of how the gravitational quasinormal frequencies vary by searching for the quasinormal frequencies of scalar perturbations, and scalar quasinormal frequencies are a lot easier to find. One hopes that the scalar frequencies will behave with D in the same manner as do the gravitational ones. Scalar perturbations in D -dimensional Schwarzschild spacetimes obey the wave equation (consult [224] for details)

$$\frac{\partial^2 \phi(\omega, r)}{\partial r_*^2} + [\omega^2 - V(r)] \phi(\omega, r) = 0. \quad (13.60)$$

The potential $V(r)$ appearing in equation (13.60) is given by

$$V(r) = f(r) \left[\frac{a}{r^2} + \frac{(D-2)(D-4)f(r)}{4r^2} + \frac{(D-2)f'(r)}{2r} \right], \quad (13.61)$$

where $a = l(l+D-3)$ is the eigenvalue of the Laplacian on the hypersphere S^{D-2} , the tortoise coordinate r_* is defined as $\frac{\partial r}{\partial r_*} = f(r) = \left(1 - \frac{16\pi GM}{(D-2)\Omega_{D-2} r^{D-3}} \right)$, and $f'(r) = \frac{df(r)}{dr}$. We have

Table 13.2: The lowest scalar quasinormal frequencies for spherically symmetric ($l = 0$) scalar perturbations of higher dimensional Schwarzschild black holes, obtained using a WKB method [13, 14]. Notice that the real part of the quasinormal frequency is always the same order of magnitude as the square root of the maximum barrier height. We show also the maximum barrier height as well as the horizon radius as a function of dimension D . The mass M of the black hole has been set to 1.

D	$\text{Re}[\omega_{QN}]$:	$\text{Im}[\omega_{QN}]$:	$\sqrt{V_{\text{max}}}$:	$1/r_+$:
4	0.10	-0.12	0.16	0.5
6	1.033	-0.713	1.441	1.28
8	1.969	-1.023	2.637	1.32
10	2.779	-1.158	3.64	1.25
12	3.49	-1.202	4.503	1.17

found the quasinormal frequencies of spherically symmetric ($l = 0$) scalar perturbations, by using a WKB approach developed by Schutz, Will and collaborators [13, 14]. The results are presented in Table 13.2, where we also show the maximum barrier height of the potential in eq. (13.61), as well as the horizon radius. (A more complete treatment using a novel sixth order WKB approach has been given by Konoplya [15]).

The first thing worth noticing is that the real part of the scalar quasinormal frequency is to first order reasonably close to the square root of the maximum barrier height $\sqrt{V_{\text{max}}}$, supporting the previous discussion. Furthermore, the scalar quasinormal frequency grows more rapidly than the inverse of the horizon radius $\frac{1}{r_+}$ as one increases D . In fact, the scalar quasinormal frequency grows with D while the horizon radius r_+ gets smaller. Note that from pure dimensional arguments, for fixed D , $\omega \propto \frac{1}{r_+}$. The statement here is that the constant of proportionality depends on the dimension D , more explicitly it grows with D , and can be found from Table 13.2. Assuming that the gravitational quasinormal frequencies will have the same behavior (and some very recent studies [15] seem to point that way), the total energy radiated will during high-energy collisions does indeed increase with D , as some studies [203, 204] seem to indicate.

13.4.2.b The gravitational energy radiated during black hole pair creation

As a new application of this instantaneous collision formalism, we will now consider the gravitational energy released during the quantum creation of pairs of black holes, a process which as far as we know has not been analyzed in the context of gravitational wave emission, even for $D = 4$. It is well known that vacuum quantum fluctuations produce virtual electron-positron pairs. These pairs can become real [225] if they are pulled apart by an external electric field, in which case the energy for the pair materialization and acceleration comes from the external electric field energy. Likewise, a black hole pair can be created in the presence of an external field whenever the energy pumped into the system is enough in order to make the pair of virtual black holes real (see Dias [226] for a review on black hole pair creation). If one tries to predict the spectrum of radiation coming from pair creation, one expects of course a spectrum characteristic of accelerated masses but one also expects that this follows some kind of signal indicating pair creation. In other words, the process of pair creation itself, which involves the sudden creation of particles, must imply emission of radiation. It is this phase

we shall focus on, forgetting the subsequent emission of radiation caused by the acceleration.

Pair creation is a pure quantum-mechanical process in nature, with no classical explanation. But given that the process does occur, one may ask about the spectrum and intensity of the radiation accompanying it. The sudden creation of pairs can be viewed for our purposes as an instantaneous creation of particles (i.e., the time reverse process of instantaneous collisions), the violent acceleration of particles initially at rest to some final velocity in a very short time, and the technique described at the beginning of this section applies. This is quite similar to another pure quantum-mechanical process, the beta decay. The electromagnetic radiation emitted during beta decay has been computed classically by Chang and Falkoff [227] and is also presented in Jackson [223]. The classical calculation is similar in all aspects to the one described in this section (the instantaneous collision formalism) assuming the sudden acceleration to energies E of a charge initially at rest, and requires also a cutoff in the frequency, which has been assumed to be given by the uncertainty principle $\omega_c \sim \frac{E}{\hbar}$. Assuming this cutoff one finds that the agreement between the classical calculation and the quantum calculation [227] is extremely good (specially in the low frequency regime), and more important, was verified experimentally. Summarizing, formula (13.56) also describes the gravitational energy radiated when two black holes, each with mass m and energy E form through quantum pair creation. The typical pair creation time can be estimated by the uncertainty principle $\tau_{\text{creation}} \sim \hbar/E \sim \frac{\hbar}{m\gamma}$, and thus we find the cutoff frequency as

$$\omega_c \sim \frac{1}{\tau_{\text{creation}}} \sim \frac{m\gamma}{\hbar}. \quad (13.62)$$

Here we would like to draw the reader's attention to the fact that the units of Planck's constant \hbar change with dimension number D : according to our convention of setting $c = 1$ the units of \hbar are $[M]^{\frac{D-2}{D-3}}$. With this cutoff, we find the spectrum of the gravitational radiation emitted during pair creation to be given by (13.54) with $m_1 = m_2$ and $v_1 = v_2$ (we are considering the pair creation of two identical black holes):

$$\frac{d^2 E}{d\omega d\Omega} = \frac{8\mathcal{G}}{(2\pi)^{D-2}} \frac{D-3}{D-2} \frac{\gamma^2 m^2 v^4 \sin^4 \theta_1}{(1-v^2 \cos^2 \theta_1)^2} \times \omega^{D-4}, \quad (13.63)$$

and the total frequency integrated energy per solid angle is

$$\frac{dE}{d\Omega} = \frac{8\mathcal{G}}{(2\pi)^{D-2}(D-2)} \frac{v^4 \sin^4 \theta_1}{(1-v^2 \cos^2 \theta_1)^2} \times \frac{(m\gamma)^{D-1}}{\hbar^{D-3}}. \quad (13.64)$$

For example, in four dimensions and for pairs with $v \sim 1$ one obtains

$$\frac{dE}{d\omega} = \frac{4\mathcal{G}}{\pi} \gamma^2 m^2, \quad (13.65)$$

and will have for the total energy radiated during production itself, using the cutoff frequency (13.62)

$$\Delta E = \frac{4\mathcal{G}}{\pi} \frac{\gamma^3 m^3}{\hbar}. \quad (13.66)$$

This could lead, under appropriate numbers of m and γ to huge quantities. Although one cannot be sure as to the cutoff frequency, and therefore the total energy (13.66), it is extremely likely that, as was verified experimentally in beta decay, the zero frequency limit, eq. (13.65), is exact.

13.4.3 Spherical coordinates in $(D - 1)$ -dimensions

In this appendix we list some important formulas and results used throughout this paper. We shall first present the transformation mapping a $(D - 1)$ cartesian coordinates, $(x_1, x_2, x_3, \dots, x_{D-1})$ onto $(D - 1)$ spherical coordinates, $(r, \theta_1, \theta_2, \dots, \theta_{D-2})$. The transformation reads

$$\begin{aligned} x_1 &= r \sin \theta_1 \sin \theta_2 \dots \sin \theta_{D-2} \\ x_2 &= r \sin \theta_1 \sin \theta_2 \dots \sin \theta_{D-3} \cos \theta_{D-2} \\ &\quad \vdots \\ x_i &= r \sin \theta_1 \sin \theta_2 \dots \sin \theta_{D-i-1} \cos \theta_{D-i} \\ &\quad \vdots \\ x_{D-1} &= r \cos \theta_1 \end{aligned}$$

The Jacobian of this transformation is

$$J = r^{D-2} \sin \theta_1^{D-3} \sin \theta_2^{D-4} \dots \sin \theta_i^{D-i-2} \dots \sin \theta_{D-3}, \quad (13.67)$$

and the volume element becomes

$$d^{D-1}\mathbf{x} = J dr d\theta_1 d\theta_2 \dots d\theta_{D-2} = r^{D-2} dr d\Omega_{D-2}, \quad (13.68)$$

where

$$d\Omega_{D-2} = \sin \theta_1^{D-3} \sin \theta_2^{D-4} \dots \sin \theta_{D-3} d\theta_1 d\theta_2 \dots d\theta_{D-2}. \quad (13.69)$$

is the element of the $(D - 1)$ dimensional solid angle. Finally, using [228]

$$\int_0^\pi \sin \theta^n = \sqrt{\pi} \frac{\Gamma[(n+1)/2]}{\Gamma[(n+2)/2]}, \quad (13.70)$$

this yields

$$\Omega_{D-2} = \frac{2\pi^{(D-1)/2}}{\Gamma[(D-1)/2]}. \quad (13.71)$$

Here, $\Gamma[z]$ is the Gamma function, whose definition and properties are listed in [208]. In this work the main properties of the Gamma function which were used are $\Gamma[z+1] = z\Gamma[z]$ and $\Gamma[1/2] = \sqrt{\pi}$.

13.5 Summary and discussion

We have developed the formalism to compute gravitational wave generation in higher D dimensional spacetimes, with D even. Several examples have been worked out, and one cannot help the feeling that our apparently four dimensional world is the best one to make predictions about the intensity of gravitational waves in concrete situations, in the sense that a small variation of parameters leads in high D to a huge variation of the energy radiated. A lot more work is still needed if one wants to make precise predictions about gravitational wave generation in D dimensional spacetimes. Since a decomposition of gravitational perturbations in higher dimensional spacetimes has recently become available [126] it is now urgent to use

this formalism to compute the gravitational radiation generated in typical processes, in a perturbation manner as described in the following chapter, i.e., assuming a curved background (for example, the background of a higher dimensional Schwarzschild black hole). The results can then be compared with the estimates presented here in a more complete fashion. One of the examples worked out, the gravitational radiation emitted during black hole pair creation, had not been previously considered in the literature, and it seems to be a good candidate, even in $D = 4$, to radiate intensely through gravitational waves.

Chapter 14

Late-time tails in higher dimensional spacetimes

Contents

14.1 Introduction	185
14.2 A brief summary of previous analytical results for a specific class of potentials	187
14.3 The evolution equations and late-time tails in the D -dimensional Schwarzschild geometry	188
14.4 Conclusions	192

14.1 Introduction

It is an everyday life experience that light rays and waves in general travel along a null cone. For example, if one lights a candle or a lighter for five seconds and then turns it off, any observer (at rest relative to the object) will see the light for exactly five seconds and then suddenly fade out completely. Mathematically this is due to the well known fact that the flat space 4-dimensional Green's function has a delta function character and therefore has support only on the light cone. There are however situations where this only-on-the light cone propagation is lost. For instance, in a curved spacetime a propagating wave leaves a "tail" behind, as shown by DeWitt and Brehme's seminal work [229]. This means that a pulse of gravitational waves (or any massless field for that matter) travels not only along the light cone but also spreads out behind it, and slowly dies off in tails. Put it another way, even after the candle is turned off in a curved spacetime, one will still see its shining light, slowly fading away, but never completely. This is due to backscattering off the potential [230] at very large spatial distances.

The existence of late-time tails in black hole spacetimes is by now well established, both analytically and numerically, in linearized perturbations and even in a non-linear evolution, for massless or massive fields [230, 231, 232, 233, 234, 88, 235, 31]. This is a problem of more than academic interest: one knows that a black hole radiates away everything that it can, by the so called no hair theorem (see [30] for a nice review), but how does this hair loss proceed

dynamically? A more or less complete picture is now available. The study of a fairly general class of initial data evolution shows that the signal can roughly be divided in three parts: (i) the first part is the prompt response, at very early times, and the form depends strongly on the initial conditions. This is the most intuitive phase, being the obvious counterpart of the light cone propagation. (ii) at intermediate times the signal is dominated by an exponentially decaying ringing phase, and its form depends entirely on the black hole characteristics, through its associated quasinormal modes [9, 10, 31, 33, 70, 37, 78, 106, 75, 34, 35]. (iii) a late-time tail, usually a power law falloff of the field. This power law seems to be highly independent of the initial data, and seems to persist even if there is no black hole horizon. In fact it depends only on the asymptotic far region. Mathematically each of these stages has been associated as arising from different contributions to the Green's function. The late-time tail is due to a branch cut [233]. The study of linearized (we note that non-linear numerical evolution also displays these tails, but here we shall work at the linearized level) perturbations in the black hole exterior can usually be reduced to the simple equation

$$[\partial_t^2 - \partial_x^2 + V(x)]\Psi = 0, \quad (14.1)$$

where the potential $V(x)$ depends on what kind of field one is considering and also, of course, on the spacetime. A detailed study of the branch cut contribution by Ching, Leung, Suen and Young [234, 88] has provided analytical results for some specific but quite broad class of potentials. These analytical results concerning the late time tails were confirmed numerically.

It is not generally appreciated that there is another case in which wave propagation develops tails: wave propagation in odd dimensional *flat* spacetimes. In fact, the Green's function in a D -dimensional spacetime [237, 99, 238] have a completely different structure depending on whether D is even or odd. For even D it still has support only on the light cone, but for odd D the support of the Green's function extends to the interior of the light cone, and leads to the appearance of tails. It is hard to find good literature on this subject, but a complete and pedagogical discussion of tails in flat D -dimensional backgrounds can be found in [238].

A study of wave physics in higher dimensions is now, more than ever, needed. It seems impossible to formulate in four dimensions a consistent theory which unifies gravity with the other forces in nature. Thus, most efforts in this direction have considered a higher dimensional arena for our universe, one example being string theories which have recently made some remarkable achievements. Moreover, recent investigations [151] propose the existence of extra dimensions in our Universe in order to solve the hierarchy problem, i.e., the huge difference between the electroweak and the Planck scale, $m_{\text{EW}}/M_{\text{Pl}} \sim 10^{-17}$. The fields of standard model would inhabit a 4-dimensional sub-manifold, the brane, whereas the gravitational degrees of freedom would propagate throughout all dimensions.

A first step towards the understanding of gravitational wave physics in higher dimensions was given by Cardoso, Dias and Lemos [99], by studying wave generation and propagation in generic D -dimensional flat spacetimes. Here we shall take a step further, by studying wave tails in higher dimensional black hole spacetimes. We will restrict the analysis to higher dimensional Schwarzschild black holes. As expected, if one now considers tails in higher dimensional black hole spacetimes two aspects should emerge: in odd dimensional spacetimes one expects the black hole contribution to the tail to be smaller than that of the background itself. Therefore for odd dimensions the tail should basically be due to the flat space Green's function. However, for even D -dimensional black hole spacetimes there is no background contribution, and one expects to see only the black hole contribution to the tail. A recent

study by Barvinsky and Solodukhin [239] has showed that such tails may not be impossible to detect. Unfortunately, the weakness of gravitational waves impinging on Earth, make this an unlikely event. We note however that they worked with small length, compact extra-dimensions, whereas we shall consider large extra dimensions. Our results will be strictly correct if the extra dimensions are infinite, but also allow us to determine the correct answer if the large extra dimensions are large enough that the timescale for wave reflection at the boundaries is larger than the timescales at which the tail begins to dominate. We shall follow closely the analysis in [240]

The evolution problem in a D -dimensional Schwarzschild background can be cast in the form (14.1), and we will show also that the potential can be worked out in such a way as to belong to the class of potentials studied in [234, 88]. Therefore, their analytical results carry over to the D -dimensional Schwarzschild black holes as well. We will verify this by a direct numerical evolution. The main results are: the late-time behavior is dominated by a tail, and this is a power-law falloff. For odd dimensions the power-law is determined not by the presence of the black hole, but by the fact that the spacetime is odd dimensional. In this case the field decays as $\Psi \sim t^{-(2l+D-2)}$, where l is the angular index determining the angular dependence of the field. This is one of the most interesting results obtained here. One can show directly from the flat space Green's function that such a power-law is indeed expected in flat odd dimensional spacetimes, and it is amusing to note that the same conclusion can be reached directly from the analysis of [234, 88]. For even dimensional spacetimes we find also a power-law decay at late times, but with a much more rapid decay, $\Psi \sim t^{-(2l+3D-8)}$. For even D , this power-law tail is entirely due to the black hole, as opposed to the situation in odd D . These results are strictly valid for $D > 4$. Four dimensional Schwarzschild geometry is special, having the well known power-law tail $\Psi \sim t^{-(2l+3)}$.

14.2 A brief summary of previous analytical results for a specific class of potentials

In a very complete analysis, Ching, Leung, Suen and Young [234, 88] have studied the late-time tails appearing when one deals with evolution equations of the form (14.1), and the potential V is of the form

$$V(x) \sim \frac{\nu(\nu+1)}{x^2} + \frac{c_1 \log x + c_2}{x^\alpha}, \quad x \rightarrow \infty. \quad (14.2)$$

By a careful study of the branch cut contribution to the associated Green's function they concluded that in general the late-time behavior is dictated by a power-law or by a power-law times a logarithm, and the exponents of the power-law depend on the leading term at very large spatial distances. The case of interest for us here, as we shall verify in the following section, is when $c_1 = 0$. Their conclusions, which we will therefore restrict to the $c_1 = 0$ case, are (see Table 1 in [234] or [88]):

(i) if ν is an integer the term $\frac{\nu(\nu+1)}{x^2}$ does not contribute to the late-time tail. We note this term represents just the pure centrifugal barrier, characteristic of flat space, so one can expect that indeed it does not contribute, at least in four-dimensional spacetime. We also note that since even dimensional spacetimes have on-light cone propagation, one may expect to reduce the evolution equation to a form containing the term $\frac{\nu(\nu+1)}{x^2}$ with ν an integer. We shall find

this is indeed the case. Therefore, for integer ν , it is the $\frac{c_2}{x^\alpha}$ term that contributes to the late-time tail. In this case, the authors of [234, 88] find that the tail is given by a power-law,

$$\Psi \sim t^{-\mu} , \mu > 2\nu + \alpha , \alpha \text{ odd integer} < 2\nu + 3. \quad (14.3)$$

For this case (α an odd integer smaller than $2\nu + 3$) the exponent μ was not determined analytically. However, they argue both analytically and numerically, that $\mu = 2\nu + 2\alpha - 2$. For all other real α , the tail is

$$\Psi \sim t^{-(2\nu+\alpha)} , \text{ all other real } \alpha. \quad (14.4)$$

(ii) if ν is not an integer, then the main contribution to the late-time tail comes from the $\frac{\nu(\nu+1)}{x^2}$ term. In this case the tail is

$$\Psi \sim t^{-(2\nu+2)} , \text{ non - integer } \nu. \quad (14.5)$$

We will now see that for a D -dimensional Schwarzschild geometry the potential entering the evolution equations is asymptotically of the form (14.2) and therefore the results (14.3)-(14.5) can be used.

14.3 The evolution equations and late-time tails in the D -dimensional Schwarzschild geometry

Here, we shall consider the equations describing the evolution of scalar, electromagnetic and gravitational weak fields outside the D -dimensional Schwarzschild geometry. We shall then, based on the results presented in the previous section, derive the late-time tails form of the waves. We will find they are always a power-law falloff.

14.3.1 The evolution equations and the reduction of the potential to the standard form

The metric of the D -dimensional Schwarzschild black hole in $(t, r, \theta_1, \theta_2, \dots, \theta_{D-2})$ coordinates is [154]

$$ds^2 = -f dt^2 + f^{-1} dr^2 + r^2 d\Omega_{D-2}^2, \quad (14.6)$$

with

$$f = 1 - \frac{M}{r^{D-3}}. \quad (14.7)$$

The mass of the black hole is given by $\frac{(D-2)\Omega_{D-2}M}{16\pi\mathcal{G}}$, where $\Omega_{D-2} = \frac{2\pi^{(D-1)/2}}{\Gamma[(D-1)/2]}$ is the area of a unit $(D-2)$ sphere, and $d\Omega_{D-2}^2$ is the line element on the unit sphere S^{D-2} . We will only consider the linearized approximation, which means that we are considering wave fields outside this geometry that are so weak they do not alter this background. Technically this means that all covariant derivatives are taken with respect to the background metric (14.6).

The evolution equation for a massless scalar field follows directly from the (relativistic) Klein-Gordon equation. After a separation of the angular variables with Gegenbauer functions (see [224] for details) we get that the scalar field follows (14.1) with a potential

$$V_s(r_*) = f(r) \left[\frac{a}{r^2} + \frac{(D-2)(D-4)f(r)}{4r^2} + \frac{(D-2)f'(r)}{2r} \right], \quad (14.8)$$

where r is a function of the tortoise coordinate r_* according to $\frac{\partial r}{\partial r_*} = f(r)$. The constant $a = l(l+D-3)$ is the eigenvalue of the Laplacian on the hypersphere S^{D-2} , and $f'(r) = \frac{df(r)}{dr}$. l can take any nonnegative integer value. Of course the evolution equation is (14.1) where the variable x is in this case the tortoise coordinate r_* . This is the standard form in which the potential is presented. However, one can collect the different powers of r and get

$$V_s(r_*) = f(r) \left[\frac{\nu(\nu+1)}{r^2} + \frac{1}{r^{D-1}} \frac{(D-2)^2 M}{4} \right], \quad (14.9)$$

where

$$\nu = l - 2 + \frac{D}{2}. \quad (14.10)$$

Asymptotically for large r_* one can show that

$$V_s(r_*) \Big|_{r_* \rightarrow \infty} = \frac{\nu(\nu+1)}{r_*^2} + \frac{1}{r_*^{D-1}} \frac{(D-2)Ml}{D-4} (3-l-D). \quad (14.11)$$

This is strictly valid for $D > 4$. In the $D = 4$ case there is a logarithm term [230]. Notice that the coefficient ν appearing in the centrifugal barrier term $\frac{\nu(\nu+1)}{r_*^2}$ is, as promised, an integer for even D , and a half-integer for odd D . The gravitational evolution equations have recently been derived by Kodama and Ishibashi [126]. There are three kinds of gravitational perturbations, according to Kodama and Ishibashi's terminology: the scalar gravitational, the vector gravitational and the tensor gravitational perturbations. The first two already have their counterparts in $D = 4$, which were first derived by Regge and Wheeler [38] and by Zerilli [219]. The tensor type is a new kind appearing in higher dimensions. However, it obeys exactly the same equation as massless scalar fields, so the previous result (14.9)-(14.11) holds. It can be shown in fact that the scalar and vector type also obey the same evolution equation with a potential that also has the form (14.11) with a slightly different coefficient for the $1/r_*^{D-1}$ term. For example, for the vector type the potential is

$$V_{\text{gv}}(r_*) = f(r) \left[\frac{\nu(\nu+1)}{r^2} - \frac{1}{r^{D-1}} \frac{3(D-2)^2 M}{4} \right], \quad (14.12)$$

where ν is defined in (14.10). Therefore asymptotically for large r_* ,

$$V_{\text{gv}}(r_*) \Big|_{r_* \rightarrow \infty} = \frac{\nu(\nu+1)}{r_*^2} - \frac{1}{r_*^{D-1}} \frac{(D-2)M}{D-4} \times [8 + D^2 + D(l-6) + l(l-3)]. \quad (14.13)$$

which is of the same form as the scalar field potential. The scalar gravitational potential has a more complex form, but one can show that asymptotically it has again the form (14.11) or

(14.13) with a different coefficient in the $1/r_*^{D-1}$ term. Since the explicit form of this coefficient is not important here, we shall not give it explicitly. Electromagnetic perturbations in higher dimensions were considered in [241]. Again, asymptotically for large r_* they can be reduced to the form (14.11) (where again $\nu = l - 2 + \frac{D}{2}$ and the $1/r_*^{D-1}$ coefficient is different), so we shall not dwell on them explicitly.

14.3.2 Late-time tails

Now that we have shown that the potentials appearing in evolution of massless fields in the D -dimensional Schwarzschild geometry belong to the class of potentials studied in [234, 88] we can easily find the form of the late-time tail. For odd dimensional spacetimes, ν is not an integer, therefore the centrifugal barrier gives the most important contribution to the late-time tail. According to (14.5) we have that the late-time tail is described by the power-law falloff

$$\Psi \sim t^{-(2l+D-2)}, \text{ odd } D. \quad (14.14)$$

According to the discussion in the introduction, this tail is independent of the presence of the black hole, and should therefore already appear in the flat space Green's function. Indeed it does [99, 238]. The flat, odd dimensional Green's function has a tail term [99, 238] proportional to $\frac{\Theta(t-r)}{(t^2-r^2)^{D/2-1}}$, where Θ is the Heaviside step function. It is therefore immediate to conclude that, for spherical perturbations, for example, the tail at very large times should be $t^{-(D-2)}$ which is in agreement with (14.14) for $l = 0$ (which are the spherical perturbations). It is amusing to note that the analysis of [234, 88] gives the correct behavior at once, simply by looking at the centrifugal barrier! We have checked numerically the result (14.14) for $D = 5$, and the results are shown in Figs. 1 and 2.

The numerical procedure followed the one outlined in [231], with constant data on $v = v_0$, where v is the advanced time coordinate, $v = t + r_*$. One final remark is in order here. When numerically evolving the fields using the scheme in [231], we have found that for $D > 5$ the tail looked always like $t^{-(2\nu+4)}$. This is a fake behavior, and as pointed out in [88] (see in particular their Appendix A) it is entirely due to the ghost potential, appearing for potentials vanishing faster than $\frac{1}{r_*}$ for a second order scheme. Technically the presence of ghost potentials can be detected by changing the grid size [88]. If the results with different grid sizes are different, then the ghost potential is present. Our numerical results for $D = 5$, presented in Figs. 1-3 are free from any ghosts.

The numerical results are in excellent agreement with the analytical predictions (14.14), and seems moreover to be quite independent of the initial data. This also means that for odd dimensional spacetimes the late time behavior is dictated not by the black hole, but by the fact that spacetime has an odd number of dimensions. To further check that it is in fact the centrifugal barrier term that is controlling the tail, we have performed numerical evolutions with a five dimensional model potential. To be concrete, we have evolved a field subjected to the potential (14.9) (with $D = 5$) but we have considered an integer value for ν , namely $\nu = 1$. The result is shown in Fig. 3. Of course the true potential has a semi-integer value for ν , but this way one can verify the dependence of the tail on the centrifugal term. Indeed if $\nu = 1$ then by (14.4), with $\nu = 1$ and $\alpha = 4$, the late time tail should be $\Psi \sim t^{-6}$. The agreement with the numerical evolution is great. It is therefore the centrifugal barrier that controls the tail in odd dimensional spacetimes. For even dimensional spacetimes, $\nu = l - 2 + \frac{D}{2}$ is an

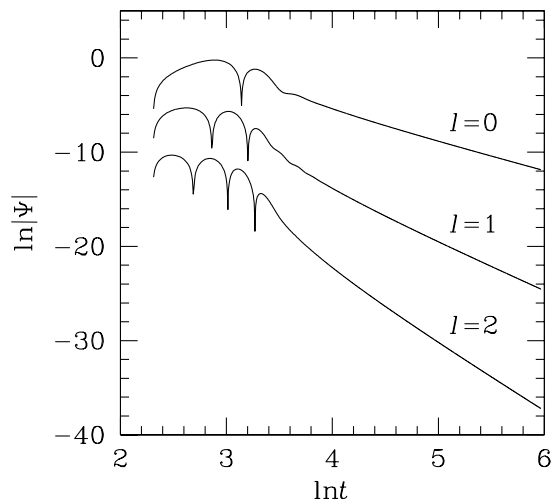


Figure 14.1: Generic time dependence of a scalar field Ψ in a five dimensional Schwarzschild geometry, at a fixed spatial position. We took as initial conditions a Gaussian wave packet with $\sigma = 3$ and $v_c = 10$. We have performed other numerical extractions for different initial values. The results for the late-time behavior are independent of the initial data, as far as we can tell. For $l = 0$ the late-time behavior is a power-law with $\Psi \sim t^{-3.1}$, for $l = 1$, $\Psi \sim t^{-5.2}$ at late times and for $l = 2$, $\Psi \sim t^{-7.3}$. The predicted powers are -3 , -5 and -7 , respectively.

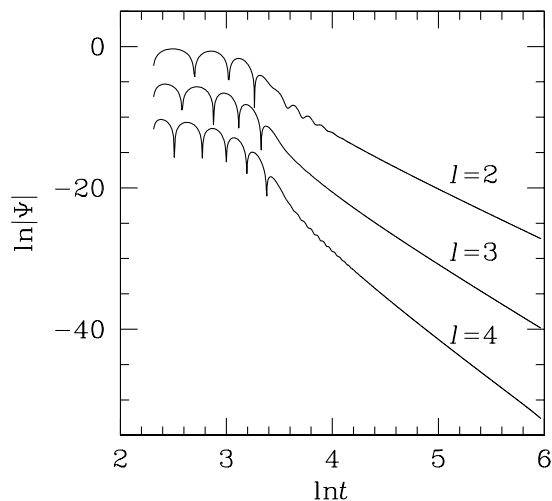


Figure 14.2: Generic time dependence of a gravitational Gaussian wavepacket Ψ in a five dimensional Schwarzschild geometry, at a fixed spatial position. The results for the late-time behavior are independent of the initial data. For $l = 2$ the late-time behavior is a power-law with $\Psi \sim t^{-7.1}$, for $l = 3$ the falloff is given by $\Psi \sim t^{-9.2}$ at late times, and for $l = 4$ it is $\Psi \sim t^{-11.4}$. The predicted powers are -7 , -9 and -11 , respectively.

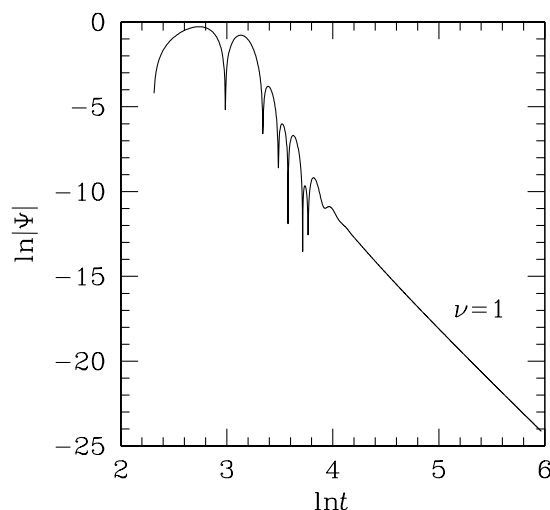


Figure 14.3: Evolution of a field subjected to a five-dimensional model potential. The potential is given by (14.9) but here we take ν as an integer, $\nu = 1$. We obtain at late times $\Psi \sim t^{-6.1}$, whereas the analytical prediction is t^{-6} . This shows nicely that for integer ν the centrifugal barrier contribution vanishes, and it is the next term in the asymptotic expansion of the potential that gives the most important contribution. We have checked that this power law is indeed the correct one, and not a numerical artifact of the ghost potential.

integer. Moreover, $\alpha = D - 1 < 2\nu + 3 = 2l + D - 1$. Therefore we are in situation (14.3). So the late time tail of wave propagation in an even D -dimensional Schwarzschild spacetime is a power-law,

$$\Psi \sim t^{-(2l+3D-8)}, \text{ even } D. \quad (14.15)$$

14.4 Conclusions

We have determined the late time behavior of massless fields (scalar, electromagnetic and gravitational) outside a D -dimensional Schwarzschild black hole. For odd D , the field at late times has a power-law falloff, $\Psi \sim t^{-(2l+D-2)}$, and this tail is independent of the presence of the black hole. It depends solely on the flat spacetime background, through the properties of the flat space odd dimensional Green's function. For even D , the late time behavior is again a power-law but this time it is due to the presence of the black hole, and is given by $\Psi \sim t^{-(2l+3D-8)}$, at late times for $D > 4$. We have focused on large extra dimensions only. Recent investigations [239], focusing on brane world models, and therefore compact extra dimensions suggest that the tail is more slowly damped if the extra dimensions are compact. In fact, for $D = 5$ they obtain a power-law $\Psi \sim t^{-5/2}$ whereas we have $\Psi \sim t^{-3}$ for spherically symmetric perturbations. This may be due to the reflection of the field at the boundaries of the extra dimension.

Bibliography

- [1] C. V. Vishveshwara, *Nature* **227**, 936 (1970).
- [2] M. Davis, R. Ruffini, W. H. Press, and R. H. Price, *Phys. Rev. Lett.* **27**, 1466 (1971).
- [3] M. Davis, R. Ruffini, and J. Tiomno, *Phys. Rev. D* **5**, 2932 (1971); R. Gleiser, C. Nicasio, R. Price, J. Pullin *Phys. Rept.* **325**, 41 (2000).
- [4] P. Anninos, D. Hobill, E. Seidel, L. Smarr, and W. M. Suen, *Phys. Rev. Lett.* **71**, 2851(1993).
- [5] R. J. Gleiser, C. O. Nicasio, R. H. Price, and J. Pullin, *Phys. Rev. Lett.* **77**, 4483 (1996).
- [6] E. Seidel, *Relativistic Astrophysics*, ed. H. Riffert et al (Braunschweig: Vieweg).
- [7] S. L. Smarr (ed.), *Sources of Gravitational Radiation*, (Cambridge University Press, 1979).
- [8] W. H. Press, *Astrophys. J.* **170**, L105 (1971).
- [9] K.D. Kokkotas, B.G. Schmidt, *Living Rev. Relativ.* **2**, 2 (1999);
- [10] H.-P. Nollert, *CQG* **16**, R159 (1999).
- [11] C. V. Vishveshwara, *Phys. Rev. D* **1**, 2870 (1970).
- [12] S. Chandrasekhar, and S. Detweiler, *Proc. R. Soc. London A* **344**, 441 (1975).
- [13] B. F. Schutz and C. M. Will, *Astrophys. Journal* **291**, L33 (1985);
- [14] C. M. Will and S. Iyer, *Phys. Rev. D* **35**, 3621 (1987); S. Iyer, *Phys. Rev. D* **35**, 3632 (1987).
- [15] R. A. Konoplya, *Phys. Rev. D* **68**, 024018 (2003).
- [16] V. Ferrari and B. Mashhoon, *Phys. Rev. D* **30**, 295 (1984).
- [17] E. W. Leaver, *Proc. Roy. Soc. Lon.* **A402**, 285 (1985).
- [18] H.-P. Nollert, *Phys. Rev. D* **47**, 5253 (1993).
- [19] A. Strominger, C. Vafa, *Phys. Lett. B* **379**, 99 (1996).

-
- [20] K. Danzmann et al., in *Gravitational Wave Experiments*, eds. E. Coccia, G. Pizzella and F. Ronga (World Scientific, Singapore, 1995).
- [21] A. Abramovici et al., *Science* **256**, 325 (1992).
- [22] C. Bradaschia et al., in *Gravitation 1990*, Proceedings of the Banff Summer Institute, Banff, Alberta, 1990, edited by R. Mann and P. Wesson (World Scientific, Singapore, 1991).
- [23] F. Echeverria, *Phys. Rev. D* **40**, 3194 (1989); L. S. Finn, *Phys. Rev. D* **46**, 5236 (1992).
- [24] H. Nakano, H. Takahashi, H. Tagoshi, M. Sasaki, gr-qc/0306082.
- [25] M. B. Green, J. H. Schwarz, E. Witten, *Superstring theory*, (Cambridge University Press, Cambridge, 1987); J. Polchinski, *String theory*, (Cambridge University Press, Cambridge, 1998).
- [26] G. 't Hooft, *Nucl. Phys. B* **72**, 461 (1974).
- [27] J. M. Maldacena, *Adv. Theor. Math. Phys.* **2**, 253 (1998); E. Witten, *Adv. Theor. Math. Phys.* **2**, 505 (1998).
- [28] O. Aharony, S. S. Gubser, J. Maldacena, H. Ooguri, Y. Oz, *Physics Reports* **323**, 183 (2000).
- [29] J. Bekenstein, *Lett. Nuovo Cimento* **11**, 467 (1974).
- [30] J. Bekenstein, in *Cosmology and Gravitation*, edited by M. Novello (Atlasciences, France 2000), pp. 1-85, gr-qc/9808028 (1998).
- [31] S. Hod, *Phys. Rev. Lett.* **81**, 4293 (1998).
- [32] J. Bekenstein and V. F. Mukhanov, *Phys. Lett. B* **360**, 7 (1995).
- [33] O. Dreyer, *Phys. Rev. Lett.* **90**, 081301 (2003).
- [34] L. Motl, *Adv. Theor. Math. Phys.* **6**, 1135 (2003).
- [35] L. Motl, A. Neitzke, *Adv. Theor. Math. Phys.* **7**, 2 (2003).
- [36] M. Bañados, C. Teitelboim, and J. Zanelli, *Phys. Rev. Lett.* **69**, 1849 (1992).
- [37] V. Cardoso and J. P. S. Lemos, *Phys. Rev. D* **63**, 124015 (2001).
- [38] T. Regge, J. A. Wheeler, *Phys. Rev.* **108**, 1063 (1957).
- [39] F. Zerilli, *Phys. Rev. Lett.* **24**, 737 (1970).
- [40] S. Chandrasekhar, in *The Mathematical Theory of Black Holes* (Oxford University, New York, 1983).

- [41] J. P. S. Lemos, *Class. Quantum Grav.* **12**, 1081 (1995); *Phys. Lett. B* **353**, 46 (1995); J. P. S. Lemos and V. T. Zanchin, *Phys. Rev. D* **54**, 3840 (1996); see also the review paper: J. P. S. Lemos, *Black holes with toroidal, cylindrical and planar horizons in anti-de Sitter spacetimes in general relativity and their properties*, “Recent developments in astronomy and astrophysics”, Proceedings of the 10th Portuguese Meeting on Astronomy and Astrophysics, edited by J. P. S. Lemos et al (World Scientific, 2001, gr-qc/0011092).
- [42] V. Cardoso and J. P. S. Lemos, *Class. Quant. Grav.* **18**, 5257 (2001).
- [43] E. Berti, V. Cardoso, K. D. Kokkotas, H. Onozawa hep-th/0307013.
- [44] E. Berti, V. Cardoso and S. Yoshida; gr-qc/0401052.
- [45] H. R. Beyer, *Commun. Math. Phys.* **204**, 397(1999).
- [46] E. S. C. Ching, P. T. Leung, W. M. Suen, S. S. Tong, and K. Young, *Rev. Mod. Phys.* **70**, 1545(1998).
- [47] S.L. Detweiler, and E. Szedenits, *Astrophys. J.* **231**, 211(1979).
- [48] G. T. Horowitz, and V. Hubeny, *Phys. Rev. D* **62**, 024027(2000).
- [49] D. Birmingham, *Phys. Rev. D* **64**, 064024 (2001).
- [50] M. W. Choptuik, *Phys. Rev. Lett.* **70**, 9(1993).
- [51] S. Fernando, hep-th/0306214.
- [52] Z-X. Shen, B. Wang, R-K. Su (CCAST World Lab, Beijing), gr-qc/0307097.
- [53] D. Birmingham, I. Sachs and S. N. Solodukhin, *Phys. Rev. Lett.* **88**, 151301 (2002).
- [54] I. Ichinose, and K. Satoh, *Nucl. Phys. B* **447**, 340(1995).
- [55] M. Bañados, M. Henneaux, C. Teitelboim, J. Zanelli, *Phys. Rev. D***48**, 1506 (1993).
- [56] G. Clément, *Class. Quantum Grav.* **10**, L49 (1993).
- [57] C. Martínez, C. Teitelboim, J. Zanelli, *Phys. Rev. D***61**, 104013 (2000).
- [58] E. W. Hirschmann, D. L. Welch, *Phys. Rev. D***53**, 5579 (1996).
- [59] M. Cataldo, P. Salgado, *Phys. Rev. D***54**, 2971 (1996).
- [60] O. J. C. Dias, J. P. S. Lemos, *JHEP* **0201**, 006 (2002).
- [61] A. R. Edmonds, *Angular Momentum in Quantum Mechanics*, (Princeton U. P., Princeton, 1957).
- [62] R. Ruffini, *Black Holes: les Astres Occlus*, (Gordon and Breach Science Publishers, 1973).
- [63] A. F. Nikiforov, V. B. Uvarov, *Special Functions of Mathematical Physics*, (Birkhäuser, Boston, 1988).

- [64] T. R. Govindarajan, and V. Suneeta, *Class. Quantum Grav.* **18**, 265 (2001).
- [65] G. B. Arfken, H. J. Weber, *Mathematical Methods for Physicists*, (Academic Press, 1995).
- [66] F. Cooper, A. Khare, and U. Sukhatme, *Phys. Rep.* **251**, 267(1995).
- [67] D. Birmingham, S. Carlip and Y. Chen, hep-th/0305113.
- [68] J. W. York, *Phys. Rev. D* **28**, 2929(1983).
- [69] J. Baez, in *Matters of gravity*, p. 12, ed. J. Pullin, gr-qc/0303027.
- [70] G. Kunstatter, *Phys. Rev. Lett.* **90**, 161301 (2003); A. Corichi, *Phys. Rev. D* **67**, 087502 (2003); J. Oppenheim, gr-qc/0307089.
- [71] E. Berti and K. D. Kokkotas, hep-th/0303029;
- [72] A. M. van den Brink, gr-qc/0303095.
- [73] D. Birmingham, hep-th/0306004 (2003).
- [74] R. A. Konoplya, *Phys. Rev. D* **66**, 044009 (2002);
- [75] B. Wang, C. Y. Lin, and E. Abdalla, *Phys. Lett. B* **481**, 79 (2000); B. Wang, C. M. Mendes, and E. Abdalla, *Phys. Rev. D* **63**, 084001 (2001); J. Zhu, B. Wang, and E. Abdalla, *Phys. Rev. D* **63**, 124004(2001); W. T. Kim, J. J. Oh, *Phys. Lett. B* **514**, 155 (2001); S. F. J. Chan and R. B. Mann, *Phys. Rev. D* **55**, 7546 (1997); A. O. Starinets, *Phys. Rev. D* **66**, 124013 (2002); Y. Kurita and M. Sakagami, *Phys. Rev. D* **67**, 024003 (2003); R. Aros, C. Martinez, R. Troncoso and J. Zanelli, *Phys. Rev. D* **67**, 044014 (2003); D. T. Son, A. O. Starinets, *J.H.E.P.* **0209**:042, (2002); S. Musiri and G. Siopsis, *Phys. Lett. B* **563**, 102 (2003)..
- [76] I. G. Moss and J. P. Norman, *Class. Quant. Grav.* **19**, 2323-2332 (2002).
- [77] V. Cardoso and J. P. S. Lemos, *Phys. Rev. D* **64**, 084017 (2001).
- [78] V. Cardoso, R. Konoplya, J. P. S. Lemos, *Phys. Rev. D* **68**, 044024 (2003).
- [79] E. Berti and K. D. Kokkotas, *Phys. Rev. D* **67**, 064020 (2003).
- [80] F. Zerilli, *J. Math. Phys.* **11**, 2203(1970).
- [81] J. Mathews, *J. Soc. Ind. Appl. Math.* **10**, 768(1962).
- [82] C. V. Vishveshwara, *Phys. Rev. D* **1**, 2870(1970).
- [83] F. Mellor, I. Moss , *Phys. Rev. D* **41**, 403(1990).
- [84] S. J. Avis, C. J. Isham and D. Storey, *Phys. Rev. D* **18**, 3565(1978).
- [85] P. Breitenlohner and D. Z. Freedman, *Phys. Lett. B* **115**, 197(1982).

- [86] C. P. Burgess and C. A. Lutken, Phys. Lett. B **153**, 137(1985); see also I. I. Cotaescu, Phys. Rev. D **60**, 107504 (1999).
- [87] A. Dasgupta, Phys. Lett. B **445**, 279(1999).
- [88] E. S. C. Ching, P. T. Leung, W. M. Suen, and K. Young, Phys. Rev. D **52**, 2118(1995).
- [89] H. Liu, Class. Quantum Grav. **12**, 543(1995).
- [90] S. Chandrasekhar, Proc. R. Soc. London, Ser. A **392**, 1(1984).
- [91] V. Hubeny, L. Susskind, and N. Toumbas, hep-th/0011164.
- [92] S. R. Das, G. Gibbons and S. D. Mathur, Phys. Rev. Lett. **78**, 417(1997).
- [93] J. A. H. Futterman, F. A. Handler and R. A. Matzner, *Scattering from Black Holes*, (Cambridge University Press, Cambridge, 1988); N. Sanchez, hep-th/9711068.
- [94] B. Carter, “General theory of stationary black hole states”, in *Black Holes*, eds B. DeWitt, C. DeWitt, (Gordon Breach, New York 1973).
- [95] E. Winstanley, gr-qc/0106032.
- [96] C. S. Peça, J. P. S. Lemos, J. Math. Phys. **41**, 4783 (2000).
- [97] H. Liu, B. Mashhoon, Class. Quantum Grav. **13**, 233 (1996).
- [98] G. Immirzi, Nucl. Phys. Proc. Suppl. **57**, 65 (1997).
- [99] V. Cardoso, O. J. C. Dias and J. P. S. Lemos, Phys. Rev. D **67**, 064026 (2003).
- [100] H. Nariai, *On some static solutions of Einstein’s gravitational field equations in a spherically symmetric case*, Sci. Rep. Tohoku Univ. **34**, 160 (1950); *On a new cosmological solution of Einstein’s field equations of gravitation*, Sci. Rep. Tohoku Univ. **35**, 62 (1951).
- [101] P. Ginsparg, M. J. Perry, *Semiclassical perdurance of de Sitter space*, Nucl. Phys. B **222**, 245 (1983).
- [102] R. Bousso, *Adventures in de Sitter space*, hep-th/0205177.
- [103] O. J. C. Dias and J. P. S. Lemos, Phys. Rev. D. (2003, in press); hep-th/0306194.
- [104] P. Brady, C. Chambers, W. Laarakkers and Eric Poisson, Phys. Rev. D **60**, 064003 (1999).
- [105] G. Pöshl and E. Teller, Z. Phys. **83**, 143 (1933).
- [106] V. Cardoso and J. P. S. Lemos, Phys. Rev. D **67**, 084020 (2003).
- [107] C. Molina, gr-qc/0304053.
- [108] A. M. van den Brink, gr-qc/0304092.

- [109] V. Suneeta, gr-qc/0303114.
- [110] A. Zhidenko, gr-qc/0307012.
- [111] S. Yoshida and T. Futamase, gr-qc/0308077.
- [112] Y. Kurita and M. Sakagami, Phys. Rev. D **67**, 024003 (2003);
- [113] Y. Ling, H. Zhang, gr-qc/0309018.
- [114] S. Musiri and G. Siopsis, hep-th/0308168.
- [115] R. A. Konoplya, hep-th/0309030.
- [116] K. H. C. Castello-Branco and E. Abdalla, gr-qc/0309090.
- [117] V. Cardoso, J. Natário and R. Schiappa, hep-th/0403132.
- [118] D. Ida, Y. Uchida and Y. Morisawa, Phys. Rev. D **67**, 084019 (2003).
- [119] J. W. Guinn, C. M. Will, Y. Kojima and B. F. Schutz, Class. Quant. Grav. **7**, L47 (1990).
- [120] V. Cardoso, J. P. S. Lemos, S. Yoshida, submitted (2003), gr-qc/0309112.
- [121] L. Crispino, A. Higuchi and G. Matsas, Phys. Rev. D **63**, 124008 (2001).
- [122] E. Berti, M. Cavaglia and L. Gualtieri, hep-th/0309203.
- [123] E. W. Leaver, Phys. Rev. D **41**, 2986 (1990).
- [124] W. Gautschi, SIAM Rev. **9**, 24 (1967).
- [125] N. Andersson, CQG **10**, L61 (1993).
- [126] H. Kodama, A. Ishibashi, hep-th/0305147 (2003); hep-th/0305185; hep-th/0308128.
- [127] A. Neitzke, hep-th/0304080 (2003).
- [128] S. Musiri, G. Siopsis, hep-th/0308168.
- [129] E. Abdalla, K. H. C. Castello-Branco, A. Lima-Santos, gr-qc/0301130 (2003).
- [130] N. Andersson, C. Howls, private communication.
- [131] H. Onozawa, Phys. Rev. D **55**, 3593 (1997).
- [132] P. T. Leung, A. Maassen van den Brink, K. W. Mak, K. Young, gr-qc/0301018 (2003).
- [133] A. Maassen van den Brink, Phys. Rev. D **62**, 064009 (2000).
- [134] S. Detweiler, Astrophys. J. **239**, 292 (1980).
- [135] E. Seidel, S. Iyer, PRD **41**, 374 (1990); K. D. Kokkotas, Class. Quant. Grav. **8**, 2217 (1991).

- [136] K. Glampedakis, N. Andersson, gr-qc/0304030 (2003).
- [137] S. Hod, gr-qc/0301122 (2003).
- [138] D. Christodoulou, Phys. Rev. Lett. **25**, 1596 (1970); D. Christodoulou, R. Ruffini, Phys. Rev. D **4**, 3552 (1971).
- [139] R. Wald, J. Math. Phys. (N.Y.) **14**, 1453 (1973).
- [140] S. Chandrasekhar, Proc. R. Soc. London **A392**, 1 (1984).
- [141] N. Andersson, Class. Quant. Grav. **11**, L39 (1994).
- [142] M. Abramowitz, I. A. Stegun, *Handbook of Mathematical Functions*, (Dover, New York, 1970); T. Oguchi, Radio Sci. **5**, 1207 (1970).
- [143] H. Bondi, Nature **179**, 1072 (1957).
- [144] K. S. Thorne, Rev. Mod. Phys, **52**, 299 (1980); K. S. Thorne, in *General Relativity: An Einstein Centenary Survey*, eds. S. W. Hawking and W. Israel (Cambridge University Press, 1989).
- [145] T. Damour, in *Gravitational Radiation*, eds Nathalie Deruelle and Tsvi Piran (North Holland Publishing Company, New York, 1983).
- [146] J. M. Weisberg and J. H. Taylor, Phys. Rev. Lett. **52**, 1348 (1984).
- [147] J. Weber, Phys. Rev. **117**, 306 (1960).
- [148] B. F. Schutz, Class. Quant. Grav. **16**, A131 (1999); B. F. Schutz and F. Ricci, in *Gravitational Waves*, eds I. Ciufolini et al, (Institute of Physics Publishing, Bristol, 2001).
- [149] S. A. Hughes, Annals Phys. **303**, 142 (2003).
- [150] M. C. Miller, E. J. M Colbert, astro-ph/0308402. R. P. van der Marel, astro-ph/0302101.
- [151] N. Arkani-Hamed, S. Dimopoulos and G. Dvali, Phys. Lett. B **429**, 263 (1998); Phys. Rev. D **59**, 086004 (1999); I. Antoniadis, N. Arkani-Hamed, S. Dimopoulos and G. Dvali, Phys. Lett. B **436**, 257 (1998).
- [152] for a review on short-ranges searches for non-Newtonian gravity, see M. Varney and J. Long, gr-qc/0309065.
- [153] J. Polchinski, TASI lectures on D-branes, hep-th/9611050.
- [154] F. R. Tangherlini, Nuovo Cim. **27**, 636 (1963).
- [155] R. C. Myers and M. J. Perry, Annals Phys. **172**, 304 (1986).
- [156] K. S. Thorne, in *J. R. Klauder, Magic without Magic*, San Francisco, 1972.
- [157] D. N. Page, Phys. Rev. D **13**, 198 (1976); Phys. Rev. D **14**, 3260 (1976).

- [158] P. C. Argyres, S. Dimopoulos and J. March-Russell, Phys. Lett. B **441**, 96 (1998); S. Dimopoulos and G. Landsberg, Phys. Rev. Lett. **87**, 161602 (2001). S. B. Giddings and S. Thomas, Phys. Rev. D **65**, 056010 (2002); S. D. H. Hsu, hep-ph/0203154; H. Tu, hep-ph/0205024; A. Jevicki and J. Thaler, Phys. Rev. D **66**, 024041 (2002); Y. Uehara, hep-ph/0205199;
- [159] V. Cardoso and J. P. S. Lemos, Phys. Lett. B **538**, 1 (2002);
- [160] V. Cardoso and J. P. S. Lemos, Gen. Rel. Grav. **35**, L327 (2003).
- [161] V. Cardoso and J. P. S. Lemos, Phys. Rev. D **67**, 084005 (2003).
- [162] V. Cardoso, J. P. S. Lemos, S. Yoshida, Phys. Rev. D (in press), gr-qc/0307104.
- [163] C. O. Lousto, and R. H. Price, Phys. Rev. D **55**, 2124 (1997); K. Martel, and E. Poisson, gr-qc/0107104.
- [164] P. D. D'Eath, in *Black Holes: gravitational interactions*, (Clarendon Press, Oxford, 1996).
- [165] P. D. D'Eath and P. N. Payne, Phys. Rev. D **46**, 658 (1992); Phys. Rev. D **46**, 675 (1992); Phys. Rev. D **46**, 694 (1992);
- [166] V. Ferrari and R. Ruffini, Phys. Lett. B **98**, 381 (1981).
- [167] V. Ferrari and B. Mashhoon, Phys. Rev. Lett. **52**, 1361 (1984).
- [168] P. N. Payne, Phys. Rev. D **28**, 1894 (1983);
- [169] T. Piran, *Gravitational Waves: A Challenge to Theoretical Astrophysics*, edited by V. Ferrari, J.C. Miller and L. Rezzolla (ICTP, Lecture Notes Series).
- [170] M. Sasaki and T. Nakamura, Prog. Theor. Phys. **67**, 1788 (1982); T. Nakamura and M. Sasaki, Phys. Lett. A **89**, 185 (1982); Y. Kojima and T. Nakamura, Phys. Lett. A **96**, 335 (1983); Y. Kojima and T. Nakamura, Phys. Lett. A **99**, 37 (1983); Y. Kojima and T. Nakamura, Prog. Theor. Phys. **71**, 79 (1984).
- [171] S. A. Teukolsky, Astrophys. J. **185**, 635 (1973).
- [172] R. A. Breuer, in *Gravitational Perturbation Theory and Synchrotron Radiation*, (Lecture Notes in Physics, Vol. 44), (Springer, Berlin 1975).
- [173] T. Nakamura and M. Sasaki, Phys. Lett. A **89**, 68 (1982); M. Sasaki and T. Nakamura, Phys. Lett. A **87**, 85 (1981).
- [174] S. A. Hughes, Phys. Rev. D **61**, 0804004 (2000); D. Kennefick, Phys. Rev. D **58**, 064012 (1998);
- [175] E. Newman and R. Penrose, J. Math. Phys. **3**, 566 (1966);
- [176] W. H. Press and S. A. Teukolsky, Astrophys. J. **185**, 649 (1973).

- [177] R. A. Breuer, M. P. Ryan Jr, and S. Waller, Proc. R. Soc. London A **358**, 71 (1977).
- [178] J. N. Goldberg, A. J. MacFarlane, E. T. Newman, F. Rohrlich and C. G. Sudarshan, J. Math. Phys. **8**, 2155 (1967);
- [179] W. H. Press, B. P. Flannery, S. A. Teukolsky and W. T. Vetterling, *Numerical Recipes* (Cambridge University Press, Cambridge, England, 1986).
- [180] S. Detweiler, Astrophys. J. **239**, 292 (1980); V. Ferrari and B. Mashhoon, Phys. Rev. D **30**, 295 (1984); V. Ferrari and B. Mashhoon, Phys. Rev. Lett. **52**, 1361 (1984); V. P. Frolov, and I. D. Novikov, in *Black Hole Physics - Basic Concepts and New Developments*, (Kluwer Academic Publishers, Dordrecht, 1998).
- [181] G. Horowitz, A. Strominger, Nucl. Phys. B **360**, 197 (1991). M. J. Duff, “TASI Lectures on Branes, Black Holes and Anti-de Sitter Space”, hep-th/9912164; A. W. Peet, “TASI lectures on black holes in string theory”, hep-th/0008241; D. Marolf, “String/M-branes for Relativists”, gr-qc/9908045.
- [182] S. S. Gubser, I. R. Klebanov, A. M. Polyakov, Phys. Lett. B **428** 105 (1998).
- [183] I. R. Klebanov, “TASI Lectures: Introduction to the AdS/CFT Correspondence”, hep-th/0009139; G. T. Horowitz, Class. Quant. Grav. **17**, 1107 (2000).
- [184] J. M. Maldacena, “Black Holes in String Theory”, Ph.D. Thesis, Princeton, hep-th/9607235; J. M. Maldacena, A. Strominger. JHEP **9812**, 005 (1998).
- [185] E. Keski-Vakkuri, Phys. Rev D **59**, 104001 (1999);
- [186] U. H. Danielsson, E. Keski-Vakkuri, M. Kruczenski, Nucl. Phys. B **563**, 279 (1999); JHEP **0002**, 039 (2000).
- [187] H. Matschull, Class. Quant. Grav. **16**, 1069 (1999).
- [188] V. Balasubramanian, P. Krauss, A. Lawrence, S. Trivedi, Phys. Rev. D **59**, 104021 (1999); V. Balasubramanian, J. de Boer, E. Keski-Vakkuri, S. F. Ross, Phys. Rev. D **64** 064011 (2001); E. Kiritsis, T. R. Taylor, hep-th/9906048.
- [189] T. Banks, M. R. Douglas, G. T. Horowitz, E. Martinec, hep-th/9808016.
- [190] L. Susskind, E. Witten, hep-th/9805114.
- [191] J. Baker, B. Brügmann, M. Campanelli, C. O. Lousto, R. Takahashi, Phys. Rev. Lett. **87**, 121103 (2001).
- [192] L. Barack and L. M. Burko, Phys. Rev. D **62**, 084040 (2001).
- [193] J. M. Cohen, R. M. Wald, J. Math. Phys. **12**, 1845 (1971).
- [194] E. Poisson, Phys. Rev. D **55**, 639 (1997).
- [195] V. Cardoso, J. P. S. Lemos, Phys. Rev. D **65**, 104032 (2002).

- [196] V. Cardoso, “Numerical Analysis of Partial Differential Equations in General Relativity and String Theory: Applications to Gravitational Radiation and to the AdS/CFT Conjecture” (Programa Gulbenkian de Estímulo à Investigação Científica, 2001).
- [197] V. Cardoso, J. P. S. Lemos, Phys. Rev. D **65**, 104033 (2002).
- [198] G. 't Hooft, gr-qc/9310026; L. Susskind, J. Math. Phys. **36**, 6377 (1995).
- [199] A. Erdelyi, W. Magnus, F. Oberlettinger, and F. Tricomi, *Higher Transcendental Functions*, (McGraw-Hill Book Co., Inc, New York, 1953); M. Abramowitz, and I. A. Stegun in *Handbook of Mathematical Functions*, (Dover, New York, 1970); A. F. Nikiforov, V. B. Uvarov, *Special Functions of Mathematical Physics*, (Birkhäuser, Boston, 1988).
- [200] M. Sasaki and T. Nakamura, Phys. Lett. B **89**, 68 (1982).
- [201] W. Kinnersley and M. Walker, Phys. Rev. D **2**, 1359 (1970); O. J. C. Dias, J. P. S. Lemos, Phys. Rev. D **67**, 064001 (2002); Phys. Rev. D **67**, 084018 (2003); hep-th/0306194.
- [202] P. Kanti and J. March-Russell, Phys. Rev. D **66**, 024023 (2002). P. Kanti and J. March-Russell, hep-ph/0212199. D. Ida, Kin-ya Oda and S. C. Park, hep-th/0212108; V. Frolov and D. Stojkovic, Phys. Rev. Lett. **89**, 151302 (2002); gr-qc/0211055;
- [203] D. M. Eardley and S. B. Giddings, Phys. Rev. D **66**, 044011 (2002).
- [204] H. Yoshino and Y. Nambu, gr-qc/0209003.
- [205] S. Weinberg, *Gravitation and Cosmology* (Wiley, New York, 1972).
- [206] J. T. Mendonca, Vitor Cardoso, Phys. Rev. D **66**, 104009 (2002); M. Servin, M. Marklund, G. Brodin, J.T. Mendonca, V. Cardoso, Phys. Rev. D **67**, 087501 (2003); J.T. Mendonca, V. Cardoso, M. Marklund, M. Servin, G. Brodin, Phys. Rev. D (in press), gr-qc/0307031.
- [207] G. N. Watson, *A Treatise on the Theory of Bessel Functions* (Cambridge University Press, 1995)
- [208] M. Abramowitz, I. A. Stegun, *Handbook of Mathematical Functions*, (Dover, New York, 1970).
- [209] R. Courant and D. Hilbert, *Methods of Mathematical Physics*, (Interscience, New York, 1962).
- [210] J. Hadamard, *Lectures on Cauchy's Problem in Linear Partial Differential Equations* (Yale University Press, New Haven, 1923).
- [211] J. D. Barrow and F. J. Tipler, *The Anthropic Cosmological Principle* (Oxford University Press, Oxford, 1986).
- [212] D. V. Gal'tsov, Phys. Rev. D **66**, 025016 (2002).
- [213] S. Hassani, *Mathematical Physics*, (Springer-Verlag, New York, 1998).

- [214] P. O. Kazinski, S. L. Lyakhovich and A. A. Sharapov, Phys. Rev. D **66**, 025017 (2002); B. P. Kosyakov, Theor. Math. Phys. **119**, 493 (1999).
- [215] B. Chen, M. Li and Feng-Li Lin, JHEP **0211**, 050 (2002).
- [216] J. M. Weisberg and J. H. Taylor, astro-ph/0211217.
- [217] P. C. Peters, Phys. Rev. **136**, B1224 (1964); P. C. Peters and J. Mathews, Phys. Rev. **131**, 435 (1963).
- [218] B. F. Schutz, *A First Course in General Relativity*, (Cambridge University Press, 1985).
- [219] F. Zerilli, Phys. Rev. D **2**, 2141 (1970).
- [220] R. Ruffini, Phys. Rev. D **7**, 972 (1973); M. J. Fitchett, *The Gravitational Recoil Effect and its Astrophysical Consequences*, (PhD Thesis, University of Cambridge, 1984).
- [221] S. Weinberg, Phys. Lett. **9**, 357 (1964); Phys. Rev. **135**, B1049 (1964).
- [222] L. Smarr, Phys. Rev. D **15**, 2069 (1977);
R. J. Adler and B. Zeks, Phys. Rev. D **12**, 3007 (1975).
- [223] J. D. Jackson, *Classical Electrodynamics*, (J. Wiley, New York 1975).
- [224] V. Cardoso and J. P. S. Lemos, Phys. Rev. D **66**, 064006 (2002).
- [225] J. Schwinger, Phys. Rev. **82**, 664 (1951).
- [226] Ó. J. C. Dias, *Proceedings of the Xth Portuguese Meeting on Astronomy and Astrophysics*, Lisbon, July 2000, eds J. P. S. Lemos et al, (World Scientific, 2001), p. 109; gr-qc/0106081.
- [227] C. S. Wang Chang and D. L. Falkoff, Phys. Rev. **76**, 365 (1949).
- [228] I. S. Gradshteyn and I. M. Ryzhik, *Table of Integrals, Series and Products*, (Academic Press, New York, 1965).
- [229] B. S. DeWitt and R. W. Brehme, Ann. Phys. (NY) **9** 220 (1965).
- [230] R. H. Price, Phys. Rev. D **5**, 2419 (1972).
- [231] C. Gundlach, R. H. Price and J. Pullin, Phys. Rev. D **49**, 883 (1994).
- [232] C. Gundlach, R. H. Price and J. Pullin, Phys. Rev. D **49**, 890 (1994).
- [233] E. Leaver, Phys. Rev. D **34**, 384 (1986).
- [234] E. S. C. Ching, P. T. Leung, W. M. Suen and K. Young, Phys. Rev. Lett. **74**, 2414 (1995).
- [235] H. Koyama and A. Tomimatsu, Phys. Rev. D **64**, 044014 (2001).
- [236] S. Hod, Class. Quant. Grav. **18**, 1311 (2001).

-
- [237] S. Hassani, *Mathematical Physics*, (Springer-Verlag, New York, 1998); R. Courant and D. Hilbert, *Methods of Mathematical Physics*, Chapter VI (Interscience, New York, 1962).
- [238] H. Soodak and M. S. Tiersten, *Am. J. Phys.* **61**, 395 (1993).
- [239] A. O. Barvinsky, S. N. Solodukhin, hep-th/0307011.
- [240] V. Cardoso, S. Yoshida, O. J. C. Dias, J. P. S. Lemos, *Phys. Rev. D* [rapid communications] (in press), hep-th/0307122.
- [241] L. C. B. Crispino, A. Higuchi, G. E. A. Matsas, *Phys. Rev. D* **63**, 124008 (2001).